

Carlos Xavier Pais Viegas

SCALABLE MODULAR MULTI-AGENT ROBOTIC SYSTEM ON AD-HOC PATHWAYS FOR AUTOMATION IN LARGE SPACES

Doctoral Thesis in Mechanical Engineering, branch of Management and Industrial Robotics, supervised by Professor Doctor Aníbal Traça Carvalho de Almeida, co-supervised by Professor Doctor Mahmoud Tavakoli and submitted to the Department of Mechanical Engineering of the Faculty of Sciences and Technology of the University of Coimbra

June, 2017



UNIVERSIDADE DE COIMBRA



Scalable Modular Multi-Agent Robotic System on Ad-hoc Pathways for Automation in Large Spaces

Doctoral Thesis in Mechanical Engineering, branch of Management and Industrial Robotics, submitted to the Department of Mechanical Engineering of the Faculty of Sciences and Technology of the University of Coimbra

Carlos Xavier Pais Viegas

Scientific Advisors: Prof. Dr. Aníbal T. de Almeida, University of Coimbra

Prof. Dr. Mahmoud Tavakoli, University of Coimbra

Department of Mechanical Engineering
Faculty of Sciences and Technology
University of Coimbra

Coimbra, June 2017

“Give me a lever long enough and a fulcrum on which to place it, and I shall move the world.”

Archimedes, Siracusa, 287 BC – 212 BC

Acknowledgements

Citing *Henry Ford*, the American visionary, founder of the Ford Motor Company and father of modern assembly lines used in mass production, “Anyone who stops learning is old, whether at twenty or eighty. Anyone who keeps learning stays young.”

This PhD dissertation is the record of an extensive research work carried out in the last four years at the Institute of Systems and Robotics of the University of Coimbra (ISR). During these long years, I struggled with many challenges, difficulties and many times frustrations. However, these were all experiences which contributed to my engineering education, as well as my personal development. The freedom which was given to me, the motivation to pursue my ideas and objectives, the stimulus to my creativity and especially the wise guidance of my scientific advisers and professors allowed me to improve the knowledge in the several fields of my research work and to overcome all obstacles I found in this endeavor. I can only express my immense gratitude to all those who made this part of my journey so pleasurable, challenging and exciting. With your help, dedication and support, I learned the true value of curiosity, perseverance and knowledge, allowing me to grow while staying forever young in mind and spirit.

Thereafter I particularly wish to express my sincere gratitude to my scientific advisers Professor Doctor Aníbal Traça de Almeida and Professor Doctor Mahmoud Tavakoli, for the valuable guidance, support and consistent encouragement during my PhD thesis. This acknowledgement is also extended to Professor Doctor David Daney, which supervised my work during my stay at Le Centre de Recherche Inria Bordeaux - Sud-Ouest, in France. I highly appreciate their outstanding scientific expertise and experience, as well as the trust and incessant care to provide me with the best possible working conditions. Their drive for scientific rigor was indispensable to the successful conclusion

of this thesis and, at the same time, a great source of inspiration for me. I would also like to acknowledge their effort in making an extensive critical review of this dissertation.

I would like to express my gratitude to Professor Doctor Rui Araújo and Professor Doctor Urbano Nunes, for their guidance during the study and development of the dynamic models of the SCALA manipulator.

I would also like to thank Doctor José Prado for the help and collaboration work in the implementation of the target identification and characterization algorithm, as well as the control of SCALA in the autonomous active surveillance demonstration.

I extend my gratitude to all people who actively worked with me in this research, and whose contributions were invaluable for this work. This includes Eng. Ricardo Dessi, Eng. Luis Bica, Eng. Pedro Lopes and Eng. Lucio Sgrigna, from ISR, for their help on the control of the SCALA agents and the development of the PCB's, sensors and all system's electrical components. In addition, I would thank Eng. João Lourenço, from ISR, Eng. Nuno Dias, from LIP and Eng. José Viana and Eng. Sergio Silva, from Fablab Coimbra, for their contribution in the fabrication of many of the SCALA prototype's components.

I would also like to acknowledge the Professor Doctor Paulo Menezes, from ISR, for lending the 6 DOF tracking solution for the SCALA testing and for the support and guidance given on how to take the best advantage of this equipment. I extend my gratitude to Professor Doctor Lino Marques, for the support given and to all the professors from the Mechanical and Electro-technical engineering departments, with whom I had the privilege and pleasure to work during my PhD. I can only hope my future work will live up to their excellence, and pay tribute to the great institution they represent, the University of Coimbra.

I also wish to thank all colleagues and friends from the ISR and INRIA research teams, for the friendly and scientifically inspiring atmosphere at both research centers.

To my friends who haven't yet been mentioned, Astrid Blin, Carolina Lourenço, Mónica Ferreira, Mariana Pinho, Leonor Gamas, Raquel Saraiva, Sofia Vieira, Rafael Batista, João Paulo, Jorge Raposo, Miguel Almeida, Rui Rocha, Adrian Peidro, André

Lopes, Ricardo Baila, Miguel Panão, Pedro Cruz, and others, I express my gratitude for their love and support.

Finally, to the people that stood closest to me, helping me maintain my motivation and focus, through their everyday love, care and support, my family and my girlfriend Carla, I wish to thank for everything.

Last but not least, I wish to acknowledge the funding entities and programs whose support was invaluable for this work to be carried out successfully, specifically the Portuguese Foundation of Science and Technology, through POPH - Programa Operacional Potencial Humano and QREN - Quadro de Referência Estratégica Nacional, contract SFRH/BD/94272/2013.



Abstract

Current industrial fabrication and automation systems are faced with the challenge of achieving fine manipulation over a large workspace. Fixed industrial arms offer high accuracy, but can only operate on a limited workspace. On the other hand, mobile robots equipped with a manipulator, do not possess the positioning accuracy required for fine manipulation. This dissertation introduces SCALA: a SCALable moduLar multi-Agent robotic system that navigates on ad-hoc pathways for automation in large spaces. It is based on the application of ad-hoc mobile agents, navigating over specially designed modular passive pathways with integrated high resolution localization systems. Modular pieces of the pathway can be installed vertically or horizontally and connected to form a bi-dimensional scaffold. This allows fast, precise and repeatable coverage of a vast and scalable bi-dimensional work grid with a low cost and scalable system. Then, one, or several reconfigurable parallel manipulators can be driven by the mobile agents and used to reach the tri-dimensional workspace. This parallel manipulator is the first of its kind, combining three different strategies for workspace extension, including reconfiguration, translation of the base and extension of the drive's ranges. With these tools, SCALA is capable of offering precise coverage of a large tri-dimensional workspace, thus fulfilling the gap between existing industrial solutions.

SCALA has applications in several fields, inside warehouses and factories. By adapting a gripper to the SCALA manipulator, one can do automation and material handling. By using a laser or a plastic filament extruder, one can do digital fabrication. The SCALA 2D agents can also be used for indoor and outdoor active surveillance in places such as shopping centers, airports, and stadiums, or as 3D tracking tool for motion capture labs. Original contributions to knowledge can be extended to three distinct domains: Introduction of a novel architecture for autonomous multi agent systems; Introduction of a

novel reconfigurable parallel manipulator architecture and development of a design methodology for parallel machines, based on geometrical parameter selection for a desired performance set; Introduction of a system for applications without "physical contact", as in the field of computer vision;

This dissertation covered the whole cycle of concept development, design, implementation and testing of the SCALA system. Until reaching the last prototype, several mechanical and mechatronic solutions were tested virtually and physically. A scale test bed was implemented for the testing and demonstration of the SCALA prototype. Demonstrations of three different applications of this system including pick and place, digital fabrication and active autonomous surveillance, were shown. These demonstrations served the purpose of validating not only the concept of SCALA, but also its actual implementation. The results are presented and discussed in detail, and future developments of this platform are proposed.

Keywords: Automation Systems, Multi-Agent Systems, Fine-Manipulation, Rail based Systems, Digital Fabrication, Parallel Manipulator, Industrial Robotics.

Resumo

Atualmente, os sistemas de automação e fabricação industriais enfrentam o desafio de obter uma elevada precisão num grande espaço de trabalho. Os manipuladores industriais fixos são capazes de atingir uma elevada precisão, mas apenas num espaço limitado. Por outro lado, robots móveis que tenham instalados braços robóticos industriais não possuem a precisão de localização necessária para tarefas de manipulação precisa. Esta dissertação introduz o SCALA: *SCAlable moduLar multi-Agent robotic system on ad-hoc pathways for automation in large spaces*, ou em português, Sistema robótico multi-agente, escalável e modular, em estruturas específicas, para automação em grandes espaços. Este sistema consiste na aplicação de agentes móveis em estruturas especialmente concebidas, modulares e passivas, e que possuem sensores de localização integrados. Os componentes modulares desta estrutura podem ser instalados vertical ou horizontalmente, para formar uma estrutura de suporte bi-dimensional. Isto permite uma cobertura rápida, precisa e fiável de uma vasta grelha de trabalho bi-dimensional, com um sistema de custo reduzido e escalável. Depois, um, ou vários manipuladores paralelos reconfiguráveis, atuados pelos agentes móveis, podem ser usados para aceder ao espaço tri-dimensional. Este tipo de manipulador paralelo é o primeiro do seu género, capaz de combinar três estratégias distintas para a extensão do seu espaço de trabalho, incluindo reconfiguração, translação da base e extensão do alcance dos atuadores. Com estas ferramentas, o SCALA oferece uma cobertura precisa de um vasto espaço tri-dimensional, preenchendo assim a lacuna existente nos sistemas industriais atuais.

O SCALA tem aplicações em várias áreas, na indústria de automação, armazenamento e fabril. Ao instalar uma garra no manipulador, é possível fazer transporte e manipulação de materiais. Da mesma forma, ao usar um laser ou um extrusor de filamento de plástico, é possível fazer fabricação digital. Os agentes móveis do SCALA

podem ser usados como sistema de videovigilância ativo em espaços domésticos e públicos, como centros comerciais, aeroportos e estádios. Outras aplicações na área da visão incluem, por exemplo, a reconstrução tridimensional de uma cena, para laboratórios ou estúdios de captura de movimentos. A contribuição deste trabalho para o estado de arte pode, desta forma, ser estendida a três domínios distintos: introdução de uma nova arquitetura de sistemas multi-agente; introdução de um novo manipulador paralelo reconfigurável e desenvolvimento de uma metodologia de projeto para máquinas paralelas, baseada na correta seleção dos parâmetros geométricos que assegure o desempenho desejado do sistema; sistemas para aplicações à distância, na área da visão computadorizada.

Esta dissertação abrange todo o ciclo de projeto, desde ao desenvolvimento do conceito, implementação e teste do sistema SCALA. Várias soluções mecânicas e mecatrônicas foram virtualmente e fisicamente testadas até chegar ao último protótipo. Foram depois demonstradas três aplicações distintas do sistema proposto, sendo elas a manipulação de objetos, fabricação digital e video-vigilância ativa e autónoma. Estas demonstrações têm como objetivo validar não só o conceito do SCALA, mas também a sua implementação. Os resultados obtidos são apresentados e discutidos em detalhe, e por fim são propostos futuros desenvolvimentos nesta plataforma.

Palavras-chave: Automação Industrial, Sistemas Multi-Agente, Manipulação de Precisão, Locomoção em Rail, Fabricação Digital, Manipulador Paralelo, Robótica Industrial.

Contents

List of Figures	xv
List of Tables.....	xxiii
Symbology and Acronyms	xxv
Chapter 1 - Introduction	1
1.1 Impact and Motivation	2
1.2 Objectives.....	6
1.3 Methodology	6
1.4 Contribution	10
1.5 Outline.....	11
Chapter 2 - Novel Multi-Agent System for Fine Manipulation over Large Workspaces	13
2.1 State-of-the-art Automation and Fine Manipulation Systems	14
2.2 Conceptual Design	28
2.2.1 Goals & innovative features	28
2.2.2 System building blocks	30
2.3 Applications	32
2.3.1 Automation and fine manipulation.....	32
2.3.2 Vision and surveillance	35
2.4 Detail Design.....	41
2.4.1 System architecture and evaluation	41
2.4.2 Control, communication and localization mechanisms.....	56
2.5 System Benchmarks and Comparison.....	58
2.6 Summary	63
Chapter 3 - Novel Reconfigurable Parallel Manipulator.....	65
3.1 Introduction to Parallel Machines	66
3.1.1 Comparison between serial and parallel robots.....	69
3.2 State-of-the-art on Reconfigurable Manipulators.....	72
3.3 SCALA Reconfigurable Manipulator	74
3.3.1 Parallel architecture.....	76
3.3.2 Kinematic model	85

3.3.3	Dynamic model	93
3.3.4	Singularities loci.....	100
3.4	Multi PKM Property Evaluation based Design Methodology.....	103
3.4.1	Existing PKM design methodologies	103
3.4.2	Novel PKM design methodology	105
3.5	Workspace and Property Evaluation	117
3.5.1	Manipulator design and parameter choice.....	117
3.5.2	Property workspaces and analysis	122
3.5.3	Workspace extension through reconfiguration.....	129
3.6	Summary	136
Chapter 4 - Implementation.....		139
4.1	Developed Prototypes.....	139
4.1.1	Generation ONE.....	140
4.1.2	Generation TWO	142
4.1.3	Generation THREE	144
4.2	Reconfigurable Manipulator Prototype	146
4.2.1	Links and joints	146
4.2.2	End-effector and tools	150
4.2.3	Prototype	153
4.3	System Electronics and Control	154
4.3.1	Drive motors.....	154
4.3.2	Agent localization system.....	155
4.3.3	Power.....	157
4.3.4	Control and communication	158
4.3.5	Graphical user interface.....	162
4.4	Vision System.....	164
4.4.1	Sensor setup.....	164
4.4.2	Mobile camera coordination.....	166
4.5	Multi-Agent Path Planning on Grid Map	169
4.6	SCALA Bill of Material (BOM) Analysis	172
4.6.1	Individual component cost	172
4.6.2	Setup cost	174
4.7	Summary	179
Chapter 5 - Results and Demonstrations		181
5.1	SCALA Test-bed.....	181
5.2	Component Testing	182
5.2.1	Mobile agent locomotion efficiency.....	183
5.2.2	Mobile agent localization accuracy	184
5.2.3	Parallel manipulator static accuracy	188

5.2.4	Parallel manipulator path following accuracy	191
5.2.5	Parallel manipulator reconfiguration	193
5.2.6	Discussion	195
5.3	Pick and Place	195
5.3.1	Methodology	195
5.3.2	Results	197
5.3.3	Discussion	198
5.4	Digital Fabrication.....	199
5.4.1	Methodology	199
5.4.2	Results	201
5.4.3	Discussion	204
5.5	Target Following.....	205
5.5.1	Methodology	205
5.5.2	Results	207
5.5.3	Discussion	213
Chapter 6 - Conclusion.....		215
6.1	Final Remarks	215
6.2	Outlook.....	220
6.3	Published Scientific Output.....	221
References		223
Appendix A - Prototype Drawings.....		241
Appendix B - Algorithms		255
Appendix C - Complementary Tables.....		259
Annex - Data Sheets.....		263

List of Figures

Figure 1-1 - From Industry 1.0 to Industry 4.0. Adapted from [3].	3
Figure 2-1 - The KUKA KR 1000 titan handling a crankshaft in a heavy-duty diesel engine factory[21].	14
Figure 2-2 - Adept Quattro™ s650HS high speed parallel manipulator[22].	15
Figure 2-3 – Few examples of different AGV types. From left to right, towing vehicle [25], load transfer vehicle[26] and forklift vehicle[27].	16
Figure 2-4 – KIVA material handling system[24].	16
Figure 2-5 - <i>Fraunhofer</i> MIMROex robot inspecting a process plant during field test on the topside of a platform[28].	17
Figure 2-6 - The Sensabot Inspection Robot, developed by the group NREC/CMU [29].	17
Figure 2-7 – KUKA youBot platform for scientists and researchers [30].	18
Figure 2-8 – Hangbot with a crane unit for cargo transport operations[33].	19
Figure 2-9 - Feed-support system of FAST[36].	20
Figure 2-10 - The Acroboter cable hanging robot's several components [38].	21
Figure 2-11 – The conCEILrge robot system [39].	22
Figure 2-12 – One of the Amazon Prime Air prototypes being tested[40].	23
Figure 2-13 – Air Drones from ETH Zürich's Institute for Dynamic Systems and Control building a 6 meter tall tower, autonomously[41].	23
Figure 2-14 – Air Drone making a cable-net structure[43].	24
Figure 2-15 - ARTIS robot with 5 modules and manipulator arm, and the robot moving on a rail[47].	25
Figure 2-16 – The Building Wall Maintenance Robot[50].	26
Figure 2-17 - Lucas Robotics System relying on motorized 3D scaffold[51].	26
Figure 2-18 – General view of the Perfect Pick relying on motorized 2D scaffold[53]. On the right, detail of actuation mechanism on Perfect Pick Rail Mesh[52].	27
Figure 2-19 – The Autostore warehouse automation system moving on passive 2D horizontal grid of rails[54].	28

Figure 2-20 - SCALA goal features place it above existing systems concerning accuracy and workspace size. 29

Figure 2-21 - Modularity of the SCALA agents. 31

Figure 2-22 - Project Escher parallel additive manufacturing concept, by Autodesk[56]. 32

Figure 2-23 – NASA’s vision for a 3D printed colony on the Moon[57]. 33

Figure 2-24 – Engineers at the 3D Print Canal House pour concrete in 3D printed molds[62]. 34

Figure 2-25 - Scale down prototype of WASP Delta mud house printer in action[63]. 34

Figure 2-26 - Two possible applications of SCALA in automation and construction. 35

Figure 2-27 - Possible SCALA application as a greenhouse automation system. 35

Figure 2-28 - Motion capture studio with multiple fixed cameras[9]. 36

Figure 2-29 - Advanced IP CamTrack Security and Surveillance Robot from Revolutionary Robotics[82]. 38

Figure 2-30 - SCALA surveillance system in a large warehouse. 39

Figure 2-31 - Examples of environments where SCALA automated surveillance system can be applied: airports, car parks, stadiums, shopping centers. 40

Figure 2-32 - SCALA as a home surveillance, support and assistance system. 40

Figure 2-33 – Different rail cross-section shapes considered for the SCALA system. 41

Figure 2-34 – Slider placement (black square) in the vicinity of a rail junction, showing the discontinuity in the slider support (hashed areas). 42

Figure 2-35 - The different architectures considered and tested for the SCALA system. 43

Figure 2-36 - System architectures with 3D agents on 3D scaffolds: a) continuous rail with 3D curves; b) perpendicular planar scaffolds with 3D agents. 43

Figure 2-37 – Mobile agent concept for *L junction* passing. a) approaching rail corner; b) rotating sliders and switching rail attachment; c) moving forward on perpendicular rail. 44

Figure 2-38 - Trainbot prototype for 3D scaffolds. 1-connection link; 2- module plate; 3-wheel module frame; 4- slider; 5- slider connection; 6- slider servo connector; 7- potentiometer. 45

Figure 2-39 - The *L junction* passing procedure, from a) to e), of the first prototype of mobile agent, tested for 3D scaffolds. 45

Figure 2-40 - Trainbot performing *X* and *L junction* crossing. 46

Figure 2-41 - Novel concept, based on the premise of having always two contact points between the slider and the rail (in red) and at least one contact point between the wheels and the rail (in green). 47

Figure 2-42 - Slider profile determination for the second prototype of mobile agent, for 3D scaffolds. 48

Figure 2-43 - Slider design for the Cambot prototype, for 3D scaffolds. 48

Figure 2-44 - Cambot prototype for 3D scaffolds. 1-New slider for continuous contact during *L junction* passing; 2- Spring; 3- Linear shaft. 49

Figure 2-45 - System architectures with 2D agents on 2D scaffolds: a) single agent fitted with a serial arm; b) parallel manipulator driven by 3 agents.	50
Figure 2-46 - Railbot prototype for 2D scaffolds. 1- Slider; 2- Big gear for the motor orientation control; 3- Anti-backlash gear for the motor orientation control; 4- Motor responsible for switching the driving motors' orientation; 5- Driving gear; 6- Driving motor.....	51
Figure 2-47 – Drawing and 3D model of Railbot, showing the fixture mechanism used for precise positioning of the agent in the center of the junction.....	52
Figure 2-48 - Railbot I prototype of mobile agent, the junction, and the rails.....	52
Figure 2-49 - Railbot I prototype passing a <i>X junction</i> on the 2D scaffold, placed horizontally upward. a) agent approaching the junction, b) agent on the junction, c) Changing the movement direction by rotating the driving motors, d) movement on the perpendicular rail.....	53
Figure 2-50 – Railbot I prototype passing a <i>X junction</i> on the 2D scaffold, placed upside down. a) agent approaching the junction, b) agent on the junction, c) Changing the movement direction by rotating the driving motors, d) movement on the perpendicular rail.....	53
Figure 2-51 - Railbot I prototype passing an <i>X junction</i> on the 2D scaffold, placed vertically on a wall. a) agent approaching the junction, b) agent on the junction, c) Changing the movement direction by rotating the driving motors, d) movement on the perpendicular rail.....	54
Figure 2-52 – Junction crossing sequence, highlighting the engaged gears at each time: a) agent approaches the junction (only one gear is engaged in the rail rack), b) agent in the middle of the junction (all four gears are engaged in the 4 perpendicular racks). At this point the mobile agent can switch its direction of movement and go to the transversal rails, or continue its longitudinal movement and proceed to c), where it is shown leaving the junction (only one gear engaged).....	55
Figure 2-53 – Detail view of the side gears engaging the perpendicular rails during junction crossing. The big arrows shows the direction of the mobile agent movement.	55
Figure 2-54 - Path planning of SCALA agents on an arbitrary 3D scaffold.....	57
Figure 2-55 - SCALA system breakdown.....	58
Figure 2-56 - Detail of the SCALA warehouse automation system.....	59
Figure 2-57 - SCALA as a 3D digital fabrication system.....	60
Figure 3-1 - Traditional types of joints[97].....	67
Figure 3-2 – Cartesian robot architecture. On the right, a gantry manipulator from Festo[98].	67
Figure 3-3 - Serial architecture and the UR5 robot arm from Universal Robots[100], on the left. Parallel architecture and the hexapod BREVA from Symétrie[101], on the right.....	68
Figure 3-4 - Parallel manipulator driven by 3 mobile agents on a rail grid.	75
Figure 3-5 - New composite joints proposed by <i>Feng Gao et al.</i> [97].....	76
Figure 3-6 - Above, the P [∧] UR limb maintains the same 4DOF whether it is moving on x or y direction. On the other hand, the CU [∧] limb, shown below, gains 1 DOF when moving on the x direction. v represents the translations and ω are the rotations with respect to three Euler's angles, α , β and γ	78

Figure 3-7 - PKM Kinematic structure and associated graph. For a clear representation, the third limb (c) is not shown anchored to the mobile platform center. 79

Figure 3-8 - 3 P^UR Manipulator architecture. Workspace block shown with the different rails and parallel manipulator’s agents identified..... 81

Figure 3-9 - Assembly modes 1 and 2 are for fine manipulation on a block, and possess several variations when the rails on which the agents move are switched. Assembly modes 3 and 4 allow the manipulator to move to other blocks in the rail grid. 82

Figure 3-10 - Workspace enlargement strategy by using the extension of the rails to the outside of the work block (highlighted in yellow), thus extending the drives ranges. 83

Figure 3-11 - Assembly Mode transitions inside a block. Above: singular transition from AM 1a to AM 2a/b/c. The same procedure is used for AM1b to AM 2d/e/f. Below: non-singular transition from AM 1a to AM 2d/e/f. The same procedure is used for AM1b to AM 2a/b/c..... 84

Figure 3-12 - Alignment of all three agents on the same rail, with same x_d distance, measured between the center points of each agent..... 84

Figure 3-13 - Assembly mode 1 referential and coordinates..... 86

Figure 3-14 - Assembly mode 2 referential and coordinates..... 87

Figure 3-15 - Assembly mode 3 referential and coordinates..... 87

Figure 3-16 - Assembly mode 4 referential and coordinates..... 88

Figure 3-17 – Dynamic control procedure. 99

Figure 3-18 - Singularities loci according to type, for AM1..... 102

Figure 3-19 - 3D Manipulator Workspace generated in MATLAB (Assembly mode 1a, $l=300\text{mm}$, agents range= 400mm , WS volume= 36.92 dm^3) 106

Figure 3-20 - PKM design study parameters. Desired workspace is represented by the yellow box. Kinematic parameters to be determined are shown in blue. 118

Figure 3-21 - Design algorithm running in serial. Inside boxes shown in green; outside boxes shown in red and purple; boundary boxes shown in white, cyan and yellow. Last image shows the final result. Calculation times (from top left to bottom right): Joint Range and Singularity Constrains- 25.52s; Accuracy Constrains- 18.27s; Force Constraints- 6.50s; Total calculation time- 50.29s..... 119

Figure 3-22 - Design algorithm running in parallel. Inside boxes shown in green; outside boxes shown in red, purple and dark blue; boundary boxes shown in white, cyan and yellow. Last image shows the final result after intersection. Calculation times (from top left to bottom right): Joint Range and Singularity Constrains- 25.52s; Accuracy Constrains- 3.00s; Force Constraints- 1.63s; Total calculation time- 25.52s..... 120

Figure 3-23 - Design Algorithm results for bisection *Rule B* (Hansen and Walster) and *classical method*. Inside boxes shown in green; outside and boundary boxes shown in white. Calculation times: *Rule B*- 50.29s; *Classical Method*-184.39s..... 121

Figure 3-24 - 3D Reachable Manipulator Workspace for AM1. Calculation time: 3375s, N. of Intervals: 100000, Min. Resolution: 25mm^3 123

Figure 3-25 - 3D Reachable Manipulator Workspace for AM2. Calculation time: 3131s, N. of Intervals: 100000, Min. Resolution: 25mm ³	123
Figure 3-26 - Workspace area on horizontal work plane at a z height from manipulator base.....	124
Figure 3-27 – Left and right, reachable workspace for AM1 and AM2, on plane $z=310$, respectively. Calculation times: 22.1s and 20.4s, N. of Intervals: 1086 and 1022, Interior area: 0.171m ² and 0.079m ²	124
Figure 3-28 - Accuracy Workspace for AM1, on plane $z=310$. Accuracy of 2mm, 1mm, 0.5mm and 0.15mm workspaces.	125
Figure 3-29 - Accuracy Workspace for AM2, on plane $z=310$. Accuracy of 2mm, 1mm, 0.5mm and 0.15mm workspaces.	126
Figure 3-30 - Force Workspace for AM1, on plane $z=310$. Payload of 0.5kg, 2kg, 3.5kg and 5kg workspaces.....	127
Figure 3-31 - Force Workspace for AM2, on plane $z=310$. Payload of 0.5kg, 2kg, 3.5kg and 5kg workspaces.....	128
Figure 3-32 - Work block mesh with m width and $2d$ length.....	129
Figure 3-33 – Reachable work areas for horizontal planes $z \in [0, l]$	130
Figure 3-34 – Reachable work areas represented on the workblock, for horizontal planes $z = 100, 200, 300, 310, 320$ and $340mm$, respectively.	131
Figure 3-35 – Reference workspace coverage for $w = 200mm$, $l = 400mm$, $d = 500mm$ and $m = 500mm$. The workplane is $z = 310mm$	132
Figure 3-36 – Left and right, workspace coverage for $w = 150mm$ and $w = 250mm$, respectively.	133
Figure 3-37 – Left and right, workspace coverage for $l = 375mm$ and $l = 425mm$, respectively. .	134
Figure 3-38 – Left and right, workspace coverage for $d = 400mm$ and $d = 600mm$, respectively.	134
Figure 3-39 – Left and right, workspace coverage for $m = 400mm$ and $m = 600mm$, respectively.	135
Figure 4-1 – SCALA generation ONE prototype.....	140
Figure 4-2 – First SCALA prototype agent model positioned in the junction center with the magnetic alignment system.....	141
Figure 4-3 – Exploded view of the first SCALA prototype agent, showing its components.	141
Figure 4-4 – SCALA generation TWO prototype, showing the mobile agent and custom made rails and junction, made in a CNC machine.	142
Figure 4-5 – Custom made rail and slider profile for the SCALA system, with embedded drive, power and localization solutions. Power solution was not tested.	143
Figure 4-6 - Exploded view of the second SCALA prototype agent, showing its components.	144
Figure 4-7 - SCALA generation THREE agent prototype, showing the top and bottom of the mobile agent.....	145
Figure 4-8 - Exploded view of the third SCALA prototype agent, showing its components.	145

Figure 4-9 – Manipulator types of joints considered: a) 3D printed universal joint; b) industrial cardan joint; c) rod end bearing; d) magnetic joint.....	147
Figure 4-10 – Range of motion in the rotation and tilt axis of the rod end bearing [235].....	148
Figure 4-11 – Section view of a magnetic joint, showing its high range of motion.....	149
Figure 4-12 - Exploded view of the SCALA manipulator end-effector with gripper.	151
Figure 4-13 - Exploded view of the SCALA manipulator end-effector with the unibody extrusion kit.	152
Figure 4-14 - Exploded view of the SCALA manipulator end-effector with laser.	152
Figure 4-15 –SCALA parallel manipulator prototype.....	153
Figure 4-16 –SCALA prototype details: 1– magnetic strip; 2– acrylic rack; 3– mobile agent; 4– aluminum rail; 5– tension string; 6– carbon fiber link; 7– steel sphere; 8– magnet; 9– bridge; 10- gripper.	153
Figure 4-17 – Pololu micro motors used and their assembly in the SCALA agents, with the driving gears coupled.	155
Figure 4-18 – AS5306 with Magnetic Multi-pole Strip Magnet for Linear Motion Measurement [243].....	155
Figure 4-19 - Encoder placement scheme on the mobile agent slider. The arrows indicate the working direction.....	156
Figure 4-20 - Section of the rail showing the initial calibration system. Gaps 1 and 2 are smaller than gap 3, meaning they are located before zero position. On the other hand, the gap 4 is bigger, meaning it is located after zero position.	156
Figure 4-21 - Arrangement of the magnetic strips to ensure there is always one encoder working during junction crossing.....	157
Figure 4-22 - Power supply solution being developed for SCALA, with embedded powerlines in the rails.....	158
Figure 4-23 - Custom made PCB for the SCALA mobile agents.	158
Figure 4-24 – Control architecture for the SCALA mobile agents.	159
Figure 4-25 - Mobile agent individual closed loop control scheme.	160
Figure 4-26 - High level centralized control scheme.	161
Figure 4-27 - Graphical user interface designed for multi-agent control.	162
Figure 4-28 - GUI for the manipulator reconfiguration control.	163
Figure 4-29 - GUI for the task performing control.....	164
Figure 4-30 - GUI for the vision applications control.....	164
Figure 4-31 – Exploded view model of SCALA surveillance agent, showing its several components.	165
Figure 4-32 – SCALA surveillance agent prototype.....	165
Figure 4-33 - Definition of camera field of vision and viewing range.....	166
Figure 4-34 - Target o_l following by mobile cameras c_1 and c_2	167

Figure 4-35 - Grid map example for a rail-based mobile robot environment.	170
Figure 4-36 - Virtual simulator for the SCALA multi-agent path planning.....	171
Figure 4-37 - Case study of a SCALA setup, for component fabrication and assembly, in a 20x10x2m room with 4 distinct areas: assembly, storage, 3D fabrication and transit....	176
Figure 4-38 – Comparable setup using existing automation solutions: 4 robotic arms, 4 delta 3D printers and 3 AGV’s equipped with a robot arm.....	177
Figure 4-39 – Scala setup cost shares for each component type.	178
Figure 5-1 - Small scale test-bed built for the SCALA, with a parallel manipulator and three mobile agents.	182
Figure 5-2 - Performance tests conducted. Images from left to right show the movement of the agent.....	184
Figure 5-3 - Setup for the Polhemus System in the agent accuracy/precision tests. 1- Sensor; 2- Source; 3- Mobile agent; 4- ABS support.....	186
Figure 5-4 - Average results with range for 10 localization accuracy trials, for each of the 5 displacements on a single rail segment. The average error of all displacements is represented by the horizontal blue dashed line.	186
Figure 5-5 - Average results with range for 10 localization accuracy trials, for each of the 2 displacements, with a junction crossing. The average error of all displacements is represented by the horizontal blue dashed line.	187
Figure 5-6 - Setup for the Polhemus System in the PM accuracy/precision tests. 1- Sensor; 2- Source; 4- ABS support; 5- Parallel manipulator.	188
Figure 5-7 - Average results with range for 10 static localization accuracy trials, for each of the PM mobile platform 5 random points in its workspace. The average error of all points is represented by the horizontal blue dashed line.	189
Figure 5-8 - Static accuracy range determined for the PM mobile platform, for 6 positions P along the y axis, in a horizontal plane $z = 310mm$	190
Figure 5-9 - Average results with range for 10 static localization accuracy trials, for each of the PM mobile platform 6 positions along the y axis, in a horizontal plane $z = 310mm$	190
Figure 5-10 - Manipulator carrying a payload of 800 g.	192
Figure 5-11 - Platform path-following accuracy tests. Plot of desired vs actual trajectory (dimensions in meters) for no load (left) and 800 g load test (right).	192
Figure 5-12 - Different test scenarios involving parallel manipulator translation or reconfiguration in the small scale test-bed: a) AM switching; b) PM translation.	193
Figure 5-13 – PM translation from one work block to another, viewed from the front.	194
Figure 5-14 - PM translation from one work block to another, viewed from the side.	194
Figure 5-15 – Task sequence implemented in the state machine, for autonomous pick and place task.	196
Figure 5-16 – Video captures during pick and place routine of the SCALA system.	198
Figure 5-17 – Digital fabrication from original source file to final output.	199

Figure 5-18 – Digital fabrication task one demonstration, by drawing on a white board. 201

Figure 5-19 - Digital fabrication task one demonstration, using the laser, on a planar and concave surface. 202

Figure 5-20 – Negatives of the results from the laser engraving demonstration on the planar surface. The desired shape is shown in red while the marks show the laser engraving/cut spots. 203

Figure 5-21 – SCALA 3D printing demonstration. 204

Figure 5-22 – Parts 3D printed by SCALA. 204

Figure 5-23 - Scheme of the test bed setup, showing cameras 1 and 2 and the target in their starting position. The target diagonal trajectory is also marked. 206

Figure 5-24 - Video captures from experience 1: a) target o_1 at the trajectory start, tracked by static camera c_1 ; b) target tracked by both c_1 and c_2 ; c) target at the end of trajectory, tracked by c_2 208

Figure 5-25 - Video captures from experience 2: a) target o_1 at the trajectory start, tracked by mobile camera c_1 ; b) target tracked by both c_1 and c_2 ; c) target at the end of the trajectory, tracked by c_2 208

Figure 5-26 - Video captures from experience 3: a) target o_1 at the trajectory start, tracked by mobile camera c_1 ; b) target leaves camera FOV and c_1 proceeds to change axis; c) target at the end of the trajectory, tracked by c_1 on a different axis. 209

Figure 5-27 - Target position tracking results using two static cameras c_1 and c_2 209

Figure 5-28 - Target position tracking results using two mobile cameras c_1 and c_2 209

Figure 5-29 - Target position tracking results using one mobile camera c_1 210

Figure 5-30 – Absolute distance to camera results of the three experiments. 210

Figure 5-31 – Distance to 2 mobile cameras, in x and y axis. 212

Figure 5-32 - Distance to 1 mobile camera, in x and y axis. 212

List of Tables

Table I - Comparison between state-of-the-art systems and SCALA Railbot II concept.	60
Table II – Comparison between different types of indoor mobile robots.	64
Table III - Feature comparison of serial and parallel robots[126].....	72
Table IV – Possible variations of the two main assembly modes.	82
Table V – Parallel manipulator geometrical parameters considered for the analysis.	122
Table VI – Effect of variation on end-effector width w	133
Table VII – Effect of variation on link length l	133
Table VIII – Effect of variation on rails 1 and 2 lengths d	134
Table IX – Effect of variation on rails 3, 4 and 5 lengths m	135
Table X –Link material properties, taken from various manufacturer catalogs.	147
Table XI – Comparison between joint variations used in parallel machines.	150
Table XII – SCALA manipulator component dimensions and mass values.	154
Table XIII – Mobile agent component and total cost.....	172
Table XIV – Rail component and total cost per meter.....	173
Table XV – Parallel manipulator component and total cost.	174
Table XVI – SCALA tools cost.	174
Table XVII – SCALA case study setup component and total cost.	177
Table XVIII – Characteristics of the developed prototypes.....	179
Table XIX – Results from the mobile agent locomotion tests.	183
Table XX – Comparison between the expected and obtained PM accuracy.....	191
Table XXI – Results for SCALA accuracy and repeatability tests.	195
Table XXII – Results from SCALA vision demonstrations.....	208
Table XXIII – technical specifications of the developed SCALA prototype.....	219
Table XXIV - Characteristics of industrial serial manipulators from ABB[266], Fanuc[267] and KUKA[268].	259
Table XXV - Characteristics of industrial parallel manipulators from ABB[266], Fanuc[267], Adept[269] and Symétrie[270].	260
Table XXVI – Spatial parallel manipulator configurations and their complexity level.....	260
Table XXVII – Main technical specifications of the commercial components used in SCALA...	261

Symbology and Acronyms

Symbology

Cambot geometrical parameters

α – rotation angle of the car when passing an *L junction*;
 R – drive wheel radius;
 d – half length of the slider;
 r – slider wheel radius;

Manipulator geometrical parameters

O – fixed Cartesian reference frame origin;
 Ω_0 – fixed Cartesian reference frame ($\Omega_0, \vec{x}, \vec{y}, \vec{z}$);
 Ω_p – moving Cartesian end-effector reference frame ($\Omega_p, \vec{x}_p, \vec{y}_p, \vec{z}_p$);
 $X(x,y,z)$ – coordinates of the end-effector relative to Ω_0 ;
 q_i – set of agent i coordinates relative to Ω_0 ;
 A_i – attach. point of limb i to agent i relative to Ω_0 ;
 B_i – attach. point of limb i to end-effector relative to Ω_0 ;
 b_i – attach. point of limb i to end-effector relative to Ω_p ;
 l_i – link L_i length;
 w – distance between b_1 and b_2 (end-effector width);
 x_d – distance between two agents A1 and A3, or A2 and A3, when in the same rail;
 d – distance between y oriented rails;
 m – distance between x oriented rails;
 v – translations along the 3 cartesian axis;
 ω – rotations with respect to three Euler's angles;
 α, β and γ – Euler's angles;
 M – mobility (of a mechanism);
 f_i – independent motion parameters of the joint i , with $i=1, \dots, k$;
 r – number of joint parameters that have lost their independence after loop closures;
 R – operational space;
 E – leg or limb;
 S – spatiality;
 R_p – rotation matrix;
 F_i – constraints equations;
 J_x – parallel jacobian matrix;
 J_q – serial jacobian matrix;
 J_{inv} – inverse jacobian matrix;

Dynamic model

ΔS – displacement;
 T – time period;
 t – time instant;
 X_0 – initial manipulator position;
 I_3 – 3×3 identity matrix;
 M – mass matrix;
 V – vector of *Centrifugal* and *Coriolis* terms;
 G – vector of gravity terms;
 τ – vector of joint efforts;
 \dot{q} – joint velocity vector;
 \ddot{q} – joint acceleration vector;
 \dot{X} – robot's end-effector velocity vector;
 \ddot{X} – robot's end-effector acceleration vector;
 m_l – mass of the links;
 m_a – mass of the actuators (agents);
 m_p – end-effector mass;
 $m_{payload}$ – manipulator payload;
 M_a – overall mass of the actuators;
 M_p – overall mass of the end-effector and payload;
 g – gravity acceleration vector;
 δW – virtual work;
 δr – virtual displacement;
 F – external forces acting on the manipulator;
 L – Lagrangian;
 K – kinetic energy balance;
 U – potential energy balance;
 p – generalized coordinate vector;
 Q – generalized external force vector;
 λ – Lagrange multiplier vector;
 τ_{fi} – friction force on joint i ;
 $f s_i$ – Coulomb friction parameter on joint i ;
 $f v_i$ – viscous friction parameter on joint i ;

Interval analysis

$[x]$ – interval real;
 $[\mathbf{x}]$ – interval vector;
 $[\mathbf{M}]$ – interval matrix;
 \underline{x} or $\inf([x])$ – infimum;
 \bar{x} or $\sup([x])$ – supremum;
 δ or $\text{rad}([x])$ – radius;
 $\text{wid}([x])$ – width/diameter;
 \tilde{x} or $\text{mid}([x])$ – midpoint/center;
 \square or \square – interval approximation of the solution set;
 \blacksquare – inner box;
 k – bisection direction;
 D – diagonal matrix;
 C_i – constraint i ;

$det()$ – determinant;
 $[p]$ – geometrical parameter interval vector;
 $[q_d]$ – joint range interval vector;
 W_i – workspace for the i performance property;
 W_{all} – workspace for a given property set;
 $[\delta q]$ – actuated joints accuracy interval vector;
 $[\Delta x]$ – end-effector positioning error interval vector;
 $[\Delta x_d]$ – desired end-effector positioning error interval vector;
 $[\tau]$ – joint forces interval vector;
 $[F]$ – external wrench exerted on the environment interval vector;
 $[D]$ – set of kinematic parameters $[p]$ which form a family of certified PKM's;
 \mathcal{L} – list of boxes;

Control and path planning

G_c – controller block;
 G_a – actuator block;
 G_p – system block;
 G_s – sensors block;
 u – control input;
 e – control signal;
 a – actuator command;
 n_i – grid map node;
 $h(s, t)_j$ – cost of a j path, from s to t ;
 f – evaluation function;
 g – direction cost;
 \hat{h} – sum of the number of horizontal and vertical nodes left to target node.

Vision

c_i – camera i ;
 o_j – target j ;
 FOV_i – field of vision of camera i ;
 rv_{cioj} – viewing range;
 α – inclination angle of the line segment connecting the camera i center to a point in the border of the camera FOV , and passing by the j target center;
 $d_{cioj}(t)$ or DTC – relative distance between camera i and target j ;
 p – position;
 v_i and v_{ij} – absolute and relative velocity, respectively;
 δ_i and δ_{ij} – absolute and relative heading, respectively;
 wo_j – priority value of target j ;
 $a_{cioj}(t)$ – camera i /target j utility function;
 Δt – reference time period;
 \hat{i} – camera movement direction;
 \hat{j} – direction perpendicular to camera movement direction;
 ϕ – occlusion factor;

Experimentation

n – number of trials;
 S_D – standard deviation;

Acronyms

ABS – Acrylonitrile Butadiene Styrene
ACO – Ant Colony Optimization
AGC – Automatic Gain Control
AGV – Automated Guided Vehicle
AM – Assembly Mode
AMS – Austria Micro Systems
CAD – Computer Aided Design
CNC – Computer Numeric Control
CW – Clockwise
CCW – Counter Clockwise
DDM – Direct Dynamic Model
DOF – Degree of Freedom
DTC – Distance To Camera
DXF – Drawing Exchange Format
ETH – Eidgenössische Technische Hochschule (Swiss Federal Institute of Technology)
EU – European Union
FAST – Five-hundred-meter Aperture Spherical radio Telescope
FCTUC – Faculdade de Ciências e Tecnologia da Universidade de Coimbra
FDM – Fused Deposition Modeling
FK – Forward Kinematics
FOV – Field Of Vision
FPS – Frames Per Second
GA – Genetic Algorithms
GPS – Global Positioning System
GUI – Graphical User Interface
IDM – Inverse Dynamic Model
IK – Inverse Kinematics
IIoT – Industrial Internet of Things
IR – Infrared
ISO – International Organization for Standardization
ICT – Information and Communication Technology
LIP – Laboratório de Instrumentação e Física Experimental de Partículas
MP – Mega Pixel
PID – Proportional–Integral–Derivative
PKM – Parallel Kinematic Machine
PLA – Polylactic Acid
PM – Parallel Manipulator
PSO – Particle Swarm Optimization
PWM – Pulse-Width Modulation
SCALA – SCALable moduLar multi-Agent robotic system for automation in large spaces
SLA – Stereolithography
SLS – Selective Laser Sintering
STL – Stereo Lithography
TC – Technical Committee
TS – Tabu Search
USB – Universal Serial Bus
VGA – Video Graphics Array

Chapter 1

Introduction

This chapter introduces the overall framework of the novel paradigms arising from the new industrial revolution. As technology and society evolve, so do all economic sectors related to them, including the industrial and manufacturing areas. The need for flexible and smart industrial systems is raised, and this constitutes the motivation behind this work. Current automation and manufacturing robotic systems deliver impressive performance in terms of accuracy or space coverage. Robotic manipulators and Automated Guided Vehicles (AGVs) have been used in industry since the fifties and sixties. While the former are used for tasks that require a high positioning accuracy and repeatability over a limited workspace, the latter are mainly applied for tasks which require navigation over a large workspace, but with lower accuracy or repeatability requirements, compared to the former. Fine manipulation over large workspaces is still a challenge. In the last decade, some solutions have been sought, in the form of combining an articulated arm with a mobile ground robot. Still, such solutions fail to provide the necessary precision, repeatability, flexibility or range needed for applications such as large scale digital fabrication, pick and place or autonomous surveillance.

In this work, a novel framework, capable of achieving high positional accuracy over a large workspace is introduced. It is conceived as a modular concept, made from specially designed ad-hoc rails and junctions which constitute a reconfigurable and scalable mesh, as dedicated pathways. A number of mobile agents can then navigate over this 2D mesh, with an excellent positional accuracy.

This platform can be used for robotics applications which do not require physical contact, such as 3D reconstruction or object tracking for surveillance. By extending the reach of the system to the tri-dimensional space, using a manipulator driven by the same mobile robots, one can perform tasks such as pick and place or digital fabrication. This framework presents novelties on several areas, comprehending the fields of mobile robots, reconfigurable parallel manipulators and also applications with no physical contact.

In the next sections of this chapter, the current and expected economic growth and impact on society of each of the proposed system's main areas of application, are discussed. The work challenges, objectives and methodology are hereby presented and defined considering the approach to the problem from the awareness to the comprehension of the new requirements for the next generation manufacturing and automation systems. To facilitate the readability and comprehension of the thesis, the structure and the main topics addressed in each chapter are presented as well.

1.1 Impact and Motivation

The manufacturing industry is, and will continue to be in the future, one of the main wealth generators of the world economy [1]. According to a report elaborated by the European Commission [2], which makes a vision of the manufacturing sector for 2020, there are 26 million enterprises in the European Union (EU). Of these, 10% are related to the manufacturing domain and represent approximately 22% of the EU National Gross Product. This data clearly reflects the importance of the manufacturing activity in Europe's and world's economy, and explains the attention devoted to the adequacy of methods and technologies to improve the productivity and competitiveness vectors.

In the last centuries, technological advances led to the birth and constant re-invention of the industrial paradigm, as illustrated in Figure 1-1. The 18th century saw the advent of mechanical production, powered by water and steam. In the end of the 19th and beginning of the 20th century, electricity revolutionized the industry. Through division of labor and introduction of assembly lines, mass production was accomplished. The development of electronics, programmable logic controllers and ICT, further automated

production in the 1970s, reconfiguring the industry for a third time. Currently we are in the dawn of a new industrial revolution. Digital Industry 4.0 sets out to shift once again the paradigm in as fundamental a way as its precursors have.

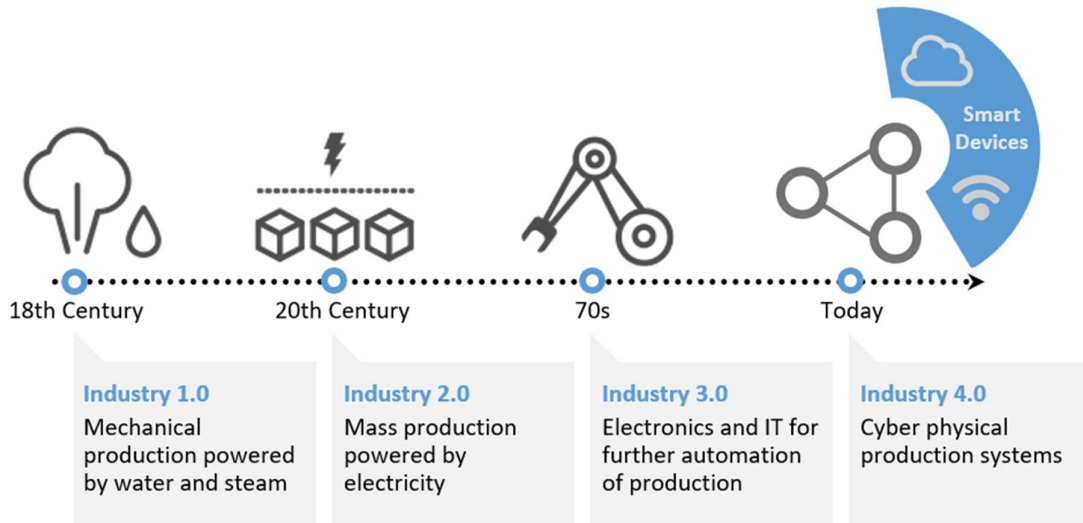


Figure 1-1 - From Industry 1.0 to Industry 4.0. Adapted from [3].

The core of Digital Industry 4.0 is highly intelligent connected systems that create a fully digital value chain, enabled by the Industrial Internet of Things (IIoT). Through the IIoT and the cloud, smart devices are able to identify themselves and communicate between each other. In a factory, machines can "talk" to products and other machines, delivering decision-critical data, which is then processed and distributed in real time, resulting in profound changes to the entire industrial ecosystem. These systems transform traditional plants into smart factories, where the idea of mass production and uniformity is changing to a more intelligent, scalable, adaptable, individual and custom-tailored production paradigm. This imposes new requirements on manufacturing systems, namely in terms of quality, response, agility, efficiency and adaptability [4].

The areas of application covered by this work range from digital fabrication to surveillance, pick and place, factory and warehouse automation.

Additive manufacturing is one of the major technological advancements behind this new digital fabrication. As opposed to subtractive methods such as CNC machining,

additive manufacturing, often referred to as 3D printing, allows the creation of three-dimensional objects by deposition or fusion of material, layer by layer. Recent studies indicate that worldwide spending on 3D printing will rise from \$1.6 billion in 2015 to around \$13.4 billion in 2018 [5], while McKinsey [6] estimates the potential economic impact of additive manufacturing to be in the range of 230 billion to 550 billion dollars, per year, by 2025. This makes it one of the most promising market rises in the near future. While still mostly used for manufacturing small scale products, large scale construction is also possible with this technology, with several advantages over traditional construction methods, making it extremely attractive to both architects and civil or environmental engineers. Contrary to using standardized elements, 3D printed designs can be customized to fit the user's needs and taste. This technology also eliminates waste, by going straight from the raw material to the final product. There are no transport costs, as designs can simply be transferred digitally and printed locally, using materials available on site, thus eliminating the local production cost variations. Additive manufacturing redesigns the supply chain around the customer, offering a big window of opportunities for innovative business models.

Today there are several systems for flexible warehouse automation and digital fabrication, as companies are willing to invest hundreds of millions of dollars to improve their workflow and efficiency. As a well-known example, Amazon invested over 775M\$ for acquiring KIVA, an autonomous material handling system [7]. Such systems often consist on automated guided vehicles (AGVs) which are capable of moving large loads, such as entire shelves, from one place to another. AGV systems have been developed and employed in large factories and warehouses for the last fifty years, and this industry is still growing. By delegating these tasks to mobile robots, one can optimize the space usage inside warehouses and factories, not needing to concern about human access or safety. It also becomes more efficient in terms of productivity, and less prone to errors than employing human workers.

Nowadays, many different types of vehicles and technologies exist with the possibility to address almost all needs for an industrial environment. Still, the main limitation resides in the fact that you can either get a mechanism, such an AGV, capable of

moving in an entire complex, while relying on an array of sensors and guiding mechanisms, or you can get a fixed base manipulator, to perform fine manipulation and precision work. However, you cannot get both. This is still a challenge that has only been briefly addressed by engineers and researchers.

Surveillance and video monitoring is another important field of research for several reasons. Recent estimations point out that the working age population in the EU will decrease by 48 million, representing a 16% reduction, between 2010 and 2050. Meanwhile, the elderly population will increase by 58 million, a gain of 77% [8]. This means an imbalance will arise between the number of elderly people and that of the caregivers. Automation of processes to provide the necessary care and support to the increasing elder population is then necessary. *Video monitoring* is a commonly-used tool for domestic and public surveillance. However, considerable human resource is required in order to monitor activities in large areas with multiple camera systems. In the case of home surveillance and assistance to elder or disabled people, the various house rooms and occluding objects demands for distribution of a large number of cameras throughout the house. An automated system, relying on multiple surveillance robots working symbiotically, could replace existing systems with clear advantages. Tri-dimensional scene and human kinematics reconstruction is another potential application of such a system, as setting up a human motion analysis laboratory is currently one of the most solicited research setups in the robotics and vision communities. Optical motion capture technologies were first used in biomechanics research studies in the late 1970s and early 1980s. Current biomechanical applications include gait analysis, ergonomics or human factors studies, orthopedic evaluations, and a wide range of sports performance studies. Optical motion capture technology is also used quite extensively in computer animation work for video games, television shows, and Hollywood movies. A typical optical motion capture system will consist of a large number of fixed cameras in combination with a computer and system controller software to automate the data collection. The number of cameras required for an application is dependent upon the number of subjects being recorded as well as the desired capture area. The more subjects and/or the larger the capture area, the more cameras will be needed for the laboratory or studio [9], and the more expensive the system becomes.

1.2 Objectives

The goal of this work is to propose and develop a solution in the form of an autonomous robotic system, capable of exploring the limitations of existing ones. This system, called SCALA, SCALable moduLar multi-Agent robotic system on ad-hoc pathways for automation and surveillance, obeys to several requirements, defined as follows:

- Capable of performing fine manipulation over a large 3D workspace in a fast, safe, reliable and repeatable fashion;
- Be scalable and modular, allowing to easily set up a custom configuration for each application;
- Be simple, low cost and efficient, with a reduced number of sensors and actuators.

The potential application areas of this platform include:

- Warehouse and factory automation;
- Digital fabrication;
- Video surveillance and 3D reconstruction;

1.3 Methodology

This research work involved the development from conceptual stage, to demonstration and validation of the SCALA prototype. The main tasks of this research work included:

1. State-of-the-art research;
2. Conceptual and detail design;
3. System implementation;
4. Multi-robot control and planning;
5. Parallel manipulator design and implementation;
6. Demonstration 1: Material handling;

7. Demonstration 2: Digital fabrication;
8. Demonstration 3: Vision application.

Each task is briefly described in this section.

State-of-the-art research

The background on existing industrial systems and solutions is the basis of all the research work. Their study is important to know their limitations and where there exists room for improvement. In particular, a detailed analysis of the state-of-the-art in the domains of automation and vision systems relying on multiple mobile robots, parallel manipulator design and reconfigurable mechanisms, was carried out. This included analysis of published scientific work, patents, videos, press communications, devices catalogs and manuals, and other available media. This stage set the requirements and standards for the proposed system, ensuring it constituted a step forward over existing systems and a valid contribution to the industry.

Conceptual and detail design

Conceptual design involved research and development of mechanisms for the SCALA components. This was followed by detail design, when all components were virtually conceived, assembled, tested and optimized to the largest extent possible prior to actual implementation. The 3D design stage in CAD software Solidworks 2014-2016 student version [10], allowed to perform structural analysis, virtual motion analysis, assembly testing and other simulations. Several prototypes were also produced until the final design, as a means of concept testing and design improvement.

System implementation

This stage included the system integration, test and validation of all components of the SCALA system. In this task, all design aspects of the whole mechatronics system

(mechanical setup, actuation, electronics) were fine-tuned. The developed prototypes were tested on a small scale test-bed, for rapid and low cost development.

Multi-robot control and planning

This task involved low level and high level trajectory planning for the distributed mobile robots on the rail mesh, through the implementation of multi-platform communication and cooperation mechanisms and algorithms. This was challenging, considering that synchronization and coordination of the mobile robots movements, in a mesh which can be heavily loaded with several agents performing distinct missions (i.e. material handling, fabrication, surveillance, patrolling, etc...), needs to be accomplished to fulfil requirements of some specific collaborative tasks.

An intuitive GUI (Graphical User Interface) was also developed in Visual Studio 2015 [11], to allow the user to control individual agents or assign missions to a group of agents. It also controlled the system functioning during the demonstrations.

Parallel manipulator design and implementation

SCALA agents are able to navigate on a bi-dimensional space. Extending the bi-dimensional workspace of the multi-agent system to a tri-dimensional workspace, can highly increase its range of applications. To achieve this, an innovative reconfigurable parallel manipulator, driven by multiple SCALA agents simultaneously, was designed and implemented.

Parallel manipulators require careful kinematics, dynamics and workspace analysis during project and design stage. When not available, novel design methodologies are developed for the conception of the system components. This was the case of the reconfigurable parallel manipulator, which due to its novel features, required specially developed design and testing algorithms, for property analysis, workspace determination and correct geometrical parameter selection. These novel design algorithms ran in Matlab R2014-16 environment [12], using special packages and tools, when necessary.

Demonstration 1: Material handling

This demonstration used the parallel manipulator to take advantage of the full tri-dimensional workspace of the SCALA prototype. For this demonstration, a gripper was mounted on the parallel manipulator end-effector. Several objects scattered around the robot workspace were picked and placed in a basket, one by one. This sets to validate the claim of SCALA as a large scale material handling system for factories and warehouses.

Demonstration 2: Digital fabrication

The second demonstration involved showing digital fabrication operations. A 3D printing extruder was fit to the manipulator tool, and several models were fabricated. A pen and a laser were also fitted to the manipulator end-effector, to draw/cut predefined patterns, thus demonstrating the capability of the system to perform precise trajectories in the same horizontal plane, which is required in applications such as laser cutting, engraving or soldering.

Demonstration 3: Vision application

The goal of this demonstration was to show one of the many applications of SCALA for tasks that do not require physical interaction of the robot with objects or humans. Applications include surveillance, target chasing, as well as 3D reconstruction, and are mostly based on robotic vision systems. The SCALA mobile agents were fitted with cameras and an existing vision algorithm was employed to detect a moving tag, fixed on a ground moving mobile robot. Then, the SCALA agents followed the moving target and tracked its precise trajectory, using the visual inputs and their own precise localization mechanism. This could be used in applications such as autonomous surveillance, and replace systems relying on fixed or 1D cameras.

1.4 Contribution

In the context of my previously developed work on mobile climbing robots for industrial inspection [13][14][15][16][17], and my master thesis work entitled “Design and implementation of an omnidirectional climbing robot for inspection of ferromagnetic structures” [18], this proposed work explores new applications in this field of mobile and service robots.

The development of the system includes challenges from conceptual design to its implementation. This dissertation involves several novelties in the conceptual and detailed design of various system components, as well as in the domain of parallel manipulators. Contributions of this work over the state of the art can be divided to three main domains:

1. Design and implementation of a novel modular multi-agent system for fine manipulation over large workspaces. This includes mobile agents and 2D ad-hoc rail grid, built from modular elements, which can be installed at any arbitrary angle, i.e., the same set of rails and agents can be used in both vertical, horizontal or over-hanging scenarios;
2. A reconfigurable parallel manipulator based on SCALA multi-agent system: to extend the 2D workspace of the agents to the 3D space, a novel reconfigurable parallel manipulator was designed and implemented. This manipulator is specially designed to take advantage of the high mobility of the robots driving it and employs several novel strategies, including reconfiguration, to achieve not only an excellent workspace to installation space ratio, but also improve its static and dynamic performances throughout said workspace;
3. Progress over state of the art systems for applications without "physical contact": taking advantage of the mobile robots high localization precision achievable by the proposed system, one can use a few cameras mounted on the mobile robots to perform several tasks in the area of computer vision, which previously required a large number of fixed cameras;

1.5 Outline

This chapter introduces the objectives and motivations of this work, while providing a brief insight on both the potential applications of the proposed system and its challenges. Furthermore, the expected outcome of this work and its scientific contribution are discussed.

Due to the variety of subjects covered in this dissertation, the state-of-the-art on each subject is presented in the related chapter.

The second chapter is dedicated to the SCALA as a novel multi-agent system for large spaces. A state-of-the-art on the existing industrial systems is presented and their strong and weak points are discussed. Then, the fundamental concepts behind SCALA are presented and developed. The conceptual and detailed design solutions for the system components, are discussed in detail. Its several fields of application are also presented, including automation, digital fabrication and vision.

The third chapter is dedicated to the design and development of the reconfigurable parallel manipulator driven by mobile agents to extend the workspace of SCALA to 3D. A state-of-the-art review on both parallel machines and their design methodology, reconfigurable robots and kinematics and dynamics of manipulators, is presented. Then, a detailed study of the main aspects of the chosen parallel architecture, as well as a novel design methodology and the study of the manipulator workspace are performed.

The fourth chapter details the concept implementation, showing the developed prototypes, the mechanical, electronical and control solutions adopted and the development of the test-bed for the demonstrations. It also contains a cost analysis of the proposed system.

The fifth chapter contains the results from the system component testing and from the demonstrations, and their discussion. The last chapter concludes this dissertation, emphasizing this research work main contributions and achievements and proposing future developments on the SCALA platform. The scientific works produced and published by

the author in peer-reviewed international journals, on the subject of this thesis, are also listed.

Chapter 2

Novel Multi-Agent System for Fine Manipulation over Large Workspaces

This chapter is dedicated to the conceptual development of the SCALA system for applications which require high accuracy and precision over a large workspace. It is an extended version of the published paper [19].

Today, there exist numerous warehouse automation solutions, each with its own characteristics and designed to suit very specific requirements or tasks. There isn't, however, a adaptable and scalable system capable of combining the best features of each automation solution, offering high accuracy, speed and safety over a large workspace, using several units which can work simultaneously.

In the first sections of this chapter, the most significant developments and systems in this field are reported and discussed in detail. The goal is to characterize the state-of-the-art and identify the current challenges in this field. These systems present valid solutions to some of the industrial challenges mentioned, while possessing limitations in other criteria.

The SCALA system concept is then built on the premise of improving current system capabilities. This conceptual design is discussed in the following sections of this chapter. From the set objectives to the design solutions for the SCALA components, every development stage is the subject of detailed analysis and discussion.

2.1 State-of-the-art Automation and Fine Manipulation Systems

Fixed base manipulators

Fixed based manipulators are tools whose base remains static and fixed to the floor or a structure. In this way, their workspace is limited by the maximum extent of their drives or links. Robotic articulated arms fall in this category of machines. Serial manipulators have been used for almost six decades in the industrial environment[20]. They constitute the largest share of industrial robots and are an indispensable tool in any modern production line. They possess several limbs connected by articulated passive or active joints, which link their base to their end-effector or tool. Decades of design and control improvement has led to modern systems which are capable of delivering impressive performance in terms of precision, speed, payload and repeatability. As an example, KUKA's KR 1000 Titan, the strongest six axis industrial arm in the market and shown in Figure 2-1, is capable of manipulating loads up to $1300kg$ with a position repeatability of $0.1mm$ and a reach of $3.6m$ [21].



Figure 2-1 - The KUKA KR 1000 titan handling a crankshaft in a heavy-duty diesel engine factory[21].

Another type of fixed-base manipulators are the parallel manipulators. Contrary to serial arms, some parallel manipulator architectures can take advantage from the fact that their actuators are fixed to their static base. This reduces the amount of moving masses and enables excellent performances in terms of speed and precision. Parallel machines such as

the Delta type Adept Quattro s650H shown in Figure 2-2, offer maximum speeds of $10ms^{-1}$ and accelerations of more than $15g$, with a position repeatability of $0.1mm$ [22].

Whether a serial articulated arm, or a parallel manipulator, repeatability and positional accuracy of these manipulators make fixed base manipulators the perfect solution for applications such as welding, painting, pick and place and component assembly. However, since they are not able to move around, their workspace is limited, even with geometrical parameter optimization[23].



Figure 2-2 - Adept Quattro™ s650HS high speed parallel manipulator[22].

Ground robots

For applications which require a large workspace, mobile robots, such as automated guided vehicles (AGV's), were developed. Ground robots constitute the biggest group of mobile robots and have been used in industry for more than 50 years [34]. They are often used to autonomously transport various materials, including pallets, rolls, racks, carts, and containers, across large factories and warehouses, with speed and efficiency. For different tasks, there are several vehicle types, as shown in Figure 2-3.

One recent example is the KIVA AGV system [24] from Amazon Robotics, for autonomous handling of shelves in a warehouse (Figure 2-4). It relies on multiple agents to transport entire shelves between distant areas inside a warehouse, by moving under them and attaching to their base.



Figure 2-3 – Few examples of different AGV types. From left to right, towing vehicle [25], load transfer vehicle[26] and forklift vehicle[27].

One of the main limitations of AGV's, including the KIVA system, is the lack of access to elevated areas.



Figure 2-4 – KIVA material handling system[24].

Some solutions which include a serial arm attached to a mobile base have been proposed, such as the *Fraunhofer* mobile robot called MIMROex [28], shown in Figure 2-5. This wheeled robot, designed to work on offshore platforms, can move through its environment autonomously and is designed to perform monitoring and inspection tasks, such as gauge reading and monitoring of gas concentrations, using its multi-DOF robotic arm.



Figure 2-5 - Fraunhofer MIMROex robot inspecting a process plant during field test on the topside of a platform[28].

Another example is the Sensabot Inspection Robot [29], developed by the group NREC/CMU (National Robotics Engineering Center from Carnegie Mellon University) in 2012. This robot is equipped with driving cameras, microphones, vibration, temperature and gas sensors, as well as a 7DOF serial robotic arm, enabling the accomplishment of multiple inspection tasks and also operation of valves, control switches, electrical panels, doors or gates. Figure 2-6 shows Sensabot performing inspection on an offshore plant during a field test and its new manipulator arm.



Figure 2-6 - The Sensabot Inspection Robot, developed by the group NREC/CMU [29].

KUKA, one of the world's largest industrial robotic solutions provider, has also launched a mobile manipulator for research and education called KUKA youBot [30], shown in Figure 2-7. This solution resembles, in a smaller scale, the above mentioned

Sensabot and MIMROex. Even though the integration of an articulated arm over the mobile base of an AGV can solve, to some extent, the problem of the limited workspace of fixed base manipulators, this highly reduces the positional accuracy of their tool. In fact, small errors in the position of the base can lead to large deviations of the manipulator end-effector from the desired pose.



Figure 2-7 – KUKA youBot platform for scientists and researchers [30].

Because AGV's move in unrestricted space with localization systems mostly based on sonar or vision, relying on multiple measures of environment references and triangulation of the obtained results, the associated errors are in the range of a few centimeters[31][32]. While this is acceptable in the context of mobile robots, a serial arm whose base location accuracy is in this range, is probably unable to perform any high precision task without the help of exteroceptive systems or external observers which can correct such error. Moving on the ground has another limitation, since they require a flat ground to operate, and also places them in direct conflict with other mobile or static obstacles and workers in the factory. This may cause severe problems in case of collision avoidance system's malfunction. Due to this high threat to safety and security, most AGV's are filled with an extensive array of collision avoidance sensors, which makes them complex, bulky and expensive. Another limitation comes from the fact that they require the installation of mechanisms, such as forklifts or robotic arms, to access the vertical space.

Robots moving on walls and ceiling

To make better use of the vertical space and avoid the crowded ground space, engineers have developed robots moving on the walls and ceiling. This not only separates the robot work area from the space humans use, improving speed and work efficiency, but also allows reaching high shelves and storage compartments. Many designs and concepts have been proposed but with limited capabilities and applications.

A simple solution consists in having a ceiling gantry robot to cover all the warehouse space. However, this solution does not allow simultaneous work of several independent units. Depending on the workspace size, one may also need large motors to drive the large and heavy moving parts of such system. Researchers from Japan recently proposed a system, shown in Figure 2-8, which relies on several individual units moving on the ceiling and using inchworm locomotion on perforated metal[33]. These units move slowly between anchor points, using actuated hooks in a complex hanging mechanism. Then a crane is employed to reach the vertical space, thus achieving full 3D manipulability.

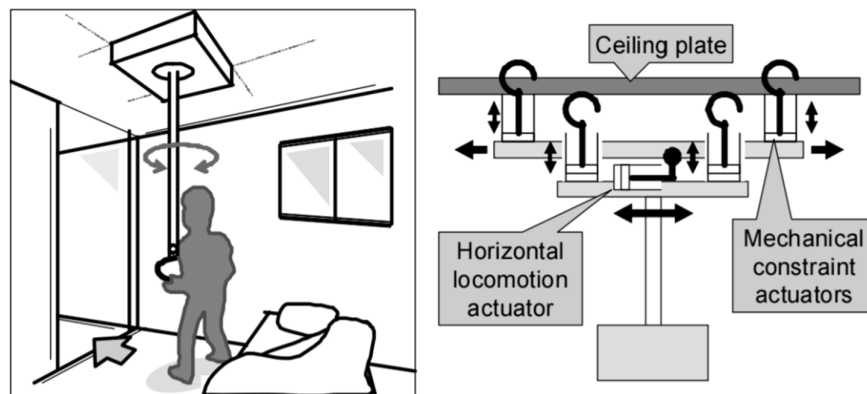


Figure 2-8 – Hangbot with a crane unit for cargo transport operations[33].

While localization accuracy can be high, the main drawback is the slow docking procedure and, consequently, slow locomotion. The WINDORO, a window cleaning robot for domestic use [34], uses one actuated wheeled unit moving on one side of the glass, connected through magnets to another unit on the opposite side of the glass. While it improves the locomotion speed, its main limitations include the risk of the payload

exceeding the capacity rate and the magnets failing to support the robot and the fact that the load is distributed by a single agent.

Cable hanging robots

Cable hanging robots are another type of mobile robots with good 3D reach. The most recognizable example is the Spidercam, used in almost every sports arena to closely follow the action in the large fields, while shooting pictures or recording videos[35]. Another similar example is the four-cable-driven parallel manipulator, developed for the orientation of the feed in the five-hundred-meter aperture spherical radio telescope (FAST) [36]. This system consists on a mobile translational platform suspended by four cables. These cables are attached to four towers, which also possess a winch mechanism to control both the length and tension of the cable, thus controlling the mobile platform position. A Stewart platform is mounted on the mobile platform so it can provide proper pose angle of feed to track celestial bodies, as shown in Figure 2-9.

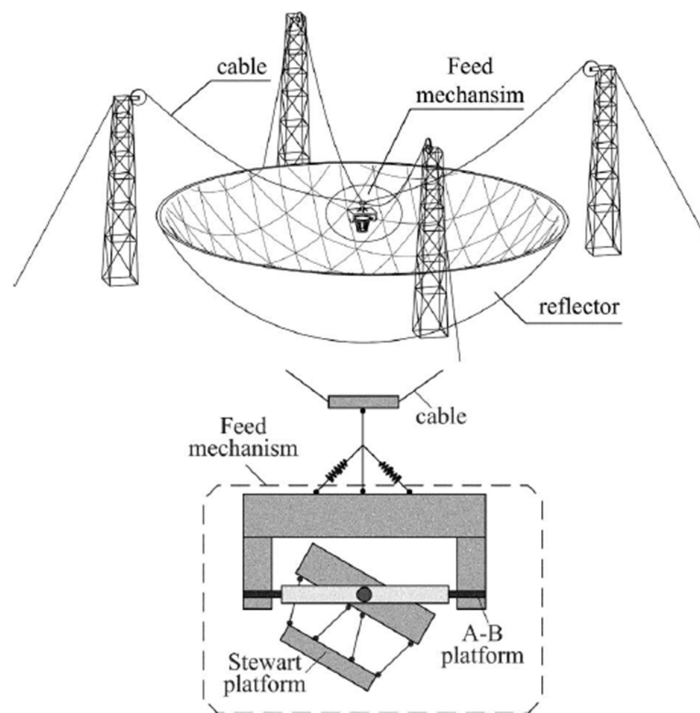


Figure 2-9 - Feed-support system of FAST[36].

However, general limitations of cable hanging systems include the fact that they can only bear tension and not compression of the cables, and are also susceptible to uncontrolled pendulum motion swinging effects when moving cargo at high speeds or when exposed to adverse exterior conditions, such as collisions or wind gusts. Adding to this, with fixed anchor points, it becomes very difficult for several units to work on the same workspace, due to the problem of cable entanglement [37]. Cable hanging robots with mobile attachment points have been proposed, such as the Acroboter[38], shown in Figure 2-10. This service robot is suspended onto the ceiling by a single cable, which is driven by a winding mechanism on a mobile ceiling platform. The mobile ceiling platform possesses two drives and is able to move from one previously placed anchor point to another. The swinging unit is equipped with ducted fan actuators that provide a free motion inside a conic volume.

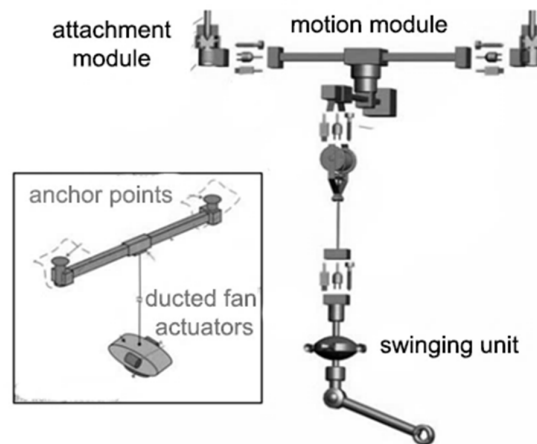


Figure 2-10 - The Acroboter cable hanging robot's several components [38].

In other words, the robot can fly around the suspension point, while the ducted fan system is also used for fine positioning and for the stabilization of the robot's motion. However this design also presents limitations regarding accuracy of the movement, due to its non-rigid nature. Autonomous manipulation of a payload by an overhead crane is difficult, due to the pendulum motion swinging effects and the requirement to do so in three dimensions simultaneously. It is important that the payload is transported in a trajectory and that the load oscillations are suppressed as quickly as possible. This non-

linear behavior raises issues of performance and safety such as: damage to the payload or to the surrounding environment, and injury to humans interacting with the robot.

Another similar concept was introduced by the *Takahiro S. et al.* with his conCEILrge robot[39], shown in Figure 2-11. This system relies on several overhead travelling units, which move above the ceiling and possess a crane mechanism to pull a cable linked to a moving platform. Instead of using ducted fans, they move the overhead travelling units and control the length and tension of the cables to move the suspended platform. However, this still has the same limitations as the Acroboter. Even with a good distribution of the load by several agents and a good tension control on the cables, moving large loads in suspended platforms is always a risk, especially in indoor and crowded environments. Also, the position control and precision of the platform is not good enough to allow tasks such as assembly or fine manipulation.

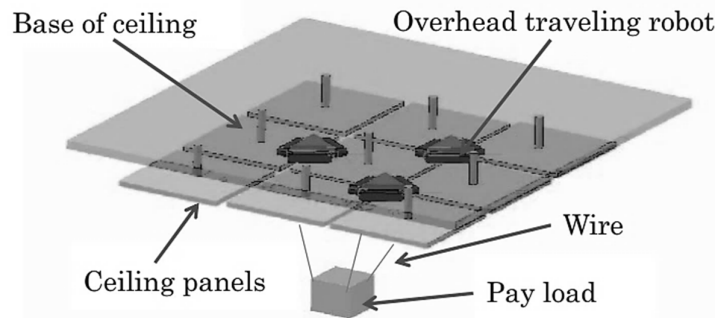


Figure 2-11 – The conCEILrge robot system [39].

Unmanned air vehicles

Recently, there has been some studies and efforts from scientists and engineers to harness the potential of Unmanned Air Vehicle (UAV) or drone technology for construction and industrial automation.

Probably the most well-known example of large scale transportation using drones is the Amazon Prime Air[40]. This future delivery system from Amazon is currently undergoing testing phase and is designed to safely get packages into customers' hands, in 30 minutes or less, using small UAV's, as shown in Figure 2-12.



Figure 2-12 – One of the Amazon Prime Air prototypes being tested[40].

In 2011, a team of roboticists from ETH Zürich's Institute for Dynamic Systems and Control, offered a glimpse of what might be possible with this technology. The researchers presented a 6-meter tall tower constructed from 1500 polystyrene bricks, shown in Figure 2-13, every one of which neatly assembled without any assistance from a human hand[41]. One by one, a fleet of flying robots dropped the pieces into place, guided by mathematical algorithms that took digital design data and translated it into flight paths.



Figure 2-13 – Air Drones from ETH Zürich's Institute for Dynamic Systems and Control building a 6 meter tall tower, autonomously[41].

This solution presents an advantage to crane systems, since it has the ability to reach any point in space. However, it still has some limitations, regarding payload limits and safety concerns. To be able to work in an indoor environment, close to humans, the size of the drones must remain small, thus limiting its range, duration of flight and payload capacity. This is something scientists have been trying to improve ever since, with new materials, lighter and more powerful batteries, more efficient motors and drone designs,

among other solutions. In the meantime, the investigation is also focusing on lightweight construction systems, particularly in the fabrication of tensile structures such as cable-net structures and three-dimensional suspension structures that could not be built with other fabrication methods [42], [43], as shown in Figure 2-14.



Figure 2-14 – Air Drone making a cable-net structure[43].

Another limitation is their flight accuracy. Without any external sensing and localization solutions, current UAV systems using onboard localization mechanisms relying on vision and multi-sensor fusion, are only capable of positioning accuracies in the range of a few decimeters[44][45]. Although engineers have been addressing all these issues, and drone technology has been evolving exponentially in the last five years[46], there is still a long way to go before we can see a reliable industrial system based on air drones.

Robots moving on rails

To address the limitations of systems based on unconstrained mobile robots, rail based systems have been proposed. These systems benefit from accurate positioning, as their movement is restricted by the single dimension rails. Furthermore, high precision localization sensors can be embedded on both rails and robots. The ARTIS robot, developed by DFKI Robotics Innovation Center and shown in Figure 2-15, is a modular rail guided robot that moves on a rectangular cross sectioned rail, and performs inspection

and maintenance tasks in ballast water tanks[47]. The robot has a polyurethane traction wheel, driven by a motor, on the upper surface of the rail and guide wheels on the sides and the bottom faces of the rail. Modules are connected using couplings composed of two ball joints and a rod.

Other very similar robots include the DORIS - Monitoring Robot for Offshore Facilities[48] and the Simple Redundant Space Robot for Space Station operation[49]. To be able to access 3D spaces, engineers used 3D rails with bends and curves. However, these rail structures are always continuous and made in a closed loop, not possessing intersections or junctions. This means that, in complex 3D environments, the shape of the rail mesh must be very well studied, and that it is difficult for multiple units to work simultaneously in the same rail mesh without interfering with each other.



Figure 2-15 - ARTIS robot with 5 modules and manipulator arm, and the robot moving on a rail[47].

To address this problem, several strategies were proposed. The Building Wall Maintenance system[50], developed by researchers at Korea University and shown in Figure 2-16, relies on several horizontal and vertical units moving on a 2D rail grid, applied on the façade of the building. The horizontal units perform the maintenance work and are carried up and down by the vertical units. Several magnets distributed along the rails, serve as localization and navigation mechanisms for the units. This robot is capable of moving large loads in a safe and precise manner, as opposed to current cable driven solutions. However, the complex docking procedure, combined with the need of having different units for moving horizontally and vertically, makes this system not as flexible as desired.

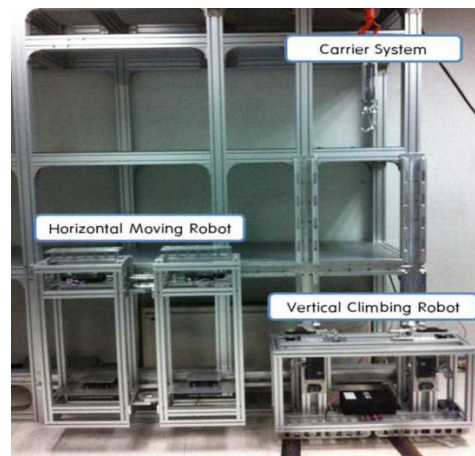


Figure 2-16 – The Building Wall Maintenance Robot[50].

Another adopted strategy was to use a rail mesh with motorized rail sections, to change the movement direction of the agents. Lucas Robotic System[51], shown in Figure 2-17, relies on several mobile units moving on a tri-dimensional mesh of rails, which possesses translational or rotational segments. These allow the mobile units to change their heading direction in the rail scaffold. While on one hand, the scaffold high automation level effectively increases the mobility and flexibility of the system, on the other hand it also increases its complexity and cost, since it requires at least one actuator per each junction.



Figure 2-17 - Lucas Robotics System relying on motorized 3D scaffold[51].

The Perfect Pick, shown in Figure 2-18, shares this same limitation [52], [53]. This system used for flexible storage in warehouses, is based on mobile robots which move on a planar rail grid. This grid possesses multiple solenoids with a linearly displaceable piston, to change the tracks configuration at junctions and select the agents moving direction (component 186 in Figure 2-18). While the scaffold automation complexity is inferior to the one employed by Lucas, it is still not optimal in terms of cost and simplicity. The workspace is also discrete, as the robots' work position is in the middle of each grid cell and there is no arm to enable access to positions between the cells.

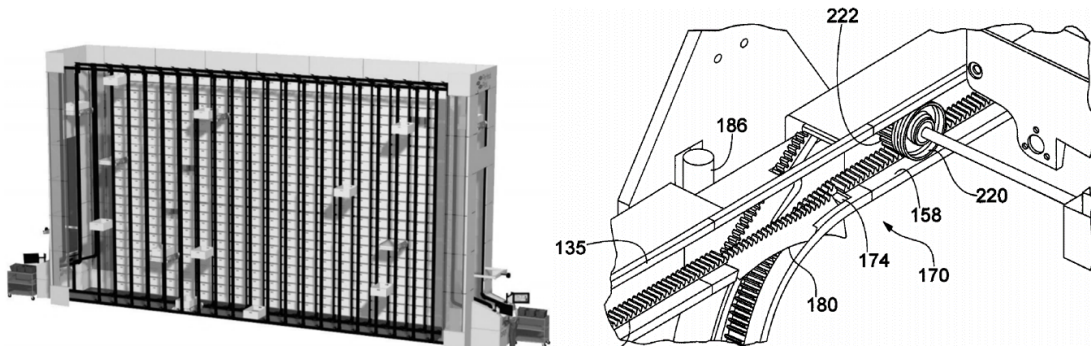


Figure 2-18 – General view of the Perfect Pick relying on motorized 2D scaffold[53]. On the right, detail of actuation mechanism on Perfect Pick Rail Mesh[52].

Autostore, shown in Figure 2-19, is an warehouse automation system relying on multiple wheeled robots, which move on a bi-dimensional passive grid mounted above storage compartments[54][55]. By using a crane, they can grab containers stored in these compartments. The advantage of this system is that the storage compartments or shelves can be fully compacted in a block, as the access is made from above, and are fully passive. The main problem is that the workspace of such system is not continuous but discrete. The tool used for accessing the 3D space, which is the crane, can only be used when the mobile robot is in the grid cell, and not in positions in between. Also, each time the robots need to switch moving direction, they need to move to the center of a work cell, stop their movement and switch the driving wheel set for the perpendicular one. This process takes valuable time and negatively affects the workflow. For this reason, this system cannot be used for flexible fine manipulation or digital fabrication.



Figure 2-19 – The Autostore warehouse automation system moving on passive 2D horizontal grid of rails[54].

2.2 Conceptual Design

In this section, the SCALA concept for fine manipulation over large workspace is introduced, with a discussion of the objectives and requisites for such system. Four specific conceptual designs are introduced, the Trainbot, the Cambot and the Railbot I and II¹. The obtained solutions are compared in detail among themselves and to the state-of-the-art systems presented previously. The best fitting concept for the objective of SCALA is then selected.

2.2.1 Goals & innovative features

In the previous section, the main capabilities and limitations of current automation systems were identified. While it is possible to have systems which offer very high precision and repeatability, and others which offer a large area of work and flexibility, the main challenge is still to find a single system capable of delivering both, with speed and

¹ The author of this thesis collaborated in the development of the Trainbot, Cambot and Railbot I, but the researcher responsible for their design was Lucio Sgrigna. They are included here as they are part of the development of SCALA and their testing contributed to the development of the Railbot II and next generation prototypes designed and developed by this thesis author.

efficiency. The proposed automation system in this dissertation work proposes to address the shortcomings of the previous systems, by fulfilling four main design objectives:

- A1 - Fine manipulation over a continuous large workspace;
- A2 - High operation speed;
- A3 - Several agents working simultaneously;
- A4 - Take full advantage of the vertical space and height in a site.

To pursue these mentioned goals, the vision for SCALA was to have autonomous mobile robots or agents, operating on specifically designed pathways, in the form of a rail mesh, made of rails and passive junctions. For these system elements, four optimization objectives were considered:

- B1 - Mobile robot simplicity;
- B2 - Rail mesh cost;
- B3 - Modularity;
- B4 - Scalability.

These features place SCALA above existing systems, as illustrated in Figure 2-20.

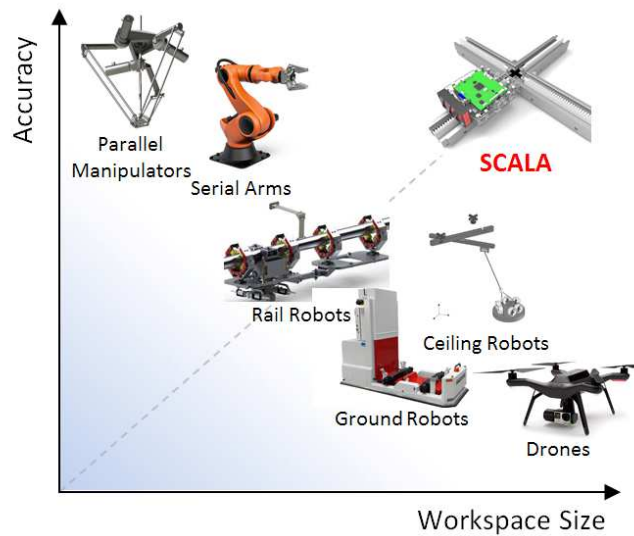


Figure 2-20 - SCALA goal features place it above existing systems concerning accuracy and workspace size.

2.2.2 System building blocks

Using several autonomous mobile robots moving on specifically designed pathways was the adopted solution, since it fulfills all main design objectives. The pathways are built by two modular elements, rails and junctions. Together, they form a mesh of rails where the mobile agents move, allowing to cover a large workspace with high speed and precision (main design objectives A1 and A2), due to integrated localization and power solutions. The rail junctions enable the robots to transit between collinear, parallel or perpendicular rails, thus allowing several units to work simultaneously and collaboratively (main design objective A3). The rail mesh can be placed on the walls, ceiling or even inclined surfaces, allowing to separate the robot environment from the human environment, thus avoiding any conflicts and increasing work efficiency (main design objective A4). In the design of the scaffold components, the adopted approach was to make only a couple of modular components which can then be connected in arbitrary configurations, just like construction blocks, to form the scaffold mesh, thus fulfilling both B3 and B4 optimization objectives.

Rails & Junctions

The main components of the scaffold are the rails. The junctions are the connecting elements of the rails. They can join two perpendicular rails, thus allowing the agents to switch the movement direction.

For the sake of scalability, and to make the investment feasible for a wide range of applications, the designs should be optimized in order to reduce the cost of the scaffold system and instead integrate any required complication into the agent. To do so, the scaffold components are totally passive (no actuator, no active sensor and no power). By using a custom-made aluminum extruded profile for the rails, one is able to produce a large amount of these rails at a reduced cost (B2 optimization objective), with a considerable low initial investment (for the extrusion mold matrix). A custom-made design also enables fine-tuning of all the necessary embedded elements. The rail junctions constitute the most expensive part of the rail mesh, since they need a higher fabrication precision to avoid problems when the agents want to change their direction of movement. However, lower

prices might be achieved when producing large quantities. Also, one of the criteria which can be implemented when designing the rail mesh is to find the minimum optimal number of rail junctions.

Agents

The mobile agents constitute the work force of the SCALA system. They possess some degree of intelligence, enough to send and receive signals to a central control station, drive its motors and receive and interpret the signals from its embedded sensors. They are also modular designed (B3 optimization objective), so the same base can accommodate several different tools for different tasks, such as a camera for surveillance or a joint module to support a manipulator, as shown in Figure 2-21. Since they continuously communicate their task and position to a central control unit, the system knows in real time the position and state of all agents. It can then send them commands and tasks, or attribute trajectories to better optimize the workflow and to avoid conflicts between them. This means that little processing power is required from the individual agents, and also no collision avoidance sensors are needed, thus making them a simple and affordable solution to acquire, run and maintain (B1 optimization objective).

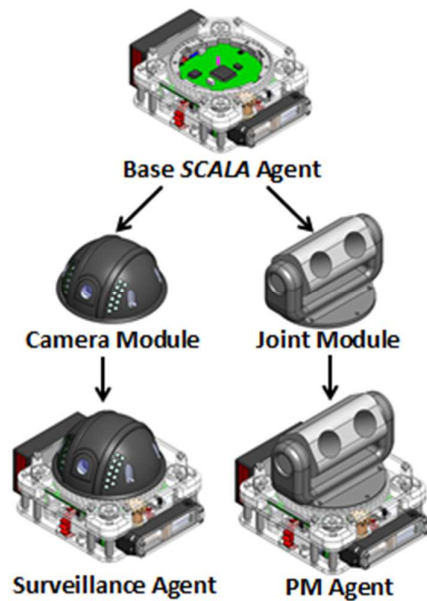


Figure 2-21 - Modularity of the SCALA agents.

2.3 Applications

2.3.1 Automation and fine manipulation

The SCALA platform primary application is automation, pick and place and 3D digital fabrication.

While current 3D printing systems can offer a very high printing resolution and object detail, current limitations include relatively slow build speed and limited object size. In an effort to improve the fabrication speed, higher velocities and accelerations were employed, up until the precision limit of both sensors and actuators. Recently, parallel additive manufacturing strategy has been tested, with the Project Escher, by Autodesk[56]. In this system, multiple independent extruders work simultaneously on the same part, as shown in Figure 2-22, thus reducing the fabrication time. Still, this concept has a large limitation in the fact that the extruder movement is not truly independent, but its range is restricted by the movement of the subsequent extruders. When the first printing head wants to move to the end of the production line, all other printing heads must also move backward and stop production.

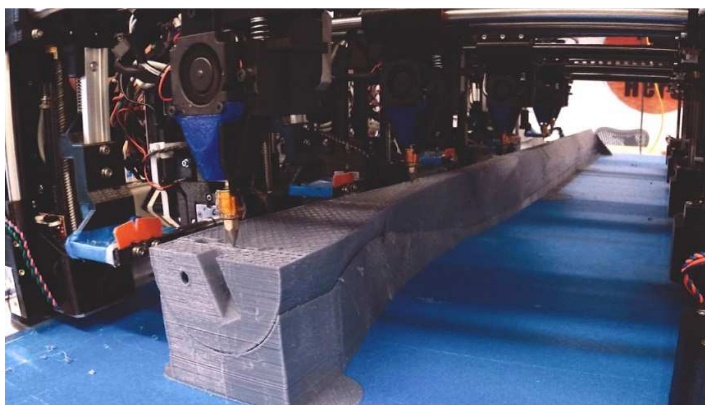


Figure 2-22 - Project Escher parallel additive manufacturing concept, by Autodesk[56].

Even though these 3D printer architectures are easily scalable, most printers are limited to small workspace volumes. However, there is also great potential in large scale 3D printing. Printing an entire house or infrastructure quickly and efficiently, without hard

human labor, using the resources available on the site and generating no waste, may be the solution in sub-developed countries, catastrophe scenarios, war zones or even establishing future colonies on other planets[57], as shown in Figure 2-23.



Figure 2-23 – NASA’s vision for a 3D printed colony on the Moon[57].

Construction is still an area where the level of automation is very low in comparison with current technological advances[58]. Some effort has been made to develop automation solutions in this field [59]–[61], but there is still a need for flexible intelligent systems for the next generation construction industry. The 3D Print Canal House project [62], shown in Figure 2-24, proposes to build a Canal House in the heart of Amsterdam to demonstrate the potential of 3D printing technology when applied to construction. Italian social business WASP[63], developed a full size portable 3D printer, shown in Figure 2-25, which prints bio-architecture houses using mud. In many parts of the world where affordable housing shortages are a growing problem, mud remains the most affordable and widely available raw material. However, building with it is an arduous and labor-intensive process. WASP prototype, consisting of a three armed, 6 meter high portable 3D printer, which can be assembled on site by two people, is capable of printing structures up to 3 meters high, in two hours. These examples show the potential of current 3D printing and fabrication technologies.



Figure 2-24 – Engineers at the 3D Print Canal House pour concrete in 3D printed molds[62].



Figure 2-25 - Scale down prototype of WASP Delta mud house printer in action[63].

SCALA, as a system capable of fine manipulation over a large space, can also be employed in large scale construction applications, performing tasks such as brick laying, tool carrying or welding, with multiple agents working simultaneously, thus largely improving the tasks' speed and efficiency, as shown in Figure 2-26.

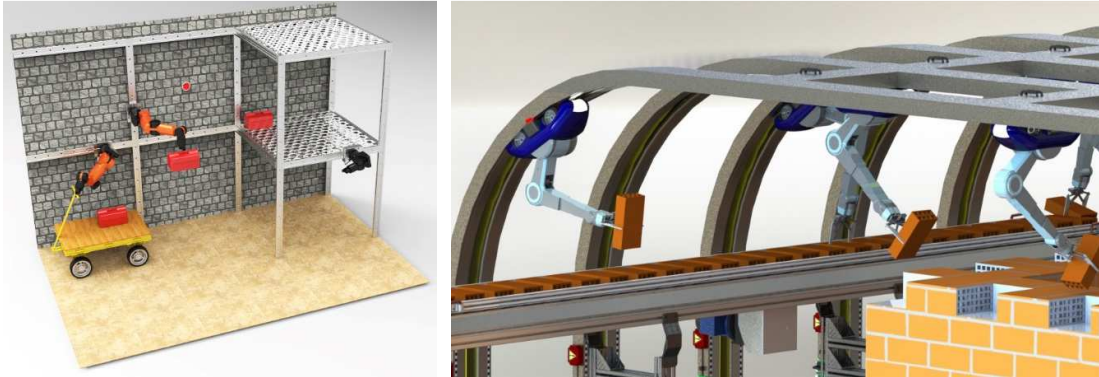


Figure 2-26 - Two possible applications of SCALA in automation and construction.

SCALA can also be used in agriculture, inside greenhouses, to attend large crops in a fully automated fashion and throughout all its phases, from the seeding, to the watering, pruning, disease detection by visual means, removing of weeds and fruit collecting (Figure 2-27).



Figure 2-27 - Possible SCALA application as a greenhouse automation system.

2.3.2 Vision and surveillance

SCALA characteristics make it an advantageous solution for applications without physical contact, relying on vision. Several tasks can be performed by the proposed architecture with superior efficiency, relatively to existing systems. This is also investigated in this dissertation work, even though it is not SCALA's primary application.

Computer vision has become, in the last years, one of the most active research fields, with many breakthroughs regarding the software and algorithms for accurate target perception and identification. This research field has a wide range of applications, including 3D reconstruction, surveillance, work flow monitoring, inspection, automated guidance, motion capture, among many others.

Optical motion capture technology has several bio-mechanical applications, including gait analysis, ergonomics or human factors studies, orthopedic evaluations, and a wide range of sports performance studies. It is also used quite extensively in computer animation work for video games, television shows, and Hollywood movies[64] (Figure 2-28).



Figure 2-28 - Motion capture studio with multiple fixed cameras[9].

For this reason, setting up a human motion analysis laboratory is currently one of the most solicited research setups in the robotics and vision communities[65]. By having multi-view images from a scene, one can extract 3D human body parts, using any of the extensive list of vision algorithms and methods available today[66]. OptiTrack [67] is the largest motion capture provider in the world and its typical system consists of at least 6 up to 48 or more fixed cameras in combination with a computer incorporating system controller software to automate the data collection.

The number of cameras required for an application is dependent upon the number of subjects being recorded as well as the desired capture area. The more subjects and/or the larger the capture area, the more cameras will be needed for the laboratory or studio[9]. This makes the whole system very expensive and complicated to set up and calibrate. *Riberto et. al.* have analyzed several setups for setting up a Motion Analysis Laboratory, and described the many problems and challenges in this field[68]. They showed that 8 cameras are required to cover an area of approximately 4x2x2m.

Multi-camera vision systems with the capacity of identification and extraction of 3D human body parts from a scene are also useful in video surveillance and elder care which has an important social impact considering the ageing of the population. Video monitoring is a commonly-used tool for domestic and public surveillance. However, considerable human resource is required in order to monitor activities in large areas with multiple camera systems.

There are already some tested and implemented algorithms developed for elder surveillance and specifically fall detection using computer vision systems that have achieved promising results[69], [70]. Yet they still require a large number of cameras distributed throughout the elevated points (i.e. ceiling) of the facility to avoid object occlusion, dead angles or aliasing effects when the camera-target distance overcomes the non-ambiguity range[71], [72].

To overcome the limitations of vision systems relying on fixed sensors, some works involving cameras mounted on mobile robotic platforms have been developed. However most of these systems use mobile robots moving on the ground to move the cameras [65], [73]–[75]. This presents several limitations, which include their low positioning accuracy, inherited from errors of the introceptive and exteroceptive perceptual system, including computer vision, GPS, wheel odometry or inertial module readings[31], [32], [76]. Even though, by means of a complex fusion of multi-sensory data, one may achieve a positioning accuracy of few millimeters [77][78][79], which is enough for navigation and other tasks, the required sub-millimetric accuracy for a reliable multi-camera 3D

reconstruction is not yet achieved. Other limitation of such systems is that, by moving on the ground, they have to share their space with people and static or moving obstacles, so they need to possess complex collision avoidance mechanisms[80], [81]. This not only limits their work flow capability, but is also far from being an unobtrusive solution. Ground mobile robots also struggle to overcome common obstacles found in indoor environments, such as steps or path obstructions, including doors or gates.

One of the most promising solutions was found to be using robots moving on rails. These possess several advantages over ground and aerial robots, including high localization precision, thanks to the possibility of embedding accurate localization sensors in the rails; infinite energy autonomy, by using electrified rails; discreet and efficient solution which can be mounted on walls or ceiling, and consequently does not have to overcome unexpected obstacles.

1D rail systems, such as the CamTrack [82], SensorRail [83] and VideoRailway [84] have been developed and commercialized for surveillance in large warehouses and supermarkets (Figure 2-29). However, their limitation to one dimensional movement makes them useless in environments with several divisions, obstacles and walls. It also becomes difficult for several surveillance units to follow simultaneously different targets, without getting in the way of each other.



Figure 2-29 - Advanced IP CamTrack Security and Surveillance Robot from Revolutionary Robotics[82].

SCALA constitutes a step forward regarding the state of the art mobile vision systems, as it is capable of having multiple mobile robots moving in an obstacle free environment, with high localization precision, and where multiple routes can be taken, thus becoming more flexible to adapt to large and complex scenarios. This includes indoor environments with several rooms, large warehouses with multiple aisles (as illustrated in Figure 2-30), etc... It is worth mentioning that a mobile camera system with a big overview of the whole system, can provide significant information for localization, path planning and fault detection of the other agents scattered in the rail mesh. This has been made for instance in a work by *Tavakoli et al.*, which involved cooperative multi agent mapping and inspection of a 3D structure with a group of terrestrial and climbing robots[85].

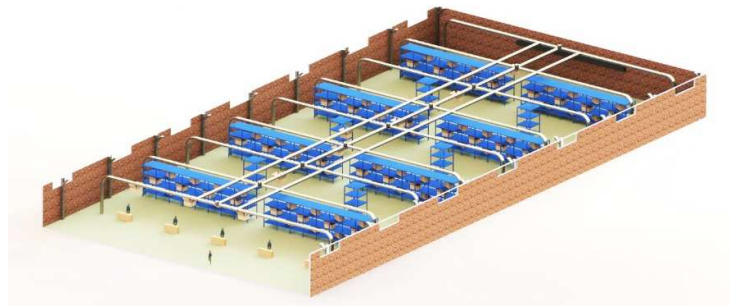
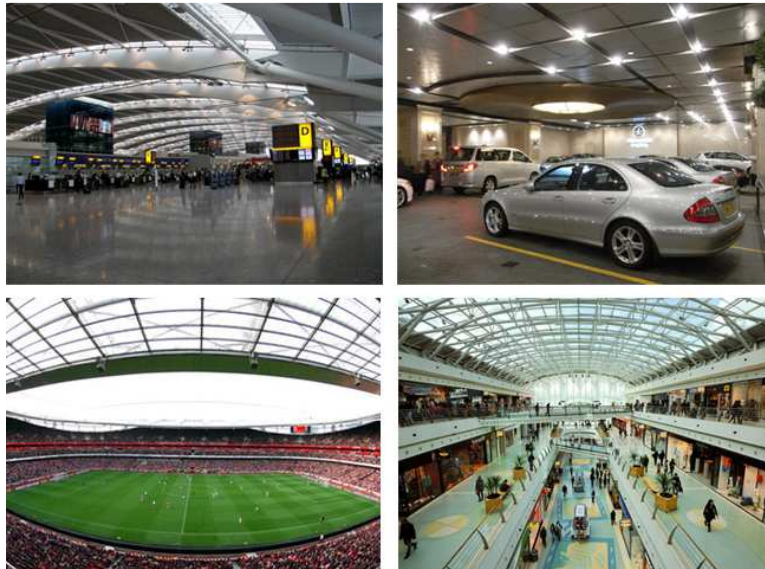


Figure 2-30 - SCALA surveillance system in a large warehouse.

It is also advantageous as a video surveillance tool in large and crowded public spaces, as the ones illustrated in Figure 2-31, where the capability of moving to another rail to get a better view of the followed target, might be invaluable to overcome current problems with object occlusion or dead angles. By knowing in real time the exact pose of each camera and being able to move the cameras to follow a scene, this system can perform precise 3D reconstruction on big spaces using fewer cameras than existing systems based on fixed sensors. This can be used for 3D reconstruction, in animation studios or for athletes in training facilities or physical rehabilitation.



**Figure 2-31 - Examples of environments where SCALA automated surveillance system can be applied:
airports, car parks, stadiums, shopping centers.**

SCALA might also be used for personal support and assistance. Not only it could allow to reach objects on shelves, but it could also perform constant surveillance and monitoring of old or disabled people and patients (Figure 2-32). By fitting the surveillance agents with the state-of-the-art vision algorithms capable of detecting falls, faints, heart attacks or other dangerous situations, it might prove to be a valuable tool in private residences, clinics, hospitals and nursing homes.



Figure 2-32 - SCALA as a home surveillance, support and assistance system.

2.4 Detail Design

In this section, different system architectures are presented and, in some cases, accompanied by a more detailed design and analysis. The goal is to fulfill the main objectives (A1-4) and evaluate the performance of system architectures, in regard with the optimization objectives (B1-4). Each system architecture moves further towards the design of the system building blocks (mobile robots, rails and junctions) which fulfills the set objectives.

2.4.1 System architecture and evaluation

The main goal of the SCALA is to perform fine manipulation over a large continuous 3D workspace. Moving robots on rails not only offers larger localization precision, but also makes it possible to install the system vertically or upside down. A rail-based solution has one main function: conduct the robots' movements between two locations. To fulfill this, three design aspects have to be considered: guidance, drive and navigation. The rail mesh is to be installed on the ceiling or on the walls, and the agents move on the rails, while carrying some payload. The rail-systems to fulfill these demands have to be form-fit, because the expected weight of the robotic system cannot be handled safely in an upside down or vertical position by mere adhesion. The combination of rail and slider design must ensure that the mobile agent has both vertical and lateral support, as shown in Figure 2-33.

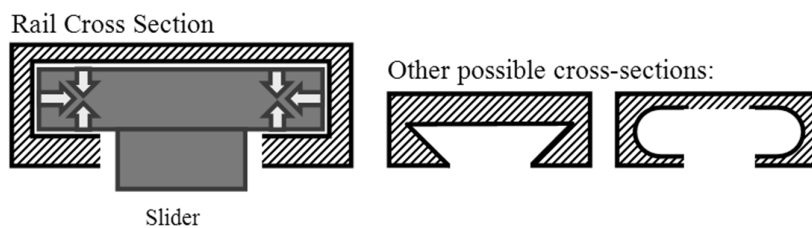


Figure 2-33 – Different rail cross-section shapes considered for the SCALA system.

For single rail systems, with no junctions or intersections, several types of cross-section shapes might be considered [47]. However, in this case, due to the existence of

junctions where the agent should be able to switch its moving direction, the choice of cross-sections was more limited. Different designs for the cross-section were evaluated during this conceptual stage (Figure 2-33), through CAD design and physics simulations. The optimized design must offer reduced friction to the movement by reducing the area of contact between the rail and slider, while still offering good support to the mobile robot. This is particularly critical in the rail intersections or junctions, where due to the discontinuity of the rail walls, as shown in Figure 2-34, the slider/rail fit must ensure full support to the robot and a good performance in the crossing of the junction.

The optimal design was found to be the C-shaped cross-section. This shape also facilitates the placement of the power and localization solutions. In the rail base, counterbores are made to allow rail fixation to the ceiling, thus avoiding problems such as rail bending and deformation.

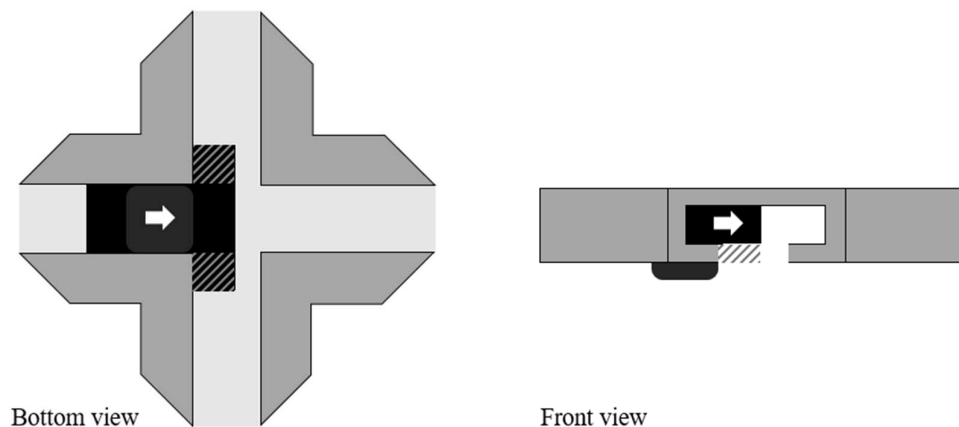


Figure 2-34 – Slider placement (black square) in the vicinity of a rail junction, showing the discontinuity in the slider support (hashed areas).

3D Workspace System

Mobility on two dimensions limits the range of SCALA applications to simple transportation tasks or applications with no contact, such as vision. To achieve fine manipulation or to perform digital fabrication, one needs to have a system with a full tri-dimensional workspace. This section is dedicated to the solution adopted to extend the

SCALA workspace from 2D to 3D. To accomplish this, several strategies can be adopted, as illustrated in the schematic Figure 2-35.

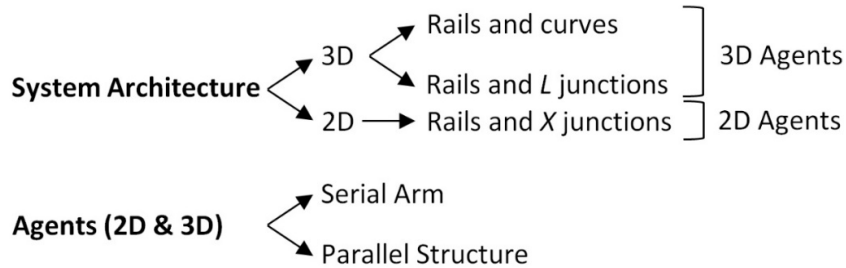


Figure 2-35 - The different architectures considered and tested for the SCALA system.

3D Scaffold Architecture

In a system where mobile robots run on rails, this can be accomplished by designing a continuous rail with 3D curves, as shown in Figure 2-36 a), which allows the agents to get to the desired areas in the workspace. This was the solution adopted by the ballast water tank inspection robots [47]. Their robot runs on a continuous rail, which passes through all the critical points of the water tank walls. The goal here was not to reach the whole workspace volume but just its boundaries. For this reason, it is possible to make a scaffold which allowed the robot to reach all necessary points.

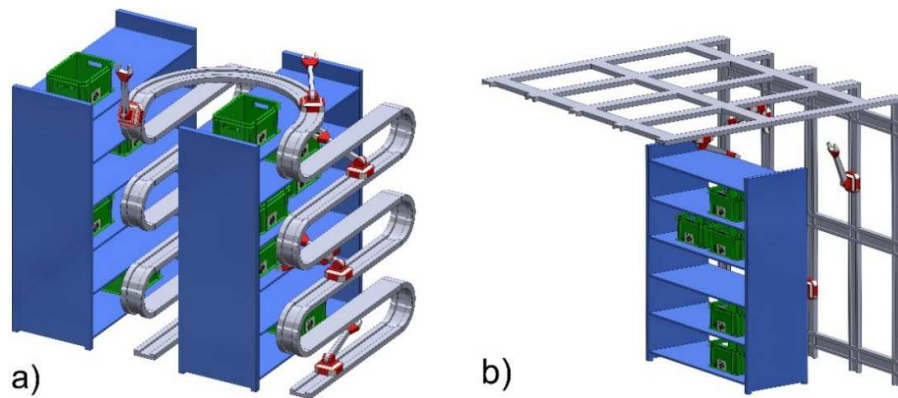


Figure 2-36 - System architectures with 3D agents on 3D scaffolds: a) continuous rail with 3D curves; b) perpendicular planar scaffolds with 3D agents.

However, in applications where one needs to access the whole volume of the workspace, the complexity and cost of the rail mesh required would render this solution

obsolete. It also constitutes an obstruction to the work environment and makes it difficult for multiple agents to work simultaneously without entering in conflict or getting in the way of each other. Due to the fact that it is a continuous rail with no branches, if one of the robots stops working, the whole line is compromised as other robots cannot pass over this robot. Thus, both A1 and A3 design objectives are not accomplished with this architecture.

One solution to address mobility on 3D scaffolds, is to build separate planar scaffolds and place them perpendicular to each other (as one in the wall and one on the ceiling), while having *L shaped junctions* to connect them, and *X junctions* in the planar scaffolds, as shown in Figure 2-36 b).

Several concepts were envisioned for this solution. One concept was to use a robot with tracks and two movable and rotating sliders. This would allow the robot to switch to a perpendicular rail in an *L shaped junction*. The process is illustrated in Figure 2-37, and starts with the robot approaching the perpendicular rail, with the slider aligned with the gap on the rail, so that it can enter inside it (Figure 2-37 a)). When the robot is in the corner of the two perpendicular rails, it rotates both sliders, so that the slider holding the robot to the previous rail aligns with the gap on the rail and releases the robot. On the other hand, the slider on the perpendicular rail, rotates in order to attach the robot to the rail (Figure 2-37 b)). The robot can then continue its movement on the perpendicular rail (Figure 2-37 c)).

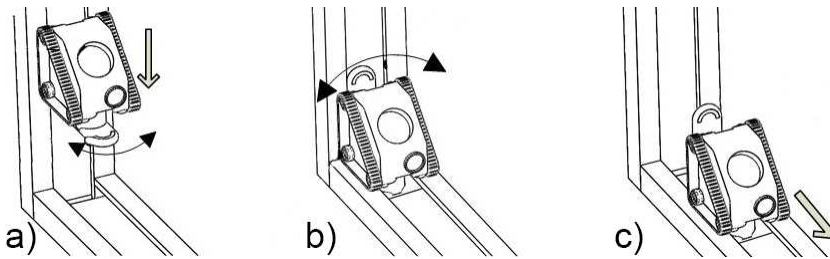


Figure 2-37 – Mobile agent concept for *L junction* passing. a) approaching rail corner; b) rotating sliders and switching rail attachment; c) moving forward on perpendicular rail.

However, this concept was not developed further due to the complexity of the mobile agent and its locomotion principle.

Another concept was explored, called Trainbot, shown in Figure 2-38.

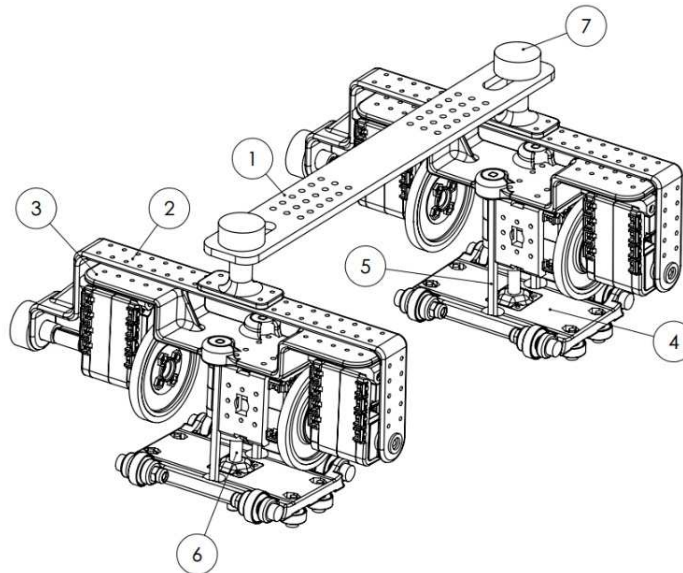


Figure 2-38 - Trainbot prototype for 3D scaffolds. 1-connection link; 2- module plate; 3-wheel module frame; 4- slider; 5- slider connection; 6- slider servo connector; 7- potentiometer.

For this concept, two differential drive modules, with a slider which goes inside the rail, were connected through a link. Each drive module possessed two drive motors and a servo motor to adjust the distance between the slider and the wheels, through a screw-nut mechanism. This enabled active traction force control, by pushing the wheels against the rail and increasing their normal force. It was also used during *L junction* passing, where the slider must keep a distance from the wheel in order to avoid hitting the rail, as can be seen in Figure 2-39.

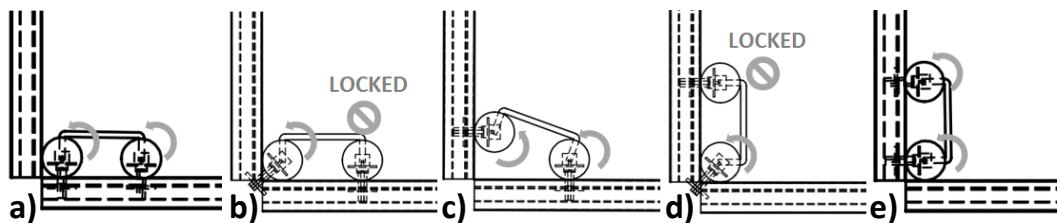


Figure 2-39 - The *L junction* passing procedure, from a) to e), of the first prototype of mobile agent, tested for 3D scaffolds.

This slider was specially designed with 8 rollers, that guaranteed contact with side plane and top plane of the inside of the rails, thus it could move along the rail with low

friction and zero clearance. To experiment this system, an early version prototype of SCALA was developed. Four potentiometers were mounted on the robot joints and reported the angle of the modules in relation to each other in two different planes, when passing the *X junction*, and when passing the *L junction*, as illustrated in Figure 2-40.

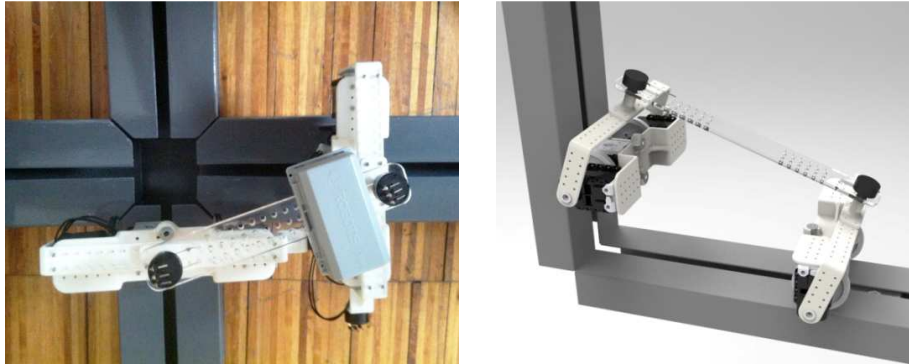


Figure 2-40 - Trainbot performing *X* and *L junction* crossing.

Chassis parts were custom designed and 3D printed in polyamide or laser cut from acrylic, while the rail segments were built from aluminum. This system had an overall of 6 actuators, which were AX-12 Robotis servo motors, and a CM-510 controller, also from Robotis[86]. To cross the *X junction*, differential drive was used. The leading module rotated 90° on the junction and moved on the new axis, until the following module reached the junction (Figure 2-40). The process was more complex for the *L junction*, involving several steps, as illustrated in the Figure 2-39. First, the robot drives to the vertical rail (a)). Then it locks the back wheels by pushing their slider against the rail and releases the front wheels by making some gap between their slider and the rail (b)). Then, the front wheels rotate, forcing the released slider to rotate 90° to the perpendicular rail (c)). At this point, both sliders are positioned for maximum wheel traction and the front wheels move up the vertical slider as the back wheels move forward. When the back wheels touch the vertical rail, the front wheels lock to allow the back slider to rotate and engage the vertical rail (d)). Then the *L junction* passing is complete (e)).

The advantage of this design was that it allowed mobility over a 3D workspace. Nevertheless, passing the *L junction* involved several steps, thus becoming highly complex and time consuming. In addition, the process of rotating the slider from one rail to the

perpendicular one required some gap to exist between this and the rail. During the experiment, it was discovered that the transition from the horizontal rail to the vertical one on the *L junction* was possible, but the transition between a vertical rail and an overhanging rail was not possible. The reason was because on step b) (Figure 2-39), the gravity helped the wheel to keep in touch with the rail and rotate the slider. However, this was not the case for the vertical to overhanging transition scenario.

These problems of crossing the *L junction* were addressed with a new design. This novel approach was based on a guaranteed contact between the wheels and sliders with the rails, in all steps of movement, as shown in Figure 2-41. In this way, the wheels have enough traction during the whole process, allowing passing the *L junction*, even in vertical to hang down scenario. To test this, a new prototype called Cambot, similar to the previous one except for the slider design, was developed. The main challenge here was to find the shape of the slider which guaranteed two constant contact points with the rail, while not colliding with the rail walls in any other point.

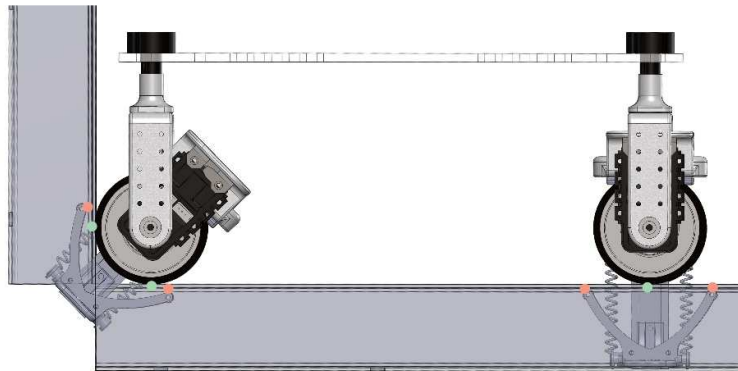


Figure 2-41 - Novel concept, based on the premise of having always two contact points between the slider and the rail (in red) and at least one contact point between the wheels and the rail (in green).

The shape of the profile was determined as a function of the rotation angle α , drive wheel radius R and the half of the length of the slider d , and corresponded to the relative position of the point P of the inside corner of the rail, relative to a slider wheel, whose radius is r . This relative position is given in terms of u and v , as shown in Figure 2-42, which translates to the following expressions:

$$\begin{aligned}
 u &= \left(\left(d - \frac{r}{\sin \alpha} \right) \frac{1}{\sin \alpha} + R(1 - \tan \alpha) \right) \cos \alpha + \frac{r}{\sin \alpha} \\
 v &= \left(\left(d - \frac{r}{\sin \alpha} \right) \frac{1}{\sin \alpha} + R(1 - \tan \alpha) \right) \sin \alpha
 \end{aligned}
 \tag{2-1}$$

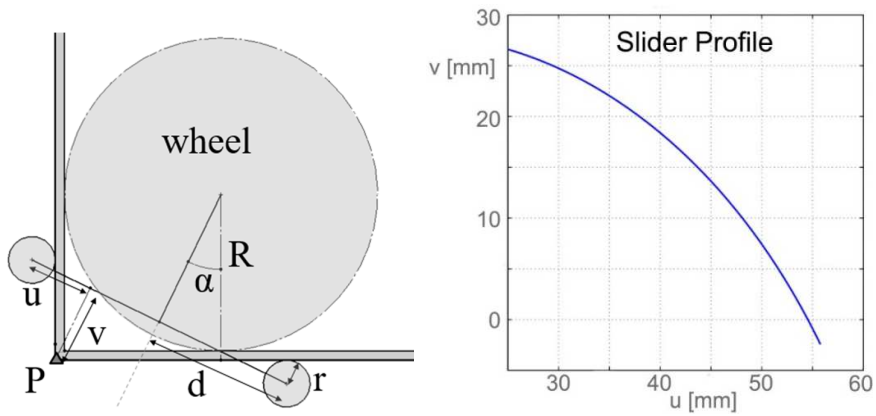


Figure 2-42 - Slider profile determination for the second prototype of mobile agent, for 3D scaffolds.

The final shape for the slider is depicted in Figure 2-43. This profile was symmetrical to be able to work in both directions with no difference.

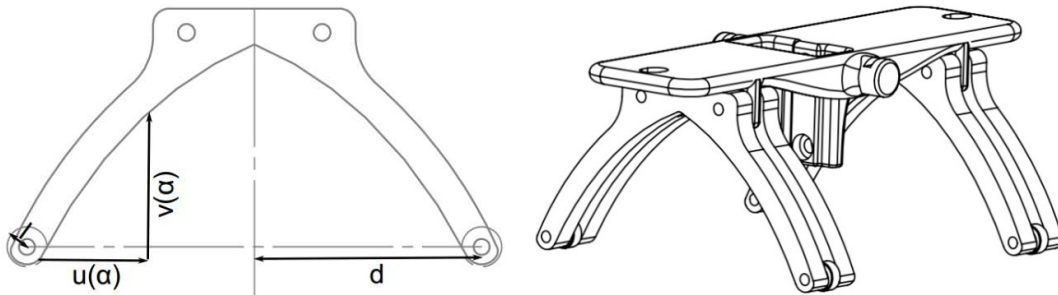


Figure 2-43 - Slider design for the Cambot prototype, for 3D scaffolds.

In addition, and since there is no need to increase the gap between slider and the wheels, during *L junction* passing, the active traction control system based on a servo motor per drive module, which worked in two directions, was replaced by a passive tension system using a linear shaft and a spring, which exerted force in one direction. This resulted in a reduction of the total number of motors from 6 to 4, as shown in Figure 2-44.

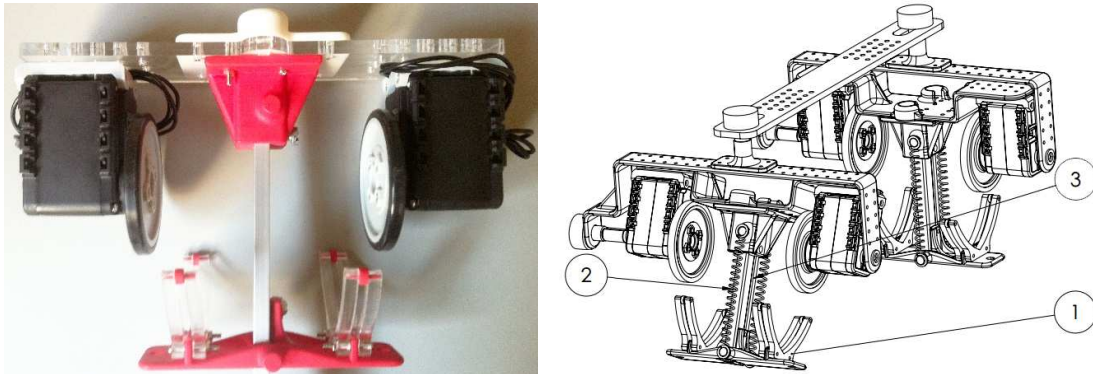


Figure 2-44 - Cambot prototype for 3D scaffolds. 1-New slider for continuous contact during L junction passing; 2- Spring; 3- Linear shaft.

Tests conducted with the new prototype showed improvements regarding the *L junction* passing procedure, due to the continuous contact of the slider and wheels with the rails and continuous traction. Still the system proved to be too complex with passive degrees of freedom which made the robot control difficult to achieve. Although removing the active traction control meant two less motors, the new prototype had no control over the traction force, meaning that moving on vertical and horizontal rails was performed under the same conditions. The springs used needed to be optimized to provide enough traction in climbing while not making too much resistance during horizontal traveling. In addition, one needed to take into consideration the possible cargo or exterior forces on the mobile agent, for both scenarios.

2D Scaffold Architecture

The 3D scaffold solutions were discarded in favor of a simpler solution where the mobile agents move on planar 2D scaffolds. Since, even for 3D scaffolds, mobile agents required an arm to reach all the continuous workspace, it would be beneficial to maintain the scaffold and agent architecture as simple and low cost as possible, since no *L junctions* nor mechanisms for passing them are required, and take advantage of efficient solutions to reach the workspace. In Figure 2-45 a), the solution adopted is to use a serial arm placed on the agent for full workspace coverage. However, when transporting large loads with high speeds and accelerations, the resulting torques on the agent may damage it or the rails.

For larger and heavier transported loads, the weight and size of the arm would also need to increase.

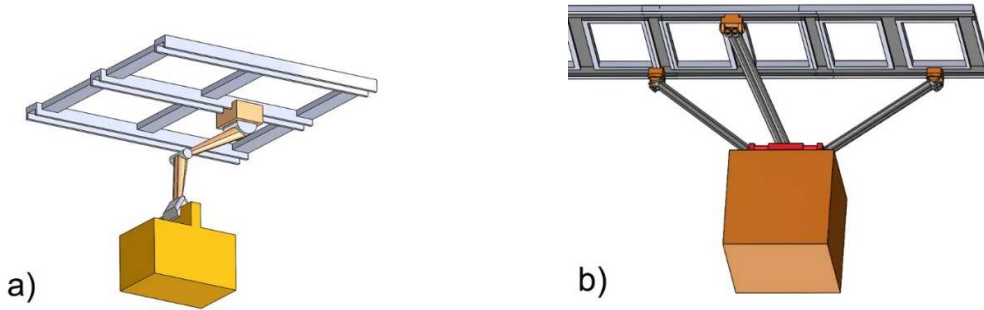


Figure 2-45 - System architectures with 2D agents on 2D scaffolds: a) single agent fitted with a serial arm; b) parallel manipulator driven by 3 agents.

To have a better load distribution, the optimal solution is to have a parallel manipulator driven simultaneously by three agents, as shown in Figure 2-45 b). This results in a much stiffer tool, capable of safely transporting cargo with large speeds and accelerations. A more detailed comparison between serial and parallel machines is presented in the next chapter. The parallel manipulator also takes advantage of the mobility of the agents to position its end-effector, not requiring any extra driving actuators or motors, as the serial arm solution requires.

The challenge on a 2D mesh of rails, which can be installed at any arbitrary angle, is to develop mobile agents which are able to move on horizontal, vertical and hang down scenarios, with the same efficiency. In this way, one guarantees a modular system that can be installed vertically to resemble a shelf, or horizontally to resemble a network of mobile robots on the ceiling.

In the previous concepts, the variations on the wheel traction caused the system to fail. To avoid slippage during agent movement, on the new prototype called Railbot, shown in Figure 2-46, the motion coupling system was changed to a gear rack drive.

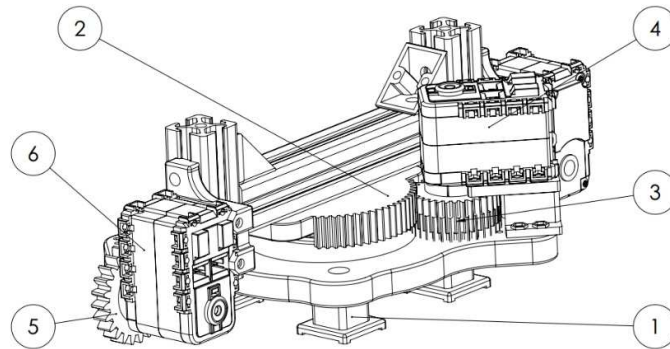


Figure 2-46 - Railbot prototype for 2D scaffolds. 1- Slider; 2- Big gear for the motor orientation control; 3- Anti-backlash gear for the motor orientation control; 4- Motor responsible for switching the driving motors' orientation; 5- Driving gear; 6- Driving motor.

Now, each motor of the agent drove one gear, which engaged a rack placed on the rail. Due to the existence of a discontinuity on the rack in the rail junctions, at least two gears and motors were required, so that there was always one gear engaged when the agent was crossing the junctions. The solution found was to use an agent with two driving motors aligned. To switch the movement direction on the *X junctions*, an auxiliary mechanism rotated the motors 90° (number 4 in Figure 2-46), measured by a shaft encoder.

For this process to be efficient, two aspects were crucial. First, when switching direction in the *X junction*, the robot should be positioned precisely in the center of the junction. To ensure this, a mechanical positioning solution in the form of spring plungers was used, that helped positioning of the robot once it reached the junction center, as shown in Figure 2-47. Three spring plungers were placed at the junction which engaged the respective holes in the sliders and center of the robot, thus locking it precisely in the junction center. Second, the mechanism for changing the orientation of the robot from one axis to a perpendicular axis, should be accurate and stiff. Otherwise, when rotating from one axis to the perpendicular one, the pinion could fail to align and engage with the rack. To solve this problem, an anti-backlash mechanism (number 3 in Figure 2-46) was employed. The anti-backlash system consisted of two gears mounted on top of each other, and a spring which pushed these two gears in opposite directions. Therefore, upon rotating around the big gear (number 2 in Figure 2-46), in clockwise (CW) or counter clockwise

(CCW) directions, at least one of the small gears was always tangent with the big gear, thus removing the gap between gears teeth and reducing backlash.

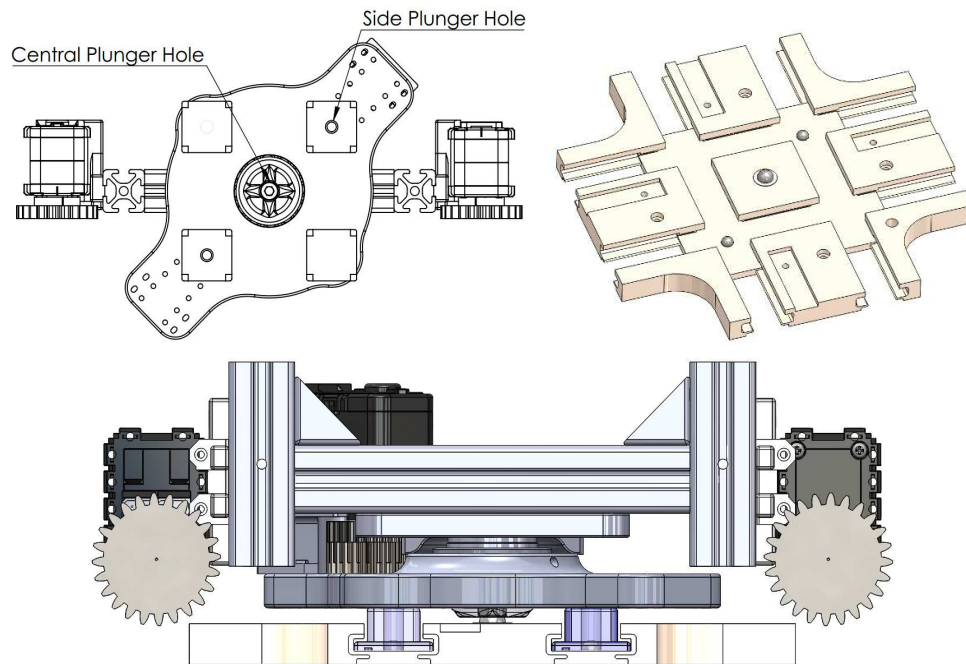


Figure 2-47 – Drawing and 3D model of Railbot, showing the fixture mechanism used for precise positioning of the agent in the center of the junction.

The Railbot I prototype developed can be seen in Figure 2-48. Overall, this architecture was much simpler than the previous concepts, integrating only 3 actuators. The chassis was made from 3D printed parts and standard aluminum profiles.

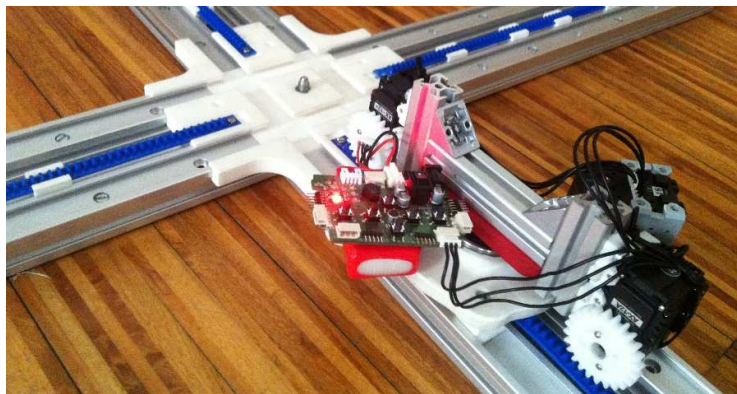


Figure 2-48 - Railbot I prototype of mobile agent, the junction, and the rails.

The motors and controller were the same from previous prototypes. The rails were aluminum extruded profiles from IGUS[87], while the junction part was 3D printed in polyamide.

Tests were conducted with the prototype moving on the 2D scaffold placed horizontally (Figure 2-49), upside down (Figure 2-50), or vertically (Figure 2-51).

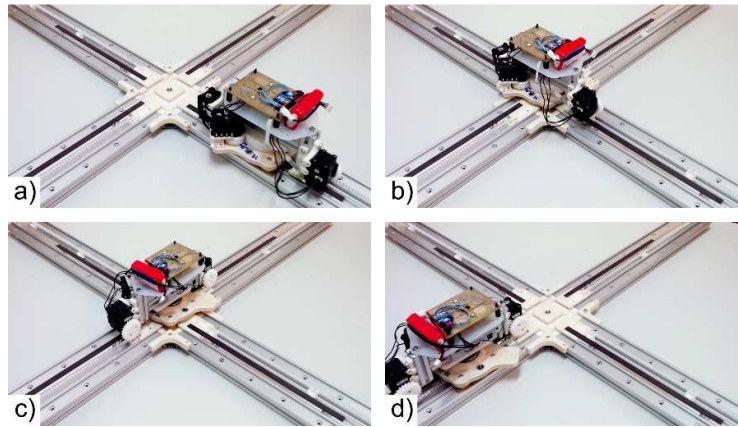


Figure 2-49 - Railbot I prototype passing a *X junction* on the 2D scaffold, placed horizontally upward. a) agent approaching the junction, b) agent on the junction, c) Changing the movement direction by rotating the driving motors, d) movement on the perpendicular rail.

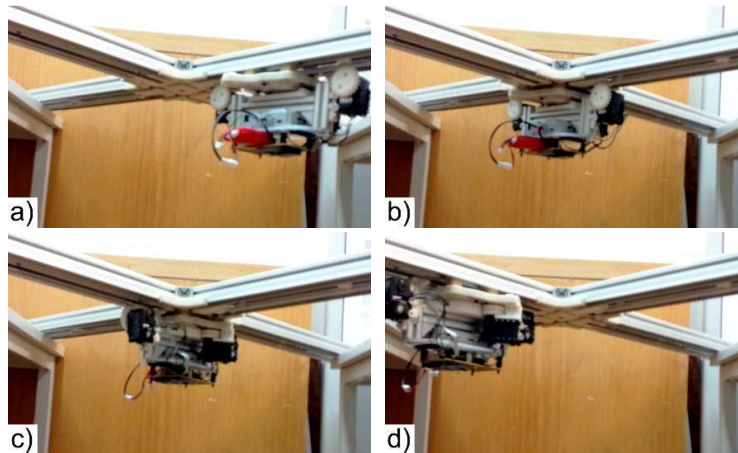


Figure 2-50 – Railbot I prototype passing a *X junction* on the 2D scaffold, placed upside down. a) agent approaching the junction, b) agent on the junction, c) Changing the movement direction by rotating the driving motors, d) movement on the perpendicular rail.

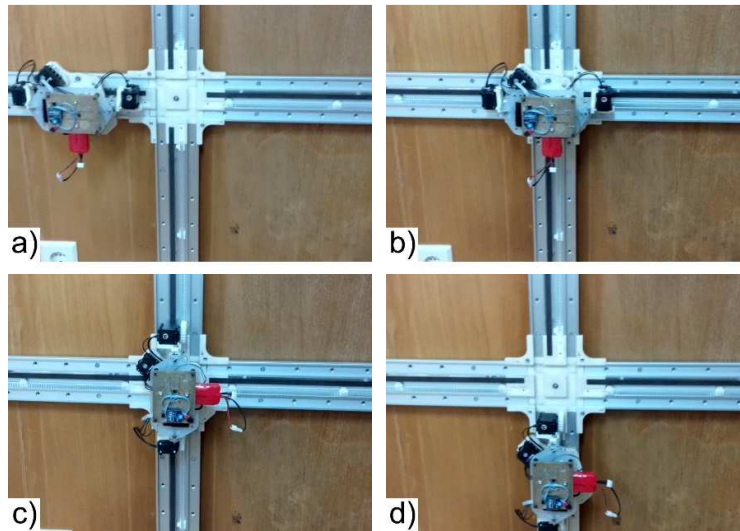


Figure 2-51 - Railbot I prototype passing an *X junction* on the 2D scaffold, placed vertically on a wall. a) agent approaching the junction, b) agent on the junction, c) Changing the movement direction by rotating the driving motors, d) movement on the perpendicular rail.

All sequences were repeated 20 times, for several directions, achieving a success rate of 100% for junction passing. Still, this design was not optimal since it meant that the robot needed to stop its movement at the junction, when it wanted to switch moving direction, for the period of time that it takes to rotate the driving wheels about 90°. This has the potential to negatively affect the workflow of the whole system.

In an effort to overcome this limitation, the final concept for the SCALA agent is developed. The Railbot II, designed and conceived by this thesis author, uses four motors, each one driving one gear, which engage the racks on the rails. In this version, for passing a junction, there is no need for a central rotation mechanism. Instead, all four gears are engaged with the four perpendicular racks, as shown by the scheme present in Figure 2-52. When reaching a junction, the robot can decide to continue its navigation on the same axis, or switch its moving direction, simply by activating the perpendicular pair of gearmotors. When the agent is crossing the rail junctions, the side gears have to smoothly engage the racks on the perpendicular rails while offering little resistance to the junction passing process. To achieve this, the gears have to be specially designed to afford a smooth engagement of the rack.

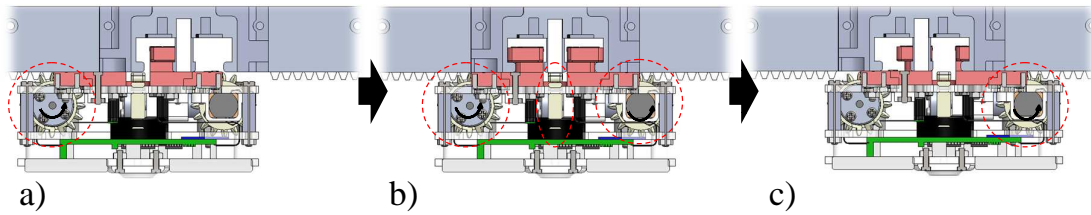


Figure 2-52 – Junction crossing sequence, highlighting the engaged gears at each time: a) agent approaches the junction (only one gear is engaged in the rail rack), b) agent in the middle of the junction (all four gears are engaged in the 4 perpendicular racks). At this point the mobile agent can switch its direction of movement and go to the transversal rails, or continue its longitudinal movement and proceed to c), where it is shown leaving the junction (only one gear engaged).

This is achieved by both tapering and crowning of their teeth (shown on the right image of Figure 2-53), in a similar solution to the one employed by *Tadakuma K. et al.* in his work on omnidirectional driving gears[88]. In his thorough analysis work, Tadakuma shows the advantage of using this solution in a bi-directional driving gear. He later employs a custom made gear with passive rollers, which offer minimal resistance to the sliding of the gear. However, given the small scale of the prototypes developed, the manufacturing challenges involved in the fabrication of the required gear, make this solution impractical. The Railbot II concept constitutes the basis of the several generations of the SCALA agents, which are presented in the following chapters of this thesis.

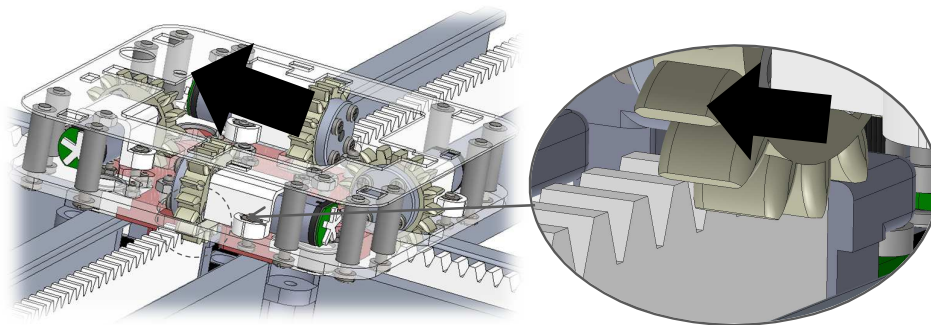


Figure 2-53 – Detail view of the side gears engaging the perpendicular rails during junction crossing. The big arrows shows the direction of the mobile agent movement.

2.4.2 Control, communication and localization mechanisms

There are several different solutions for the navigation and localization of mobile agents. Wire following was used by the first AGV, by Barrett Electronics of Northbrook, Illinois, in the 1950s [89]. The principle behind it is a wire placed in the ground which transmits a radio signal. This signal is detected by the sensors on the AGV and is used to steer the vehicle.

Today, most automated vehicles are laser navigated. Reflective tape is distributed throughout the AGV environment. The AGV carries a laser transmitter and receiver on a rotating turret. Then it determines its position by measuring the angle and distance to any reflectors that are in its line of sight, and comparing this information to the map of the reflector layout stored in its memory.

Guide tape, whether magnetic or coloured, is another solution. The AGV is fitted with the appropriate guide sensor to follow the path of the tape. One major advantage of tape over wired guidance is that it can be easily removed and relocated if the course needs to change. It is also a passive and unpowered solution.

Inertial navigation is based on the inputs from an inertial measurement unit, mounted in the AGV. This unit possesses a combination of accelerometers and gyroscopes, capable of measuring and report a body's specific force and angular rate, thus detecting the slightest change in the direction of the vehicle and acting in order to keep the AGV on its path, with a margin of error of a few millimetres [77][78]. Inertial navigation can also include the use of magnets embedded in the floor of the facility that the vehicle can read and follow [90].

Natural targeting navigation and geo-guidance have the advantage of not requiring retrofitting of the workspace. Typical systems employ range-finding sensors or cameras to record features along a route and use these features as references for their navigation. Using these fixed references, they can position themselves, in real time and determine their shortest route. The advantage of such systems is that they are highly flexible for on-demand delivery to any location. They can handle failure without bringing down the entire manufacturing operation, since AGVs can plan paths around the failed device. They are also quick to install, with less down-time for the factory [75].

In the SCALA system, the positioning precision is critical both for visual applications, such as 3D reconstruction, and also for fine manipulation tasks. Given the fact that the agents' movement is restricted by the rails, one can embed the localization system in the rail. The movement along the rail is one dimensional, so localization in the rail can be achieved with a low cost magnetic strip and linear encoder solution. By establishment of selective cuts on the magnetic strips, the localization of agents is reset, in order to compensate possible incremental errors. These cuts can also be used as a means to identify the rail in which the robot is moving. This is then communicated via wireless (radio, Wi-Fi or Bluetooth) to the central control station, which possesses a pre-loaded map of the structure, and is capable of knowing in real time the exact position and task of each mobile agent in the rail mesh.

In return, the central control sends commands, tasks, or trajectories to the robots. For task allocation and path planning, as shown in Figure 2-54, cost functions are considered, taking into account task priority, disturbance to other agents, concurrent movement of multiple collaborative agents, task execution time or minimum junction passages.

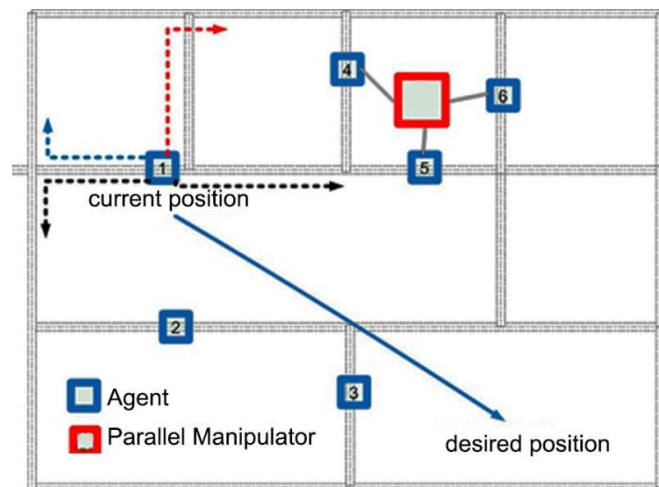


Figure 2-54 - Path planning of SCALA agents on an arbitrary 3D scaffold.

This central control station is also programmed to work automatically, requiring no human intervention or supervision.

Power solutions to the agents include rails with embedded power lines or on-board batteries and charging stations. The first solution has been widely used in rail based automation systems. Cooper tracks and brushes can be used to feed power to the agents. This solution has the advantage of enabling uninterrupted work, as the agents do not need to stop to re-charge their batteries, as in the second solution. From the maintenance point of view, it is also preferable, as it is cheaper to replace damaged brushes than degraded batteries.

2.5 System Benchmarks and Comparison

Having clearly defined not only the system requirements but also its detail design, one can break SCALA in its main components, as shown in Figure 2-55.

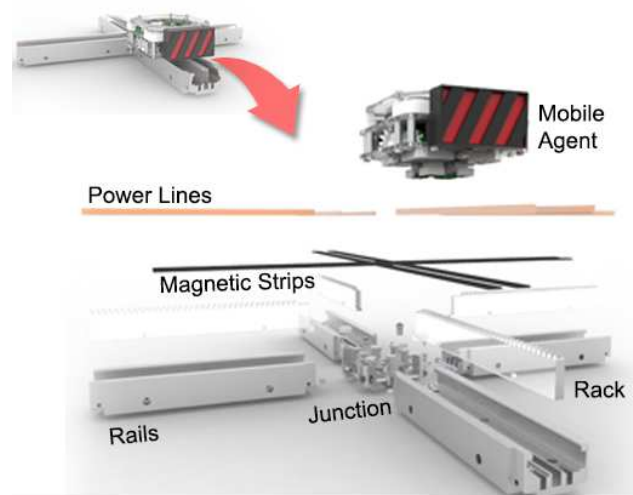


Figure 2-55 - SCALA system breakdown.

These constitute the basis for the SCALA implementation. Taking advantage of the high mobility degree of its agents and the fact that the scaffold can be mounted in any orientation, one can use the rails for both shelves and ceiling, using mobile agents on the shelves to pick up individual objects and ceiling agents to transport these objects inside the

warehouse. Surveillance agents can also be added to the system, to visually inspect the work-flow and quickly detect any problem or malfunction (Figure 2-56).

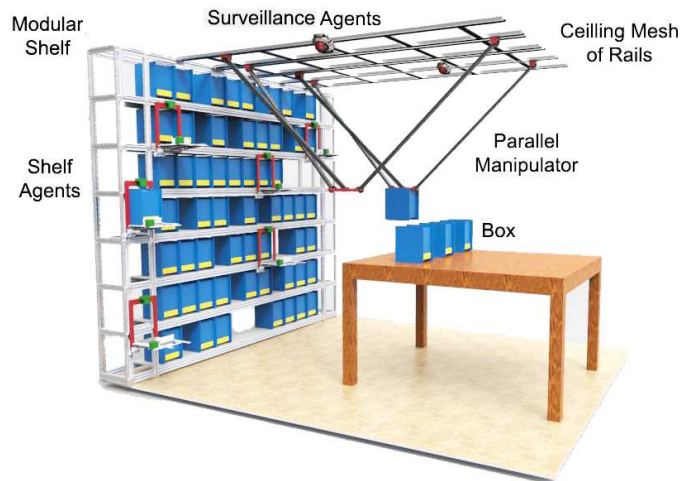


Figure 2-56 - Detail of the SCALA warehouse automation system.

The parallel manipulator is also a crucial component of the system, by enabling access to the 3D workspace. This parallel manipulator also has the advantage of being able to move from one workblock to another and to change its configuration. By changing the working rail of the agents, a new manipulator is formed which is advantageous in terms of workspace. Most of the components of the parallel manipulator are modular, including connection points to agents, tools, links and joints. Different tools can be installed on the manipulators and furthermore, by changing the length of the parallelogram, different workspaces for the manipulators can be achieved. By fitting the end-effector with a laser cutter or a filament extruder, one can transform the platform in a large scale 3D digital fabrication system, where multiple agents can work simultaneously on the same job and with different materials (Figure 2-57).

This will be, to the best of the author's knowledge, the first time that a complex fabrication like this will be carried out by an overhanging fully autonomous system.

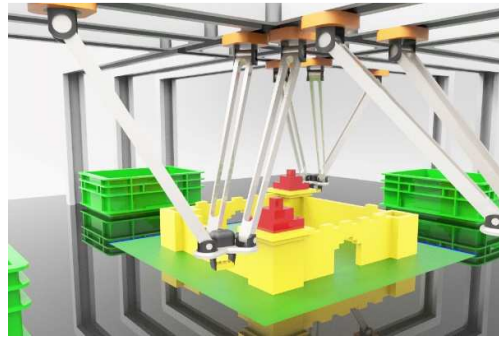


Figure 2-57 - SCALA as a 3D digital fabrication system.

The Table I summarizes a direct comparison between the state-of-the-art systems and the SCALA Railbot II concept.

Table I - Comparison between state-of-the-art systems and SCALA Railbot II concept.

System	Drive Motors	Sensors	Scaffold	Locomotion	Localization System
Hangbot [33]	4	3 potentiometers 3 linear encoders	Perforated steel plate	Step-by-step	Linear encoders
KIVA [24][91]	2	8 IR sensors 1 pressure sensor QR reading sensors	Ground	Continuous	2D QR/Datamatrix codes on floor
Lucas R. S. [92][51]	NA	NA	3D actuated rail mesh	Discontinuous	NA
Perfect Pick [52][53]	1	1 hall sensor	2D actuated rail mesh	Continuous	Hall sensor on drive motor
Autostore [93][54]	10	8 encoders	2D passive rail mesh	Discontinuous	Rotary encoders on wheels
SCALA Trainbot	6	4 potentiometers 2 linear encoders	3D passive rail mesh	Discontinuous	Linear encoders
SCALA Cambot	4	4 potentiometers 2 linear encoders	3D passive rail mesh	Continuous	Linear encoders
SCALA Railbot I	3	1 shaft encoder 4 linear encoders	2D passive rail mesh	Discontinuous	Linear encoders
SCALA Railbot II	4	4 linear encoders	2D passive rail mesh	Continuous	Linear encoders

Hangbot represents the advantages and disadvantages of docking mobile robots. While it can achieve high localization precision, through the use of encoders combined with a preloaded mapping of all docking points with their exact coordinates, its docking process is slow and thus not suitable for an industrial use.

KIVA system utilizes many solutions often employed by ground AGV based automation systems[24][91]. KIVA agents drive system is one of the simplest. It uses six wheels and differential drive. The two motors in KIVA robot drive two wheels, while the remaining four wheels are passive caster wheels. Each motor boasts about $3Nm$ of torque and stall power of almost $1kW$. The motors are coupled to a gearbox which performs a 25:1 reduction. While no max speed or acceleration figures could be found, they most certainly are limited to a safe range, as these robots share their workspace with human workers. Precisely for safety concerns, they are fitted with 8 infrared (IR) sensors for obstacle detection and 1 pressure sensor for collision detection. These numerous sensors increase the complexity level and price of each agent. Quick Response (QR) codes embedded on the floor (black markings visible on the floor in Figure 2-4) are used for localization of each agent. Localization mechanisms based on vision or QR codes are reported to have an accuracy in the order of 1 to $2cm$ [31][32], thus not suitable for high precision tasks. In addition, they do not possess any means to access 3D space, through a robotic arm, for example.

The advantage of systems moving on scaffolds is that they can reach high speeds and accelerations, as they do not share their workspace with humans. Lucas Robotic System drive solution is rack and pinion. No information on the number of drive motors, nor the self-localization solution employed, could be found. Still, their actuated rail positioning precision is said to be in the order of $0.05mm$ [92]. These motorized rail modules exhibit both translational and rotational degrees of freedom, to allow changing the rails or the direction of the agents' movement, as depicted in Figure 2-17. In fact, this is their biggest disadvantage, in relation to systems based on a passive rail mesh. The high automation level of their scaffold increases not only the complexity but also the cost of the system.

Perfect Pick shares this same limitation [52][53]. While the drive system requires only one motor to drive four wheels, each junction in the rail mesh possesses solenoids with a linearly displaceable piston to change the tracks configuration at junctions and select the agents moving direction in the grid. While the scaffold automation level is inferior to the one employed by Lucas, it is still not optimal in terms of cost and simplicity. The workspace is also discrete, as the robots work position is in the middle of each grid cell and there is no arm to enable access to positions between the cells.

Autostore [93][54] relies on cars with four wheels for each moving direction. When the car is on a grid cell, it can switch moving direction by raising a set of four wheels and lowering the perpendicular four wheel set. While as few as four motors can be employed for this [93], by using pulleys and belts, the current system needs up to ten motors for locomotion, as it uses a motor per wheel plus two motors for the raising mechanism. It also shares the same limitation of the Perfect Pick system, regarding the access to positions in between cells and the consequent discrete workspace. Localization system is similar to the one on Perfect Pick. It is, however, based on a large and redundant number of sensors. One can assume this is due to the possibility of wheel slippage, which does not happen in the Perfect Pick system, as its drive system is based on gears and racks. Nevertheless, localization methods based on rotary encoder readings, which are coupled to either the wheels or drive motors of a robot, are known to be inaccurate, even after filtering, with localization estimate errors in the order of *1 percent* [76].

Regarding the developed solutions for SCALA, even though all strategies tested fulfilled the main design objectives set (A1-4), one of the approaches stands out as the preferable, regarding the optimization objectives set (B1-4). Considering the concepts for 3D scaffolds, Cambot is preferable to the Trainbot not only due to having less motors, but also because its movement was continuous, even when passing the *L type junctions*, whereas the Trainbot needed to perform a complex multi-step operation, described and illustrated in Figure 2-39. However, the concept of agents moving on 3D scaffolds proved to involve complex mobile agent designs and mechanisms, as well as multiple sensors and motors for the control of the agents' behavior and locomotion, thus going against the

pursuit for simple mobile agents (optimization objectives B1). The 3D scaffold also required one more junction type (L) than the 2D, thus making it more expensive (optimization objectives B2). In terms of scalability (optimization objectives B4), the 2D scaffold is easier and cheaper to scale since it has less dimensions than the 3D scaffold. In fact, due to these problems, and since mobile agents will always require an arm or parallel manipulator to reach the 3D space, both for bi and tri-dimensional scaffolds, the 2D scaffold approach is the most promising solution for the SCALA. For this approach, Railbot II is also preferable to Railbot I, in the sense that its movement is continuous at the junction, thus being this the base concept for future developments and implementation. Regarding localization precision, the mechanism employed by the SCALA prototypes is based on a magnetic strip embedded on the rails, and magnetic encoders on the agents. This system typically provides accuracy in the range of tenths of a millimeter, depending on the encoder and magnetic strip employed. Still, the SCALA mechanical realization will determine the system final accuracy, due to drive system backlash or tolerances on the slider/rail fitting, which bear a negative impact on the precision. Dynamic properties of the SCALA prototypes are also highly dependent on the motor, gearbox and wheel specifications.

2.6 Summary

In this chapter, the SCALA concept as a flexible system for automation, digital fabrication and vision applications, was presented. The most relevant state-of-the-art systems were analyzed in detail, and their limitations were exposed. Then, the several concepts for SCALA design were studied and some early stage prototypes were presented. This study constituted the development basis for each element of SCALA, which will be the subject of the next chapters.

To the best of the author knowledge, SCALA is the first system in the world that offers the possibility of simultaneous and independent movement of several agents on 2D scaffolds, 2D mobility over a large space and climbing ability on rails which can be installed at arbitrary angles, with a non-actuated junction system, and agents with

continuous motion (in contrary to slower docking systems). Table II presents an early comparison of SCALA and the presented state-of-the-art systems.

Table II – Comparison between different types of indoor mobile robots.

Mobile Robots	Agent Cost	3D Space Reach	Localization Precision	Safety	Energy Autonomy	Low Initial Investment
Ground	★	★	★	★	★★	★
Walls & Ceiling	★★	★★	★★	★★	★★	★★
Rails	★★	★	★★★	★★★	★★★	★★★
Air Drones	★★	★★★	★	★	★	★★★
SCALA	★★	★★★	★★★	★★★	★★★	★★★

Ratings: ★ Not Satisfactory, ★★ Moderately Satisfactory, ★★★ Very Satisfactory

SCALA fills the gap between these existing systems. By relying on multiple mobile agents, moving on special designed scaffolds with integrated power lines and localization sensors, which can be placed vertically on walls or hanging out of the ceiling, SCALA enables access to 3D spaces with safety, repeatability, accuracy and better energy autonomy. Thanks to its modular design, one can shape the scaffold according to each individual application. Given that all modular components of the scaffold are passive and do not require actuators, data transmission and energy supply, one can assemble a system with a reduced initial investment.

Several applications for this platform, in the fields of automation, pick and place, digital fabrication, surveillance and 3D reconstruction, are proposed. Other applications can also take advantage of this multi-purpose system. In the field of computer vision, this system has advantages over fixed camera systems since it allows to cover a vast space with a reduced number of sensors. It can also overcome problems such as target occlusion, dead angles or large camera/target distances. Regarding the proposed mobile camera systems, this offers more freedom and flexibility by allowing 2D movement on the walls and ceiling. This developed platform can be considered as a new framework in robotics, which can benefit different fields of automation and robotics such as digital fabrication, 3D reconstruction, surveillance, service robotics, among others.

Chapter 3

Novel Reconfigurable Parallel Manipulator

This chapter is dedicated to the development of the SCALA reconfigurable parallel manipulator. While SCALA multi-agent system allows navigation on a bi-dimensional space, by using a parallel manipulator driven simultaneously by three mobile agents, one can extend the SCALA workspace to three dimensions, thus enabling manipulation and digital fabrication tasks. Such tasks require accuracy, repeatability, high operating speeds, and accelerations. In the last decades, researchers and engineers have studied extensively machines for component handling and assembly, based on parallel kinematic structures, on account of their high speed and stiffness and low inertia and positioning errors. However, these machines also suffer from a few drawbacks, including kinematic complexity, the existence of singularities, anisotropic behavior or low workspace to installation space ratio. For this reason, it is important to perform a rigorous study of all their particular aspects prior to developing the final solution for the SCALA system.

The first section of this chapter is dedicated to parallel kinematic machines, and their characteristics as well as their state-of-the-art. After this, reconfigurable parallel machines are introduced. Then, the whole cycle of SCALA reconfigurable parallel manipulator development is detailed, including the choice of architecture, kinematic, dynamic and workspace analysis. The last section introduces a proposed PKM design methodology based on multi property analysis and workspace determination. This chapter

is an extended version of two published articles[94], [95], and provides progress over state-of-the-art in two domains:

1. A novel grid-based reconfigurable spatial parallel mechanism with large workspace;
2. Performance analysis and design of parallel kinematic machines using interval analysis.

3.1 Introduction to Parallel Machines

Manipulators are mechanisms which are able to control the pose of an end-effector or tool, including position and orientation DOF. All manipulators contain a base and an end-effector, and then several links and joints connecting both. The traditional types of joints are rotational joint (R), prismatic joint (P), spherical joint (S), cylinder joint (C), helix joint (H), and universal joint (U)², as shown in Figure 3-1.

The number and type of links and joints, and the way they are installed in the manipulator, is what defines its mobility and is referred to as the manipulator architecture. The simplest manipulator architecture is made up of three mutually perpendicular

² **Rotational joints** have one DOF and are used to describe rotational movements (with 1 DOF) between objects. Their configuration is defined by one value which represents the amount of rotation about the *rotation axis*.

Prismatic joints have one DOF and are used to describe translational movements between objects. Their configuration is defined by one value that represents the amount of translation along the *translation axis*.

Spherical joints have three DOF and are used to describe rotational movements (with 3 DOF) between objects. Their configuration is defined by three values which represent the amount of rotation around the *x*, *y* and *z axes*. The three values that define a spherical joint's configuration are specified as *Euler angles*.

Cylinder joints have two DOF, being a combination of one translation and one rotational movement about the same translational axis. Their configuration is defined by one value that represents the amount of rotation and another value which represents the amount of translation, along the same axis.

Helix joints can be seen as a combination of revolute joints and prismatic joints (with linked values). They have one DOF and are used to describe a movement similar to a screw. Their configuration is defined by a single value, that represents the amount of rotation about its *rotation/translation axis*, and a pitch parameter which relates this amount of rotation to a linear displacement.

Universal joints have two DOF and are a combination of two revolute joints whose axis are perpendicular to each other. Their configuration is defined by two values that represent the amount of rotation around their *reference axes*.

prismatic joints, as shown in Figure 3-2. This type of architecture is called Cartesian. Cartesian robots move their tool on the three Cartesian coordinates associated with their three prismatic joints. Their kinematics and workspace are very easy to describe. This architecture is used for robots mounted on rails above their workspace, also called gantry robots[96], in construction sites or for small scale applications, such as 3D printers.

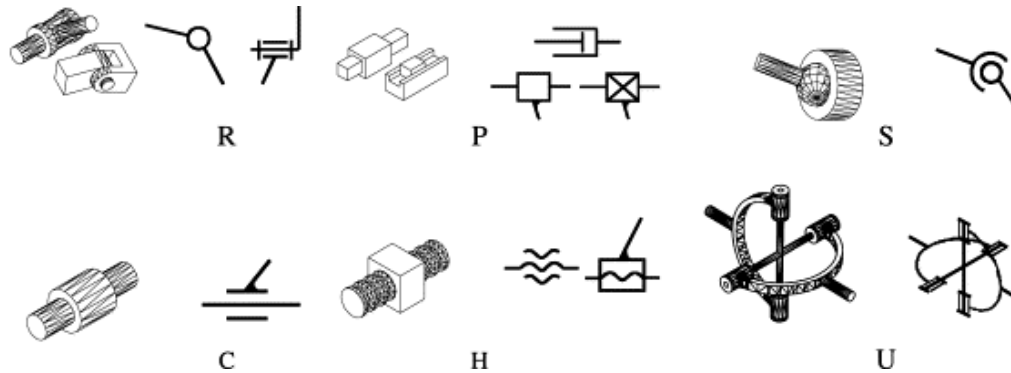


Figure 3-1 - Traditional types of joints[97].

However, this architecture can only allow the control of the 3 translations of the end-effector, whereas serial and parallel architectures can offer up to 6DOF manipulability.

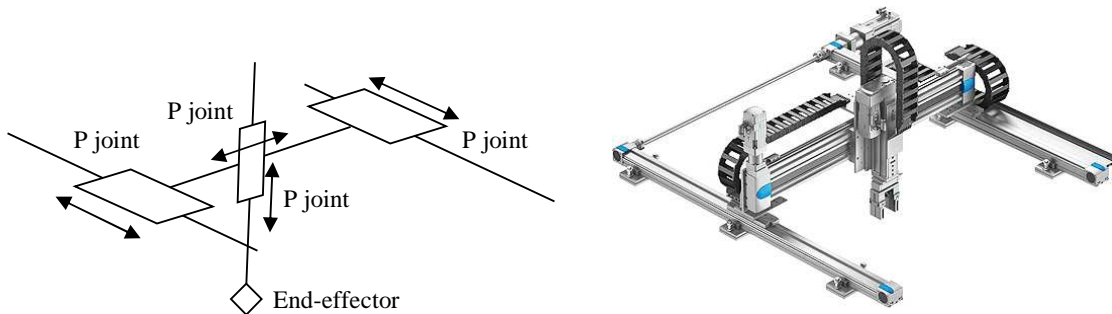


Figure 3-2 – Cartesian robot architecture. On the right, a gantry manipulator from Festo[98].

To understand the characteristics and distinguish between each one of these architectures, the notion of connection degree will be introduced [99].

For each link of a manipulator, the connection degree is the number of rigid bodies attached to this link by a joint. On simple kinematic chains, the connection degree of all members is always less or equal to 2. Serial manipulators fall in this category, as all their components possess a connection degree equal to 2, except for two of them, the base and

the end-effector, with connection degree 1. Such a chain is also called an open-loop kinematic chain, and is exemplified in Figure 3-3. A closed-loop kinematic chain is characterized by having at least one of its members, but not the base, with a connection degree greater than or equal to 3. This is the case of parallel machines, as shown in Figure 3-3. A generalized parallel manipulator can then be defined as a closed-loop kinematic chain mechanism whose end-effector is linked to the base by several independent kinematic chains.

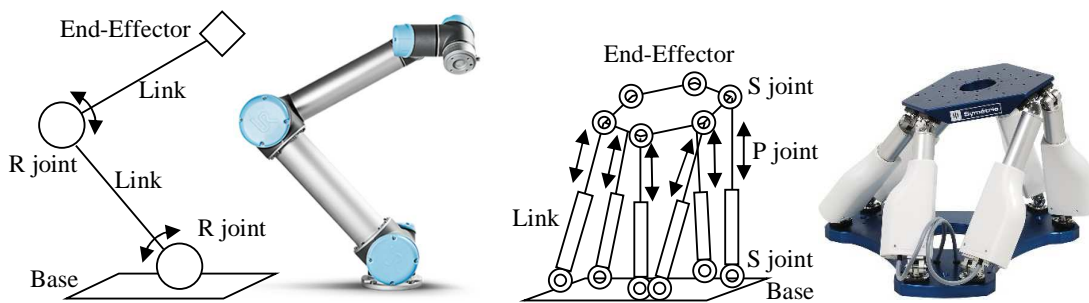


Figure 3-3 - Serial architecture and the UR5 robot arm from Universal Robots[100], on the left. Parallel architecture and the hexapod BREVA from Symétrie[101], on the right.

For almost four centuries, closed-loop kinematic chain structures have drawn the interest of mathematicians as they offered interesting problems. *Christopher Wren*, in 1645 mentioned some theoretical problems linked to this type of structures. Then *Cauchy* in 1813 [102] and *Bricard* in 1897 [103]. However, at that time, the technology was not able to deal with any practical applications of this type of structures. The very first application arrived 60 years later and was proposed by *Gough* for a tire test machine [104][105], although parallel structures were really put in practice in the 1970's for a flight simulator with the patent of *Cappel* in 1964 [106] and the seminal paper of *Stewart* [107]. The first robotics applications were proposed in the early 1980's [108],[109],[110]. Since then many different types of designs, configurations and prototypes for parallel kinematic structures have been proposed [111], [112]. Recently, there has been a growing tendency to focus on parallel manipulators with 3-translational degrees of freedom (DOF) [113]–[121]. In this case, the end-effector can only translate, along the three Cartesian axes X-Y-Z, with respect to the base, exhibiting a spatial movement. The Delta robot, designed in 80's by *Prof. Raymond Clavel* from EPFL – École Polytechnique Fédérale de Lausanne, is one of

the most famous translational parallel manipulators [122]–[124]. Parallel manipulators are widely used in industry, as they offer great dynamic properties, including high accuracy, stiffness and velocity. However, their workspace to installation space ratio is small when compared with serial manipulators. The next section will focus on explaining the differences between the two architectures.

3.1.1 Comparison between serial and parallel robots

Serial manipulators or serial articulated robotic arms are constituted by a succession of rigid bodies, each of them being linked to its predecessor and its successor by a one-degree-of-freedom joint. This means that their reach and dexterity is usually very high, resulting in large workspace to installation space ratios. However, that also means that each link must not only support the load being manipulated, but also the weight of all segments following it. This means that the links in the beginning of the serial chain (closer to the base), are subject to large flexure torques. To counteract this effect, such links are stiffened, which in turn makes them heavier and bulkier. A low transportable load to mass ratio is, thus, inherent in the serial mechanical architecture of existing manipulators. Another consequence of serial arrangement of the limbs is the low positioning accuracy. In fact, links magnify errors in a way that a small measurement error in the internal sensors of the first one or two joints will quickly lead to a large error in the position of the end-effector. Consider, for example, for a one meter long link, a revolute joint measurement error of *0.1 degrees* leads to an error of almost *2mm* in the position of the link end. If more links are added after this, their error will be magnified. The presence of a drive with a reduction gear also induces a backlash which leads to inaccuracy. In addition, flexural deformations, which are not measured by the robot internal sensors, are also sources of positioning errors.

Larger elements and higher moved masses also increase the manipulator inertia, centrifugal and Coriolis forces, during high velocity operations, making the control of the robot complex. Inertia and friction forces act on different scales, and this effect is especially critical on serial robots: inertia forces essentially vary with the square of the lengths of the links, while friction forces are relatively unaffected by such dimensions.

This means that one cannot design a micro serial robot simply by scaling down a larger version; under such scaling, the inertia forces are reduced while the friction forces remain relatively unchanged[125].

On Table XXIV, available in Appendix C – Complementary Tables, some examples of industrial serial manipulators are presented, along with their characteristics according to the manufacturers notice. Notice that the repeatability of a manipulator represents the maximum distance between two positions of the end-effector reached for the same desired pose from different starting positions. It is one measure of the manipulator precision and accuracy. Notice also that for the base size, one considers the largest base dimension. Bases typically are either rectangular or circular shaped. Given that all robots here presented are of spherical type, meaning their serial chain contains only revolute joints, their work volume can be roughly represented by a sphere, with the radius equal to the robots' reach. Then, the workspace to installation space ratio (*WorkS/InstS*) approximate value presented in the table was determined as:

$$\frac{WorkS}{InstS} = \frac{\pi.Reach^2}{\pi.(Base_Size/2)^2} \quad (3-1)$$

This value is just indicative and for comparison purposes. One can see that serial robots show a low load to mass ratio, with the highest value being *0.185*. However, their average workspace to installation space ratio is very high. Still, the maximum velocities and accelerations achieved by their tool center point are relatively low. One concludes that serial robots are inappropriate for tasks requiring either the manipulation of heavy loads with good positioning accuracy at very high speeds or accelerations.

These tasks are, usually, more suited for manipulators based on parallel architectures. Because the external load can be shared by the actuators, parallel manipulators tend to have a large load-carrying capacity. Contrary to serial robots, where the maximum force is limited by the minimum actuator force, for parallel manipulators, the forces of several actuators are combined to increase the force capacity of the manipulator. The use of base-mounted actuators and low-mass links results in very low inertia and

moved masses, allowing their end-effector to achieve accelerations of up to $15G$ in industrial applications[22]. The highly coupled movement of the closed-chain structure induces an averaging effect on the position error of the end-effector on parallel machines. Since several independent kinematic chains, each one with its individual positioning error, are linked together, the final error will be, approximately, an average of all errors[126]. Stiffness is also superior to the one of serial robots, thanks to the closed-chain structure of limbs.

The parallel manipulators main drawback is the fact that they have small workspaces to installation space ratios, when compared to serial robots. There are, however, several strategies which can and will be used by the SCALA parallel manipulator to improve such ratio, and whose analysis will be the subject of the following sections.

On Table XXV, available in Appendix C – Complementary Tables, some examples of industrial parallel manipulators are presented, along with their characteristics according to the manufacturers notice. The first five examples are Delta type manipulators, while the last five are hexapods. The reach, base size and workspace to installation space ratio ($WorkS/InstS$) hold the same meaning as previously for the serial robots.

Immediately, one can see that parallel manipulator performances vary significantly according to parallel architecture chosen. Delta type manipulators exhibit very high speeds, but low load to mass ratios. On the other hand, hexapods can move, with very high precision, loads two times bigger than their own mass, but at significantly lower velocity. However, all parallel manipulators have in common the high precision and low workspace to installation space ratio. Parallel machines are then most suitable for small scale, fast and high precision tasks, or very high precision positioning of large loads.

This section's conclusions are summarized in Table III. Some other criteria can be used to compare both architectures, but still the presented criteria perfectly serve the purpose of justifying the use of a parallel architecture for the SCALA manipulator. For a more in-depth analysis and comparison between serial and parallel robots, the following works are suggested [127][126].

Table III - Feature comparison of serial and parallel robots[126].

Feature	Serial Robot	Parallel Robot
Workspace	Large	Small and Complex
Position Error	Accumulates	Averages
Accuracy and Repeatability	Low	High
Maximum force	Limited by minimum actuator force	Combination of all actuator forces
Stiffness	Low	High
Dynamics characteristics	Poor	High
Inertia	High	Low
Payload/weight ratio	Low	High*
Velocities and Accelerations	Low	High*
Workspace/Installation-space ratio	High	Low

**depends on the architecture type*

3.2 State-of-the-art on Reconfigurable Manipulators

Researchers and engineers have studied extensively machines for handling and assembly based on parallel kinematic machines (PKM), on account of their promising potential for highly dynamic movement and low inertia and positioning errors, as seen and discussed in the previous section. However, the main drawbacks of parallel structures are their small workspace to installation-space ratio, and also the existence of singularities in their workspace. This drove the scientists to pursue strategies which allow to extend the workspace of parallel machines.

For special structures with linear drives and a parallel arrangement of the drives' axes, one can extend the workspace in the direction of the drives' axes by increasing the positioning range of the drives. Several structures and prototypes using this build-up have been described, e.g. the Linear Delta [128], Triglide [129], Linapod [130], Urane SX [131], or Gantry-Tau [132]. This layout allows for long drawn-out workspaces, by enabling the workspace extension in one direction. But it is only a small step towards a better workspace to installation-space ratio, since larger positioning ranges of the drives lead to

larger bases and thus to larger installation-spaces. Another approach to extending the range of the manipulator's drives, is to translate its base, as done by *Brogardh* [132]. In his work, driven carriages carry an entire manipulator over the workspace. Drawbacks to this approach are the higher moved masses and the fact that each end-effector can only reach the workspace of one assembly mode.

Reconfigurable robots were developed as a scalable and flexible solution for modern automation and fine manipulation systems [133], by gathering the advantages of several robotic architectures in a single system. They consist on structures capable of changing their configuration to better suit a specific task [134]. Reconfiguration can happen statically or dynamically[135]. Static reconfiguration requires physical intervention from the user, to add or remove links or connecting elements to the structure. Examples include the PARTNER multi-DOF robotic manipulator [136] or the RPPM planar parallel manipulator [137]. In both examples, the parallel robots are made with several identical links which can be added or removed to the structure to change its characteristics. In the works of Plitea, a 6 DOF reconfigurable parallel manipulator [138][139] is designed so the user can suppress one or more DOF by manually attaching connecting elements on the structure's links. Dynamic reconfiguration can happen online and is certainly the most flexible of the two solutions. Several mechanisms are employed for this purpose. The 6-DOF reconfigurable hybrid parallel manipulator by *Coppola et al.* [140] uses variable length joints on its base for its reconfiguration. A similar system is employed by *Zhang and Bi* on its Reconfigurable 5-axis Parallel Kinematic Machine [133], where the angle of the prismatic joints on the manipulator base can be changed to allow its reconfiguration. Adaptive joints that can block one DOF in operation are also used in the works of *Grosh et al.* and *Palpacelli et al.* [141][142]. The first used a universal joint where one DOF could be dynamically suppressed, while the later used a spherical joint, capable of blocking alternately one of two suppressible DOF, thus transforming it in a variable configuration universal joint. An electromagnetic brake clutch was used by *Chablat et al.* in the NaVARo manipulator [143] to allow it to switch between eight assembly modes.

Reconfiguration serves many purposes. Whether it is to enlarge their workspace [136],[133], change its dynamic properties [137],[140],[144], its degrees of freedom [138],

[139],[145],[146] or to avoid singular poses [147], reconfiguration has proven to be a solid strategy used for flexible production machines.

In this thesis work, reconfiguration is used primarily to extend the manipulator workspace. For a planar structure such an implementation has been described in [148], showing that the approach to use the workspaces of several assembly modes can be successfully used to gain a larger overall workspace. For spatial movements several structures are proposed in [132], allowing the use of different workspaces, which are either of unequal size or feature a different platform orientation. Budde recently proposed a Triglide spatial manipulator capable of changing its assembly mode, making use of two symmetrical workspaces without a change in platform orientation. This reconfigurable manipulator achieved a workspace volume to installation-volume ratio of 0.96 [149]. Still there are some limitations regarding this design, such as the workspace shape and orientation (essentially longitudinal), only two configuration modes and the impossibility of having more than one manipulator working in the structure at a given time.

3.3 SCALA Reconfigurable Manipulator

The solution proposed in this thesis, for the SCALA manipulator, is in the form of a reconfigurable grid-based planar parallel manipulator, which increases its workspace using three strategies including drive range extension, base translation and dynamic joint reconfiguration. This novel concept relies on the premise that the parallel manipulator is driven by 3 SCALA agents, simultaneously, as shown in Figure 3-4.

The mobile agents move on a bi-dimensional mesh of rails. They can transport rapidly the parallel platform all over the workspace and then stay in one of the blocks to do fine manipulation. The agents can also move from one rail to another, thus changing the shape of the manipulator and forming a new configuration, referred in this thesis as Assembly Mode (AM). This high degree of mobility can also be used to allow simultaneous functioning of several agents and manipulators in the same structure, which is highly desirable in large warehouses or industrial environments. This new concept of a

mobile reconfigurable parallel manipulator possesses the following advantages relative to other existing solutions:

- Fine manipulation over a large workspace;
- Possibility of shaping the manipulator's workspace to desired standards by changing the arrangement of the modular network of rails;
- Dynamic reconfiguration to, at least, 4 different assembly modes and several variations of these assembly modes;
- Structure reconfiguration without changing the number of DOF;
- Possibility of having several units working simultaneously on the same installation space;

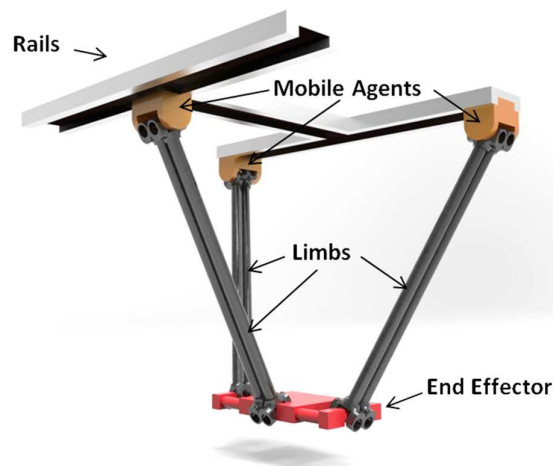


Figure 3-4 - Parallel manipulator driven by 3 mobile agents on a rail grid.

To the author's knowledge, this is the first concept to combine all these advantages and all three workspace enlargement strategies in a single system. The manipulator's tool may be fitted with a printing nozzle for additive manufacturing, a simple grasping unit for material handling or a laser for laser cutting/engraving tasks. While additive manufacturing requires a full 3D workspace, pick and place or laser cutting tasks do not require a large vertical extension of the work volume, nor a regular shape of this volume. In turn, they privilege a large planar workspace and small vertical displacements of the tool. For this

reason, in this thesis work, focus will be given on the extension of a planar workspace, parallel to the base of the manipulator.

In the following sections, the entire process of the concept development, from the choice of parallel architecture to kinematic analysis is discussed. Then, for validation purposes, a case study PKM is considered and an algorithm based on interval arithmetic is used to obtain the certified robot workspace given the actuator limits and singularity constraints, for its several assembly modes.

3.3.1 Parallel architecture

Limb Structure

To determine the most suitable PKM architecture, the following requirements were considered:

- Spatial movement (3 DOF for translations and 0 DOF for rotations);
- As simple and lightweight as possible, with the least number of DOF and joints;

By using only the traditional joints, it becomes difficult to design parallel robotic mechanisms with specific DOF's. The reason for this is that it is hard to obtain the limbs with specific DOF and to determine the kinematic characteristics of their end-effectors because of the coupled motions. *Feng Gao et al.* [97] made a comprehensive study of the several types of composite joints, which are very useful for designing parallel robotic mechanisms. Among the new types of composite joints are the pure translation universal joint (U^*) and the translation and rotation universal joint (\hat{U} or U^\wedge), which are shown in Figure 3-5.

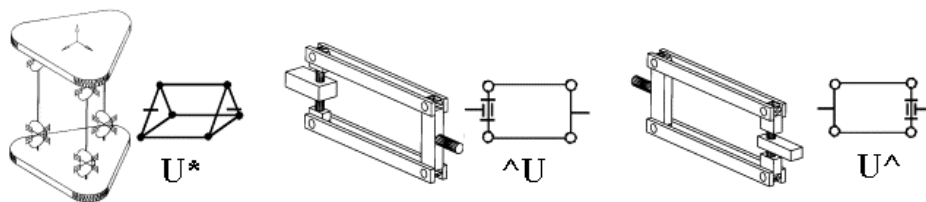


Figure 3-5 - New composite joints proposed by *Feng Gao et al.*[97].

Then they elaborated a table for classification of parallel robot mechanisms which is partly reproduced in Table XXVI, available in Appendix C – Complementary Tables, along with our measure of the complexity level of the mechanisms in the form of total number of joints and links of the PKM.

To select the ideal architecture for the PKM from the available options, solutions with more than 4DOF per limb are excluded, since this means either a large number of joints, or joints with a high number of DOF. Both present challenges in the mechanical realization of the robot, and because only one DOF per limb is actuated, all extra passive DOF are potential and uncontrollable sources of error. The actuated DOF is, necessarily, the first joint of each limb, since it is the one which links to the base of the manipulator. Since the mobile agents are translational and serve as actuators for the PKM, the only joints which can mimic this are the prismatic and cylinder joints. Configurations with more than 6 links are also excluded because of the high quantity of moving masses, which should always be minimized in mobile machines. After applying these criteria, the only options remaining are the 3-P[^]UR and 3-CU[^]. These two architectures are very similar. The difference is that for the P[^]UR limb, the rotational joint is independent from the first prismatic joint, whereas in the CU[^] limb they are combined to form the first cylindrical joint. This constitutes the limitation of the CU[^] limb. Because these limbs are attached to mobile agents moving on a 2D grid, they are required to perform equally in two perpendicular directions, where the only joint which is reconfigured is the first joint (P or C respectively). However, in the case of the CU[^] limb, it gains one DOF when the C joint is reconfigured to a new moving direction, as can be seen in Figure 3-6, resulting in a change in the manipulator's mobility. For this reason, the optimal joint pair is the P[^]UR.

Limb Arrangement and Manipulator Mobility

The choice of the joint configurations for the manipulator's limbs does not guarantee, *per se*, the desired final degrees of freedom for our end effector. For this, careful limb arrangement is necessary so that the several closed loops combined result in a manipulator with the desired spatial movement.

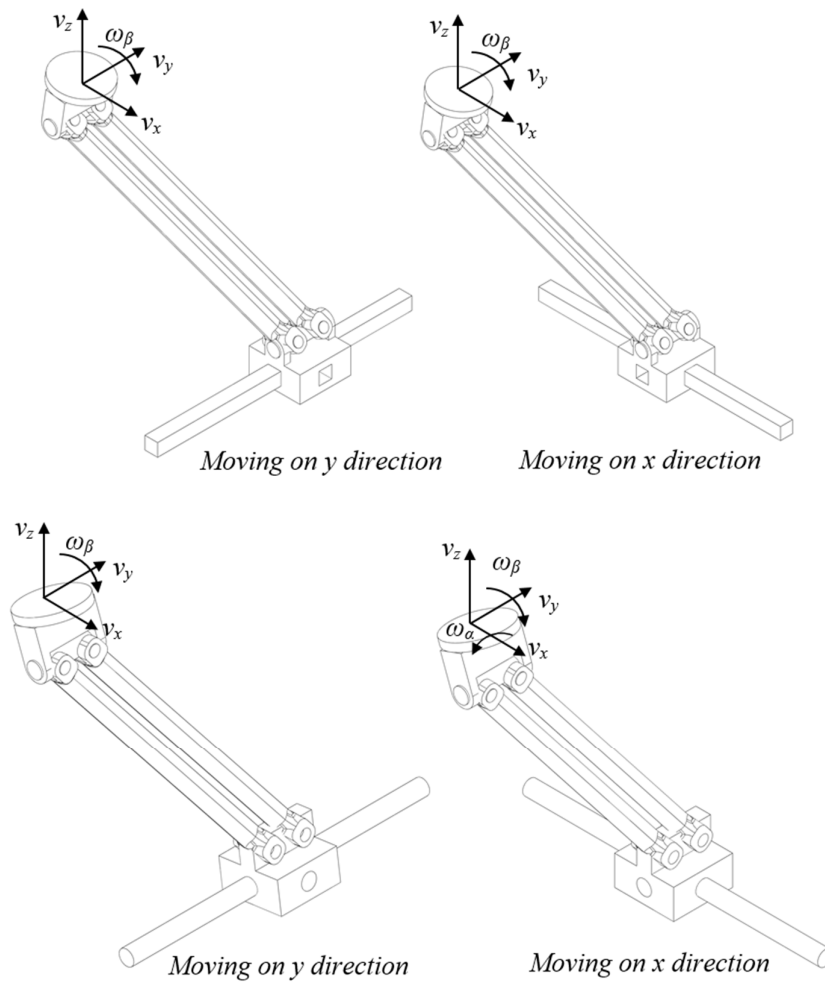


Figure 3-6 - Above, the P^{UR} limb maintains the same 4DOF whether it is moving on x or y direction. On the other hand, the C^U limb, shown below, gains 1 DOF when moving on the x direction. v represents the translations and ω are the rotations with respect to three Euler's angles³, α , β and γ .

In robotics, the most used formula for determining the mechanism's mobility M the (i.e., the total degrees of freedom which need to be controlled in the mechanism for every link to be in a specific position), with k number of joints, is given by the difference

³ The three Euler angles describe the orientation of a rigid body. In this work the adopted Euler angles are alpha, beta and gamma (or α , β and γ), used to describe a rotation composed by three elemental rotations:

$$Q = Rx(\alpha).Ry(\beta).Rz(\gamma)$$

Where Rx , Ry and Rz represent elemental rotations about axes x , y and z respectively, of the absolute reference frame.

between the number of independent motion parameters of the joints $\sum_{i=1}^k f_i$, before loop closures provide further constraints and the number of joint parameters that have lost their independence after loop closures r [150]:

$$M = \sum_{i=1}^k f_i - r \quad (3-2)$$

This formula is a variation of the one usually attributed to *Grübler* and *Kutzbach* and allows the basic calculation for a mechanism's mobility, often called its degrees of freedom [151], [152][153]. The manipulator kinematic structure and associated graph are shown in Figure 3-7.

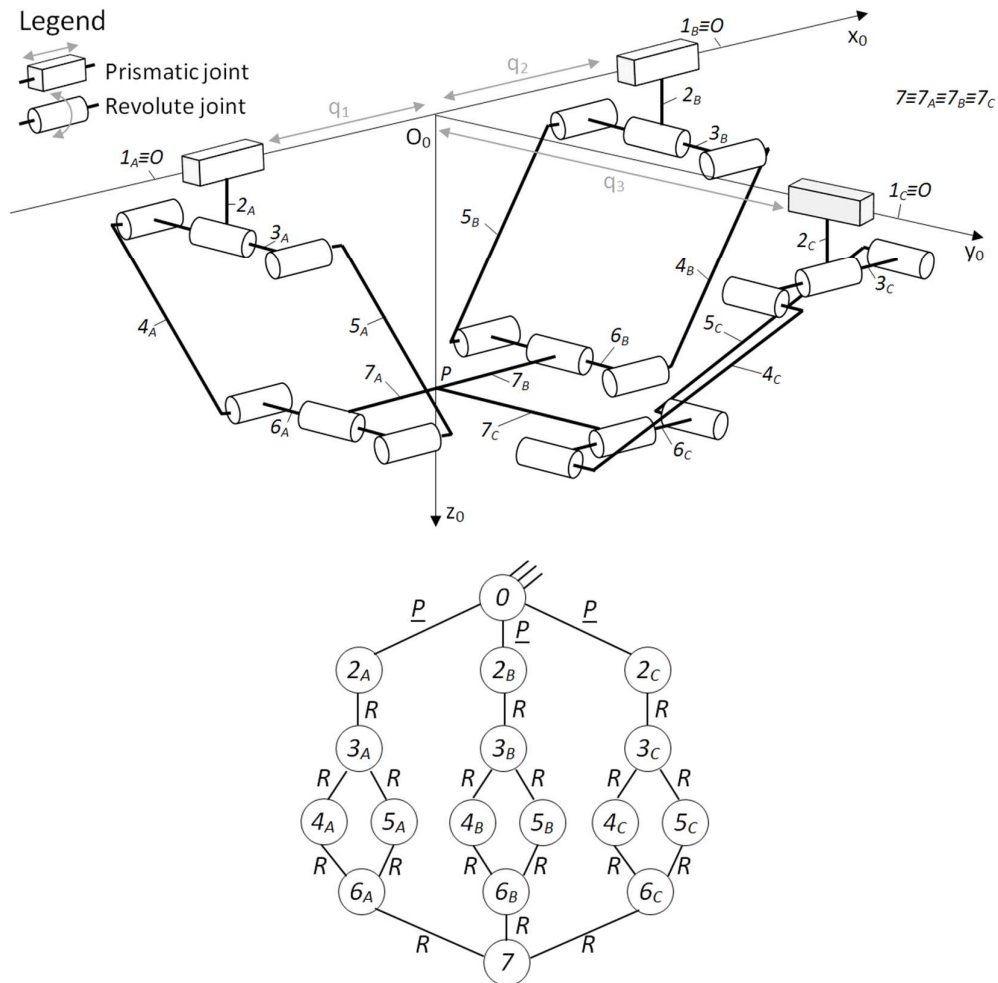


Figure 3-7 - PKM Kinematic structure and associated graph. For a clear representation, the third limb (c) is not shown anchored to the mobile platform center.

The operational space R_{Ei} for each complex leg E of the mechanism, given this arrangement, is: $R_{E1} = (v_x, v_y, v_z, \omega_\beta)$, $R_{E2} = (v_x, v_y, v_z, \omega_\beta)$ and $R_{E3} = (v_x, v_y, v_z, \omega_\alpha)$; where, v (v_x, v_y, v_z) and ω ($\omega_\alpha, \omega_\beta, \omega_\gamma$) express the translations and rotations with respect to three *Euler's angles* α, β and γ .

The spatiality of each limb (the number of independent finite displacements between the extreme elements) is $S_{Ei} = \dim(R_{Ei}) = 4$. The spatiality of the mobile platform in the parallel mechanism S_{PM} is given by:

$$S_{PM} = \dim(R_{E1} \cap R_{E2} \cap R_{E3}) = 3 \quad (3-3)$$

The same three relative independent velocities (v_x, v_y, v_z) exist between the mobile and reference platforms in the PKM. While the chosen P^{UR} limb possesses four degrees of freedom, being 3 translations and 1 rotation, the end-effector should only have spatial movement, meaning one should arrange the limbs in a way that the rotational DOF is suppressed. Placing one limb perpendicular to the other two is enough to change the Euler angle of its rotational DOF and when coupling the movement of all limbs, get the desired spatial movement. For instance, in the case of the Delta configuration, since the limbs have 5 DOF's each, it is necessary to suppress 2 rotational DOF, thus all limbs should have different Euler angles of rotation and the 120° arrangement is chosen.

The parallel mechanism has 18 revolute and 3 prismatic joints ($\sum_{i=1}^k f_i = 21$). Spatiality of the elementary open chain associated with each planar parallelogram closed loop is three, that is the three closed loops serially concatenated in the complex legs cancel the independence of $t_l = 3 \times 3 = 9$ joint variables. The total number of joint parameters that have lost their independence after loop closures r is given by:

$$r = \sum_{i=1}^3 S_{Ei} - S_{PM} + t_l = 4 + 4 + 4 - 3 + 9 = 18 \quad (3-4)$$

Thus, the mobility of the parallel robotic manipulator is $M = 21 - 18 = 3$. Three variables q_i of the prismatic joints connecting each leg to the base element are used to command the position of the mobile platform.

Assembly Modes

Since the PKM structure is reconfigurable, in a way that allows the re-arrangement of the mobile agents on different rails, it is possible to switch to different assembly modes. In Figure 3-8 it is shown the manipulator in a workspace, with the rails identified and assuming one of the possible assembly modes.

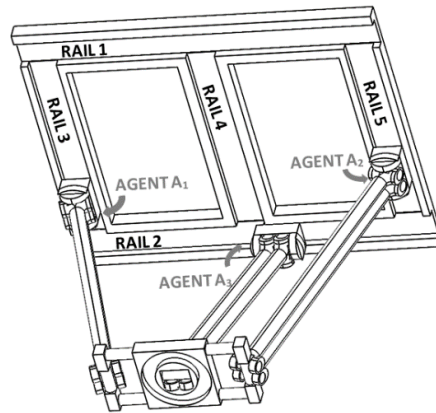


Figure 3-8 - 3 P^UR Manipulator architecture. Workspace block shown with the different rails and parallel manipulator's agents identified.

In this thesis work, two main AM's for manipulation and two for translations on the grid will be considered. In the manipulation AM's, agents A1 and A2 move in the same direction, while agent A3 moves in a perpendicular direction to these two.

In the translation AM's, all three agents move in the same direction. To help cover the full workspace block area, the two main AM's for manipulation can be reconfigured into several different configurations, as shown in Figure 3-9 and Table IV. Then, translation AM's can be used to move to other workspace blocks, thus achieving a large planar workspace. Some more variations can be made from AM1 and AM2. One can have AM1, where agents A1 and A2 move on different parallel rails, such as rail 1 and rail 2, respectively. One can also have AM2, where agents A1 and A2 move on the same rail, for instance rail 3. However, these variations are not optimal due to the link attachment point arrangement and orientation of the end-effector, resulting in residual workspaces with no practical use. For this reason, these AM variations were not included in this work.

Table IV – Possible variations of the two main assembly modes.

	Rail 1	Rail 2	Rail 3	Rail 4	Rail 5
Assembly Mode 1a	A ₁ , A ₂			A ₃	
Assembly Mode 1b		A ₁ , A ₂		A ₃	
Assembly Mode 2a	A ₃		A ₁		A ₂
Assembly Mode 2b	A ₃		A ₁	A ₂	
Assembly Mode 2c	A ₃			A ₁	A ₂
Assembly Mode 2d		A ₃	A ₁		A ₂
Assembly Mode 2e		A ₃	A ₁	A ₂	
Assembly Mode 2f		A ₃		A ₁	A ₂

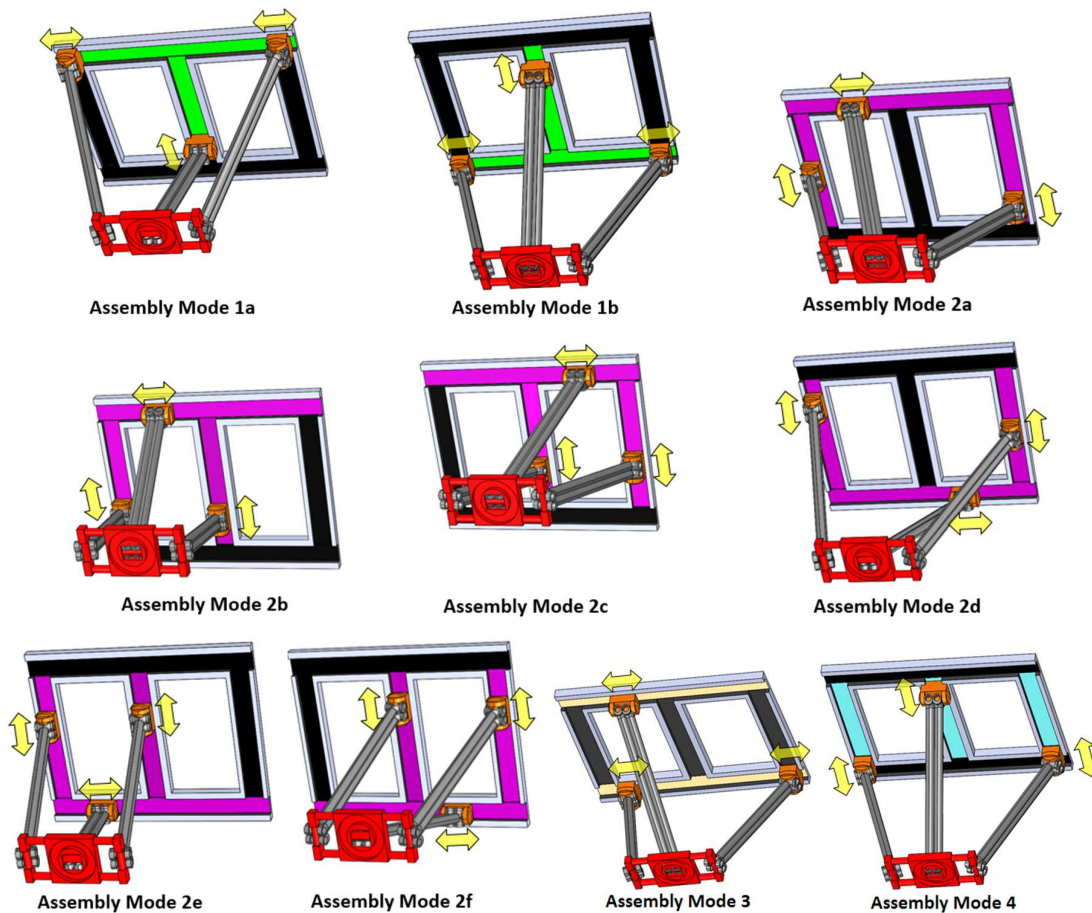


Figure 3-9 - Assembly modes 1 and 2 are for fine manipulation on a block, and possess several variations when the rails on which the agents move are switched. Assembly modes 3 and 4 allow the manipulator to move to other blocks in the rail grid.

Considering a mesh of rails with many adjacent workspace blocks, the agents are free to move outside their current workspace block, even though they are still working on it, to extend the tool range inside that work block, as illustrated in Figure 3-10.

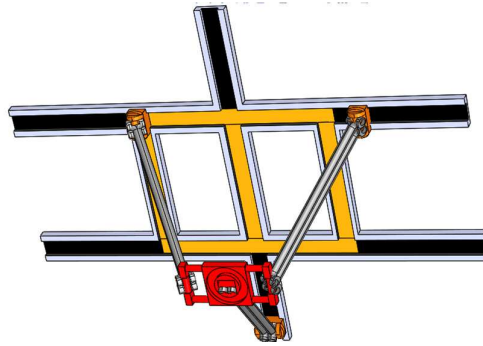


Figure 3-10 - Workspace enlargement strategy by using the extension of the rails to the outside of the work block (highlighted in yellow), thus extending the drives ranges.

Assembly Mode Switching

To switch between AM's, the agents often not only change the rail they are working on but also the orientation of their movement. The agents trajectories, when passing from one rail to another or when switching working blocks, must be carefully planned as the platform may enter a singular configuration, losing its stiffness and risking losing its control in the process [154],[155],[156]. The process of AM switching inside a single work block is illustrated in Figure 3-11. All transitions are reversible.

In [147],[157], it is shown that it is possible to make non-singular transitions between AM's of parallel manipulators. In fact, a non-singular transition from AM 1a to AM2d/e/f is illustrated in the lower part of Figure 3-11. However, in some occasions and depending on the rail size and mesh design, AM switching may require an alignment of agents 1 or 2 with agent 3 on the same rail (a variation of Assembly Mode 3). This happens during AM 1a to 2a/b/c or AM 1b to AM 2d/e/f, as illustrated in the top of Figure 3-11. During this alignment, the manipulator enters a combined singularity and this may lead to failure in switching AM and even system breakdown. To avoid this, when all three agents align in the same rail, two agents should maintain a relative distance x_d . This allows all links to stay on a vertical plane, as shown in Figure 3-12. Distance x_d corresponds to the

half the distance between the extreme anchor points of the limbs on the end-effector, noted by w .

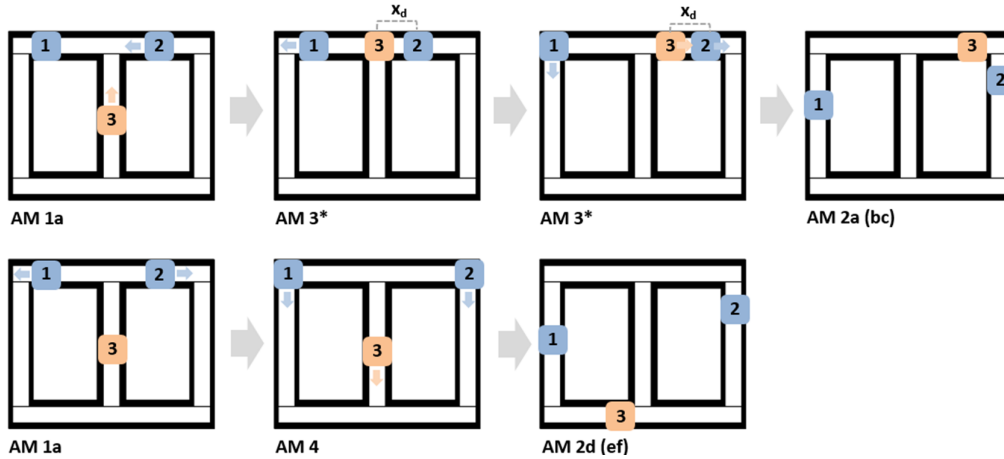


Figure 3-11 - Assembly Mode transitions inside a block. Above: singular transition from AM 1a to AM 2a/b/c. The same procedure is used for AM1b to AM 2d/e/f. Below: non-singular transition from AM 1a to AM 2d/e/f. The same procedure is used for AM1b to AM 2a/b/c.

This pose where all three agents are aligned in a single rail is, in fact, a singular pose of the third type. The robot loses a translational DOF in y direction, while gaining a rotational DOF about the x axis. However, one can take advantage of gravity, which points downwards and helps maintaining balance and manipulator integrity.

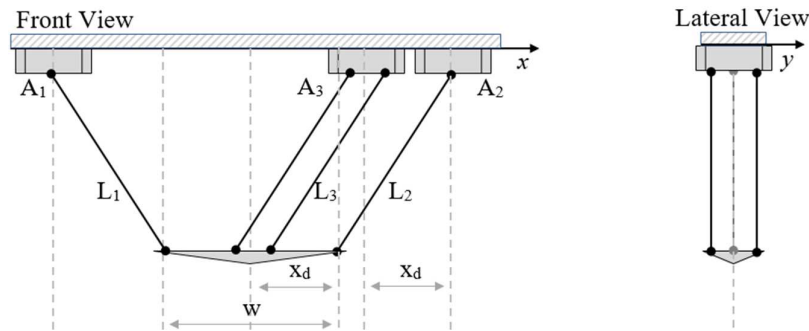


Figure 3-12 - Alignment of all three agents on the same rail, with same x_d distance, measured between the center points of each agent.

3.3.2 Kinematic model

Kinematic analysis allows to model the manipulator behavior given the positions of the mobile agents or the end-effector. Given the multiple configurations possible for this PKM, to fully characterize it, one has to consider all four assembly modes.

For the kinematic analysis of the manipulator, the following geometrical parameters will be considered:

- Ω_0 - fixed Cartesian reference frame ($\Omega_0, \vec{x}, \vec{y}, \vec{z}$);
- Ω_p - moving Cartesian end-effector reference frame ($\Omega_p, \vec{x}_p, \vec{y}_p, \vec{z}_p$);
- $X(x,y,z)$ - coordinates of the end-effector relative to Ω_0 ;
- q_i - set of agent i coordinates relative to Ω_0 ;
- A_i - attach. point of limb i to agent i relative to Ω_0 ;
- B_i - attach. point of limb i to end-effector relative to Ω_0 ;
- b_i - attach. point of limb i to end-effector relative to Ω_p ;
- l_i - link L_i length;
- w - distance between b_1 and b_2 (end-effector width);
- d - distance between y oriented rails;
- m - distance between x oriented rails;

With $i = 1,2,3$.

The fixed Cartesian reference frame's origin is in the point O , which is the intersection point between rail 1 and 4, in the working block. The fixed Cartesian reference frame's origin is in the point O . All links are equal in length ($l_1 = l_2 = l_3 = l$). Agent's A_1 and A_2 limbs are anchored at the extremities of the end-effector. Agent's A_3 limbs are anchored at the center point P of the end-effector. Let b_i be the position vector of the attachment point of limb i to end-effector relative to the moving Cartesian end-effector reference frame P . Then b_i coordinates are given by:

$$b_1 = [-w/2,0,0]^T \quad , \quad b_2 = [w/2,0,0]^T \quad , \quad b_3 = [0,0,0]^T \quad (3-5)$$

The transformation from the moving platform to the fixed base can be described by a position vector $p = \overline{OP}$ and a 3x3 rotation matrix R_P . Since the manipulator displays

spatial movements with only translations and no rotations, by calibration, the 3x3 rotation matrix R_P will be equal to the identity matrix. The position vector B_i with respect to the fixed coordinate system is obtained by the following transformation:

$$B_i = P + R_P b_i \quad i = 1,2,3 \quad (3-6)$$

All rails are considered to be installed on the horizontal plane, $z = 0$. In the first main AM, agents A_1 and A_2 move on a rail coincident with the x axis. The agent A_3 moves on a rail coincident with the y axis. Figure 3-13 shows the first main AM configuration.

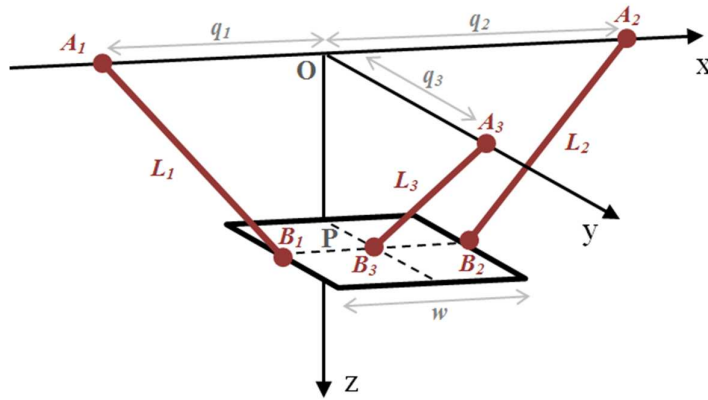


Figure 3-13 - Assembly mode 1 referential and coordinates.

Agents position coordinates are given by the following vectors:

$$A_1 = [q_1, 0, 0]^T, \quad A_2 = [q_2, 0, 0]^T, \quad A_3 = [0, q_3, 0]^T \quad (3-7)$$

In the second main AM, agents A_1 and A_2 move on different rails, coincident or parallel to the y axis. The parallel rails are separated by a distance d . In turn, the agent A_3 moves in a rail coincident with the x axis. Figure 3-14 illustrates the geometry of the second main AM. Agents position coordinates are given by the following vectors:

$$A_1 = [-d, q_1, 0]^T, \quad A_2 = [0, q_2, 0]^T, \quad A_3 = [q_3, 0, 0]^T \quad (3-8)$$

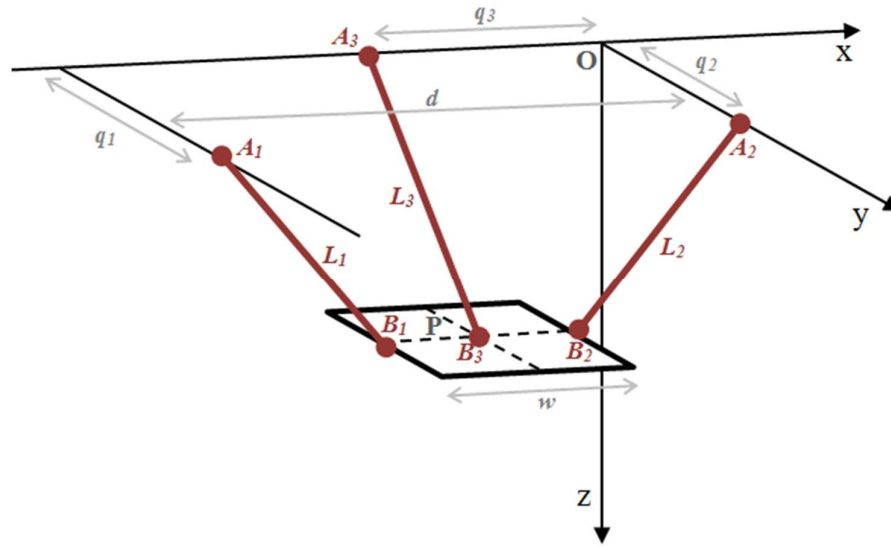


Figure 3-14 - Assembly mode 2 referential and coordinates.

In the third AM, all agents move on x oriented rails. Agents A_1 and A_2 move on the same rail, coincident with the x rail, while agent A_3 moves on a parallel rail, separated by a distance m . Figure 3-15 illustrates the geometry of the third AM. Agents position coordinates are given by the following vectors:

$$A_1 = [q_1, 0, 0]^T, \quad A_2 = [q_2, 0, 0]^T, \quad A_3 = [q_3, m, 0]^T \quad (3-9)$$

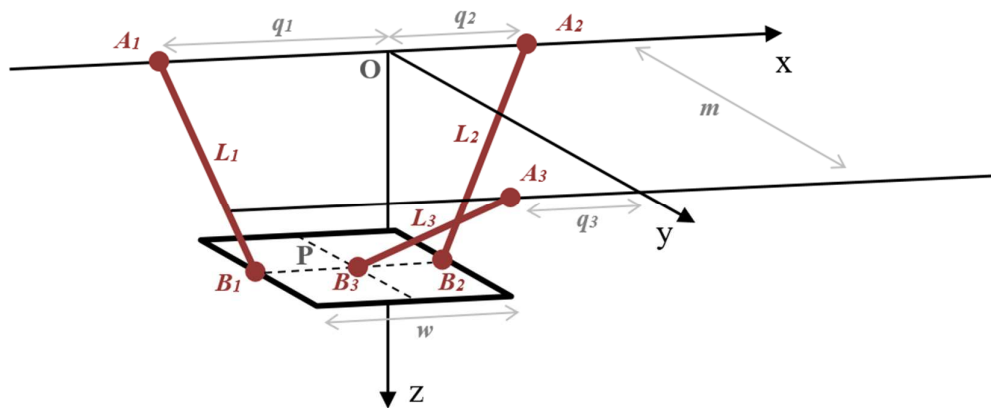


Figure 3-15 - Assembly mode 3 referential and coordinates.

In the fourth AM, all agents move on y oriented rails. Agents A_1 and A_2 move different parallel rails, separated by a distance d . Agent A_3 moves either on another parallel

rail, or can move in one of the rails where A_1 or A_2 move. Figure 3-16 illustrates the geometry of the fourth AM.

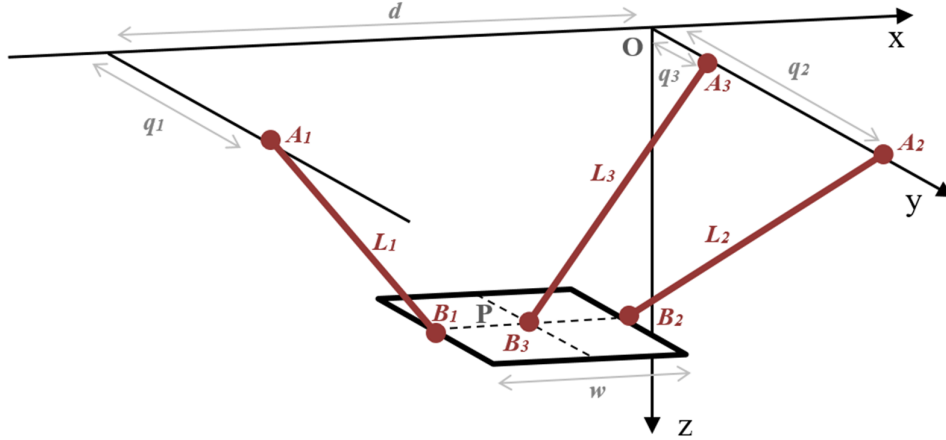


Figure 3-16 - Assembly mode 4 referential and coordinates.

Agents position coordinates are given by the following vectors:

$$A_1 = [-d, q_1, 0]^T, \quad A_2 = [0, q_2, 0]^T, \quad A_3 = [0, q_3, 0]^T \quad (3-10)$$

Inverse Kinematics Problem

The inverse kinematic implicit model (IK) is obtained by using the three closure equations, constraints of the kinematic chains, which link the Cartesian space variables to the joint space variables. The three F constraint equations for the robot are given by:

$$F_i(X, q) = \|P(X) + I_3 \cdot b_i - A_i(q_i)\|^2 - l_i^2 \quad i = 1, 2, 3 \quad (3-11)$$

For this specific problem there are 2^3 different sets of solutions to the inverse kinematics problem, i.e., for a given location of the end-effector, several sets of agents' positions are possible. These correspond to the positive and negative (\pm) roots. In this work, it is considered a unique solution of interest, which is indicated in brackets.

With equations (3-5), (3-6), (3-7) and (3-11), one obtains the IK implicit model equations (3-12) for the first main AM (Figure 3-13):

$$IK_{AM1} = \begin{cases} q_1 = x \pm \sqrt{l^2 - y^2 - z^2} - \frac{w}{2} & (-) \\ q_2 = x \pm \sqrt{l^2 - y^2 - z^2} + \frac{w}{2} & (+) \\ q_3 = y \pm \sqrt{l^2 - x^2 - z^2} & (+) \end{cases} \quad (3-12)$$

For the second main AM (Figure 3-14), the IK model is given by:

$$IK_{AM2} = \begin{cases} q_1 = y \pm \sqrt{l^2 - (d + x - w/2)^2 - z^2} & (+) \\ q_2 = y \pm \sqrt{l^2 - (x + w/2)^2 - z^2} & (+) \\ q_3 = x \pm \sqrt{l^2 - y^2 - z^2} & (+) \end{cases} \quad (3-13)$$

For the third AM (Figure 3-15), the IK model is given by:

$$IK_{AM3} = \begin{cases} q_1 = x \pm \sqrt{l^2 - y^2 - z^2} - \frac{w}{2} & (-) \\ q_2 = x \pm \sqrt{l^2 - y^2 - z^2} + \frac{w}{2} & (+) \\ q_3 = x \pm \sqrt{l^2 - (m - y)^2 - z^2} & (-) \end{cases} \quad (3-14)$$

For the fourth AM (Figure 3-16), the IK model is given by:

$$IK_{AM4} = \begin{cases} q_1 = y \pm \sqrt{l^2 - \left(d + x - \frac{w}{2}\right)^2 - z^2} & (+) \\ q_2 = y \pm \sqrt{l^2 - \left(x + \frac{w}{2}\right)^2 - z^2} & (+) \\ q_3 = y \pm \sqrt{l^2 - x^2 - z^2} & (-) \end{cases} \quad (3-15)$$

Forward Kinematics Problem

The forward kinematics problem (FK) can be obtained by solving the three F constraint equations (3-11) in order to the end-effector coordinates. Once again, for a given set of drive positions there are two possibilities for the position of the end-effector, which correspond to the intersection points of three spherical surfaces. By considering that the Z coordinate is always positive, one finds the single solution to the problem.

For the first main AM (Figure 3-13), the FK model is given by:

$$FK_{AM1} = \begin{cases} x = \frac{q_1 + q_2}{2} \\ y = \frac{(q_1 + w/2)(q_2 - w/2) + q_3^2}{2q_3} \\ z = \pm \sqrt{l^2 - \left(\frac{q_2 - q_1 - w}{2}\right)^2 - y^2} \end{cases} \quad (+) \quad (3-16)$$

In the z coordinate expression, y was used instead of its corresponding expression for simplification purposes. For the second main AM (Figure 3-14), the FK model is given by:

$$FK_{AM2} = \begin{cases} x = \frac{(q_1 - q_2)(q_1 q_2 - w^2/4 + q_3^2) + q_2 d(d - w)}{q_2(w - 2d - 2q_3) + q_1(2q_3 + w)} \\ y = \frac{(d - w)(2x + d) + q_1^2 - q_2^2}{2(q_1 - q_2)} \\ z = \pm \sqrt{l^2 - y^2 - (x - q_3)^2} \end{cases} \quad (+) \quad (3-17)$$

On the y and z coordinate expressions, x and y were used instead of their corresponding expressions for simplification purposes. For the third AM (Figure 3-15), the FK model is given by:

$$FK_{AM3} = \begin{cases} x = \frac{q_1 + q_2}{2} \\ y = \frac{(x - q_3)^2 - (q_1 - x - w/2)^2 + m^2}{2m} \\ z = \pm \sqrt{l^2 - (x - q_3)^2 - (m - y)^2} \end{cases} \quad (+) \quad (3-18)$$

On the y and z coordinate expressions, x and y were used instead of their corresponding expressions for simplification purposes. For the fourth AM (Figure 3-16), the FK model is given by:

$$FK_{AM4} = \begin{cases} x = -\frac{(q_2 - y)^2 + (q_3 - y)^2 + (w/2)^2}{w} \\ \frac{w}{2d} = \frac{(q_2 - y)^2 + (q_3 - y)^2 + (w/2)^2}{(q_1 - y)^2 + (q_2 - y)^2 + 2(q_3 - y)^2 + (d - w/\sqrt{2})^2} \\ z = \pm \sqrt{l^2 - (y - q_3)^2 - x^2} \end{cases} \quad (+) \quad (3-19)$$

On the x and z coordinate expressions, x and y were used instead of their corresponding expressions for simplification purposes.

Jacobian and Inverse Jacobian Matrix

Differentiating the F constrain equations (3-11) leads to the velocity model, written in matrix form as:

$$J_x \cdot \dot{X} + J_q \cdot \dot{q} = 0 \quad (3-20)$$

Where $\dot{X} = [\dot{x} \ \dot{y} \ \dot{z}]^T$ is the vector of the end-effector velocities, and $\dot{q} = [\dot{q}_1 \ \dot{q}_2 \ \dot{q}_3]^T$ is the vector of actuated joint rate. The J_x is the 3x3 parallel Jacobian matrix (reduced since the end-effector does not have angular velocities) and J_q is the 3x3 serial Jacobian matrix. Jacobian matrices are useful for determining the singularity loci and manipulator property workspace. For this reason, they are of great interest to obtain for the manipulation assembly modes, but are of limited interest for the translation assembly modes. In this work, jacobian matrices and property workspace will only be obtained for the first and second main assembly mode, but the same methods can be used to obtain these for the other assembly modes. Thus, for the first assembly mode they are given by:

$$J_{x1} = \begin{bmatrix} \sqrt{l^2 - y^2 - z^2} & y & z \\ -\sqrt{l^2 - y^2 - z^2} & y & z \\ x & -\sqrt{l^2 - x^2 - z^2} & z \end{bmatrix} \quad (3-21)$$

And:

$$J_{q1} = \begin{bmatrix} \sqrt{l^2 - y^2 - z^2} & 0 & 0 \\ 0 & -\sqrt{l^2 - y^2 - z^2} & 0 \\ 0 & 0 & -\sqrt{l^2 - x^2 - z^2} \end{bmatrix} \quad (3-22)$$

For the second AM, and considering, for simplification purposes, $a = d + x - w/2$ and $b = x + w/2$, the jacobians are given by:

$$J_{x2} = \begin{bmatrix} a & -\sqrt{l^2 - a^2 - z^2} & z \\ b & -\sqrt{l^2 - b^2 - z^2} & z \\ -\sqrt{l^2 - y^2 - z^2} & y & z \end{bmatrix} \quad (3-23)$$

$$J_{q2} = \begin{bmatrix} -\sqrt{1^2 - a^2 - z^2} & 0 & 0 \\ 0 & -\sqrt{1^2 - b^2 - z^2} & 0 \\ 0 & 0 & -\sqrt{1^2 - y^2 - z^2} \end{bmatrix} \quad (3-24)$$

By differentiating the velocity model equation (3-20) with respect to time, one obtains the acceleration model. This model can be used to calculate the joint accelerations \ddot{q} of the PKM:

$$\ddot{q} = J_{inv} \dot{\dot{X}} + \dot{J}_{inv} \dot{X} \quad (3-25)$$

Where J_{inv} is the inverse jacobian matrix ($J_{inv} = -J_q^{-1} \cdot J_x$), \dot{X} is the robot's end-effector velocities vector and $\dot{\dot{X}}$ is the end-effector acceleration vector. When J_q is not singular, i.e., $det(J_q) \neq 0$, one can obtain the inverse jacobian matrix. Thus, for the first and second AMs, respectively, one obtains:

$$J_{inv1} = \begin{bmatrix} 1 & \frac{y}{\sqrt{1^2 - y^2 - z^2}} & \frac{z}{\sqrt{1^2 - y^2 - z^2}} \\ 1 & -\frac{y}{\sqrt{1^2 - y^2 - z^2}} & -\frac{z}{\sqrt{1^2 - y^2 - z^2}} \\ -\frac{x}{\sqrt{1^2 - x^2 - z^2}} & 1 & -\frac{z}{\sqrt{1^2 - x^2 - z^2}} \end{bmatrix} \quad (3-26)$$

$$J_{inv2} = \begin{bmatrix} -\frac{a}{\sqrt{1^2 - a^2 - z^2}} & 1 & -\frac{z}{\sqrt{1^2 - a^2 - z^2}} \\ -\frac{b}{\sqrt{1^2 - b^2 - z^2}} & 1 & -\frac{z}{\sqrt{1^2 - b^2 - z^2}} \\ 1 & -\frac{y}{\sqrt{1^2 - y^2 - z^2}} & -\frac{z}{\sqrt{1^2 - y^2 - z^2}} \end{bmatrix} \quad (3-27)$$

Motion model

Given the kinematic model, for a wanted linear trajectory, one can determine the motion characteristics of the manipulator actuators in time. Given a total 3D displacement ΔS , a time period T and an initial position of the manipulator X_0 , the position, velocity and acceleration characteristics of the platform, for an instant t , can be determined by:

$$X(t) = X_0 + \frac{\Delta S}{2} \left[1 - \cos\left(\frac{\pi t}{T}\right) \right] \quad (3-28)$$

$$\dot{X}(t) = \frac{\Delta S \pi}{2 T} \sin\left(\frac{\pi t}{T}\right) \quad (3-29)$$

$$\ddot{X}(t) = \frac{\Delta S}{2} \left(\frac{\pi}{T}\right)^2 \cos\left(\frac{\pi t}{T}\right) \quad (3-30)$$

By combining these expressions with the manipulator's kinematic models (expressions (3-12) until (3-19)), the velocity model (equation (3-20)) and the acceleration model (equation (3-25)), one can relate the motion of the manipulator to the motion of the actuators. Then, one is able to determine the position, velocity and acceleration required for each actuator to perform a given linear trajectory.

3.3.3 Dynamic model

The inverse dynamic model (IDM) and direct dynamic model (DDM) of robots play an important role in design and control. For robot design, the IDM can be used to select actuators [158]–[160], as it allows to compute the actuator efforts, which are needed to achieve a desired motion [161]. It is also used to identify the dynamic parameters that are necessary for both control and simulation applications [162]–[165]. On the other hand, the DDM is employed to carry out simulations that test the performance of the robot and to study the relative merits of possible control schemes [166].

Several approaches have been proposed for the development of the dynamic model of PKM, based on the *Newton-Euler's method* [167]–[169], the *Lagrangian formulation* [170]–[172], the *principle of virtual work* [173]–[175], the *principle of Hamilton* [176], the *Denavit & Hartenberg method* [177], among others [178]. All these methods vary in terms of complexity or computation labor. Therefore, selection of an efficient kinematic modeling convention is very important for simplifying the complexity of the dynamics problems in PKM's.

In this section, a dynamics model of the SCALA manipulator is developed in terms of actuator coordinates, using the two most simple and common methods, the *Virtual Work Principle* and the *Lagrangian Formulation*. For a manipulator with n actuated joints, its

rigid body dynamics, assuming no user force applied on the end-effector, is governed by the following equation:

$$\tau = M(q)\ddot{q} + V(q, \dot{q})\dot{q} + G(q) \quad (3-31)$$

Where $M(q)$ is the $n \times n$ mass matrix of the manipulator and a function of the joint positions q , $V(q, \dot{q})$ is an $n \times 1$ vector of *Centrifugal* and *Coriolis* terms and a function of both joint positions q and velocities \dot{q} , $G(q)$ is a $n \times 1$ vector of gravity terms and a function of joint position q , and τ is a $n \times 1$ vector of joint efforts (forces or torques).

The two approaches developed allow to obtain the symbolic expressions for the dynamic parameters and, consequently, the inverse and direct dynamic models. As a simplification, the inertia of rotation and the rotation of the parallel links are neglected, since link mass is typically much inferior to the mass of the other mobile parts of a PM. Many models adopt this simplification without significant loss of precision [174][179]. Due to the architecture of the 3 P[^]UR PKM, these moving bodies' (end effector and agents) frames are always parallel to the fixed reference frame Ω_0 , exhibiting only spatial movement. Therefore, the rotational motion terms in the models can be neglected. The mass of the links m_i is considered to be equally distributed between A_i and B_i . Thus the overall mass of the actuators M_a , and overall mass of end-effector and payload M_p are considered equal to:

$$M_a = m_a + \frac{m_i}{2} \quad , \quad M_p = m_p + \frac{3m_i}{2} + m_{payload} \quad (3-32)$$

The vector $g = [0 \ 0 \ 9.81]^T$ is the gravity acceleration vector, which points in the positive direction of z axis, because of the referential orientation choice.

Virtual Work Principle

The *Virtual Work Principle* states that, at equilibrium, the virtual work, δW , done by all n external forces, F , acting on a body during any virtual displacement, δr , consistent with the structural constraints imposed on the body is equal to zero [179]:

$$\delta W = \sum_{i=1}^n F_i \cdot \delta r_i = 0 \quad (3-33)$$

Since internal forces, such as constraint and reaction forces, do not produce any virtual work, they are ignored in (3-33), and only external forces are considered. The *virtual work principle* is traditionally applied to static problems. However, there is an extension to this principle, which considers the inertia forces as a result of the t body's mass, m , and acceleration a , allowing to deal with dynamic problems. This is known as *D'Alembert's principle* [180] and is illustrated mathematically below:

$$\delta W = (\sum_{i=1}^n F_i - \sum_{i=1}^t m_i a_i) \cdot \delta r_i = 0 \quad (3-34)$$

Considering the end-effector of the manipulator, the forces applied to it are the force due to gravity, $F_G = M_p g$, and the inertia force, $F_A = M_p \ddot{X}$, due to its acceleration:

$$(M_p g - M_p \ddot{X}) \cdot \delta X = 0 \quad (3-35)$$

As for the agents, they have applied the manipulator actuation forces, τ , and the inertia forces, $F_A = M_a \ddot{q}$. The gravity force is not considered since the vertical movement of the agents is constrained, so there is no work done by gravity. Their virtual work equation is then expressed as follows:

$$(\tau - M_a \ddot{q}) \cdot \delta q = 0 \quad (3-36)$$

With the dynamic parameters for the individual components of the manipulator calculated, the complete manipulator dynamics can now be developed. From the *D'Alembert's principle* (3-34), the sum of all virtual work done on the system by all external forces and torques must be equal to zero. Therefore, adding both expressions (3-35) and (3-36) one obtains:

$$(M_p g - M_p \ddot{X}) \cdot \delta X + (\tau - M_a \ddot{q}) \cdot \delta q = 0 \quad (3-37)$$

Since $\delta X = J \delta q$ and \ddot{X} can be obtained from expression (3-25), equation (3-37) becomes:

$$(M_p g - M_p (J \ddot{q} + \dot{J} \dot{q})) \cdot J \delta q + (\tau - M_a \ddot{q}) \cdot \delta q = 0 \quad (3-38)$$

Which, after re-arrangement, leads to:

$$\tau = (M_a I_3 + M_p J^T J) \ddot{q} + (M_p J^T \dot{J}) \dot{q} - M_p J^T g \quad (3-39)$$

Lagrangian Formulation

The *Lagrange formulation* describes the behavior of a dynamic system in terms of work and energy stored in the system. The basic concept behind this method is that the variation of the energy of a system is equal to the work of the non-conservative forces applied to the system[166]. The energy balance of the system is given by the Lagrangian L :

$$L = K - U \quad (3-40)$$

Where the potential energy U (due to gravity effects, deformations, etc.) is subtracted to the system's kinetic energy K . Kinetic energy results from the agents and end-effector movements, while the end-effector also possesses gravitational potential energy. The potential energy of the agents is neglected since their vertical movement is constrained. The energy balance for the system is then given by:

$$L = \frac{M_p}{2} \dot{X}^2 + \frac{M_a}{2} \dot{q}^2 - M_p g z \quad (3-41)$$

Where z is the vertical distance, between the mobile platform mass center and the system's fixed reference frame origin. The Lagrangian equations are written in the form:

$$\tau = \frac{d}{dt} \left(\frac{\partial L}{\partial \dot{p}} \right)^T - \left(\frac{\partial L}{\partial p} \right)^T \quad (3-42)$$

Where p is the vector of *generalized coordinates*, i.e. the vector of independent parameters that describe the configuration of the system. For rigid robots, p is equal to the vector of active joint variables q . Thus, in the case of robots without any closed loops, q is the vector of the joint coordinates. In a similar fashion, \dot{p} is the vector of *generalized velocities*, the vector of parameters that describe the velocity of any body.

For closed loop robots, the expression of kinetic and potential energies is difficult to obtain as a function of the active joint variables q and velocities \dot{q} only. Therefore, it is preferable to introduce into the vector of *generalized coordinates* p additional variables that will help in obtaining kinetic and potential energies in a simpler form. Those variables are, in the case of a parallel robot, all passive joint variables and platform Cartesian

coordinates. Obviously, these additional variables are not independent and can be linked to the active joint variables through the use of the f_i constraint equations. Three redundant coordinates which are x , y , and z , are chosen, besides the active joint variables q_1 , q_2 and q_3 . Thus the $n = 6$ generalized coordinates p are:

$$p = (x, y, z, q_1, q_2, q_3) \quad (3-43)$$

The *Lagrangian model* for the inverse dynamics is then expressed by:

$$\frac{d}{dt} \left(\frac{\partial L}{\partial \dot{p}_j} \right) - \left(\frac{\partial L}{\partial p_j} \right) = Q_j + \sum_{i=1}^k \left(\lambda_i \frac{\partial f_i}{\partial p_j} \right) \quad (3-44)$$

for $j = 1$ to n , where:

- j is the *generalized coordinate index*;
- n is the number of generalized coordinates;
- i is the constraint index;
- p_j is the j^{th} *generalized coordinate*;
- k is the number of *constraint functions*;
- f_i is a *constraint equation*;
- Q_j is a *generalized external force*;
- λ_i is the Lagrange multiplier.

Expression (3-44) represents a system of six equations in six variables, where the six variables are λ_i for $i = 1, 2$, and 3 , and the three actuator forces, Q_j for $j = 4, 5$, and 6 . The *external generalized forces*, Q_j for $j=1, 2$, and 3 , are the forces applied to the end-effector, which are null:

$$Q = (0,0,0, \tau_1, \tau_2, \tau_3) \quad (3-45)$$

Solving (3-44) for $j = 1;2; 3$, one obtains:

$$M_p(\ddot{X} - g) = J_{inv}^T \lambda \quad (3-46)$$

Solving (3-44) for $j = 4, 5, 6$, one obtains:

$$M_a \ddot{q} = \tau - \lambda \quad (3-47)$$

Combining both (3-46) and (3-47), and replacing \ddot{X} using (3-25), one obtains:

$$\tau = (M_a I_3 + M_p J^T J) \ddot{q} + (M_p J^T \dot{J}) \dot{q} - M_p J^T g \quad (3-48)$$

Inverse Dynamic Model

The formal *inverse dynamic model* is given by (3-31). From the *Virtual Work Principle* and the *Lagrangian Formulation*, equations (3-37) and (3-48), respectively, one obtains this formal model. Both models resulted in the same symbolic expressions for the *dynamic parameters*, given by:

$$M(q) = (M_a I_3 + M_p J^T J) \quad (3-49)$$

$$V(q, \dot{q}) = (M_p J^T \dot{J}) \dot{q} \quad (3-50)$$

$$G(q) = -M_p J^T g \quad (3-51)$$

This model can be used for control or simulation purposes. One can determine the actuator force requirements based on a desired motion and task. This procedure is illustrated in Figure 3-17. The user sets the start position and motion of the mobile platform. The static solution determines the static forces and actuator positions for the manipulator starting pose. From then, motion planning in conjunction with the kinematic models generates the position, velocity and acceleration profiles for the actuators, for each time instant. This, in combination with information about external forces and torques, is used as an input for the dynamic model, which then determines the required forces on each actuator to perform such motion step. Then, the time instant is incremented and this process is repeated until the end of motion.

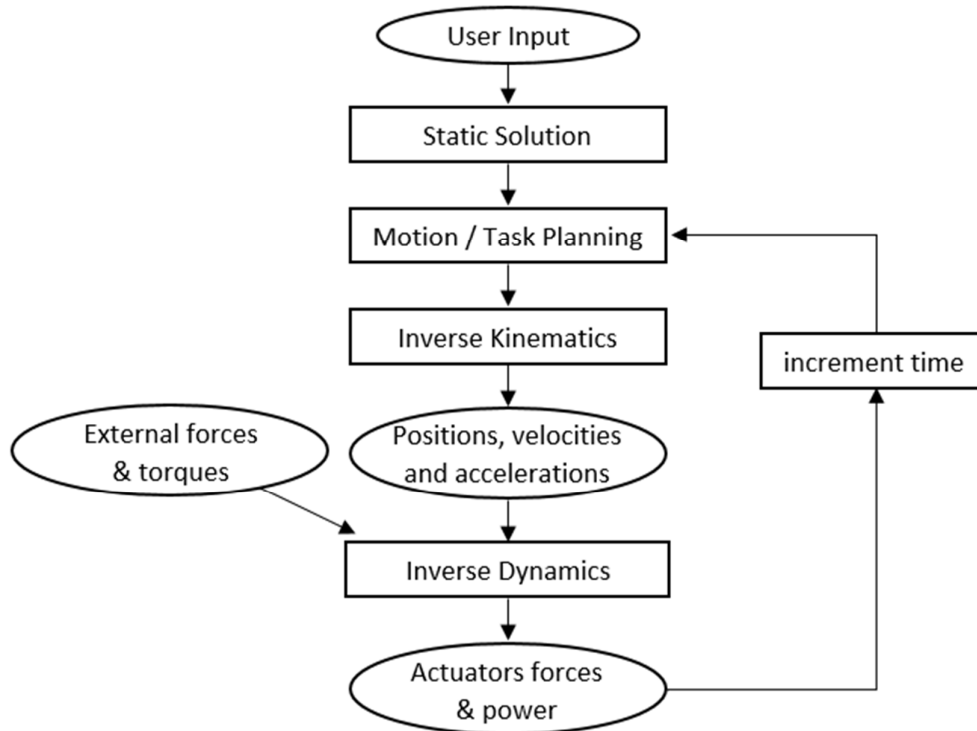


Figure 3-17 – Dynamic control procedure.

Direct Dynamic Model

The DDM of the PKM, expresses the input joint accelerations \ddot{q} as a function of the input efforts τ and it is given by:

$$\ddot{q} = M(q)^{-1}(\tau - V(q, \dot{q})\dot{q} - G(q)) \quad (3-52)$$

Having previously developed the IDM and obtained the *dynamic parameters* (*Inertial, Coriolis-Centrifugal and Gravity Matrices*), it is trivial to develop the DDM.

Considering Friction on the Joints

When using a robot's dynamic model for design or control purposes, it is important that it faithfully reproduces the behavior of the robot in the real world and takes into consideration all the forces involved during its movement. The friction force plays a significant role in this behavior, as it may limit the quality of the robot performance. Non-compensated friction produces static errors, delays, and limits cycle behavior[181].

Many works have been devoted to studying friction torque in joint and transmission systems and various friction models have been proposed in literature [182]–[184]. The model employed in this dissertation is the most often employed model, and is composed of Coulomb friction together with viscous friction. The model based on Coulomb friction assumes a constant friction component that is independent of the magnitude of the velocity. On the other hand, viscous friction is generally considered to be proportional to the joint velocity⁴.

Therefore, the friction forces or torques, τ_{fi} , at a joint i are given by:

$$\tau_{fi} = fs_i \cdot \text{sign}(\dot{q}_i) + fv_i \cdot \dot{q}_i \quad (3-53)$$

Where fs_i and fv_i are the Coulomb and viscous friction parameters, respectively. These terms are quantified during the prototype experimentation process and vary as a function of the load in the joints[185], [186]. However, for simplification purposes, they can be considered constant, thus obtaining a linear model which is simpler to use.

3.3.4 Singularities loci

Singularity configurations are particular poses of a parallel manipulator, in which the mechanism loses its rigidity and degrees of freedom or becomes uncontrollable. Hence, singularities should be avoided at all costs for most applications. As in the work by Gosselin[187], the analysis of the manipulator's two Jacobian matrices, parallel and serial, to establish three types of singularities is proposed:

- First kind singularities: they occur when the determinant of the serial Jacobian matrix is null. This leads to the loss of one or more DOF.
- Second kind singularities: they occur when the determinant of the parallel Jacobian matrix is null. The robot gains one or more DOF.

⁴ Experimental studies have pointed out the Stribeck phenomenon that arises from the use of fluid lubrication, which results in decreasing friction with increasing velocity at low velocity. After a certain point, the friction becomes proportional to velocity [269]. This effect, however, is not considered in the adopted friction model in this dissertation work.

- Third kind singularities: also called combined singularity, they occur when both serial and parallel Jacobian matrices are not full rank. In this situation, the robot gains and loses DOF and may become uncontrollable.

Singularities for AM1

The determinant of the J_{x1} reduced parallel Jacobian matrix of the first AM (3-21) is given by:

$$|J_{x1}| = 2z(y + \sqrt{l^2 - x^2 - z^2})(\sqrt{l^2 - y^2 - z^2}) \quad (3-54)$$

Which in turn is equivalent to:

$$|J_{x1}| = -q_3(q_1 - q_2 + w)z \quad (3-55)$$

The determinant of the J_{q1} serial Jacobian matrix of the first AM (3-26) is trivial to calculate since it is a diagonal matrix:

$$|J_{q1}| = (\sqrt{l^2 - x^2 - z^2})(l^2 - y^2 - z^2) \quad (3-56)$$

Which in turn is equivalent to:

$$|J_{q1}| = \left(x - \frac{w}{2} - q_1\right) \left(x + \frac{w}{2} - q_2\right) (y - q_3) \quad (3-57)$$

As already mentioned, singularities occur when the determinants of the jacobians are null. By equaling equations (3-54) and (3-56) to zero, one obtains the expressions for the singular loci surfaces, shown in Figure 11. In this case, all singularities happen in the vicinity or at the boundary of the robot's workspace, which in turn guarantees the nonexistence of singularities on the inside of the robot workspace, for the first AM. In fact, when met, this set of 3 conditions ensures that one never reaches a singular pose:

$$\left\{ q_1 < x - \frac{w}{2}, \quad q_2 > x + \frac{w}{2}, \quad q_3 > y \right\} \quad (3-58)$$

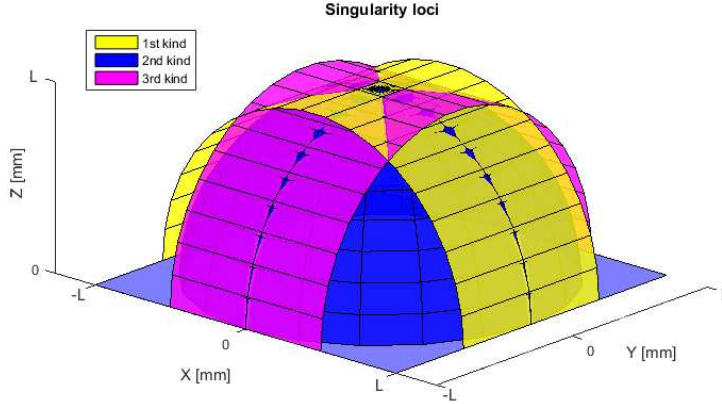


Figure 3-18 - Singularities loci according to type, for AM1.

Singularities for AM2

The determinant of the J_{x2} reduced parallel Jacobian matrix of the second AM (3-23), considering again for simplification purposes, $a = d + x - w/2$ and $b = x + w/2$, is given by:

$$|J_{x2}| = z \left(by - ay + \sqrt{l^2 - y^2 - z^2}(\sqrt{l^2 - a^2 - z^2} - \sqrt{l^2 - b^2 - z^2}) + b\sqrt{l^2 - a^2 - z^2} - a\sqrt{l^2 - b^2 - z^2} \right) \quad (3-59)$$

Which, simplifying and replacing the corresponding expressions for a and b , is equivalent to:

$$|J_{x2}| = z \left(q_1 \left(q_3 + \frac{w}{2} \right) + q_2 \left(\frac{w}{2} - d - q_3 \right) \right) \quad (3-60)$$

The determinant of the J_{q2} serial Jacobian matrix of the second AM (3-24) is:

$$|J_{q2}| = -(\sqrt{l^2 - y^2 - z^2})(\sqrt{l^2 - a^2 - z^2})(\sqrt{l^2 - b^2 - z^2}) \quad (3-61)$$

Which in turn is equivalent to:

$$|J_{q2}| = (y - q_1)(y - q_2)(x - q_3) \quad (3-62)$$

Given the complexity of the determinant of the reduced parallel Jacobian matrix for AM 2 (3-59), it is more difficult to find the expressions for the parallel singularity loci. For this reason, they are not represented here but it will be taken into account in the workspace determination. The trivial solution is $z=0$, which in fact never occurs. The serial singularities are easy to find and occur when the agents, links and platform become aligned. In fact, when met, this set of 3 conditions ensures that one never reaches a serial singular pose in the AM2:

$$\{q_1 > y, q_2 > y, q_3 > x\} \quad (3-63)$$

3.4 Multi PKM Property Evaluation based Design

Methodology

Given the characteristics of PKM, such as their anisotropic properties and existence of singularities, their design and development becomes crucial to fully understand and predict their final behavior. PKM design process, through property evaluation and workspace characterization, allows to determine the values of the PKM kinematic parameters which will improve or certify the properties of the parallel machine.

In this section, a novel design methodology based on interval evaluation of the PKM property workspace is proposed. This methodology is also compared with existing design methods. This sub chapter is an extended version of [95]. The novelty of this methodology is the combination of PKM workspace analysis and design, for several properties of different nature, in a single method.

3.4.1 Existing PKM design methodologies

Design methodologies often follow two distinct philosophies: optimization or certification. The first approach consists of an optimization of a weighted criteria depending on the robot parameters, as it chooses the solution which offers the best

compromise in terms of performance. Examples of this approach include Atlas approach [188], [189], the cost function approach [190], [191], dual expansion [192], compromise programming methodology [193], physical programming methodology [194] among others [195], [196].

The second approach, on the other hand, defines the performance parameters in terms of constraints and not as subjects of optimization. It addresses the design problem in terms of feasibility, by determining a set of solutions for the kinematic parameters which ensure all performance requirements are met [110]. This approach has several advantages relative to design optimization as it is capable of dealing with manufacturing tolerances and other deviations from the nominal design parameter values. It can also deal with a large number of different properties or design parameters which is something that optimization methods usually struggle with. Optimization methods may also converge to a single solution, which might or might not be global optimal, and depends on the weights given to the performance criteria considered or the compromises made between conflicting criteria.

The proposed design methodology focuses on the second approach. Its goal is to design a PKM which fulfills certain desired performance thresholds over its workspace. In other words, one wishes to obtain the set of kinematic parameters for a PKM with a desired workspace, characterized by its joint range limits, absence of singularities, with a desired motion accuracy and force properties. Other parameters such as the occurrence of link and platform collisions or PKM stiffness can be easily added to this model but are not subject to study in the present work. The workspace is the common variable and serves to unify the properties and certify the set of kinematic parameters. Interval analysis [197]–[199] is used to evaluate the constraints and Branch-and-Prune to characterize the constraint workspace. Interval arithmetic, proposed by Moore [200], has been used for PKM property analysis, such as accuracy [201], [202], sensitivity [203], force workspace [204], existence of singularities [205], among others. It deals with continuous intervals instead of discrete points, thus allowing a continuous evaluation of the entire workspace of the PKM as well as the entire range of its design parameters. The proposed design method is based on an

algorithm which uses some well-known interval analysis techniques. Some strategies employed to improve the efficiency of this algorithm are also presented and discussed.

Some works have been made on parallel robot property analysis using constraints, Branch-and-Prune and interval analysis. In [206], a certified enclosure of the generalized aspects is computed. It is used to obtain connected sets of non-singular configurations for path planning of planar robots with 2 and 3 DOF, but in theory can be added additional constraints for any parallel robot case. In that work, arm and obstacle collision as well as joint limits constraints were demonstrated. However, few works have been made addressing the design of a PKM with certified performance. In [207] a robot with certified dynamic performance over a workspace is designed. As an example, a range of design parameters is determined, which ensure that a 2DOF robot with pre-selected actuators can perform a designated task, consisting on following trajectory with a specific velocity and acceleration. In [208], a method is proposed for synthesizing the largest tolerances in the model parameters of a PKM while keeping the pose error below a given limit. A similar work is done in [202].

3.4.2 Novel PKM design methodology

Most works on PKM design either focus on less than 3-DOF PKM's or on a single property. The proposed design methodology, which uses interval analysis methods, addresses the evaluation of several PKM properties of different nature, including singular poses, joint limits, accuracy and force, for an entire workspace, while also taking into account possible variations or uncertainties of the geometrical parameters. Same methodology also enables the design of a PKM with multiple DOF, taking into account different performance requirements.

In this section, the interval analysis tool is introduced. The performance parameter evaluation method is discussed in detail and an outline of the design algorithm developed is presented.

Interval Analysis

The discrete approach to the study of a manipulator's workspace has been widely used for its simplicity. For instance, by varying the actuators' positions in their range, and applying the forward kinematics, one is able to generate a cloud of points inside the workspace and its boundary, as shown in Figure 3-19. However, being able to evaluate the workspace continually (and not in a discrete way) is important since singularities or particular poses of the robot where its performance in terms of accuracy and forces is not satisfactory may occur between two certified workspace points. One can refine the evaluation by adding more points at the expense of computation velocity and efficiency. For this reason, the most robust approach of Interval Analysis (IA) is used for design certification, since it deals with a continuous set of points instead of some particular discrete points. In this sense, IA can certify an entire workspace, since it provides simple tools to evaluate the lower and upper bounds for a function with interval unknowns. It can perform more evaluations on critical areas of the workspace close to singular or boundary regions, while performing much less calculations on large non-critical areas, thus largely improving computation velocity and efficiency.

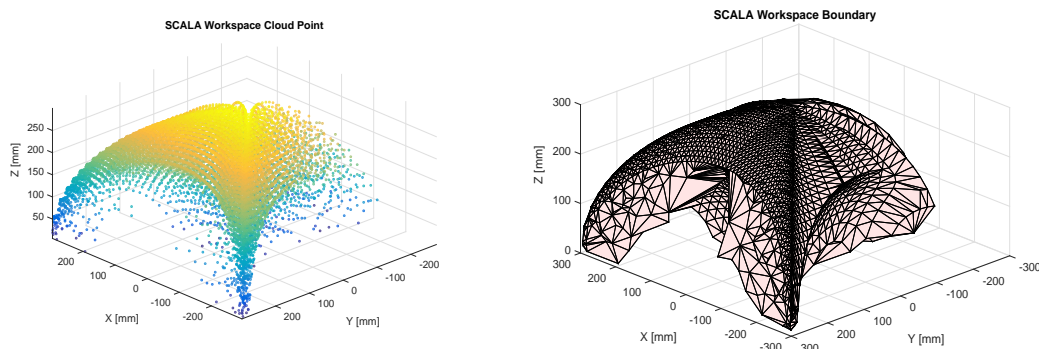


Figure 3-19 - 3D Manipulator Workspace generated in MATLAB (Assembly mode 1a, l=300mm, agents range=400mm, WS volume=36.92 dm³)

An application is when some parameters are not known exactly but are bounded, such as the physical realization of the mechanical components of a robot with its

manufacturing tolerances [209]. It can also be used to take into account computer round-off errors [202].

In this work the usual interval notation will be used:

- Interval real - $[x] \in \mathbb{R} = [\underline{x}, \bar{x}] = \{x \in \mathbb{R} \mid x \leq x \leq \bar{x}\}$;
- Interval vector - $[x] \in \mathbb{R}^n = [\underline{v}_i, \bar{v}_i]$ for $i = 1, \dots, n$;
- Interval matrix - $[M] \in \mathbb{R}^{m \times n} = \begin{bmatrix} [a_{11}] & \cdots & [a_{1n}] \\ \vdots & \ddots & \vdots \\ [a_{m1}] & \cdots & [a_{mn}] \end{bmatrix}$;
- Infimum - $\underline{x} = \inf([x]) \triangleq \inf\{a \in \mathbb{R} \mid \forall x \in [x], a \leq x\}$;
- Supremum - $\bar{x} = \sup([x]) \triangleq \sup\{b \in \mathbb{R} \mid \forall x \in [x], x \leq b\}$;
- Radius - $\delta = \text{rad}([x]) \triangleq \frac{\bar{x} - \underline{x}}{2}$;
- Width/Diameter - $2\delta = \text{wid}([x]) \triangleq \bar{x} - \underline{x}$;
- Midpoint/Center - $\tilde{x} = \text{mid}([x]) \triangleq \frac{\bar{x} + \underline{x}}{2}$;
- Interval approximation of the solution set - $\square = \square$;
- Inner box - \blacksquare ;

As, for example, in the real interval $[-3, 5]$ the *infimum* is -3 , the *supremum* is 5 , the *radius* is 4 , *diameter* is 8 and the *midpoint* is 1 .

Interval arithmetic allows to implement basic operators $(+, -, \times, \div, ^n, \sqrt{\quad}, \sin, \cos, \text{etc} \dots)$, such that[200]:

$$[x] \circ [y] \subseteq \{x \circ y \mid x \in [x], y \in [y]\} \quad (3-64)$$

Then, it is possible to provide an *interval extension* or *inclusion*, noted $[f]$ to real function f as:

$$\forall [x] \in \mathbb{R}, [f]([x]) \supseteq \{f(x); \forall x \in [x]\} \quad (3-65)$$

There exist several types of interval extension, such as *Natural Inclusion*, where every classical operator is replaced by its interval counterpart, or *Taylor Extension*.

The main problem with interval analysis is the overestimation of the resulting interval extension bounds, which may lead to pessimist evaluations of interval arithmetic. Indeed, in interval arithmetic, the several occurrences of variables are treated as independent and are not correlated:

$$[x] - [x] = \{x - y | x \in [x], y \in [y]\} \supset \{x - x | x \in [x]\} \quad (3-66)$$

This, in most cases, leads to loss of properties and to overestimation, where the upper (or lower) bound of $[F]$ is not exactly \max (or \min) $f(x)$ for $x \in [x]$ [200]⁵.

Interval Extensions of Robot Properties

The design methodology proposed can be divided into two steps: Verification and Design.

Verification: The workspace W of the robot is the common denominator in this study. One will analyse the robot's static configurations and determine the workspace for each of the performance thresholds. The workspace W_i for the i performance property, characterized by m inequality constraints noted C_i , formulated as conjunctions and/or disjunctions of inequalities, for a real or interval set of n kinematic parameters, p or $[p]$ respectively, can be defined as:

$$W_i([p_t]) = \{x | \forall p \in [p_t], C_i(x, p)\} \quad (3-67)$$

The exact description of the workspace is difficult to obtain formally. In fact, one is interested in the inner approximation of these sets described by interval boxes. Continuous intervals, depending on their dimensions, can be graphically represented by boxes (lines for 1D, rectangles for 2D, parallelepipeds for 3D, and hypercubes for superior dimensions) with their sides parallel to the reference axis of the chosen parameters. These boxes are tested and labelled as internal or external according to whether or not they are part of the

⁵ Consider, for example, the function $f: x \rightarrow x^3 - 3x^2 + x$. If one uses the interval arithmetic to evaluate f for $x=[2,3]$, one gets $x^3 - 3x^2 + x = [2,3]^3 - 3 \times [2,3]^2 + [2,3] = [8,27] - 3 \times [4,9] + [2,3] = [-17,18]$. This is, in fact a very bad result, since in reality the range $f([2,3])=[-2,3]$. The problem of pessimism is related to the multiple occurrences of the same variable in one expression, by not taking into account the correlation between these variables.

solution set, defined by its *constraints*. A box (ex : $[x_t]$) is internal to W_i , if the condition $\forall x \in [x_t]; C_i(x, p)$ is met. For W_{all} , the condition for an interior box is $\forall x \in [x_t]; \forall i \in [1, \dots, m]; C_i(x, p)$. This set of inner boxes is denoted $\blacksquare W_i([p_t])$ and such as $\blacksquare W_i([p_t]) \subset W_i$. This allows us to ensure that one is fully inside the workspace. External boxes are boxes where the constraint evaluation deems results which lie completely outside the solution set.

An undetermined box is characterized by having parts which belong to the solution set while others lie outside of it. In this case one cannot be sure if the effect of the interval overestimation might be pessimistic, so the box is bisected in two and the resulting boxes are re-evaluated.

One then obtains an inner approximation of the final workspace:

$$W_{all}([p_t]) = \{x | \forall i = [1, \dots, m], \forall p \in [p_t], C_i(x, p)\} \quad (3-68)$$

By intersecting all performance workspaces such that:

$$\blacksquare W_{all}([p_t]) = \bigcap_{i=1}^m \blacksquare W_i \quad (3-69)$$

Design: In Design, one finds all possible values of the n kinematic parameters p vectors for a family of PKM whose performance is certified and complies with all k desired performance parameters, characterized by m inequality constraints noted C_i in a given interval workspace box noted $[x_d]$:

$$D([x_d]) = \{p | \forall i = [1, \dots, m], \forall x \in [x_d], C_i(x, p)\} \quad (3-70)$$

For the design problem, if a box (ex : $[p_t]$) is internal, a condition $\forall p \in [p_t]; [x_d] \subset W_{all}(p)$ or $[x_d] \subset W_{all}([p_t])$ must be met.

In the design methodology, there are boxes for both the search space (geometrical parameters of the PKM) and the variation domain of the parameters (workspace). Bisecting on the variation domain of the parameters and evaluating smaller domains reduces the pessimism and can improve the results of the box evaluation, thus constituting an improvement on the method efficiency and ensuring the convergence of the algorithm. Being $[x]$ the search space and $[y]$ the variation domain, for a given quantified constraint

($\forall \mathbf{x} \in [\mathbf{x}]; \forall \mathbf{y} \in [\mathbf{y}]; f(\mathbf{x}, \mathbf{y}) \leq 0$) one can compute the following interval evaluations $[z] := f([\mathbf{x}], [\mathbf{y}])$, $[z]^1 := f([\mathbf{x}], [\mathbf{y}]^1)$ and $[z]^2 := f([\mathbf{x}], [\mathbf{y}]^2)$, where $[\mathbf{y}]^1$ and $[\mathbf{y}]^2$ are obtained by bisecting the variation domain $[\mathbf{y}]$, and knowing that the interval hull $\square([\mathbf{z}]^1 \cup [\mathbf{z}]^2) \subseteq [z]$. Then, if either $[z]^1$ or $[z]^2$ lies outside the solution set, one can discard the entire parameter set $[\mathbf{x}]$. To know when to perform a bisection on parameter domains, in a similar fashion to the work of *Goldsztein* [210], one defines a threshold on the ratio:

$$\frac{\text{wid}(\square([\mathbf{z}]^1 \cup [\mathbf{z}]^2))}{\text{wid}([z])} \quad (3-71)$$

Below which the parameter domains are bisected. This solution relies on three interval evaluations of the function f , which, as the previous author states, is cheap with respect to the use of interval contractors. The calculations in this work were carried out using a threshold of 0.80, shown to lead to good performances in average. Other methods exist in literature [211], [212] and although not discussed here may be tested in the future to compare with this method.

Once chosen the domain for bisection, the right bisection direction choice is also critical for the efficiency of the algorithm. The classical method for the subdivision process is the bisection of the box $[\mathbf{x}]$ perpendicular to a direction of maximum width. For an interval $I^k = [a_k, b_k]$, bisection occurs at its middle point in order to create two new intervals $I_1^k = [a_k, (a_k + b_k)/2]$ and $I_2^k = [(a_k + b_k)/2, b_k]$. However, the evaluation function f might not variate as much for that direction of bisection as for others, resulting in the creation of an unnecessary large number of boxes. For this reason, one should look for efficient methods for the selection of the direction of bisection to reduce the number of sub-boxes generated, thus reducing the required computation space and time. *Ratz* has studied four different rules for the selection of subdivision directions[213]. Each of the rules selects a direction k by using a merit function:

$$k = \min\{j | j \in [1, \dots, n] \text{ and } \mathcal{R}(j) = \max_{i=1}^n \mathcal{R}(i)\} \quad (3-72)$$

Where $\mathcal{R}(i)$ is determined by the given rule. They have empirically proved, using a wide spectrum of unconstrained test problems, that the correct choice of bisection rules can

effectively reduce calculation time and function evaluations by around 20% and the space complexity by around 15%, when compared with the *classical rule* which selects the direction of maximum width ($R(i) = \text{wid}[\mathbf{x}_i]$). The most effective bisection rules were *Rule B* (Hansen and Walster), defined by:

$$\mathcal{R}(i) = \text{wid}(\nabla f_i([\mathbf{x}]))\text{wid}([\mathbf{x}_i]) \quad (3-73)$$

And *Rule C* (Ratz), defined by:

$$\mathcal{R}(i) = \text{wid}(\nabla f_i([\mathbf{x}]))([\mathbf{x}_i] - \text{mid}([\mathbf{x}_i])) \quad (3-74)$$

The relative efficiency of each bisection method depends on each problem and for one specific case, one method might present serious advantages or disadvantages over all others. For the proposed algorithm, three different bisection methods were tested to find the most efficient one. Bisection can occur until a minimum box size is achieved. In this case, if one still cannot draw any conclusion about the nature of the box, it is characterized as a boundary box. This minimum box size is called study minimum resolution. This is the principle of the *Branch and Prune* algorithm and constitutes the basis of the design algorithm. Property evaluations require solving by intervals linear equality or inequality constraints. For the equality constraint problem, one can apply the method proposed in [214]. However, since they can also be interpreted as inequalities with no prejudice to the result or method, and in an effort to maintain coherence throughout the whole text, one opted to use inequality constraints, which will be discussed in detail in the next section, but can be roughly represented by the following linear interval system:

$$\underline{\mathbf{b}} \leq \mathbf{Ax} \leq \bar{\mathbf{b}}, \mathbf{A} \in [\mathbf{A}] \quad \text{or} \quad \mathbf{Ax} = \mathbf{b}, \mathbf{A} \in [\mathbf{A}], \mathbf{b} \in [\underline{\mathbf{b}}, \bar{\mathbf{b}}] \quad (3-75)$$

Where $[\mathbf{A}]$ is composed by invertible matrices. The problem consists in finding out the subset \mathbf{x} , in the form of an interval vector:

$$\Sigma \exists, \exists([\mathbf{A}], [\mathbf{b}]) := \{\mathbf{x} \in \mathbb{R}^n \mid \exists \mathbf{A} \in [\mathbf{A}], \exists \mathbf{b} \in [\mathbf{b}], \mathbf{Ax} = \mathbf{b}\} \quad (3-76)$$

In this case, and in a similar way to the evaluation of interval polynomial equations, a simple adaptation of scalar algorithms is not feasible. The main source of difficulties connected with computing the solution set \mathbf{x} is its complicated structure, which is generally nonconvex.

Oettli and Prager first proposed a technique to deal with this problem, in 1964 [215]. Taking advantage from the fact that the intersection of the solution set \mathbf{x} with each orthant is, in fact, a convex polyhedron, *Oettli* [216] proposed, using a linear programming procedure in each orthant to determine the infimum and supremum for the solution set. Though this method effectively allows one to obtain larger solution boxes than other methods, it is extremely computation intensive, since it requires an evaluation of the linear system for each orthant.

For this reason, for the proposed algorithm, a theorem proposed by *Beaumont*[217], which is an evolution of the *Oettli-Prager theorem*, is employed:

$$\Sigma \exists, \exists([\mathbf{A}], [\mathbf{b}]) \subset \square \left\{ \mathbf{x}; \begin{pmatrix} A_c - \delta_A D_\alpha \\ -A_c - \delta_A D_\alpha \end{pmatrix} \mathbf{x} \leq \begin{pmatrix} \bar{b} + \delta_A \beta \\ -\underline{b} + \delta_A \beta \end{pmatrix} \right\} \quad (3-77)$$

Where D_α is a diagonal matrix whose elements are α_i and β is a vector whose elements are given are the β_i . Both this scalar matrix and vector depend on an initial approximation of the solution set \mathbf{x} and are given by:

$$\alpha_i = \frac{|\bar{x}_j| - |x_j|}{\bar{x}_j - x_j}, \quad \beta_i = \frac{\bar{x}_j |x_j| - |x_j| \bar{x}_j}{\bar{x}_j - x_j} \quad (3-78)$$

While it does not require an evaluation for each orthant, it is an iterative method, which might turn out to be computation intensive. However, our tests have shown that, with a good initial approximation to the solution set, one obtains sharper results than *Oettli and Prager*, for only one or two iterations.

To reduce the effect of the overestimation and contract the bounds of the solution sets, *filtering methods* are employed:

$$[\mathbf{x}_{new}] = \text{Filtering}([\mathbf{x}_{old}], C([\mathbf{x}])) \text{ so that } [\mathbf{x}_{new}] \subseteq [\mathbf{x}_{old}] \quad (3-79)$$

Filtering can be made using *2B*, *3B*, *Gauss Elimination*, *Taylor*, *Hansen-Blink*, *Newton*, among other methods[199]. If the filtering leads to an empty box, this box is sent to the list of outside boxes.

Robot Properties Characterization

Joint Range: To obtain the manipulator's workspace limited by the reachable extent of its drives and joints, called *reachable workspace*, one has to first develop the kinematics of the robot. The interval extension of the inverse kinematics problem (IK) to a box $[\mathbf{x}]$ ($\forall \mathbf{p} \in [\mathbf{p}_t]$) allows to overestimate all possible variations of the joint coordinates for all $\mathbf{x} \in [\mathbf{x}]$. The *constraint* for joint range property checks if the joint coordinates obtained are inside the defined joint ranges, noted $[\mathbf{q}_d] = [\underline{\mathbf{q}}_d, \overline{\mathbf{q}}_d]$, for the property workspace W :

$$C_1([\mathbf{x}], [\mathbf{p}]) \Leftrightarrow \underline{\mathbf{q}}_d \leq \square (IK([\mathbf{x}], [\mathbf{p}])) \leq \overline{\mathbf{q}}_d \quad (3-80)$$

In this case, if $IK([\mathbf{x}], [\mathbf{p}]) \subset [\mathbf{q}_d]$, it is an internal box. Otherwise, if $IK([\mathbf{x}], [\mathbf{p}]) \cap [\mathbf{q}_d] = \emptyset$, it is an external box.

Singularities: As seen previously, singularities occur when the determinant of the inverse jacobian matrix is null. Thus, the singularity constraint to a box $[\mathbf{x}]$ ($\forall \mathbf{p} \in [\mathbf{p}_t]$) is defined as:

$$C_2([\mathbf{x}], [\mathbf{p}]) \Leftrightarrow \det(J_{inv}([\mathbf{x}], [\mathbf{p}])) < 0 \vee 0 < \det(J_{inv}([\mathbf{x}], [\mathbf{p}])) \quad (3-81)$$

If $[0,0] \notin \det(J_{inv}([\mathbf{x}], [\mathbf{p}]))$, one is sure there is no singular pose in the workspace of the robot. Another approach is to check the regularity of a matrix ($\forall \mathbf{x} \in [\mathbf{x}_t] | \forall \mathbf{p} \in [\mathbf{p}_t], J_{inv}(\mathbf{x}, \mathbf{p})$ are regular) as an alternative to the evaluation of the Jacobian determinant [218], [219]. A different approach is used in [220], where the authors compute the determinant of the jacobian for single poses corresponding to the upper and lower bound of an interval, and try to find inversions of the signal of the determinant, meaning

that there is a singularity inside the pose interval, as the determinant of J_{inv} is a real valued continuous and differentiable function.

Motion Accuracy: Error analysis is an essential study for any PKM design exercise, as it is shown by the numerous works on this subject [209], [221]–[226]. It consists on finding the positioning errors of a given robot at some specific location within the workspace, by solving the following interval linear system of equations:

$$J_{inv}([\mathbf{x}], [\mathbf{p}])[\Delta\mathbf{x}] = [\delta\mathbf{q}] \quad (3-82)$$

Which relates the positioning errors $[\Delta\mathbf{x}]$ of the end-effector with the actuated joints accuracy $[\delta\mathbf{q}]$, through the inverse jacobian matrix J_{inv} , which is pose dependent but also depends on the geometrical parameters $[\mathbf{p}]$ that define the geometry of the robot (considered as intervals to account for the bounded manufacturing errors). While this is actually a first order approximation of the pose error, near singularities the whole process may turn out to be non-reliable. An approximation to the distance to singularities can be found in [227], where the authors avoid singularities by restraining the workspace to a set of static poses where the joint forces do not exceed a certain threshold. A similar solution is employed for our force workspace determination (*constraint C4*), and can be used for the same purpose, to improve on the reliability of this method.

The PKM moves within a given workspace W that is defined as intervals for $[\mathbf{x}]$ parameters. The desired vector of maximal positioning errors $[\Delta\mathbf{x}_d]$ is defined as a set of allowed ranges for the errors on $[\mathbf{x}]$. The goal is to find robot geometries for which one can ensure that whatever is the pose of the robot within the workspace, the positioning error will be included in $[\Delta\mathbf{x}_d]$. Solving by interval the problem for a given accuracy $[\delta\mathbf{q}]$, the internal box $[\mathbf{x}]$ ($\forall \mathbf{p} \in [\mathbf{p}_t]$) test condition consists of checking if the obtained accuracy $[\Delta\mathbf{x}_{res}]$, which is an overestimation of the real accuracy, is inside a desired accuracy interval $[\Delta\mathbf{x}_d]$ is done by:

$$C_3([\mathbf{x}], [\mathbf{p}]) \Leftrightarrow \underline{\Delta\mathbf{x}_d} \leq \square \sum_{\exists, \exists} J([\mathbf{x}], [\mathbf{p}])[\delta\mathbf{q}] \leq \overline{\Delta\mathbf{x}_d} \quad (3-83)$$

If $J([\mathbf{x}], [\mathbf{p}])[\delta\mathbf{q}] \subseteq [\Delta\mathbf{x}_d]$ then it is an internal box. Otherwise, if $J([\mathbf{x}], [\mathbf{p}])[\delta\mathbf{q}] \cap [\Delta\mathbf{x}_d] = \emptyset$ it is an external box.

Joint Forces: Static analysis reveals one very interesting phenomenon in the vicinity of singularities, characterized by the existence of a load such that the internal forces in the joints of the structure tend to infinity[227]. Large payloads also require bigger actuation forces. Such large forces can lock the entire mechanism and in the worst scenario lead to its breakdown. To avoid this, the designer can define a threshold τ_{max} for the maximum internal forces in the joints. The areas of the manipulator workspace in which the internal forces in the joints do not exceed this threshold constitute the *force workspace*. At static equilibrium, the fundamental relation between the joint forces interval vector $[\boldsymbol{\tau}]$, the external wrench exerted on the environment $[\mathbf{F}]$ and the transpose of the inverse kinematic jacobian matrix J_{inv}^T , is given by:

$$J_{inv}^T([\mathbf{x}], [\mathbf{p}])[\boldsymbol{\tau}] = [\mathbf{F}] \quad (3-84)$$

This same expression can be obtained from the manipulator dynamic model, for instance in equation (3-48), considering static condition. The wrench $[\mathbf{F}]$ contains all forces applied by the geometrical center of the end-effector, i.e. in the origin of its reference frame, to the environment. When, for instance, the manipulator carries an $[m]$ payload, where $[m]$ is the interval mass of the payload, the end-effector must counterbalance the weight $[\mathbf{F}]=[m]\cdot\mathbf{g}$, where \mathbf{g} is the gravity acceleration vector. Solving by interval the linear problem for a given wrench $[\mathbf{F}]$, the force constraint for a box $[\mathbf{x}]$ ($\forall \mathbf{p} \in [\mathbf{p}_t]$), consists on checking if the obtained joint forces $[\boldsymbol{\tau}_{res}]$ are inferior to the maximum joint forces τ_{max} , and can be defined as:

$$C_4([\mathbf{x}], [\mathbf{p}]) \Leftrightarrow \forall \mathbf{F} \in [\mathbf{F}], \underline{\boldsymbol{\tau}} \leq \square \sum_{\exists, \exists} (J([\mathbf{x}], [\mathbf{p}])^T \mathbf{F}) \leq \bar{\boldsymbol{\tau}} \quad (3-85)$$

With $[\boldsymbol{\tau}] = [-\tau_{max} \ \tau_{max}]$.

If $J([\mathbf{x}], [\mathbf{p}])^T[\mathbf{F}] \subseteq [\boldsymbol{\tau}]$ then it is an internal box. Otherwise, if $J([\mathbf{x}], [\mathbf{p}])^T[\mathbf{F}] \cap [\boldsymbol{\tau}] = \emptyset$, it is an external box.

Algorithm Outline

It is presented here an outline of the algorithm developed for the study and design of the parallel manipulator, using interval analysis. For the verification routine Algorithm 1, whose pseudo-code is available in Appendix B, the user obtains the workspace for the robot characterized by the unique set of manipulator *geometrical parameters* \mathbf{p} such as the length of the limbs l_i or the width of the end-effector w .

In the design Algorithm 2, whose pseudo-code is available in Appendix B, the result is a set $[\mathbf{D}]$ of kinematic parameters $[\mathbf{p}]$ which form a family of certified PKM's. Then, even if the physical realization of the robot differs from the theoretical model while staying within the given manufacturing error bounds, one can then certify the robot design for the required performance parameters.

If p_j^m is used as the nominal value of a given geometrical parameter p_j , for the manufacturing process one may assume that the real value of p_j will lie in the range $[p_j^m - \varepsilon_j, p_j^m + \varepsilon_j]$. This implies that if one finds a solution interval $[\mathbf{p}_j] = [a, b]$ for the parameter p_j , whose width is larger or equal to $2\varepsilon_j$, then one is able to guarantee that the real robot will satisfy property (3-70), by choosing as theoretical manufacturing value a number in the range $[a + \varepsilon_j, b - \varepsilon_j]$, as this guarantees that the real value will be in $[\mathbf{p}_j]$.

Notice that, even though the inclusion tests show as performed in serial, they can also be performed in parallel fashion for both routines. Both strategies have their advantages and disadvantages, demonstrating higher speeds and efficiency depending on the calculation conditions, as will be discussed further in the next section. Notice also that in the Algorithm 2, line 22, bisection occurs on the variation domain of the parameters, in this case, the workspace $[\mathbf{W}]$. While not shown in the pseudo-code, this is followed by new evaluations of the constraint for a smaller part of the workspace, in order to reduce the overestimation effect. If a single of these evaluations, results in an outside box, then the entire parameter set $[\mathbf{bnew}]$ can be discarded.

3.5 Workspace and Property Evaluation

In this section, the design algorithm is used to find the geometrical parameters set for the SCALA manipulator. After this, a workspace and property evaluation is performed for the two assembly modes of the manipulator, using the property verification algorithm. Finally, it is shown that the workspace extension strategies successfully extend the manipulator workspace and improve its workspace to installation space ratio.

The interval analysis algorithm, proposed in the last section, was developed in the Matlab R2015a environment, with the INTLAB V7.1 package, developed by Siegfried M. Rump, head of the Institute for Scientific Computing at the Hamburg University of Technology, Germany, Copyright (c) 1998 – 2013, under academic licenses. It ran on a computer with an AMD A6-7400K Radeon R5 6 Compute Cores (2C+4G) at 3.50 GHz and 8Gb of RAM.

3.5.1 Manipulator design and parameter choice

For the PKM design, first, it is necessary to establish the characteristics for the desired workspace, namely its volume, guaranteed accuracy and payload capacity. After this, the algorithm determines the set of geometrical parameters (link length and platform width) which guarantees such workspace. It is important to mention that in this design study, a single assembly mode is considered, which is the AM1. The desired workspace was defined as a box of 200 by 200 by 40 millimeters, centered on the point (0,0,300), as shown in Figure 3-20. Inside such work volume, an accuracy of 1mm and a payload of 1kg, for all poses, is ensured.

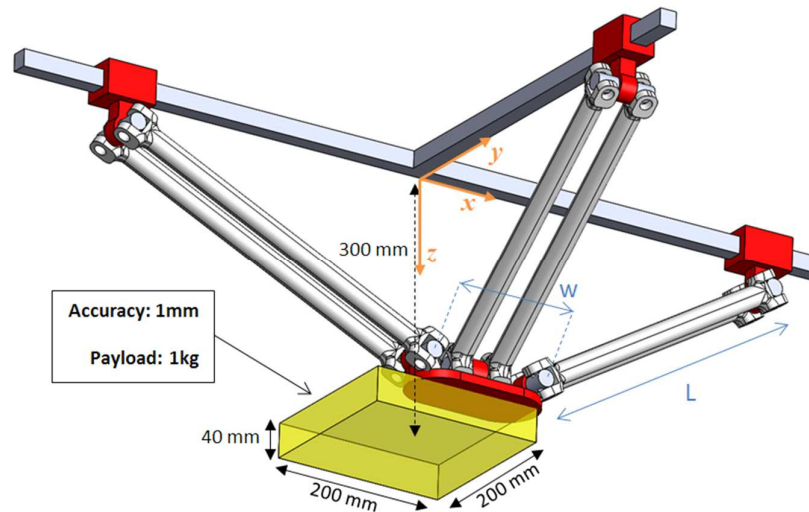


Figure 3-20 - PKM design study parameters. Desired workspace is represented by the yellow box.

Kinematic parameters to be determined are shown in blue.

The design algorithm is run in two fashions: the first one performing the constraint tests in serial (starting from joint limits constraints, then accuracy constraints and then force constraints) and the other one in parallel. When performing serial calculation, the first property constraint is applied to the entire search space. However, for the subsequent evaluations, only the inside boxes of the previous evaluation are used. The search space is then much inferior to parallel calculation, where all search space is used for each property constraint. The final result is the intersection of each property evaluation. Results are shown in Figure 3-21 and Figure 3-22, for serial and parallel calculations, respectively.

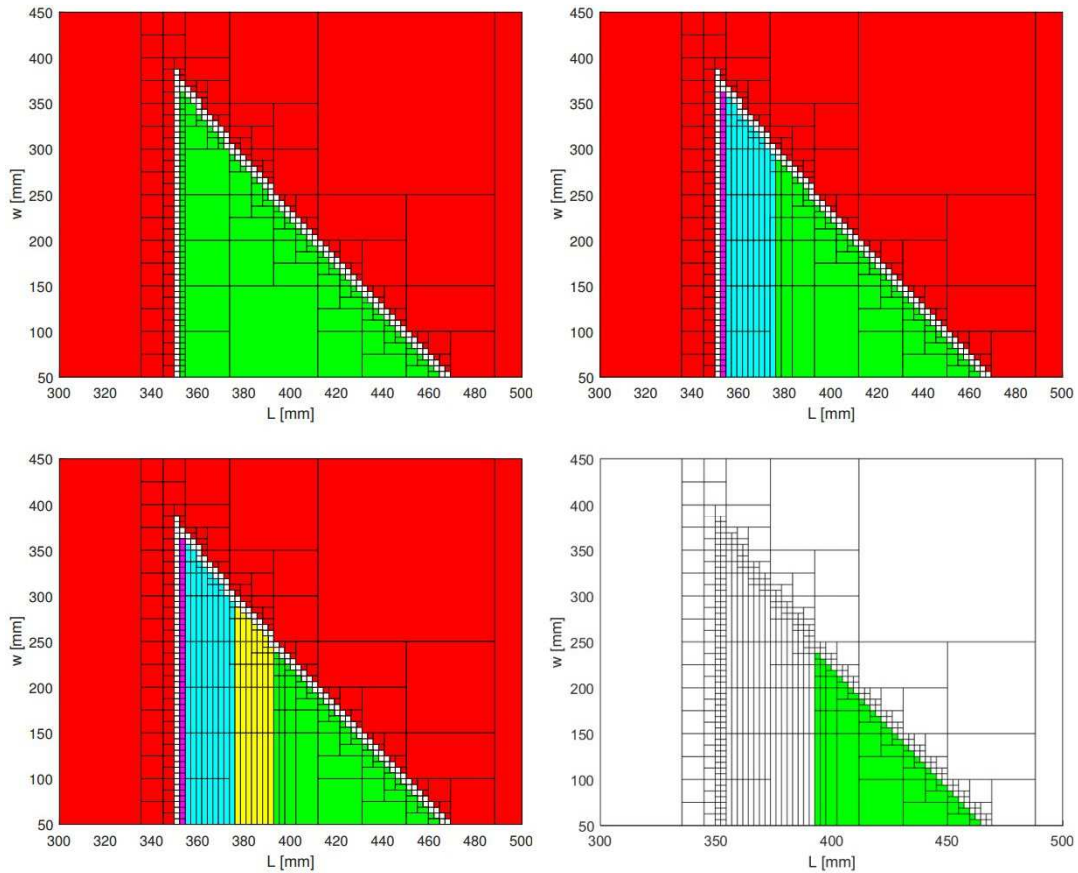


Figure 3-21 - Design algorithm running in serial. Inside boxes shown in green; outside boxes shown in red and purple; boundary boxes shown in white, cyan and yellow. Last image shows the final result. Calculation times (from top left to bottom right): Joint Range and Singularity Constrains- 25.52s; Accuracy Constrains- 18.27s; Force Constraints- 6.50s; Total calculation time- 50.29s.

One can see that the accuracy and force workspace calculation times are much lower than joint range workspace. In fact, the bisection for the former only occurs for one of the design parameters (this particular robot's Jacobian matrices can be expressed only in terms of L and X coordinates of the end-effector with the end-effector width w bearing no influence on the results). For this reason, the number of boxes is much lower as well as the calculation times. Serial calculation is the most efficient when only one computer is available to run the algorithm. However, one can see that the final calculation time for the parallel calculation is inferior to the serial calculation.

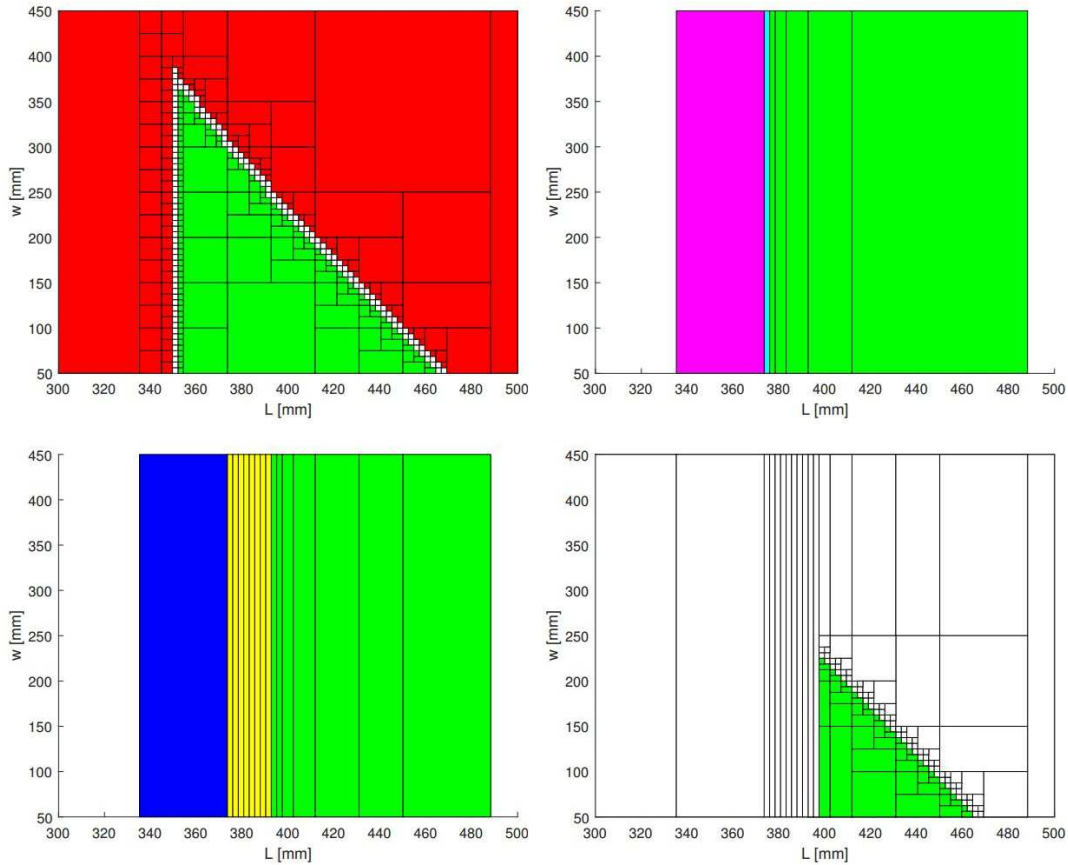


Figure 3-22 - Design algorithm running in parallel. Inside boxes shown in green; outside boxes shown in red, purple and dark blue; boundary boxes shown in white, cyan and yellow. Last image shows the final result after intersection. Calculation times (from top left to bottom right): Joint Range and Singularity Constrains- 25.52s; Accuracy Constrains- 3.00s; Force Constraints- 1.63s; Total calculation time- 25.52s.

This is because one is using a distributed approach, i.e. using a set of computers: a master program will manage the list \mathcal{L} and send boxes to process to a free slave computer \mathcal{S} . This slave computer is responsible for a single property constraint and evaluates its own boxes list \mathcal{L}_s until either \mathcal{L}_s is exhausted or that the number of boxes in \mathcal{L}_s has reached a given threshold. Then the slave computer will return to the master program the list \mathcal{L}_s (possibly empty) that has to be processed together with the remaining sets (also possibly empty) of synthesis solutions. The result is that the calculation time is equal to the longer property evaluation time, in this case, the accuracy constraints.

However, a new serial run of the algorithm was performed, but this time the constraint evaluations were done in order of time efficiency, i.e., Force Constraints (1.63s), then Accuracy Constraints (0.69s) and finally Joint Range (10.71s), obtaining a final calculation time of 12,71s.

The efficiency of the bisection method adopted was also tested. Figure 3-23 shows the results for bisection *Rule B* (Hansen and Walster) and *classical method* (bisect biggest interval). One can see that *Rule B* generates less boundary and outside boxes, meaning its more efficient as a bisection method. The average gain in space complexity is 58% relative to the *classical method*.

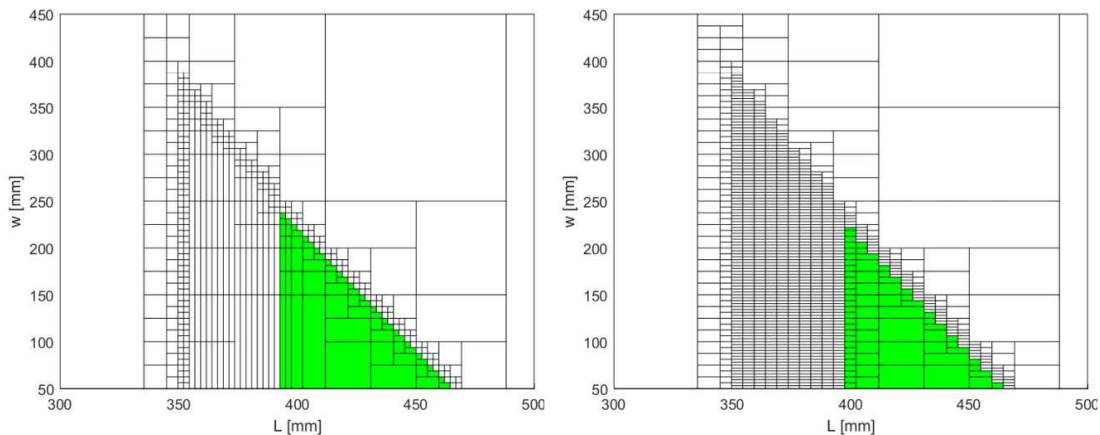


Figure 3-23 - Design Algorithm results for bisection *Rule B* (Hansen and Walster) and *classical method*. Inside boxes shown in green; outside and boundary boxes shown in white. Calculation times: *Rule B*-50.29s; *Classical Method*-184.39s.

This is also shown by the average 63% reduction on the calculation times, relative to the *classical method*. *Rule C* (Ratz) was also tested, and while it was not as efficient as *Rule B*, still an average improvement of 57% in calculation time and 56% in space complexity was obtained, when comparing to the *classical method*. The reason why the *classical bisection* method deems such bad results is thanks to not being able to detect the independency of the parameter w in the accuracy and force constraints evaluation. Thus, it creates many more boxes by bisecting on two design variables. For this reason, and in problems of this nature, a good selection of the bisection method is crucial to obtain a fast and efficient algorithm. The resulting green area constitutes the set of *geometrical*

parameters for the manipulator, which ensure that the desired workspace is achieved. From this set, the designer is free to choose any combination of values. In order to select nominal values for the parameters, the link lengths and end-effector width of the SCALA manipulator were given the values of 400mm and 200mm , respectively. These values also have a good tolerance margin, as one can see for instance in Figure 3-23.

3.5.2 Property workspaces and analysis

In this section, the verification algorithm is used to evaluate the workspace and performance of the manipulator, for AM1 and AM2, given the geometrical parameters present in Table V.

Table V – Parallel manipulator geometrical parameters considered for the analysis.

Parameter	Value [mm]
l (link length)	400
$[q_i]$ (Joint ranges) AM1/AM2	([-500,500] [-500,500] [0,500]) ([0,500] [0,500] [-500,500])
w (end-effector width)	200
δq (actuator accuracy)	0.1
τ_{max} (actuator max force in Newton)	15

Reachable Workspace

Given these parameters as input, the verification algorithm determines the workspace for a given property. Considering the reachable workspace, one obtains the workspace volumes depicted in Figure 3-24 and Figure 3-25, for the first and second assembly modes, respectively.

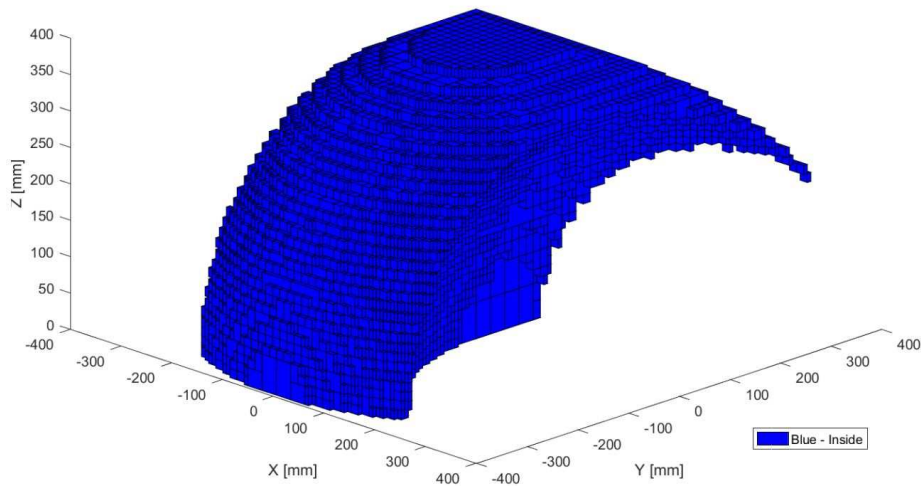


Figure 3-24 - 3D Reachable Manipulator Workspace for AM1. Calculation time: 3375s, N. of Intervals: 100000, Min. Resolution: 25mm³.

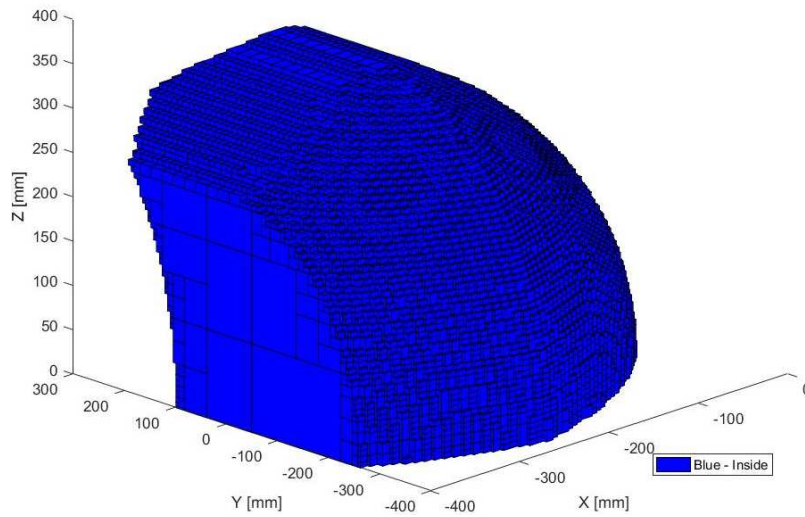


Figure 3-25 - 3D Reachable Manipulator Workspace for AM2. Calculation time: 3131s, N. of Intervals: 100000, Min. Resolution: 25mm³.

When one compares these figures with Figure 3-19, the main difference is that with interval analysis, an entire volume is certified, whereas in discrete point analysis (as in Monte Carlo for instance), results depend on the resolution adopted and do not allow to check the space between each point. This is useful to give an idea of the overall shape and size of the workspace, but due to the high number of intervals (100000), it consumes a lot

of time and processing power. It also becomes more difficult to analyze interior parts of the workspace volume. In fact, most of the time, one is only interested in the behavior and properties of the robot on a specific horizontal plane, or workspace area, as shown in Figure 3-26. For this reason, from this point forward, the workspace analysis will be made on a horizontal plane situated 310mm above the rails ($z=310$).

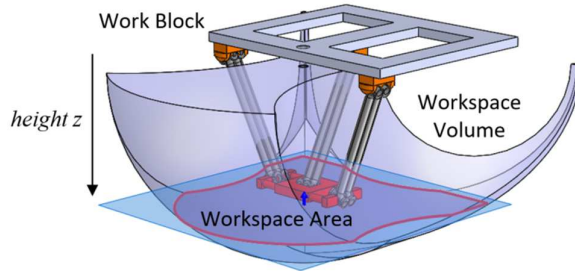


Figure 3-26 - Workspace area on horizontal work plane at a z height from manipulator base.

Figure 3-27 shows the 2D reachable work areas for AM1 and AM2 on this horizontal plane.

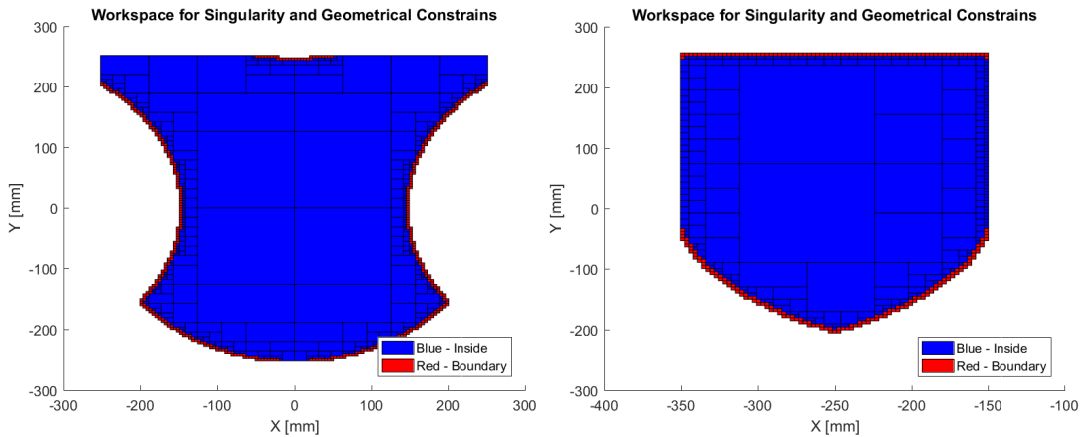


Figure 3-27 – Left and right, reachable workspace for AM1 and AM2, on plane $z=310$, respectively.

Calculation times: 22.1s and 20.4s, N. of Intervals: 1086 and 1022, Interior area: 0.171m^2 and 0.079m^2 .

The interior area is equal to 0.171m^2 and 0.079m^2 for AM1 and AM2, respectively. The minimum resolution considered was 25mm^2 . This calculation took into consideration the singularity constraints. Notice the red boundary boxes separating the interior boxes from the exterior space. Where there is no such boundary is the place where boundary singularities occur. The fact that both workspaces possess no interior gaps, means that

there are no interior singularities, as expected. Notice also the much lower computation times comparatively to the 3D analysis (Figure 3-24 and Figure 3-25).

Accuracy Workspace

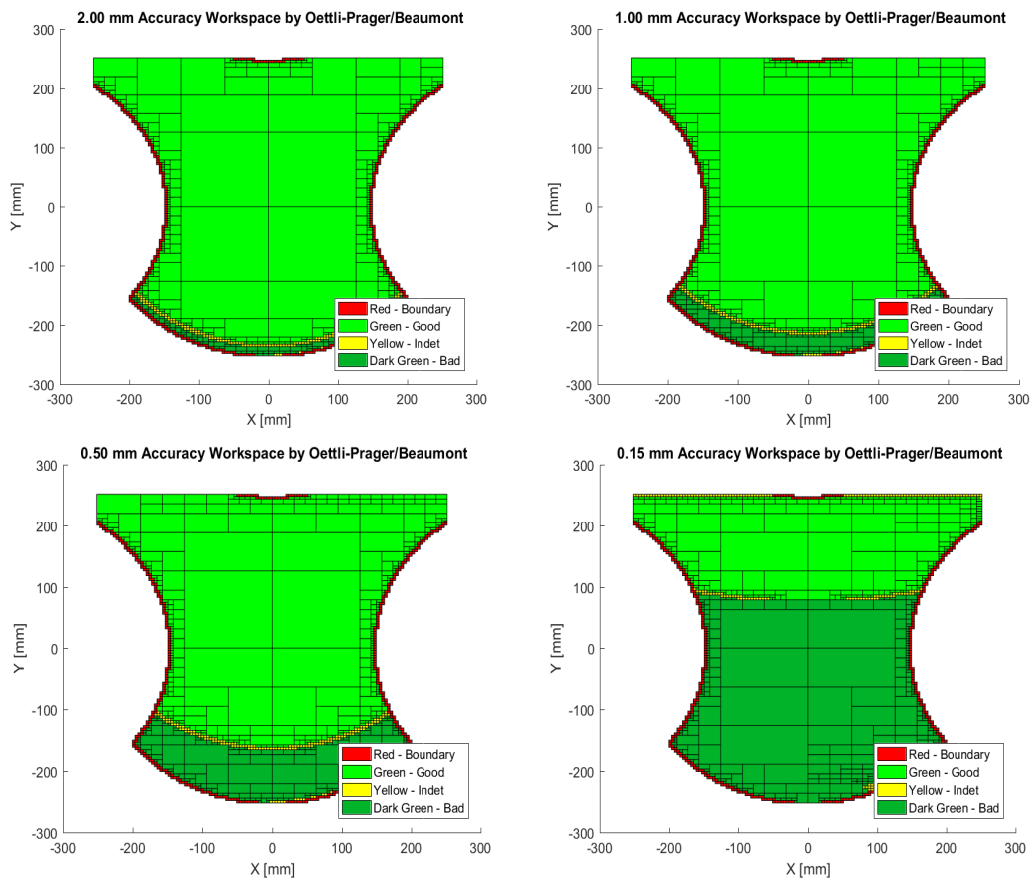


Figure 3-28 - Accuracy Workspace for AM1, on plane z=310. Accuracy of 2mm, 1mm, 0.5mm and 0.15mm workspaces.

The manipulator accuracy workspaces are shown in Figure 3-28 and Figure 3-29, for AM1 and AM2, respectively. The useful work area (shown in bright green) reduces comparatively to the whole workspace area (delimited by the red boundary boxes) as one demands more accuracy from the manipulator. Yellow boxes represent the boundary of the useful work area. For an accuracy of 2mm, 1mm, 0.5mm and 0.15mm, one gets and certified work area of $0.164m^2$, $0.156m^2$, $0.139m^2$ and $0.068m^2$, respectively, for the AM1.

In the case of AM2, certified work area values for the same accuracies are $0.076m^2$, $0.073m^2$, $0.065m^2$ and $0.019m^2$.

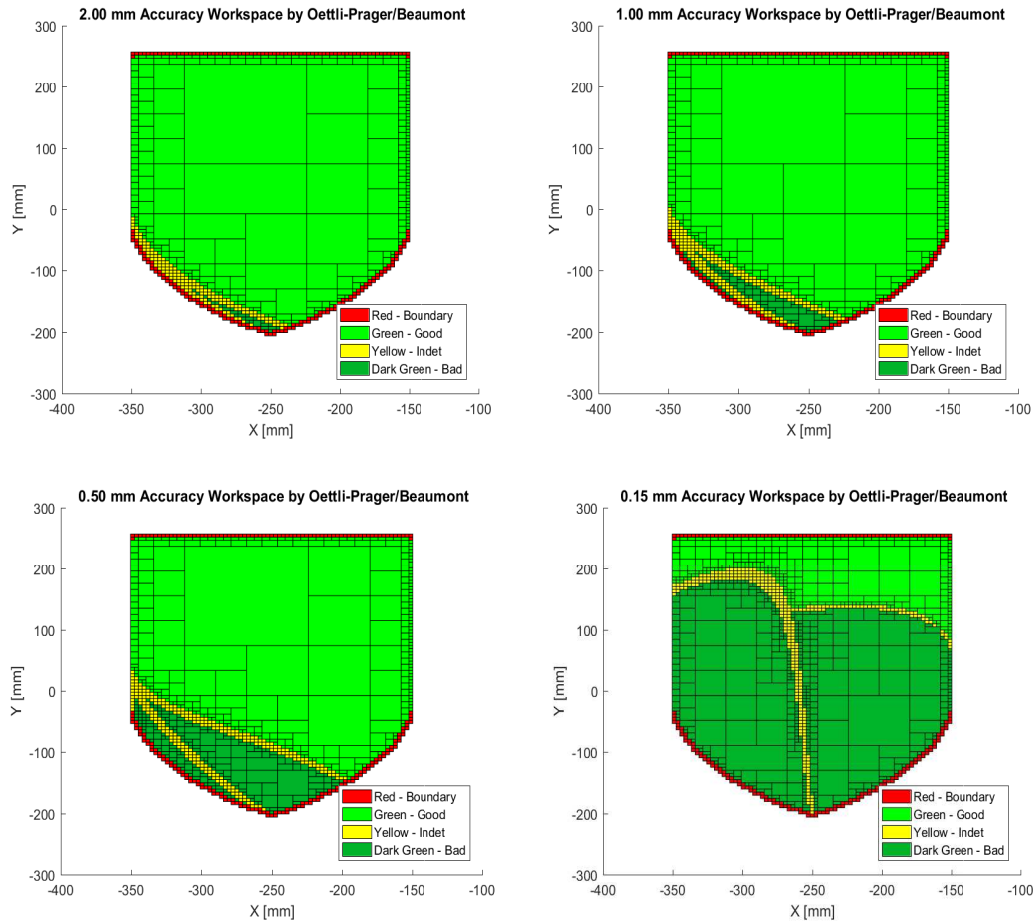


Figure 3-29 - Accuracy Workspace for AM2, on plane $z=310$. Accuracy of 2mm, 1mm, 0.5mm and 0.15mm workspaces.

Force Workspace

Force workspaces for AM1 and AM2 were obtained as a function of the manipulator’s payload, and are shown in Figure 3-30 and Figure 3-31, respectively. As expected, by increasing the load on the manipulator, the internal forces on the joints also increase to the point where in some robot poses they overcome the maximum achievable force to the actuated joints, thus reducing the useful area of work (shown in bright green).

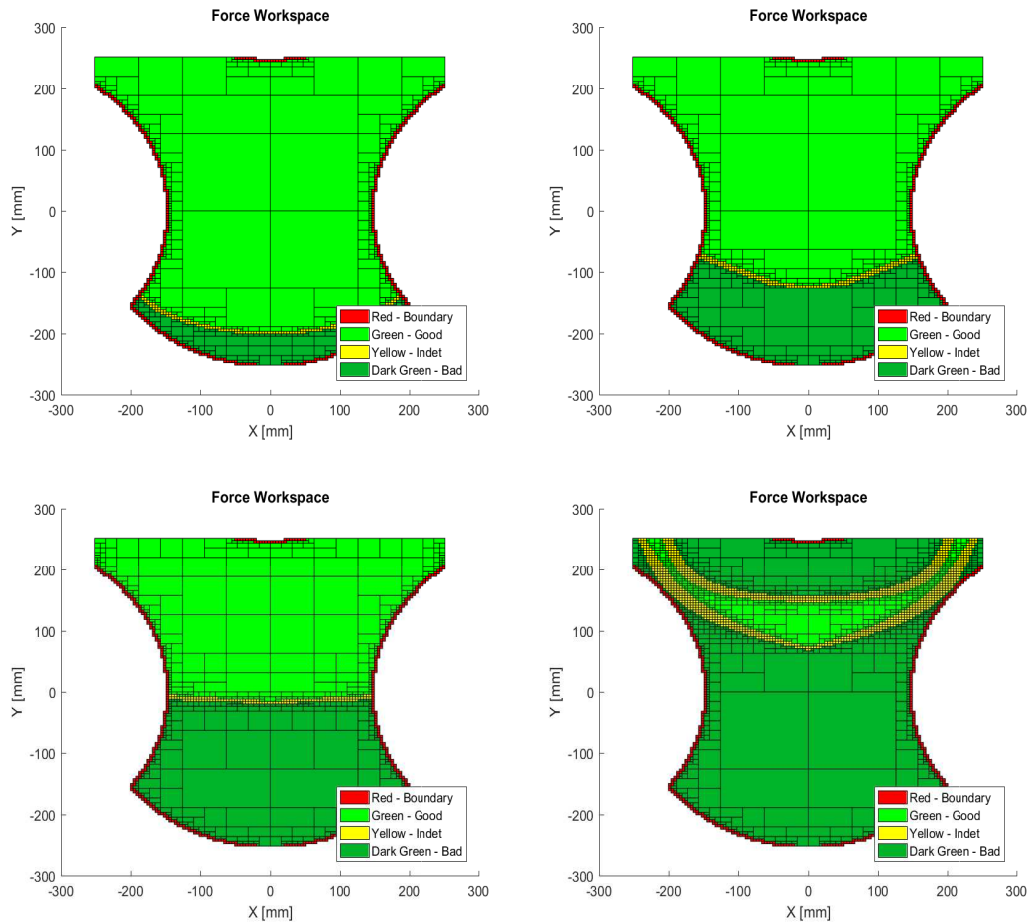


Figure 3-30 - Force Workspace for AM1, on plane z=310. Payload of 0.5kg, 2kg, 3.5kg and 5kg workspaces.

For a payload of *0.5kg*, *2kg*, *3.5kg* and *5kg*, corresponding to certified work areas of $0.154m^2$, $0.125m^2$, $0.098m^2$ and $0.019 m^2$, for AM1, and $0.057m^2$, $0.027m^2$, $0.006m^2$ and $0m^2$, for AM2. Compared to the AM1, the AM2 exhibits weaker performance, regarding both the accuracy and force properties.

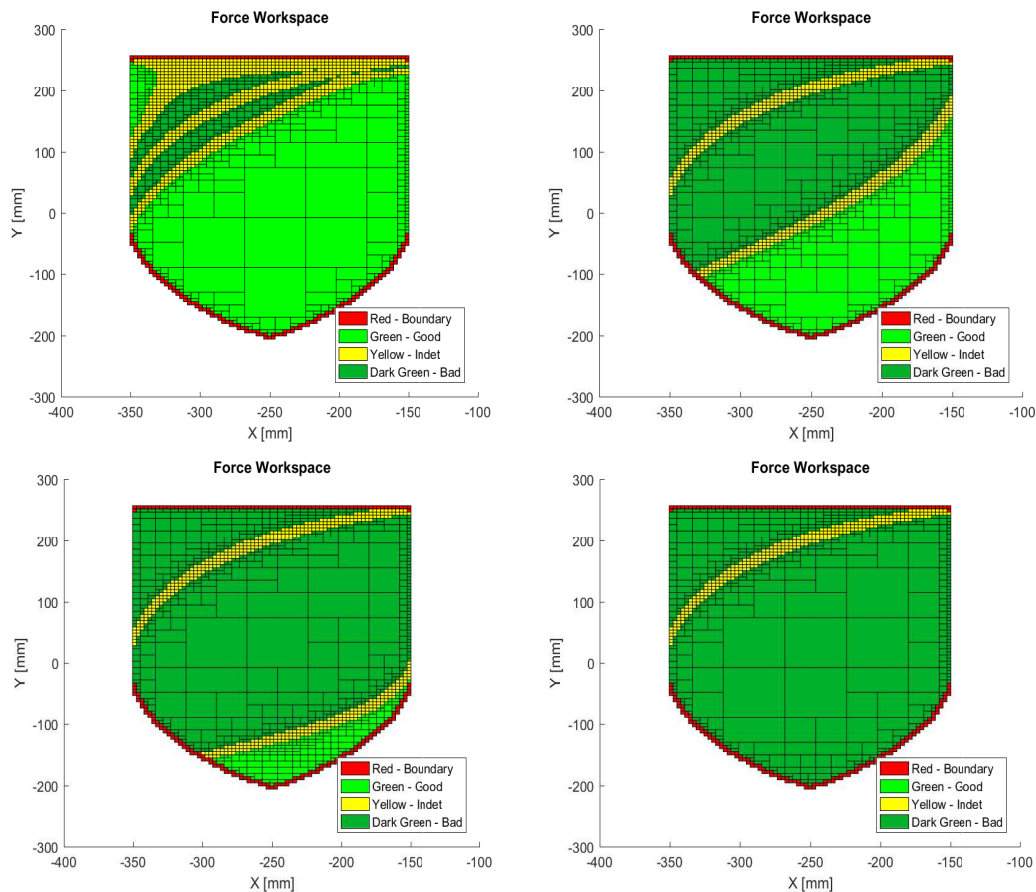


Figure 3-31 - Force Workspace for AM2, on plane $z=310$. Payload of 0.5kg, 2kg, 3.5kg and 5kg workspaces.

Notice that the property workspace for AM2 does not have a symmetry axis, as it is observed in AM1, where the symmetry axis is the line or plane $x=0$. This happens because the assembly of AM1 is, in fact, symmetric, whereas in AM2, there is no general symmetry in the assembly. There are also some indeterminate areas in the middle of the outside box region for AM2. Because the formal expression of the Jacobian matrices is more complex for AM2 than it is for AM1, some effects may occur which can prejudice the accuracy of the verification algorithm. For instance, and since the algorithm does not take into account the dependency of the components in the inclusion function, a large repetition of variables may lead to overestimation of the results[199]. This effect should be further investigated in future work.

3.5.3 Workspace extension through reconfiguration

To show the potential of this reconfigurable platform, a case study was prepared, where the goal was to determine the work area to installation area ratio in a single work block of 5 rails, as shown in Figure 3-32.

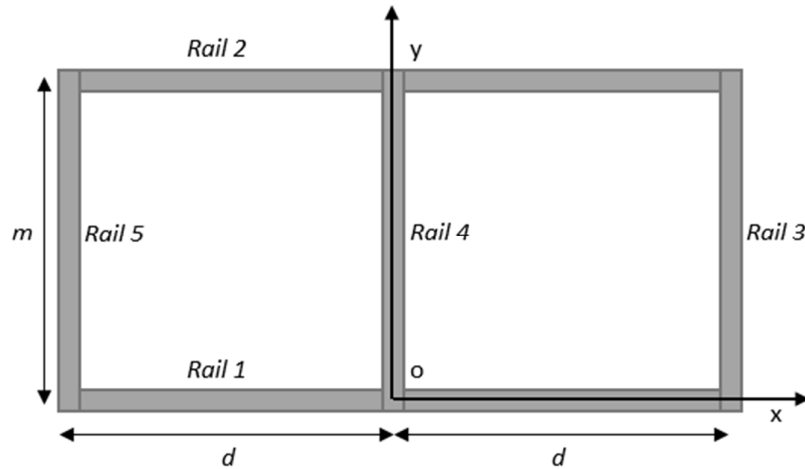


Figure 3-32 - Work block mesh with m width and $2d$ length.

The workblock considered is made from equal linear $500mm$ long rails, thus both $d = 500mm$ and $m = 500mm$. Rails 1 and 2 are made from two of these rails. The agents can move until the ends of the work block, thus setting their limits. In fact, the only strategy for workspace enlargement demonstrated in this case study will be reconfiguration, as the driving agents will be working on a single work block and won't be allowed to move outside of it. The manipulator geometrical parameters are the same present in Table V, with a link length l of $400mm$ and an end-effector width w of $200mm$.

The purpose of this case study is to show how the workspace coverage in a horizontal work plane can be improved by using multiple AM's of the same manipulator.

The workspaces were determined for all AM's present in Table IV, with the exception of AM 2a and 2d. These two are impossible to achieve with this link and rail length combination, since the distance between rails 3 and 5 is $1000mm$ and the manipulator links are only $400mm$ long. The manipulator's workspace is determined by the verification algorithm proposed.

First, the reachable workspace for all AM's is determined, in this workblock, for several horizontal planes, from $z = 20mm$ to $z = 400mm$.

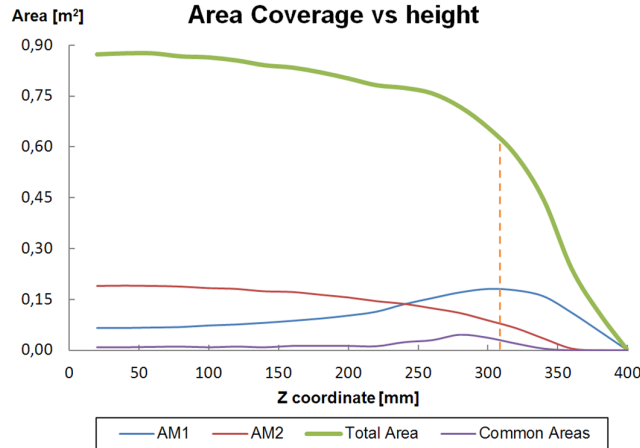


Figure 3-33 – Reachable work areas for horizontal planes $z \in [0, l]$.

The variation of the area coverage for AM1, AM2, all AM's combined and the common areas, with the workplane height, is shown in Figure 3-33. One can see that the total area coverage constantly diminishes with the increase in workplace height. This tendency is also followed by the area of the second assembly mode. However, the area of the first assembly mode increases steadily until $z = 310mm$, and after it also decreases. The common areas maintain a steady low value from $z = 0mm$ to $z = 220mm$. After this point, they increase up until $z = 280mm$, and then go to $0m^2$. This graph is not enough to draw conclusions regarding the workspace coverage of the several assembly modes, thus the workspaces for the several heights were represented and are depicted in Figure 3-34.

This figure allows to understand how the size and shape of the coverage areas change according to the workplane height. One can see that low heights favor the AM2, while higher heights favor AM1. Analyzing both Figure 3-33 and Figure 3-34, one can conclude that for this set of geometrical parameters, the optimal height for the workplane is $z = 310mm$, for three reasons: first, even though it does not offer the best total workspace coverage, it offers a big range of $310mm$ for the vertical displacement of the manipulator tool; second, it favors AM1, which, as seen previously, possesses better performances in terms of accuracy and force properties than AM2; third, the workspace coverage does not

have any interior gap, and it is a continuous workarea. All other workareas include interior gaps, which are not desirable in the workspace of a PM.

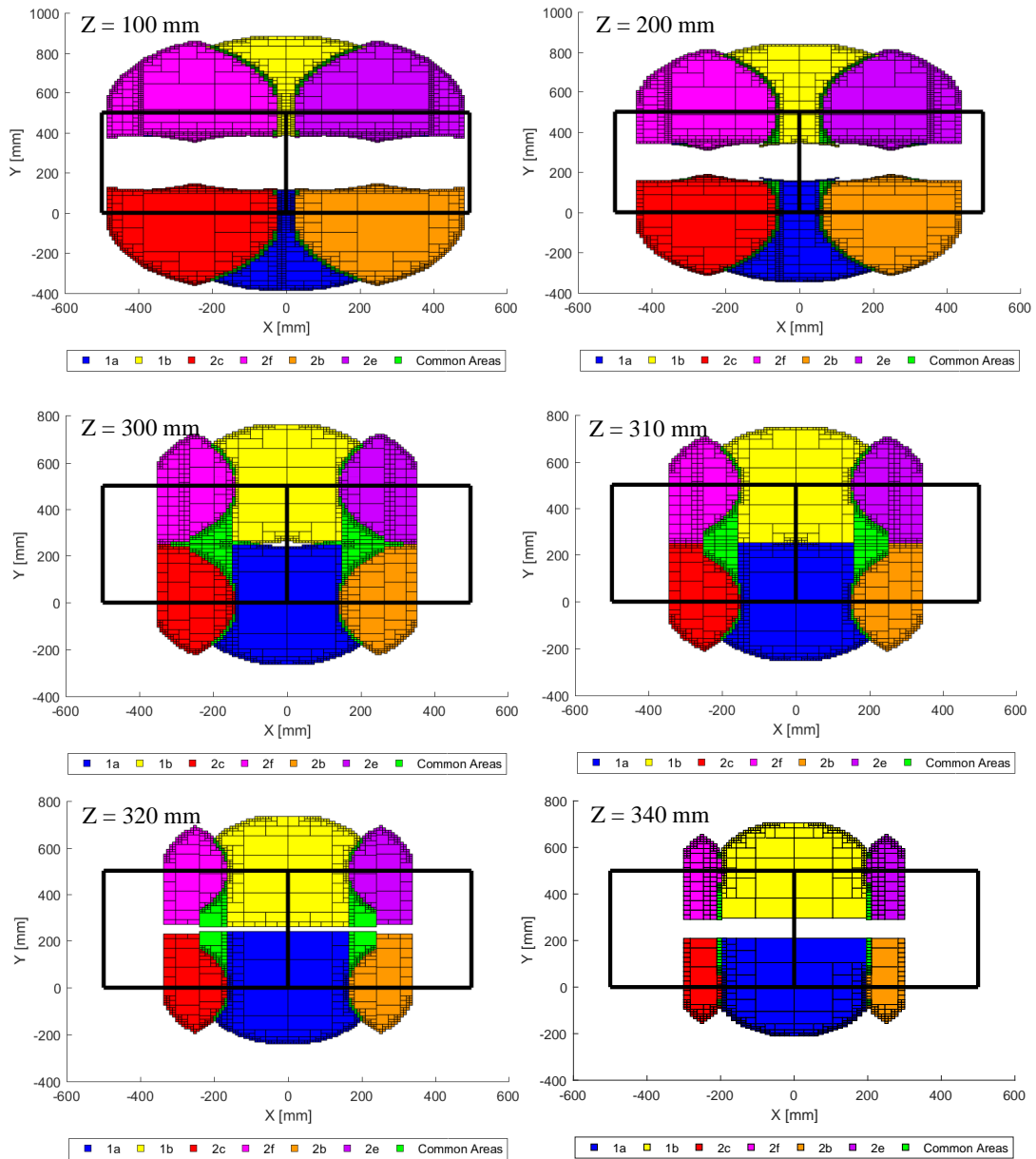


Figure 3-34 – Reachable work areas represented on the workblock, for horizontal planes $z = 100, 200, 300, 310, 320$ and 340 mm, respectively.

For the workplane $z = 310\text{mm}$, total area covered is 0.627m^2 , with common areas of 0.024m^2 . This represents a workspace to installation space ratio of 1.25, achieved for a single workblock and only through PM reconfiguration. However, through geometrical parameter fine-tuning, one can still improve such parameters, as will be demonstrated in the next analysis.

Manipulator Geometry Variation Effect on Workspace Coverage

In this section, the influence of the geometrical parameter variations of both the manipulator and the work block is studied, to see how a fine tuning can improve the workspace coverage. The purpose is not to search for an optimal set of parameters, but to demonstrate that by parameter fine tuning, it is possible to shape the parallel manipulator workspace to suit a specific task or requirement. When analyzing a particular parameter, all other parameters assume the values previously considered in the case study, which are $w = 200\text{mm}$, $l = 400\text{mm}$, $d = 500\text{mm}$ and $m = 500\text{mm}$. The workplane is $z = 310\text{mm}$. The reference workspace coverage is shown in Figure 3-35.

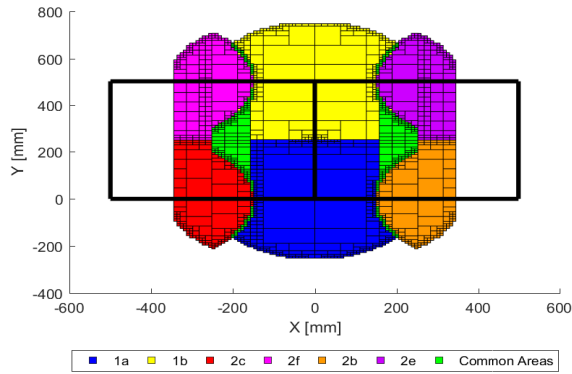


Figure 3-35 – Reference workspace coverage for $w = 200\text{mm}$, $l = 400\text{mm}$, $d = 500\text{mm}$ and $m = 500\text{mm}$. The workplane is $z = 310\text{mm}$.

The first parameter studied was the end-effector width w . The work areas were determined for $w = 150\text{mm}$ and $w = 250\text{mm}$. Results are shown in Table VI and Figure 3-36. As one can see, increasing the end-effector width has distinct effects for AM1 and AM2. While the AM1 area reduces, the AM2 area increases.

Table VI – Effect of variation on end-effector width w .

End-effector width w	150	200	250
Work Area [m ²]	0.569	0.627	0.686
Common Area [m ²]	0.024	0.024	0.029
Work/Installation Area Ratio	1.14	1.25	1.37

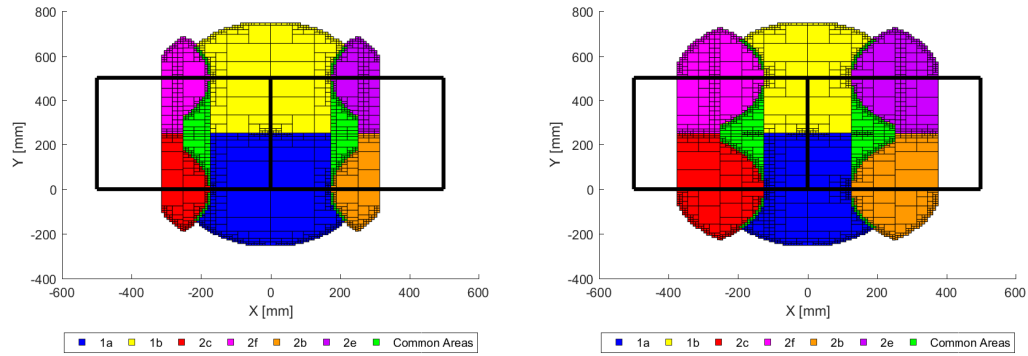


Figure 3-36 – Left and right, workspace coverage for $w = 150mm$ and $w = 250mm$, respectively.

The overall effect is an increase in the workspace coverage with an increase of the end-effector width, at the prejudice of AM1. The common areas also tend to increase.

The second parameter studied was the link length l . The work areas were determined for $l = 375mm$ and $l = 425mm$. Results are shown in Table VII and Figure 3-37.

Table VII – Effect of variation on link length l .

Link length l	375	400	425
Work Area [m ²]	0.444	0.627	0.725
Common Area [m ²]	0.005	0.024	0.041
Work/Installation Area Ratio	0.88	1.25	1.45

The workspace coverage shows great variations with the link length variation. Increasing the link length allows the manipulator to reach further outside the work block, increasing the total area covered. However, it can also cause gaps in the middle of the work block.

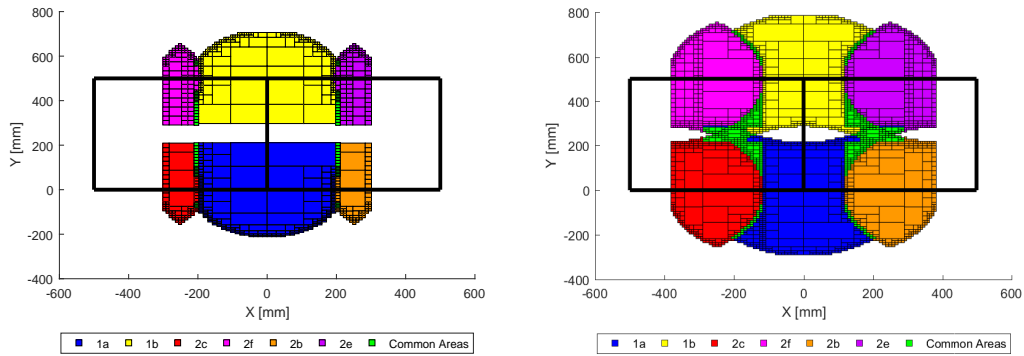


Figure 3-37 – Left and right, workspace coverage for $l = 375mm$ and $l = 425mm$, respectively.

The third parameter studied was the rails 1 and 2 lengths d . The work areas were determined for $d = 400mm$ and $d = 600mm$. Results are shown in Table VIII and Figure 3-38.

Table VIII – Effect of variation on rails 1 and 2 lengths d .

Rails 1 and 2 lengths d	400	500	600
Work Area [m ²]	0.641	0.627	0.600
Common Area [m ²]	0.035	0.024	0.000
Work/Installation Area Ratio	1.60	1.25	1.00

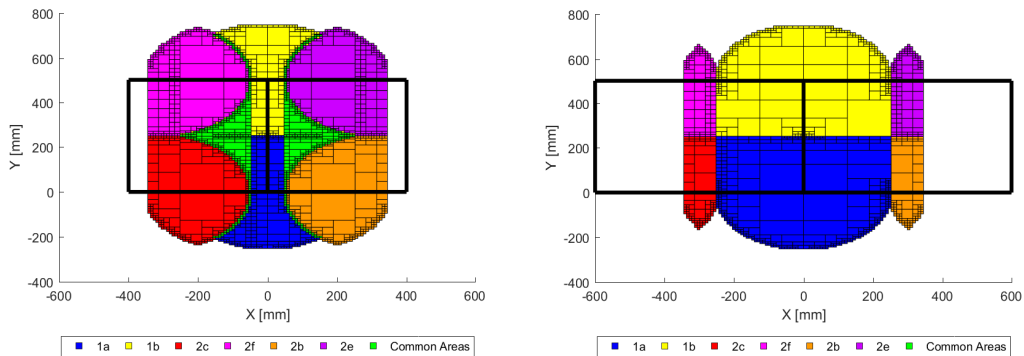


Figure 3-38 – Left and right, workspace coverage for $d = 400mm$ and $d = 600mm$, respectively.

Longer rails 1 & 2 allow the mobile agents to travel further on AM1, thus enlarging this workspace. On the contrary, since it increases the distance between rails 3, 4 & 5, it reduces the workspace of the second AM. The shorter work block has the best work/installation area ratio, so in the case of having a single workblock, this is preferable. However, when it is possible to have several workblocks adjacent to each other, the longer rails are a better solution which offers a big AM1 area and reduced common areas.

The last parameter studied was the rails 3, 4 and 5 lengths m . The work areas were determined for $m = 400\text{mm}$ and $m = 600\text{mm}$. Results are shown in Table IX and Figure 3-39.

Table IX – Effect of variation on rails 3, 4 and 5 lengths m .

Rails 3, 4 and 5 lengths m	400	500	600
Work Area [m ²]	0.528	0.627	0.626
Common Area [m ²]	0.043	0.024	0.024
Work/Installation Area Ratio	1.32	1.25	1.04

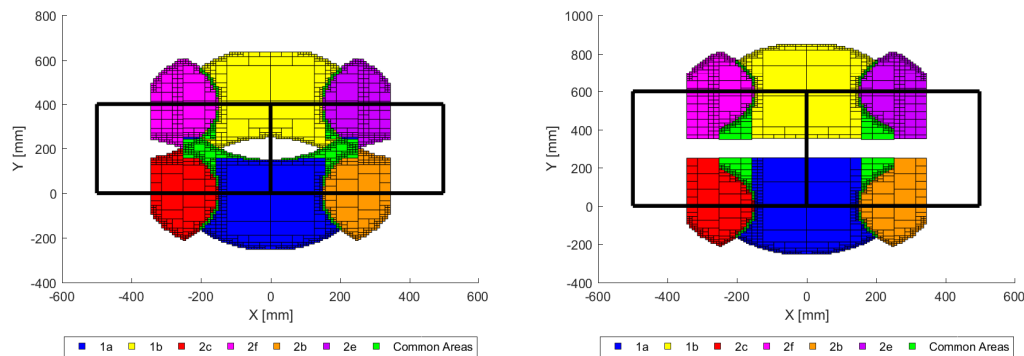


Figure 3-39 – Left and right, workspace coverage for $m = 400\text{mm}$ and $m = 600\text{mm}$, respectively.

Increasing the length of the rails 3, 4 & 5 increases the separation of the work areas. As the size of the work block also increases with the increased rail lengths, the work/installation area ratio decreases.

3.6 Summary

In this chapter, a novel reconfigurable parallel manipulator with a large workspace, driven by the SCALA mobile robots, was presented. The mobile robots move on a 2D mesh of rails, granting them a high degree of mobility. This mobility was used for 3 different strategies for workspace enlargement, including extension of the drive ranges, translation of the robot base and reconfiguration. These allow the robot to cover a large planar area in its workspace and overcome the limitations of current systems. For a single work block, reconfiguration proved to be an efficient strategy for large work area coverage, given the right geometrical parameters for the robot and the desired application. In the case study presented, a workspace area to installation area ratio of 1.60 was achieved (when $d = 400mm$), by combining the workspaces of all different assembly modes. This value is on the same level of the best performing parallel robots commercially available today, as seen in the state-of-the-art section (Table XXV). Still the authors believe this value can be improved after parameter optimization. Parameter fine tuning can also be used to shape the manipulator workspace to suit specific requirements. Such manipulator can be used for fine manipulation or digital fabrication tasks such as large scale 3D printing, laser cutting or pick and place.

The development of the architecture was performed from the choice of limb and joint pairs to kinematic and dynamic analysis and modelling. For the PKM property evaluation and design, a novel methodology was presented. This method, based on an Interval Analysis algorithm, was explained in detail, and applied to the parallel manipulator for demonstration purposes. It proved to be a useful and efficient tool for the analysis and design study of the parallel manipulator, and can be used not only for this PKM but also for any other parallel architecture. With the results obtained, one can design any PKM machine being sure that its kinematic parameters ensure the required performance over its workspace. The advantage of having sets of values for these parameters is that one can choose the nominal values for the PKM kinematic parameters to be in the middle of the resulting sets, thus having some margin of error to consider the manufacturing tolerances. These geometric uncertainties are unavoidable during the manufacturing process, and may

not be compensated by calibration, thus severely affecting the overall behavior of the manipulator.

However, there is still room for improvement of the proposed algorithm. Failure of the algorithm may occur if the terms of the inclusion function have a very complex form. Indeed interval analysis will usually overestimate the ranges for these components and the size of this overestimation increases with the complexity of the analytical form of the terms. A consequence of this overestimation is that the procedure may fail to determine if all solutions of the linear systems are included in the set of solutions, even if the size of the ranges for the geometry and workspace parameters is small. Another possible cause of failure is due to not taking into account the dependency of the components in the inclusion function. While some strategies employed to improve the efficiency of the proposed algorithm are discussed and employed, it can still be further improved by using different filtering methods or different solvers, such as RSolver[212],[228], IBEX [229],[230] and Alias[231], although this was not explored further in this dissertation work.

The implementation of the manipulator, which is the subject of the next chapters, allows validation of the theoretical models here presented, including not only the kinematic models, but also the property workspaces.

Chapter 4

Implementation

This chapter is dedicated to the implementation of the SCALA. All the mechanical, mechatronics challenges and solutions are presented and discussed, for all three generations of SCALA prototypes developed. The first section is dedicated to the realization of the SCALA prototypes, including both agents and scaffold elements. Second section shows the implementation of the parallel manipulator. The third section is about the system electronics and control. The fourth section describes the SCALA as a vision system. The fifth section is dedicated to multi-agent control and path planning. The last section details the costs for the SCALA prototype and a full scale system setup.

4.1 Developed Prototypes

The concepts explored in Chapter 2, established the basis for detail design and development of the SCALA prototypes. Three generations were implemented, all sharing the same philosophy of using four gearmotors to drive the agents, on a bi-dimensional rail mesh, through a rack and pinion drive system. Electronics also remained the same in all generations. All SCALA mobile agent prototypes used four magnetic encoders, on board Li-Po battery or tethered power feed, and a homemade processing and control board, with wireless communication.

However, throughout the generations, the designs and materials employed evolved, in order to improve the system performance.

4.1.1 Generation ONE

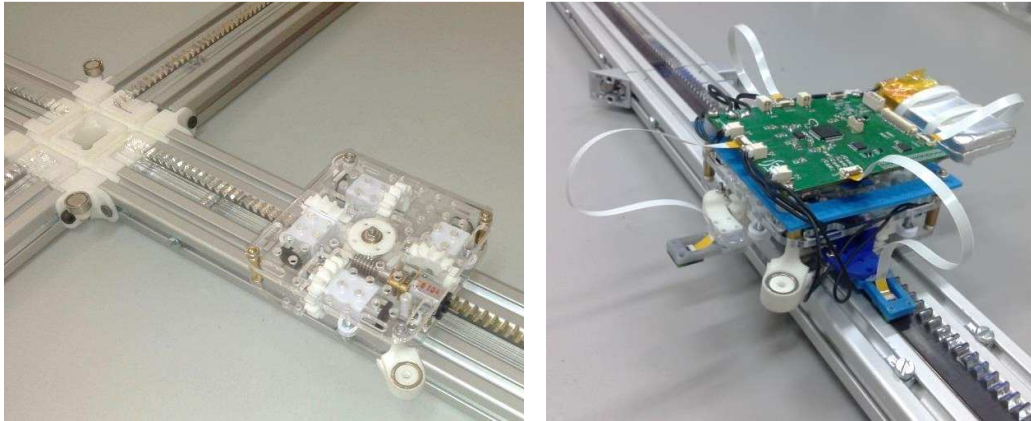


Figure 4-1 – SCALA generation ONE prototype.

In the first generation prototype, shown in Figure 4-1, the rail was made from commercially available aluminum extruded profiles from *ITEM* [232]. This solution proved to be relatively cheap, with a rail cost of approximately $30\text{€}/\text{m}$ (already including rack and magnetic strip costs). Because the magnetic encoders were placed outside the agent body, a single magnetic strip was required and placed in the middle of the rail. The M1.5 rack was made from 6mm laser cut acrylic and placed in the center of the rails. The junction was 3D printed using Selective Laser Sintering (SLS) technology, and was made in polyamide [233], with a cost of 30€ . The agent sliders and the M1.5 16T drive gears were also 3D printed in polyamide using SLS technology. This fabrication method allows manufacturing accuracies in the range of $\pm 0.15\text{mm}$. Both the agent and the junction possessed integrated magnets, with the purpose of aligning the robot in the middle of the junction. This passive and no contact solution was preferred to using plungers, as it does not offer a large resistance to the agent movement. By alignment of the magnetic fields, the agent is precisely positioned in the center of the junction, as shown in Figure 4-2.

The mobile agents were modular built on three levels, separated by 3mm laser cut acrylic plates, as shown in Figure 4-3. The base level possesses the slider which goes inside the rail. The second level encloses the drive motors, the magnetic encoders and the magnets for junction alignment. The third level served as a support for the PCB to control

the agent and the batteries. For this first prototype, no tools were used, since its purpose was to test and validate the drive and localization systems. The detailed drawings of the generation ONE prototype of SCALA are available in the Appendix A1.

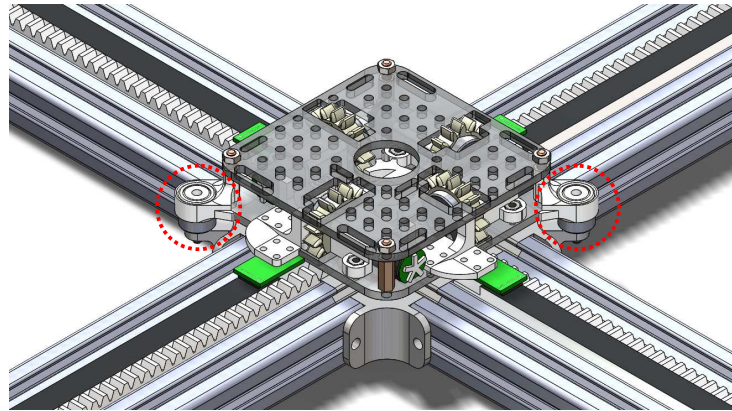


Figure 4-2 – First SCALA prototype agent model positioned in the junction center with the magnetic alignment system.

Initial tests revealed that using 3D printed junctions and sliders was not optimal. Due to the high tolerance in the manufacturing of these parts, junction crossing was very difficult to achieve, with most trials resulting in the robot getting stuck.

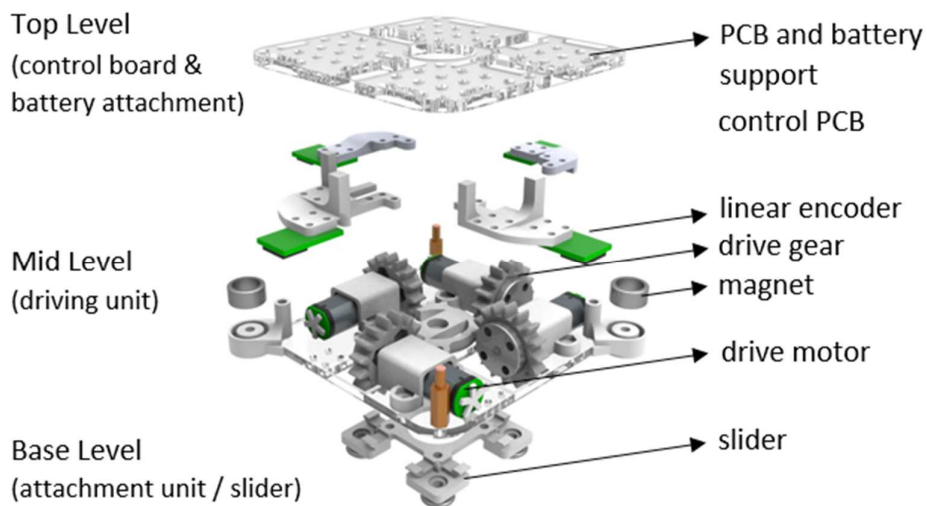


Figure 4-3 – Exploded view of the first SCALA prototype agent, showing its components.

This effect was even worse due to the high friction between the sliders and the junction, both made of polyamide. However, the localization mechanism of the robot, relying on magnetic encoders, proved to be very effective, as well as the passive mechanism to help the agent approach the center of the junction, using magnets. Using standard extruded aluminum profiles also presented a challenge for the placement of the localization solutions and the rack in the rail. Using a custom made profile, would allow to optimize the displacement of the embedded elements in the rail.

Although this prototype proved that the concept was feasible, the choice of materials and manufacturing processes would need to change, in order to obtain a functional system.

4.1.2 Generation TWO

In the prototype for the SCALA second generation, the rails and junctions were custom fabricated in a CNC machine, in aluminum, shown in Figure 4-4.



Figure 4-4 – SCALA generation TWO prototype, showing the mobile agent and custom made rails and junction, made in a CNC machine.

To reduce the friction, the sliders were also made in a CNC machine, in Polytetrafluoretilene (PTFE), a very low friction and self lubricating composite material. This solution enabled to achieve lower manufacturing tolerances (in the range of $\pm 0.01mm$) and to make rails, junctions and sliders at the same time. The advantage of using custom made profiles is that it becomes easier to integrate localization, drive and power

solutions on a smaller profile, as opposed to using standard elements, as shown in Figure 4-5. However, production costs are much higher, with an approximate cost of 400€/m for the rails, 150€ per junction and 50€ per slider. Nevertheless, after the rail design is fixed, one can extrude the rails to reduce the cost, as further explained in section 4.7.

Once again, the M1.5 rack was made from 6mm laser cut acrylic and placed in the center of the rails.

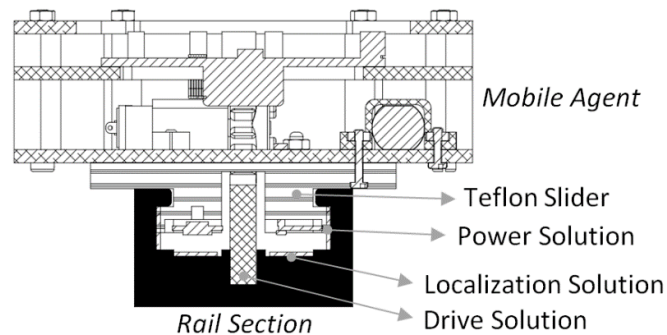


Figure 4-5 – Custom made rail and slider profile for the SCALA system, with embedded drive, power and localization solutions. Power solution was not tested.

This time, the mobile agents were modular built on four levels, separated, once again, by 3mm acrylic plates, as shown in Figure 4-6. The base level contained the slider and four magnetic encoders, which were integrated on the slider, resulting in a more compact design. This meant, however, that two magnetic strips were needed per rail. The magnets, for junction alignment, were also maintained and integrated on the agent's slider, although testing revealed they were no longer necessary given the high manufacturing precision and consequent slider/junction fit precision. On the second level rested the driving motors and the batteries, which were moved below to lower the agent center of gravity. Third level contained, once again, the control and communications board. The top level was used for modular tool attachment. The detailed drawings for the second generation prototype of SCALA are available in the Appendix A2.

The changes on the arrangement of the encoders and the battery, allied to the increased manufacturing quality of the rails and slider, resulted in a more efficient and smoother locomotion on the rails.

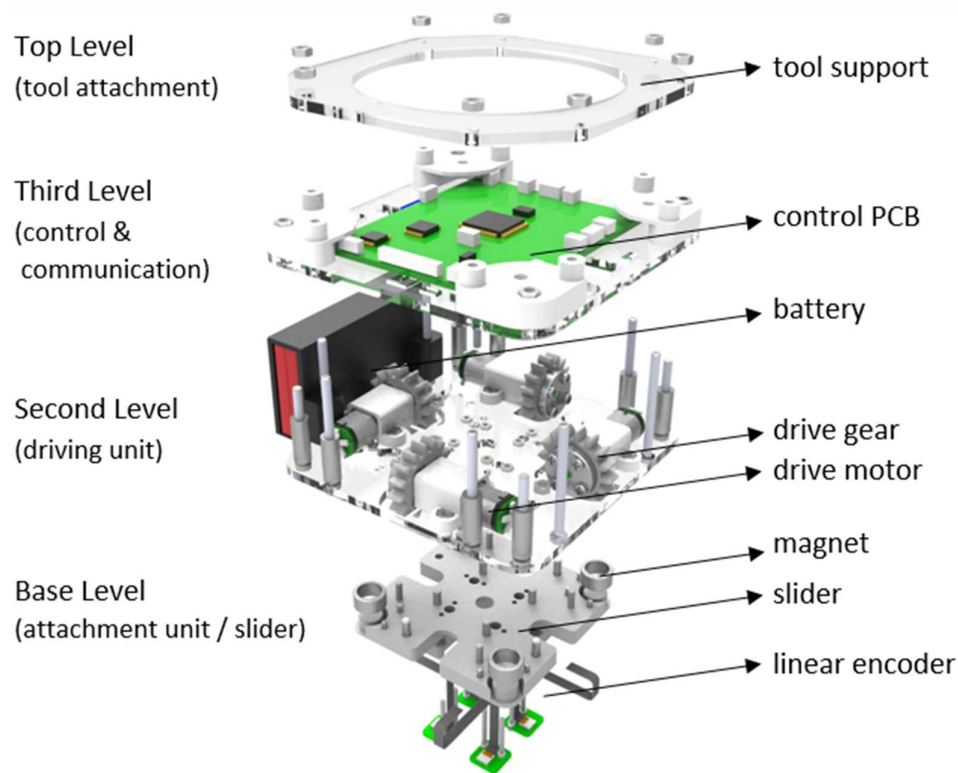


Figure 4-6 - Exploded view of the second SCALA prototype agent, showing its components.

However, since the agents' chassis was mostly made of acrylic laser cut parts, it was not stiff enough, often bending due to the torque of the drive motors. It was also not rigid enough to support the tools and the parallel manipulator. A more robust solution was needed to improve the performance of the system.

4.1.3 Generation THREE

The third generation of the SCALA system maintained most aspects of the previous generation, including the location and arrangement of the electronics and the exact same scaffold. Changes included only the design and materials used for the mobile agent, shown in Figure 4-7. As before, the mobile agents are modular built on four levels.

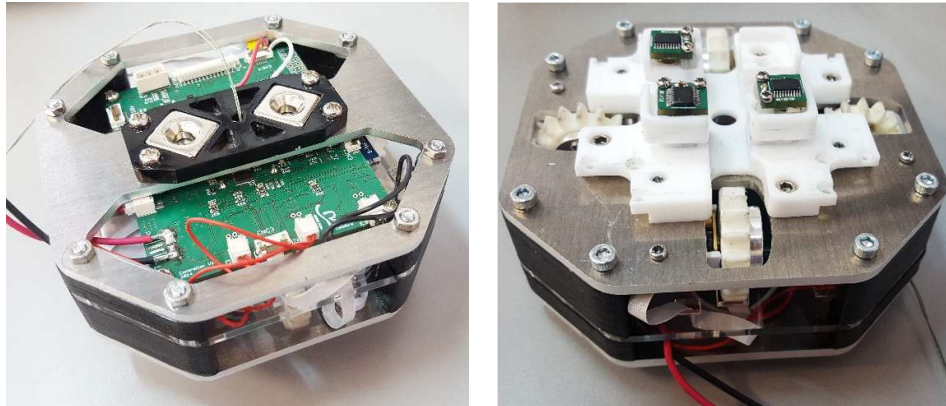


Figure 4-7 - SCALA generation THREE agent prototype, showing the top and bottom of the mobile agent.

This time, however, *3mm* aluminum plates were used to separate these levels. This chassis reinforcement effectively eliminated the problems with the previous generation, and allowed the agent to support both the tools and the parallel manipulator. The testing results of this system are discussed in the next sections. The detailed drawings of the third generation prototype of SCALA are available in the Appendix A3.

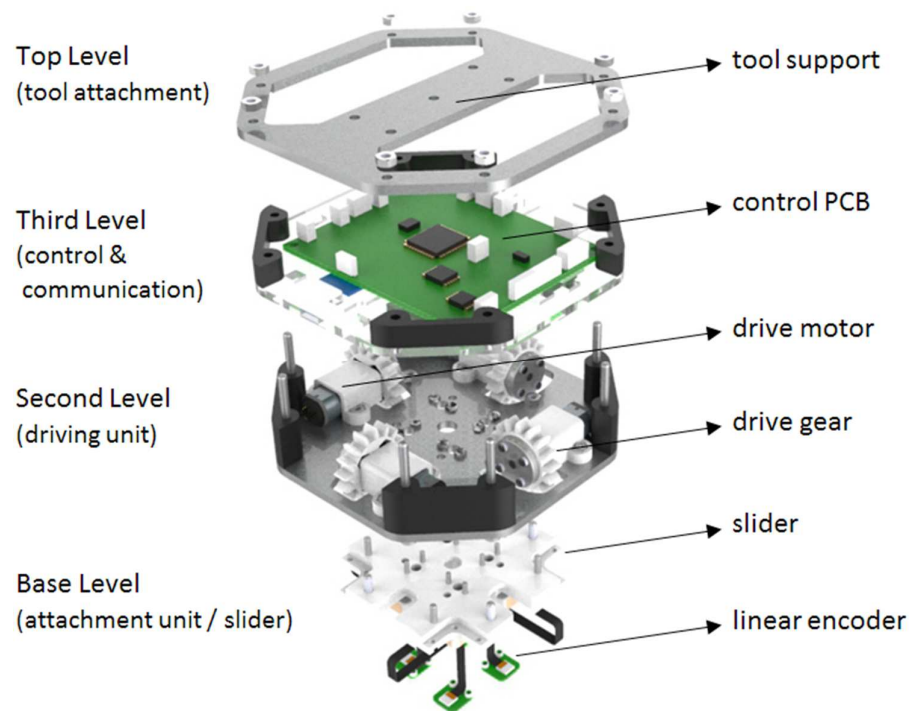


Figure 4-8 - Exploded view of the third SCALA prototype agent, showing its components.

4.2 Reconfigurable Manipulator Prototype

The kinematic and dynamic properties of the parallel manipulator were discussed during the conceptual design, but there are still uncertainties and parasitic errors on non-wanted DOF (orientation), which are a function of the mechanical tolerances, system backlash, or implementation defaults. Some of the mechanical tolerances and backlash between components are unavoidable, even after system calibration, and may severely affect the positioning accuracy, stiffness and overall behavior of the manipulator. The only way to mitigate these undesired effects is to adopt tight manufacturing tolerances, when possible, on the several components of the parallel manipulator, including links, joints and end-effector.

In addition, the PKM design should allow modification of the workspace, by quick changing of the link set to another longer link set. That is, the design should afford a modular approach, where one can quickly replace the links of the PKM with a different set. This is especially vital during the prototyping phase.

This section describes the implementation of the SCALA manipulator driven by three mobile agents, and the mechanical solutions adopted in its construction.

4.2.1 Links and joints

The parallel manipulator links are one of the most important elements of the system, providing the connection between the agents and the end-effector and transferring the movements of the former to the later. The links, as all moving parts of the manipulator, should be as light and stiff as possible.

Several link materials were considered, but the chosen solution was *8mm* carbon fiber tubes, as they offered a good compromise between mechanical properties, weight and cost, as shown in Table X.

Table X –Link material properties, taken from various manufacturer catalogs.

	Aluminum (6061-T6)	Steel (316L SS)	Carbon Fiber*
Density [kg/m ³]	2700	7850	1400
Elastic Modulus [GPa]	68.9	210	175
Poisson's Ratio	0.33	0.3	0.3
Tensile Strength [MPa]	460	990	110
Yield Strength [MPa]	276	1700	469
Hardness [Brinell 3000kg]	95	149-627	120
Cost of 8mm tube [€/m]	2	20	3

*properties vary according to manufacturer and product

Joints are crucial elements of a parallel manipulator, as the precision of the end-effector positioning depends not only on the link length, but also on a correct nodal point. In contrast to a cartesian manipulator, the error on a parallel manipulator is dependent on the end-effector pose within the workspace. Moreover, a small backlash or positioning error on the joint, largely affects the manipulator pose and stiffness, since it is magnified by the length of the PKM links.

The 3-P^{UR} architecture chosen for the SCALA manipulator, depicted for instance in Figure 3-8, is based on limbs with two links arranged in a parallelogram, which possess two joints in their extremities. These joints have two DOF each, which have to be precisely aligned, in order for the parallelogram to function correctly. To select the best joints for the manipulator, several different solutions were considered, as shown in Figure 4-9.

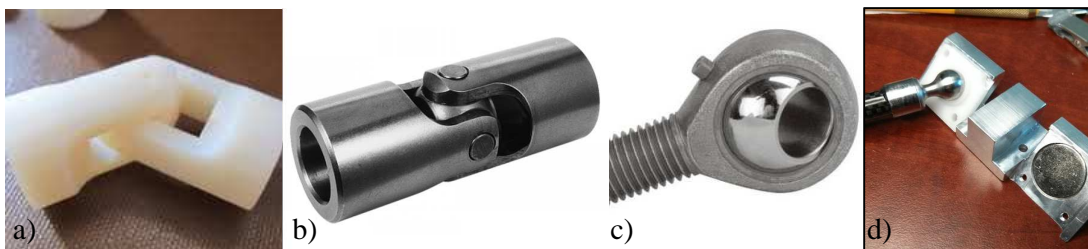


Figure 4-9 – Manipulator types of joints considered: a) 3D printed universal joint; b) industrial cardan joint; c) rod end bearing; d) magnetic joint.

Some home-made parallel 3D printers use printed cardan joints. Based on this technique, they can be made at a very low cost per unit. However, the manufacturing often lacks the required precision. This design is also prone to backlash and misaligned nodal points, for vertical and horizontal axis.

Many remote controlled cars, helicopters and boats use machined industrial cardan joints. They are ready to use, have low friction, and high manufacturing precision. However, they have high costs per unit and their design only allows the joint to be tilted 90° in four directions. In the intermediate directions, the usable angle is limited to about 30° . For this reason, they have to be constructed in a 45° angle to minimize joint limits and have to be mounted in the optimal working direction.

Some manufacturers such as IGUS [87] provide rod end bearing joints made from self-lubricant plastic. As in industrial cardan joints, they are ready to use, have very low friction, and high precision. However, this joint design presents a severe disadvantage since at rotation axis the joint is designed for endless rotation, but at the tilt axis the joint is limited by construction, as shown in Figure 4-10. As reported in the manufacturer documentation, tilt angle is limited to $\pm 30^\circ$ [234]. Any parallel machine pose requiring a tilt angle of its joints superior to that, is simply not possible to achieve. As a result, machines using this type of joint have a limited work area.

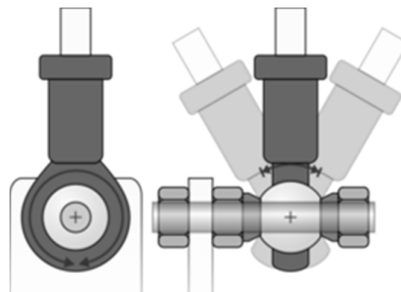


Figure 4-10 – Range of motion in the rotation and tilt axis of the rod end bearing [235].

Thus, to take full advantage of the manipulator workspace, one requires a high range of motion from the joints. There is also a high number of joints, so it is important that they have high precision and no backlash, to limit the positioning errors in the tool.

Magnetic joints are being used in many parallel machines for their advantages. They are simple, low cost, easy to assemble and disassemble, and do not suffer from backlash. Therefore, good stiffness and precision can be achieved, while the possibility of quickly changing the links, for the sake of modularity, can be fulfilled. They consist on a metal ball which is attracted to a cylindrical magnet, and slides over the surface of the magnet. Usually, this magnet, or the resting place of the metal ball has a groove to maintain the ball in place, as shown in Figure 4-11. These joints exhibit a high range of motion in all directions, which also depends on the relative diameters of the ball and link used.

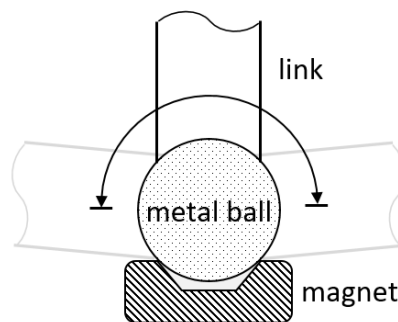


Figure 4-11 – Section view of a magnetic joint, showing its high range of motion.

Their main disadvantage is their limited holding force. One can employ stronger magnets with the drawback of increasing the joint friction and possibly shorten their life cycle due to abrasion. To solve the abrasion problems, one can place a low friction self-lubricating material between the metal ball and the magnet. The metal ball should also possess a high quality surface finish and sphericity, for superior joint performance and longevity.

The Table XI summarizes the advantages and disadvantages of the common joint variations used in parallel machines. To fulfill the SCALA requirements, the only suitable type of joint is the magnetic joint. This solution allows to switch between different link lengths in an easy and fast fashion, with no need for tools. With magnetic joints, the user can also easily switch the end-effector to have either a 3D printer, a manipulator or a laser cutter.

Table XI – Comparison between joint variations used in parallel machines.

Joint Variations	Advantages	Disadvantages
DIY Cardan Joint	<ul style="list-style-type: none"> • Very low cost • Can be printed to any size and shape 	<ul style="list-style-type: none"> • Highly prone to manufacturing and assembling errors • Prone to backlash and misaligned nodal points for vertical and horizontal axis
Industrial Cardan Joint	<ul style="list-style-type: none"> • Low friction • High precision 	<ul style="list-style-type: none"> • High cost per joint • Have to be constructed at a 45° angle to minimize limits • Have to be mounted in the optimal working direction
Rod End Bearing	<ul style="list-style-type: none"> • Low friction • High precision 	<ul style="list-style-type: none"> • Limited work area
Magnetic Joint	<ul style="list-style-type: none"> • Precision by design • No backlash • Implicit correct and well known nodal point • Low cost • Simple construction • Easy assembly and disassembly 	<ul style="list-style-type: none"> • Limited holding force • Increased friction • Permanent magnets are sensitive to shock and high temperatures

This was the solution adopted for the manipulator joints. For the metal balls, 10 grade 10 mm bearing steel spheres were used. These fit on N35 grade Neodymium 15mm block magnets, from HKCM [236]. Magnetic joints such as these are of spherical type, thus possess 3DOF. In order to suppress one degree of freedom, a bridge between two links was used. A cable tensioned with spring was used to give more rigidity to each parallelogram, and also acts as a safety feature in case of system breakdown.

4.2.2 End-effector and tools

The end-effector was designed so that the user can easily switch its modular tools. It consists on a 4mm thick laser cut aluminum plate, for its light weight and stiffness properties. It then possesses a tool attachment, 3D printed in ABS, where the user can attach a gripper, for pick and place applications, a plastic filament extruder, for 3D printing applications, and a laser for cutting or engraving tasks.

The gripper was custom designed for SCALA and consists on a single actuator (Pololu micro motor[237]) three finger claw, as shown in Figure 4-12. Its body was 3D printed from ABS. This tool is capable of not only grabbing any object up to a diameter of $80mm$, but also carry a pen or a laser pointer. It also included a $30mm$ electromagnet, from Eclipsemagnetics[238], for picking metallic objects.

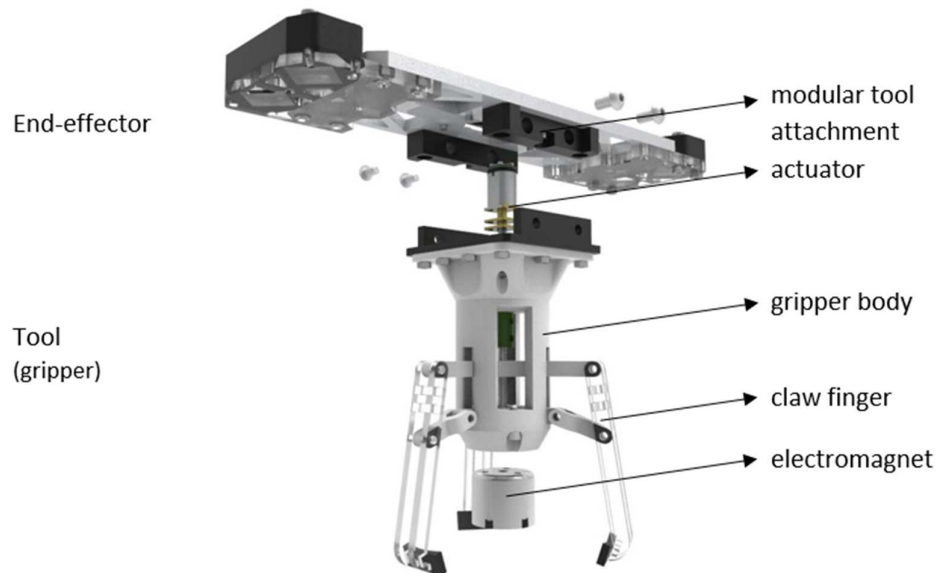


Figure 4-12 - Exploded view of the SCALA manipulator end-effector with gripper.

The plastic filament extruder used was a heatcore unibody extrusion kit from BQ[239]. A complete description and the main specs of the extrusion kit are available in the Annex F. A 3D printed ABS support was made for the kit. The assembly is shown in Figure 4-13.

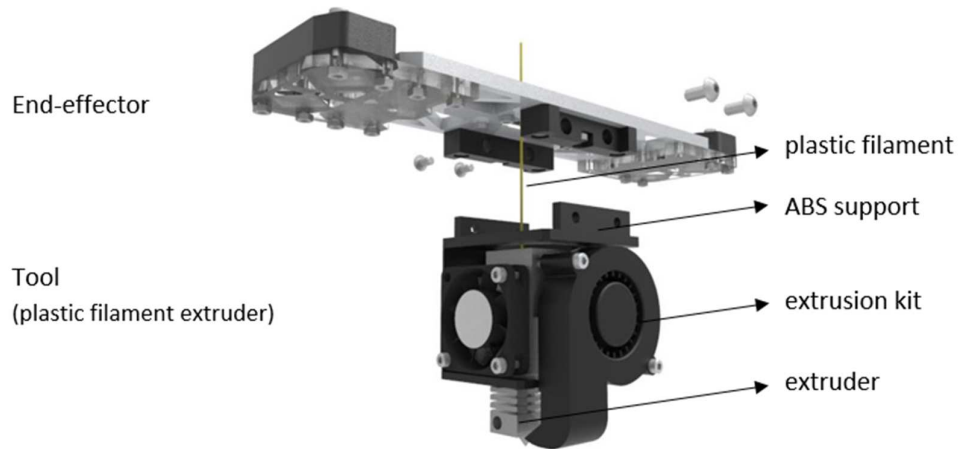


Figure 4-13 - Exploded view of the SCALA manipulator end-effector with the unibody extrusion kit.

For the laser cutter tool, a PL TB450B blue laser diode from OSRAM [240], was used. This laser has an optical output power (continuous wave) of $1.6W$, and a typical emission wavelength of $450nm$. The complete laser specs are included in Annex E. For cooling purposes, a $30mm$ cooling fan was mounted on top of the laser module. An acrylic support was cut to hold both the laser assembly and a driver board. This is shown in Figure 4-14.

The detailed drawings for the SCALA manipulator components, end-effector and tools are available in the Appendix A4.

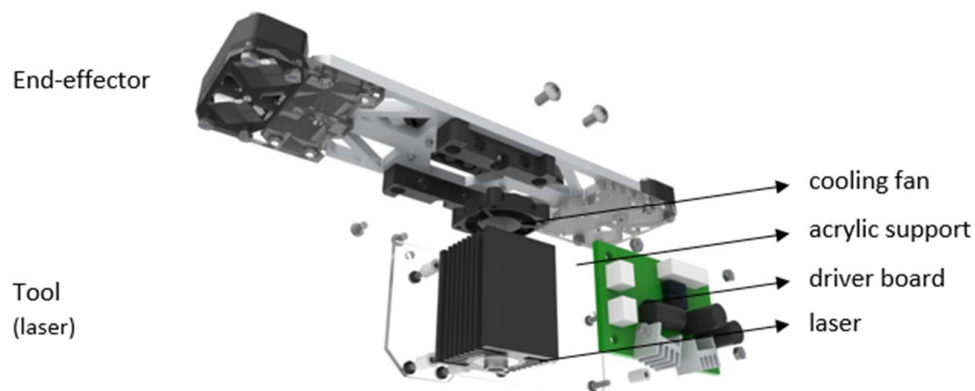


Figure 4-14 - Exploded view of the SCALA manipulator end-effector with laser.

4.2.3 Prototype



Figure 4-15 –SCALA parallel manipulator prototype.

The prototype for the parallel manipulator is shown in Figure 4-15. Some details of the mechanical solutions adopted are shown in Figure 4-16. The dimensions and mass of the SCALA manipulator components, including limbs, end-effector and tools, are presented in Table XII.

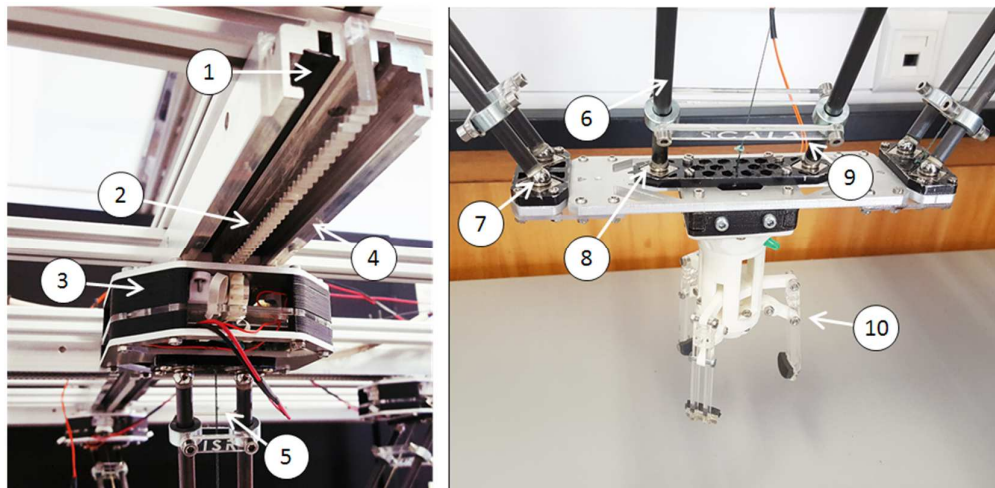


Figure 4-16 –SCALA prototype details: 1– magnetic strip; 2– acrylic rack; 3– mobile agent; 4– aluminum rail; 5– tension string; 6– carbon fiber link; 7– steel sphere; 8– magnet; 9– bridge; 10– gripper.

Table XII – SCALA manipulator component dimensions and mass values.

Components	Dimensions [mm]	Mass [g]
Limbs	8 x 400	28
End-effector w/ gripper	130 x 225 x 60	352
End-effector w/ extruder	100 x 225 x 64	736
End-effector w/ laser	70 x 225 x 60	385

4.3 System Electronics and Control

In this section, the system electronics and the control strategy implemented are discussed in detail.

4.3.1 Drive motors

SCALA mobile agent prototypes use four DC motors for their drive system. The motors were selected from the range of brushed DC gear micromotors from Pololu [237], considering a desired velocity of $0.10m.s^{-1}$ and $15N$ driving force (enough to allow the manipulator to handle $1kg$ payloads in most of its workspace). The micromotor range from Pololu offers powerful and robust motors with small dimensions, which are perfectly suited for this type of prototypes. The DC motor itself is always the same, but it comes coupled to different metal gearboxes, thus having a range of speed and torque performances. The selected micromotors, shown in Figure 4-17, are coupled to a small metal gearbox with a $298:1$ reduction ratio, offering a balanced compromise between speed and torque with a low power consumption. The keyspecs of the motors are: $100RPM$ and $120mA$ with no load, $0.5N.m$ and $1.6A$ at stall, at $6V$. The motors full spec sheet is available in the Annex A.

Each motor has a $24mm$ nominal diameter drive gear, coupled to its shaft. This drive gear has a 16 teeth and a 1.5 metric size, and fits on a 1.5 metric size rack. Running the motors at 25% of the stall torque and considering a typical efficiency of 97% for a typical rack and pinion drive system[241], one obtains a maximum theoretical drive force of $19.8N$, which in reality, and given the friction on the drives, translates to around $15N$.

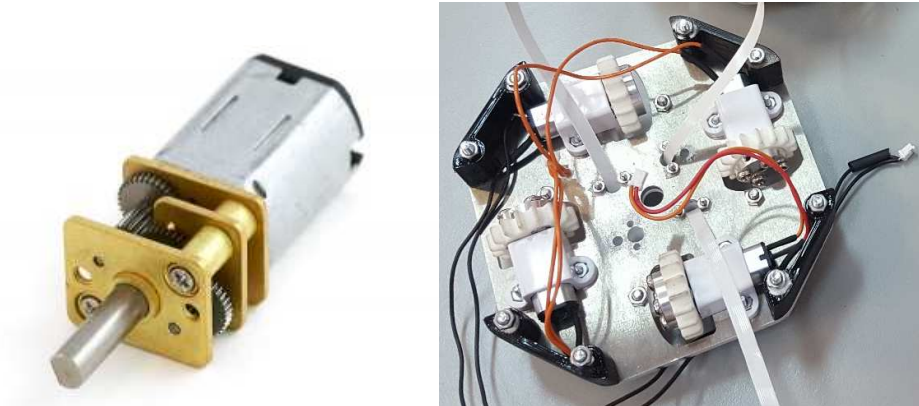


Figure 4-17 – Pololu micro motors used and their assembly in the SCALA agents, with the driving gears coupled.

They also ensure a maximum theoretical speed for the agents of $0.12m.s^{-1}$, although measured maximum speeds were equal to $0.10m.s^{-1}$.

4.3.2 Agent localization system

The real-time localization system for the SCALA agents relies on the so-called *Hall effect*, which can be used to create a low-cost non-contact sensor to measure linear motion[242]. Since it is a contact-less technology, it has the benefits of long life and high reliability, due to limited component wear and degradation. It also has advantages over optical or laser based systems, as it is not affected by dust or different lighting conditions, so it is a robust solution for an industrial application.

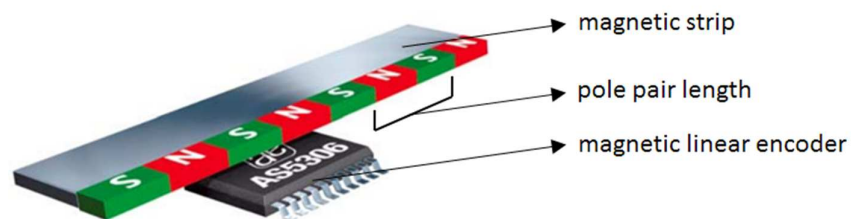


Figure 4-18 – AS5306 with Magnetic Multi-pole Strip Magnet for Linear Motion Measurement [243].

The MS20-150 magnetic strips, from Austria Micro Systems (AMS) [243], with pole pair lengths of $4mm$ (see Figure 4-18), are embedded on the rails and junction. To read the strips, each mobile agent possesses four AS5306 magnetic linear sensors with 160

pulses per pole pair length, installed on the slider, as shown in Figure 4-19. This combination allows a maximum system resolution of $0.025mm$. The datasheets for the magnetic encoders and strips used, are available in the Annex B and C, respectively.

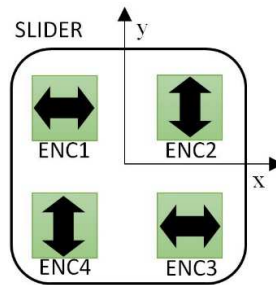


Figure 4-19 - Encoder placement scheme on the mobile agent slider. The arrows indicate the working direction.

To increase the stability of the encoder signals and reduce noise and jitter, one can average multiple readings, at the expense of resolution. In this system, two distinct sets of magnetic strips which are read by two magnetic encoders are used for each moving direction. One set (magnetic strip A) is continuous and is used for incremental localization on the rail, while the second set (magnetic strip B) has gaps in predetermined spaces, as shown in Figure 4-20.

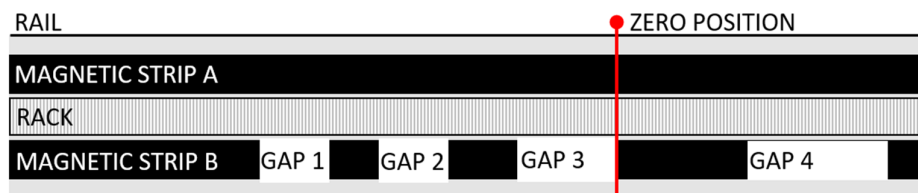


Figure 4-20 - Section of the rail showing the initial calibration system. Gaps 1 and 2 are smaller than gap 3, meaning they are located before zero position. On the other hand, the gap 4 is bigger, meaning it is located after zero position.

This second set is used to reset the incremental error on the encoders and also for initial calibration when the system runs for the first time. The process works as follows: each agent moves in a random direction until it detects a gap. Then, the encoders are reset and the length of the gap is measured by the encoder on the continuous strip. The zero position is determined at the end of a gap with a specific length. If the measured length is

smaller than this specific length, it means that the robot must travel further to reach position zero. Otherwise, if the measured gap is bigger than the specific length, then the robot must move backwards to reach its position zero.

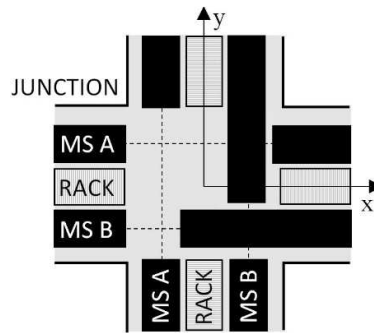


Figure 4-21 - Arrangement of the magnetic strips to ensure there is always one encoder working during junction crossing.

To detect a junction, the strategy adopted was to place a gap on the magnetic strip A, to differentiate from the calibration gaps. Due to the crossing of perpendicular magnetic strips on the junction, some gaps will exist. However, and since there are four encoders, if one arranges the encoders and magnetic strips as depicted in Figure 4-19 and Figure 4-21 respectively, there will always be at least one encoder per moving direction reading the position, so no tick counts are lost during junction passing and there is no prejudice on the localization precision.

4.3.3 Power

In SCALA generation THREE, each agent is fed $9V$ at $0.3A$ through a cable. Alternatively, a battery can be used. However, the rails are designed and ready to have embedded power lines, as shown in Figure 4-22. These can constantly feed energy to the moving agents through copper brushes on the sliders (Fig. 11), thus eliminating the need for large batteries or power cables. Still, small batteries or capacitors are required for an event of a power failure, and also for junction crossing, were due to the gaps, the power lines are interrupted.

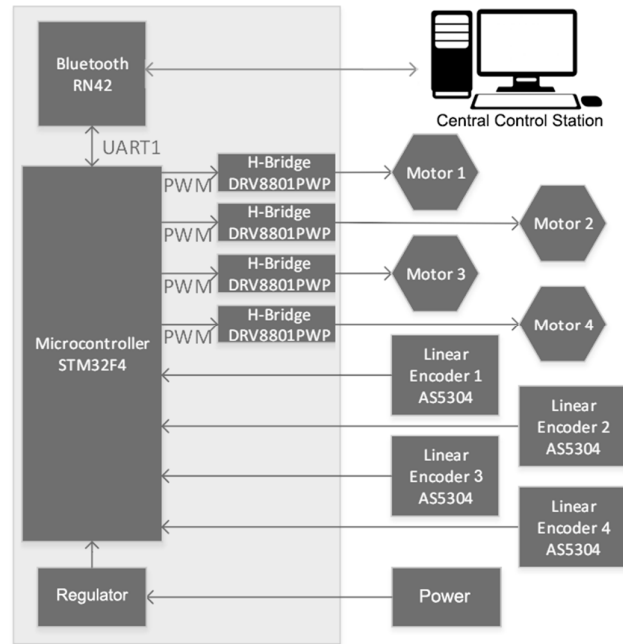


Figure 4-24 – Control architecture for the SCALA mobile agents.

As can be seen in Figure 4-24, each motor is derived by one H-bridge. The 4 hall sensors are installed in the slider and wired to the PCB. A RN42 Bluetooth communication module[245], integrated on the control PCB, enables the agents to send and receive wireless signals to a central control station in real time. This central control station is responsible for multiple agent coordination, path planning and task allocation. This reduces the amount of information each agent needs to process, and improves the workflow. The central control can also receive information from surveillance agents on the mesh, and identify any problems, disturbances or malfunctions in the system. Then it can decide the best route for each agent in the rail mesh, taking into account factors such as task priority, task execution time, minimum distance of travel, traffic ahead or disturbance to other agents, as will be described in the multi-agent path planning section.

Low level control

Each SCALA agent can work as an independent unit, thanks to its processing and control board. This board can interpret signals from the encoders and autonomously control the agent motors, without needing to communicate with the central control station.

This is due to the low level control scheme implemented in the SCALA agents. The control architecture was implemented within a *MSc* dissertation work[246].

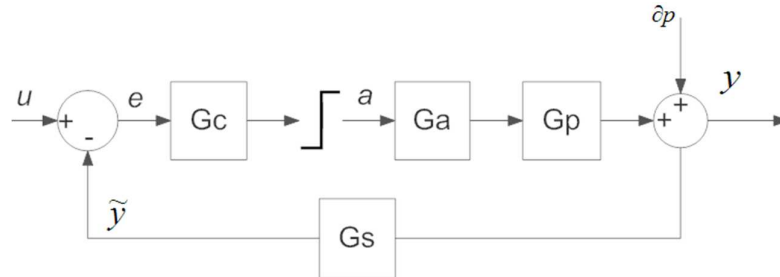


Figure 4-25 - Mobile agent individual closed loop control scheme.

The low level control scheme is illustrated in Figure 4-25. It consists on a standard configuration with four main transfer function blocks: the controller G_c , the actuator G_a , the system G_p and the sensors G_s . The sensors G_s are the four magnetic encoders, which measure the output of the system (agents position on the rail), and close it in retro-action with the reference position input u . The result of the retro-action produces a new signal e , which defines the error and is the input quantity of the controller. The controller itself produces the output command a , that is directly passed to the actuator, the DC motor. Then, to account for any external disturbances on the agents⁶, a summing node is added immediately after the process block. The transfer functions, which model G_a and G_p , were obtained through direct evaluation of the input and output signals and system parameter identification. In this specific case, a step reference signal a of 100 was provided, which corresponds to the amplitude of the PWM square signal which drives the electric motor, and in output y , the position of the agent on the rail with respect to the set zero reference, that is given in mm , was collected. It is important to underline that, due to the system configuration, the only acquirable signals are the input and output (in the G_a/G_p open-loop), so no internal signal can be acquired, such that the final transfer function will take into consideration the overall system G_a plus G_p .

⁶ These external disturbances can be, for instance, when three agents are connected and forming the parallel manipulator, each agent is subject to static and dynamic coupling forces, resulting from the movement of the other agents and the moving platform.

High level control

When synchronization between several agents is required, as for instance, to drive the parallel manipulator, high level control is needed. For this, a centralized control, shown in Figure 4-26, takes into consideration the three different errors, and provides the correct PWM saturation speed, such that all agents achieve their position at the same time.

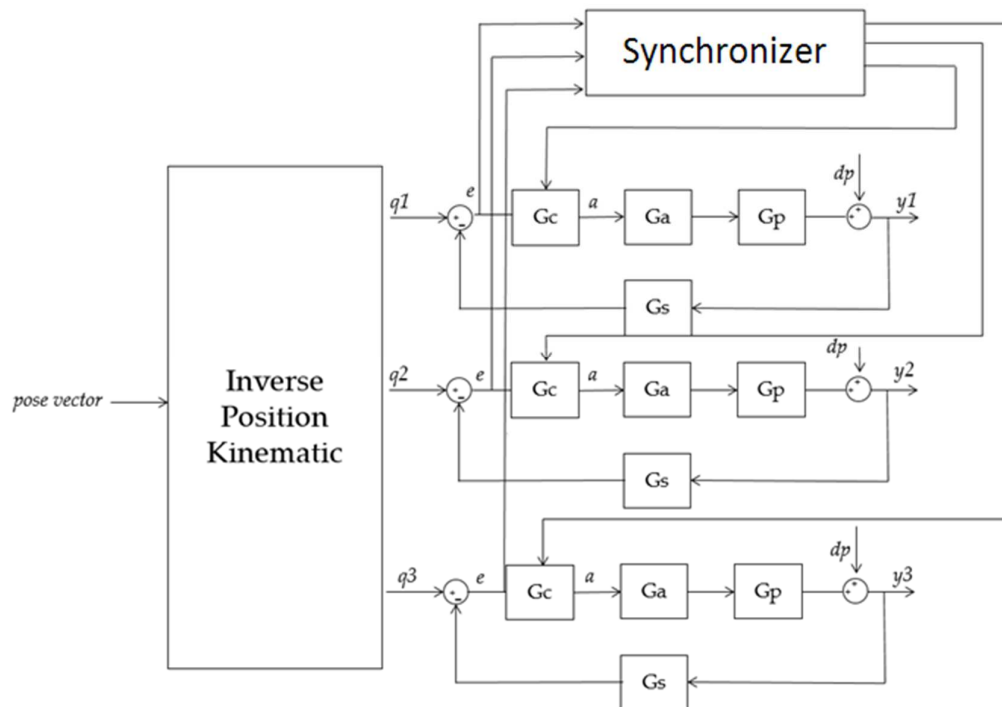


Figure 4-26 - High level centralized control scheme.

This is done by software, by using a synchronizer with a PID (proportional integrative and derivative) controller, whose parameters online tuning is made through *Ziegler-Nichols* method[246]. The SCALA control was implemented in *Microsoft Visual Studio Community 2015*. A state machine using a timer, set to a frequency rate of 33Hz, constitutes the system's real time control implemented. In the timer function, the systems inputs are read and processed and the commands are sent to all agents. For the user to control the system, a Graphical User Interface (GUI) was conceived.

4.3.5 Graphical user interface

A GUI, shown in Figure 4-27, was designed so that the user can control the SCALA agents and manipulator. The program shows the communication data it receives in real time from all agents, including current status, task, encoder signals and voltage. Then, the program determines the position of each agent on the rail mesh and represents it graphically, again in real time, in the image of the mesh located on the upper right corner. The user can command each agent separately or all simultaneously, to perform pre-programmed tasks, which include moving the manipulator to a specific location in its workspace. In the lower left there are four buttons, one to open or close the Bluetooth communications, one to manually reset the agent positions, one to send them to "Home" positions, a button for the agents automatic calibration and positioning, and a large red "STOP" button to immediately cease the movement of all agents.

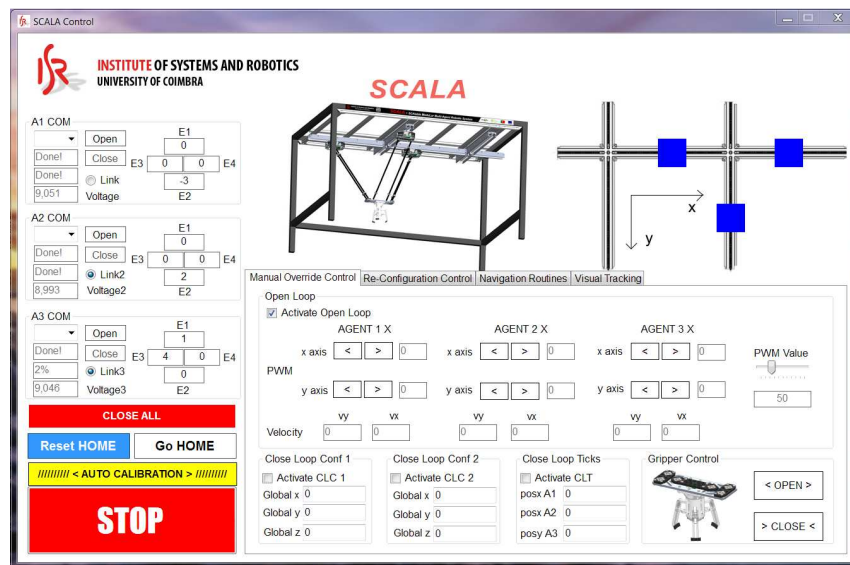


Figure 4-27 - Graphical user interface designed for multi-agent control.

Control commands for the agents and manipulator are divided into four separate sections.

First section, shown in Figure 4-27, allows a manual control of the agents, manipulator and manipulator gripper, by open loop (the user directly sends the agents

forward or backward at a set speed), or closed loop (the user sets the coordinates where he wants the agents or the end-effector to move to).

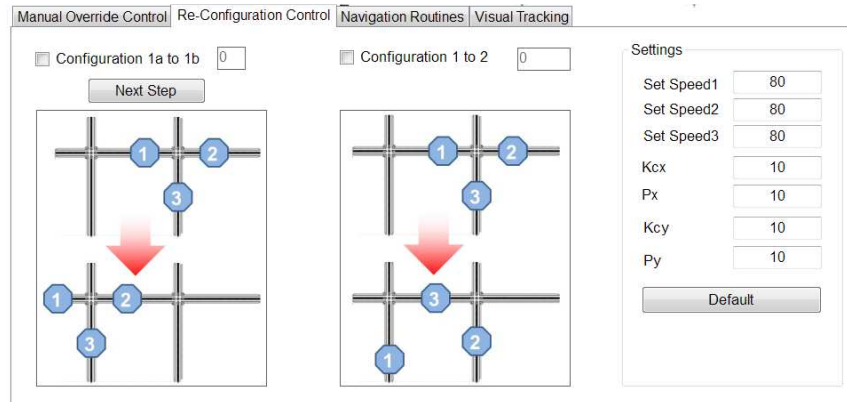


Figure 4-28 - GUI for the manipulator reconfiguration control.

The second section, shown in Figure 4-28, is about the reconfiguration control. This allows the manipulator to automatically change its configuration to access points that are outside its workspace. The agents automatically move to other rails to perform this change, in a synchronized fashion. On the right, a settings panel allows the user to choose the PID parameters for the agents' control.

The third section, shown in Figure 4-29, is the control for the agents or the manipulator to perform predefined tasks, such as pick and place, trajectory following or 3D printing. In the pick and place task, the agents and the parallel manipulator follow a programmed script, consisting of several events, such as move to point x , open griper, return home, etc. In the trajectory following task, the user can run a *G-code*, containing the coordinates for the path the manipulator should follow. This is used, for instance, in 3D printing, laser cutting, or other digital fabrication tasks. The 3D printing section allows to control several parameters of the process, such as layer thickness, base plane height and part height, if one desires to print only a part of the entire model.

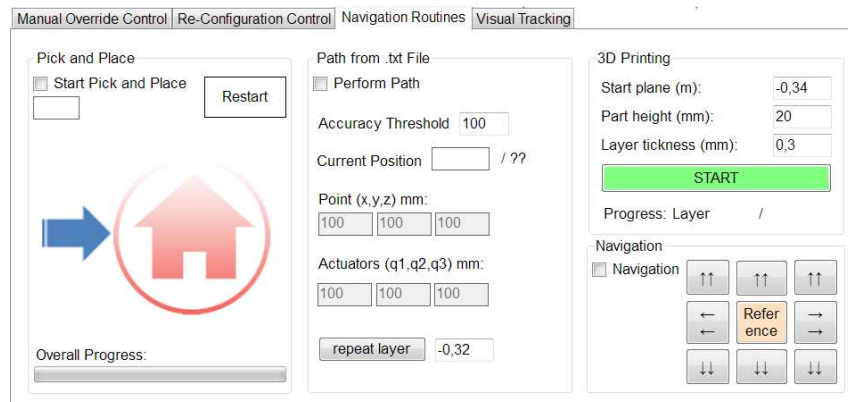


Figure 4-29 - GUI for the task performing control.

The last section, shown in Figure 4-30, is the control of the autonomous surveillance tasks, including the initialization of the vision sensors, the selection of the number of agents to use and other control parameters.

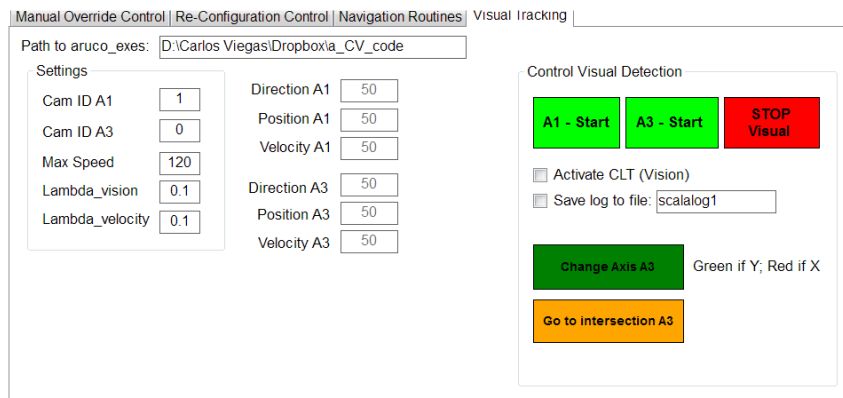


Figure 4-30 - GUI for the vision applications control.

4.4 Vision System

4.4.1 Sensor setup

For applications in the field of vision, a camera was mounted on top of each mobile agent, as shown in Figure 4-31, and directly connected through cable to the central control station.

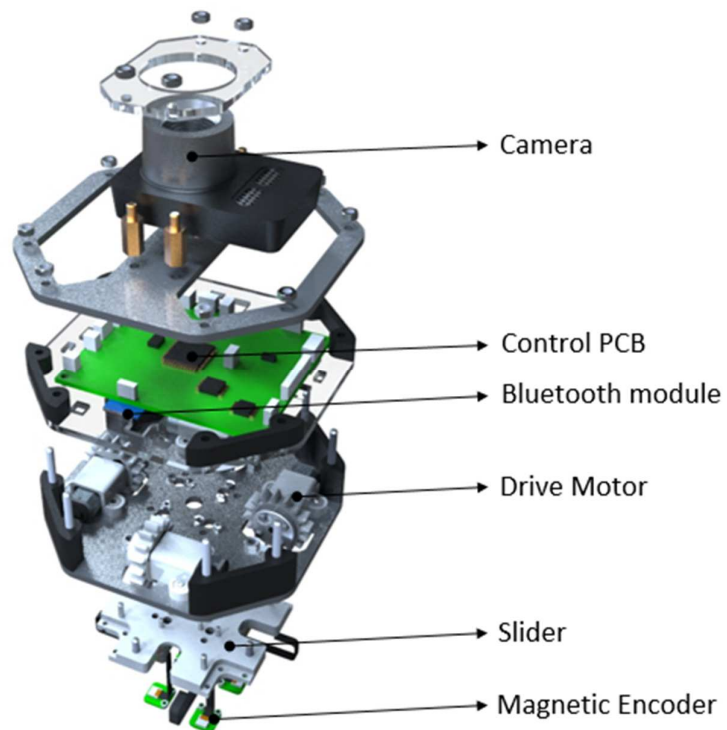


Figure 4-31 – Exploded view model of SCALA surveillance agent, showing its several components.

The vision sensor employed was a Philips SPZ5000 webcam, with a resolution of 1.3 MP (1280 x 1024 pixels), F2.6 and 80 degrees wide-angle lens, capable of capturing video at a maximum resolution of 2.0MP (software enhanced) and at 60 FPS @VGA. The camera orientation is fixed. The SCALA surveillance agent prototype is shown in Figure 4-32.

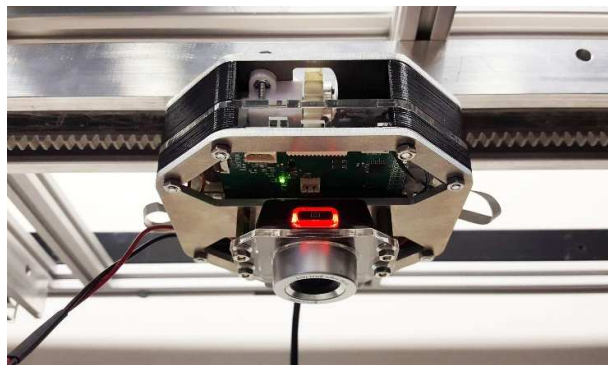


Figure 4-32 – SCALA surveillance agent prototype.

4.4.2 Mobile camera coordination

The vision agents carrying a camera c_i are used in the SCALA vision system to characterize and follow a target o_j .

The *field of vision* (FOV_i) of a camera c_i is a rectangle centered on the camera position, whose dimensions (width and height) are equal to the camera image resolution, as shown in Figure 4-33.

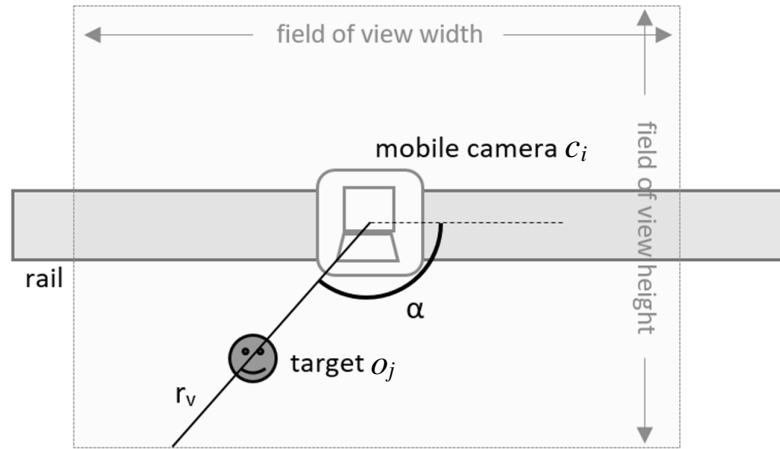


Figure 4-33 - Definition of camera field of vision and viewing range.

The viewing range rv_{cioj} is equal to the length of a line segment, connecting the center of the camera c_i to a point on the border of the camera FOV , and passing by the o_j target center. It can be determined as a function of the inclination angle α of the line:

$$rv_{cioj} = \begin{cases} FOVwidth/2 \times \sec(\alpha), & \text{if } |\tan(\alpha)| \leq 1 \\ FOVheight/2 \times \csc(\alpha), & \text{if } |\tan(\alpha)| > 1 \end{cases} \quad (4-1)$$

A target is in the camera FOV if its distance to the camera $d_{cioj}(t)$ is inferior to the viewing range rv_{cioj} . Once a target enters the FOV of a camera, its current position $po_j(t)$, velocity $vo_j(t)$ and heading $\delta o_j(t)$ are identified, and a priority value wo_j is attributed to it, as illustrated in Figure 4-34.

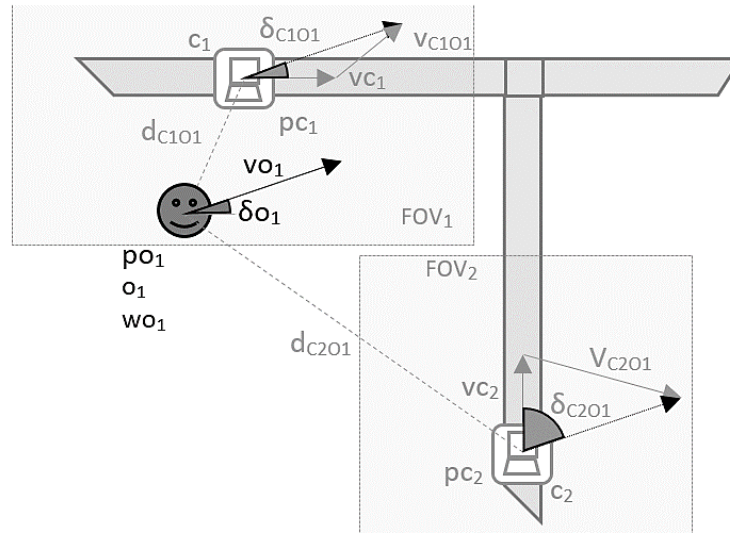


Figure 4-34 - Target o_1 following by mobile cameras c_1 and c_2 .

Camera/target pairing is done using a cost function. A similar approach has been used in [247]. Targets are sorted according to their priority, from the highest to lowest. Then each target is attributed a camera, based on the value of the camera/target utility function $a_{cijo}(t)$. This function is inversely proportional to the energy cost for the mobile camera to capture the target and is time variable, so the pairings can dynamically change to ensure best tracking efficiency.

The energy cost function takes into account not only the target/camera distance $d_{cijo}(t)$, but also their relative velocity $v_{cijo}(t)$ and heading $\delta_{cijo}(t)$. The energy cost is approximated as the expected robot-target distance $\widehat{d_{cijo}}(t)$ after a time period Δt , assuming the relative velocity $v_{cijo}(t)$ to be constant during Δt :

$$\widehat{d_{cijo}}(t) = |d_{cijo}(t) - v_{cijo}(t)\Delta t| \quad (4-2)$$

Where $\Delta t = 1$ second in this work, $d_{cijo}(t) = p_{ci}(t) - p_{oj}(t)$ and the relative velocity $v_{cijo}(t)$ is given by:

$$v_{cijo}(t) = [v_{oj}(t) \cos(\delta_{cijo}(t)) - v_{ci}(t)] \hat{i} + [v_{oj}(t) \sin(\delta_{cijo}(t))] \hat{j} \quad (4-3)$$

Where \hat{i} is defined as the mobile camera movement direction and \hat{j} is its perpendicular direction. Notice that in Figure 4-34, this direction is different for agents c_1 and c_2 .

The relative heading is the angle between the mobile camera movement direction and the target velocity:

$$\delta_{ij}(t) = \angle \hat{i} \overrightarrow{v_0} \quad (4-4)$$

If the relative heading $|\delta_{c_{ioj}}(t)| > \frac{\pi}{4}$ (for instance c_2 in Figure 4-34) the mobile camera has two options, either look for another camera/target pair with lower utility value, or switch to a perpendicular rail to be able to continue following the target.

To account for occlusion, an occlusion factor ϕ was added, which is equal to 1 if the camera can clearly capture the target, or 0 if the camera cannot capture the target.

The utility function $a_{c_{ioj}}(t)$ is then defined as:

$$a_{c_{ioj}}(t) = \phi - \frac{\widehat{d_{c_{ioj}}}(t)}{rv_{c_{ioj}}} \quad (4-5)$$

The camera/target pairs are selected considering the highest utility values. Utility values lower than or equal to zero, indicate that either the target is not in the viewing range of the camera, or it is occluded from camera view. During target tracking and following, the utility function should be maximized, meaning the camera/target distance and relative velocity should be kept to a minimum.

4.5 Multi-Agent Path Planning on Grid Map

Multi-agent systems require careful control and planning in order to function efficiently. One of the most widely researched fields in robotics is an autonomous agent's ability to operate without human intervention. For this, an autonomous robot should possess the following attributes[248]:

- a way to represent the environment;
- an attributed target or goal position;
- an efficient method to reach its target.

Regarding the environment characterization, it can be considered static or dynamic. The robot target is given as a function of its current task or even other autonomous agents' tasks. For instance, if one agent is blocking the passage of another agent, whose mission is of higher priority, it might be asked to temporarily suspend its task and move out of the way of the high priority robot. To efficiently manage a large number of robots in a grid, ensuring all reach their targets in the minimum time possible and with the lowest energy costs, while avoiding obstacle collisions or impediment to other agents, is the problem of path planning. When the robot has complete knowledge about the environment, this problem is known as global path planning. On the contrary, if the robot has a partial knowledge, this problem is classified as local path planning [249]. The SCALA path planning is a typical problem of global path planning in static grid maps.

Several heuristic solutions have been proposed to solve the global path planning problem such as *Ant Colony Optimization (ACO)* [250], *Genetic Algorithms (GA)* [251], *Particle Swarm Optimization (PSO)* [252], *Tabu Search (TS)* [253], [254], and the *A* algorithm*, which is regarded as the gold standard for search algorithms [255], [256].

For task allocation and path planning of the multiple SCALA agents on the rail mesh, an A* type algorithm was used. A graph or grid map G is defined as a set $\{n_i\}$ of elements called nodes. These nodes are arranged in a matrix form and possess the *value* of 1 or 0 whether they can or cannot be travelled to, as shown in the example in Figure 4-35.

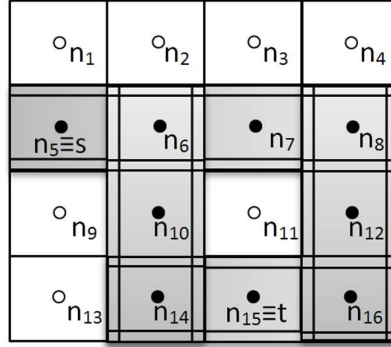


Figure 4-35 - Grid map example for a rail-based mobile robot environment.

In this way, it is possible to build a grid map, where $value(n) = 1$ are the n nodes which represent the rails and $value(n) = 0$ is the empty space in between (nodes with a black circle and a white circle in the Figure 4-35, respectively). The agents are only allowed straight moves in the four cardinal directions (4-connect grid). These movements have costs associated with them, which take into account the current heading of the agent and the direction to take. Since switching the moving direction costs time and energy, as the agent has to stop at a rail junction and accelerate again in a different direction, trying to maintain the same heading and finding a path with minimum direction changes is preferable.

A path from n_1 to n_k is an ordered set of nodes (n_1, n_2, \dots, n_k) with each n_{i+1} a successor of n_i . The search algorithm employed determines the optimal path by beginning the calculation on a starting node. In this node n_i , the *scores* for the available adjacent nodes (nodes to which the agent can travel to) are determined, based on the evaluation function $f(n_j)$, given by:

$$f(n_i)_j = g(n_{i+1}) + \hat{h}(n_{i+1}) \quad (4-6)$$

Where j is the index of the immediate above, below, left and right available nodes, $g(n_j)$ is the cost of moving from the node n_i to n_j and $\hat{h}(n_{i+1})$ is the sum of the number of horizontal and vertical nodes left until reaching the target node t . A $direction(n_j)$ variable is used to store the information relative to the heading needed to move from node n_i to n_j . This is used to determine the parent node to n_j , as well as the $g(n_j)$ cost. If $direction(n_j) =$

$direction(n_i)$, then $g(n_j)$ is equal to 1, otherwise it is equal to 3. After determining the evaluation function scores for the adjacent nodes, the algorithm adds the nodes to an open node list \mathcal{L}_{open} . Then, from that list, it selects the node with the lowest score, removes it from the open node list, and repeats the process of calculating the scores for its adjacent nodes. This is done until the target node is reached. Once this happens, the algorithm finds the optimal path by starting on the target node and proceeding backwards, using the variable $direction(n_j)$ which stored the directions taken to reach each node. This optimal path is the path which has the smallest cost over the set of all paths from s to t . The path cost is obtained by adding the individual costs of each node transition ($g(n_j)$, for $j = s, \dots, t$).

The principle of the algorithm is available as pseudo-code in Appendix B (algorithm 3). This algorithm was implemented in a virtual simulator, shown in Figure 4-36, for testing purposes. In this simulator, any map size or number of agents can be used. The user selects the starting and target nodes for each agent, and their tasks. The simulator takes into account the agents speed and acceleration to calculate their best paths. It also determines if there are collisions between agents.

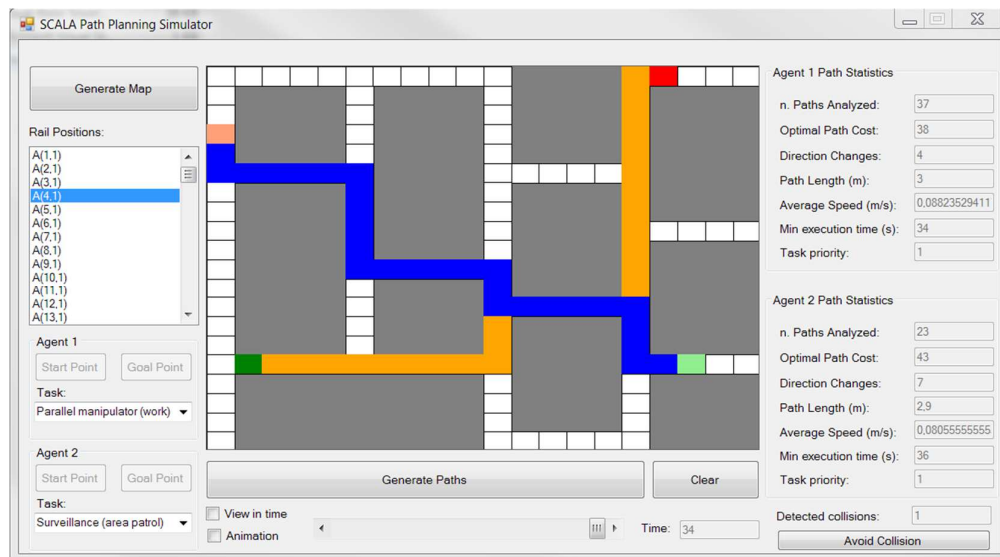


Figure 4-36 - Virtual simulator for the SCALA multi-agent path planning.

Agents are treated as dynamic obstacles. The algorithm determines their position in time, taking into account the mobile robot's velocity and acceleration properties, and

calculates if multiple agents occupy the same node, or adjacent nodes while moving in opposing directions, at the same time. Then, it determines an alternative path for the agents with lowest priority tasks, in order to prevent the collision. When no alternative path is available, the low priority agents stop while the other agents move on the common path nodes. This path planning method constitutes an efficient management strategy for SCALA.

4.6 SCALA Bill of Material (BOM) Analysis

This section details the costs of the proposed system, including the price of the individual components used in the prototype realization, and the estimated costs for setting up the system for an example real world application.

4.6.1 Individual component cost

The cost of the individual components of the SCALA mobile agent is detailed in Table XIII.

Mobile agents

Table XIII – Mobile agent component and total cost.

Mobile Agent Components	n°	Cost per unit [€]	Total[€]
Micromotors	4	12.8	51.2
PCB	1	30	30
3D Printed Parts	1	4	4
Motor hubs	4	2.4	9.6
Motor Supports	4	2	8
Encoders	4	4	16
Slider	1	50	50
Laser cut parts	1	15	15
Screws & nuts	1	16	16
Total			200

Rails

As explained earlier, SCALA concept was built on a philosophy of simple and low cost scaffolds. It is vital to keep the price of the rails as low as possible, because the claim of fine manipulation over large workspaces is only viable, if the rails are achievable at a reasonable cost. The cost of the prototype rails was described in section 4.1.2. The cost of 400€ per meter was due to the fact that they were produced by a CNC. Nonetheless, the rail profile is designed for possible future production by extrusion, at reduced costs. Feasibility of using standard custom-made rails was already proved in prototype I of the SCALA. An inquiry was sent to several national companies dedicated to the production of aluminum extruded profiles, to know what would be the cost for the production of the rails by extrusion. The best price was 800€ for the extrusion matrix and then a rail production cost of 6€ per meter. This is the price which is considered in Table XIV, for the rail costs.

Table XIV – Rail component and total cost per meter.

Rail Components	Cost per meter [€]
Rack	4
Magnetic strip	15
Rail Aluminum	6
Total	25

Junctions

The junction price for the prototype was 150€. Once again, it was a highly specialized CNC production of only two units. By placing large orders, it is often possible to obtain significant cost reductions, thus the final price considered was 50€ per junction.

Parallel manipulator and tools

The costs of the parallel manipulator components, and the tools both the manipulator and agents can carry, are given in Table XV and Table XVI, respectively. The Philips SPZ5000 webcam used in the vision applications is no longer commercially available, thus the typical cost of a USB camera was considered.

Table XV – Parallel manipulator component and total cost.

Parallel Manipulator Components	n°	Cost per unit [€]	Total [€]
Links	6	1.2	7.2
Spherical Joints	12	0.4	4.8
Laser cut parts	1	20	20
Link collars	12	1	12
Screws & nuts	1	6	6
Total			50

Table XVI – SCALA tools cost.

Tools	Cost per unit [€]
Camera	50
Gripper	60
BQ HeatCore DDG Extruder Kit	150
Laser	80

4.6.2 Setup cost

Let us consider a SCALA setup for mechanical part construction and assembly, as depicted in Figure 4-37. This setup consists in a *20m by 10m* room, *2m* high, with four distinct areas: a *storage area*, containing a *6m by 2m* shelf with a vertical SCALA rail mesh applied to it and four mobile agents, in this specific case called shelf agents, moving on it to retrieve items (similarly to what was shown previously in Figure 2-56). The *3D fabrication area* contains four SCALA manipulators dedicated to 3D printing of components. The *transit area* is a low density rail zone, which is used to quickly move

between the other areas. The *assembly area* possesses four SCALA manipulators with grippers for component assembly. Besides this, there is one more SCALA manipulator with a gripper for picking parts from the *storage* or *3D fabrication area* and five surveillance agents which supervise the operations in all areas. Also, five mobile agents were included as backup, to replace the active agents in case of malfunction.

Even though in this work it is demonstrated that SCALA mobile agents can move in a vertical rail mesh, the shelf agents with a specific tool for item retrieval from a shelf were not developed. In this case, one considered a cost of 250€ per each of these agents. The parallel manipulator link length was also increased by four times, as well as the workblock dimensions. These larger dimensions of the manipulators would require also larger mobile agent actuators, but since this is a case study whose results are just an initial approach of the real cost of an actual system implementation, the same components and prices for the SCALA prototype were maintained. A central control station, with a cost of 2000€ was also included, since the actual SCALA prototype can be controlled by a personal computer with Bluetooth communication.

Considering the costs of the SCALA components given in the last section 4.6.1, the costs for this setup are presented in Table XVII. The total cost of the installation amounts to 18400€. This setup includes four parallel manipulators for digital fabrications, five parallel manipulators for transport and assembly (total of twenty seven agents), and fourteen individual agents for the shelves, surveillance and as back up. It should be noted that, due to modularity of the system components, the agents and the parallel manipulators' missions and tools may change, depending on the dynamics of the work in progress.

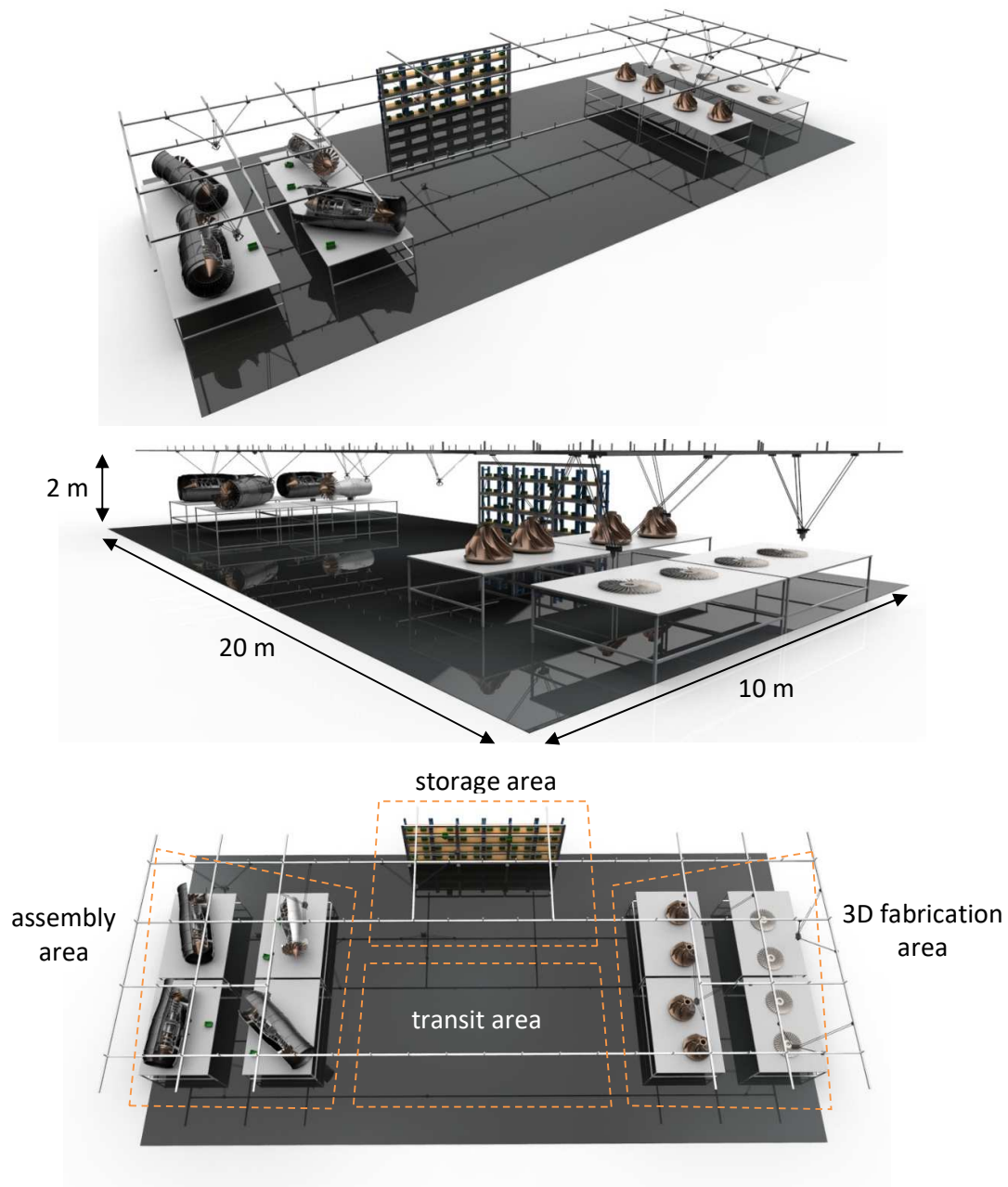


Figure 4-37 - Case study of a SCALA setup, for component fabrication and assembly, in a 20x10x2m room with 4 distinct areas: assembly, storage, 3D fabrication and transit.

For instance, a manipulator assigned to digital fabrication at a certain time, may move to the assembly area. Also, the surveillance or shelf agents can be used to drive an extra manipulator, if necessary. In fact, the modularity of the components means that

any changes or extensions of the setup can be easily made, and even these same components can be used in another space and with a different application.

Table XVII – SCALA case study setup component and total cost.

Setup Components	n°	Cost per unit [€]	Total [€]
Rails (meters)	160	25	4000
Junctions	48	50	2400
Mobile agents + backup agents	37	200	7400
Shelf agents	4	250	1000
Parallel manipulators	9	50	450
Grippers	5	60	300
Plastic filament extruders	4	150	600
Cameras	5	50	250
Central control station	1	2000	2000
Total			18400

The current cost evaluation is a rough estimate of an autonomous fabrication and storage cell, and the actual cost of a commercial SCALA solution might increase, to consider the scaling up the prototype components (e.g. for dealing with larger loads), installation costs and profit margins.



Figure 4-38 – Comparable setup using existing automation solutions: 4 robotic arms, 4 delta 3D printers and 3 AGV's equipped with a robot arm.

Still, a similar installation using existing industrial systems, would require at least three AGV's with storage retrieval capacity, four robot arms and four delta printers, plus cameras and external sensors, as depicted in Figure 4-38. Considering a typical cost of 20000€ for each AGV and 25000€ for each manipulator[257], plus independent control systems for each robot type, one would have a total setup cost of around 300000€. Even considering a commercial setup price for SCALA, existing solutions are more costly and require at least three different types of industrial robots and their control systems.

The Figure 4-39 depicts each component cost share in the total cost of this setup. One can see that mobile agents constitute the largest share of the total system costs. However the scaffold (rails and junctions) also represents 35% of the total cost. This is still a large share, which might be reduced by rail and junction design and fabrication optimization.

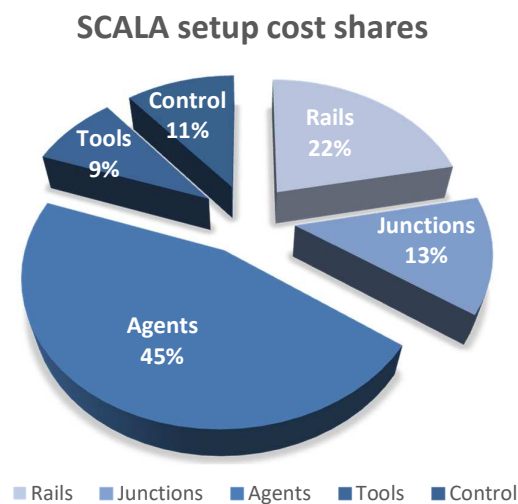
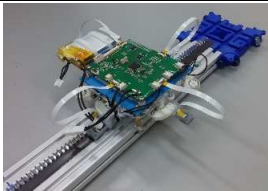
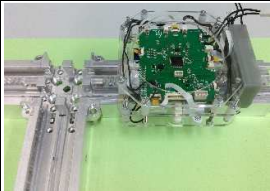



Figure 4-39 – Scala setup cost shares for each component type.

4.7 Summary

In this chapter, the implementation of the SCALA prototypes was described. This included a description of the several generations developed and the evolutionary process behind such iterations, which is summed up in Table XVIII.

Table XVIII – Characteristics of the developed prototypes

			
	Generation ONE	Generation TWO	Generation THREE
Mobile Agent			
Locomotion	4 DC gear micro motors		
Self-Localization	4 Integrated magnetic encoders + magnetic strip (resolution of 15 micrometers)		
Control	Homemade PCB with 32-bit ARM Cortex M4F processor		
Communication	Bluetooth 2.0 module		
Power	On-board Li-po battery or direct power feed		
Sliders	3D printed Polyamide	CNC Teflon	
Chassis*	ABS/ Acrylic/Polyamide	Acrylic/ABS	Aluminum/ABS/Acrylic
Dimensions	120x120x29 mm	115x100x54 mm	105x105x54 mm
Mass	200 g	300 g	345 g
Rails			
Production/Material	Standard Extruded Aluminum Profiles	CNC Custom Made Aluminum Profile	
Cost	30 €/m	400 €/m / 25 €/m **	
Dimensions (section)	23x56 mm	27x50 mm	
Mass	960 g/m	1920 g/m	
Junction			
Production/Material	3D printed Polyamide	CNC Custom Made Aluminum Profile	
Cost	30 €/uni.	150 €/uni. / 50 €/uni. **	

*in order of material usage; **prototype costs vs estimated costs for a final system.

The several SCALA generations pushed the design and performance of the system forward. The parallel manipulator was also implemented, including its several tools for the different tasks proposed, being pick and place and digital fabrication. The mechatronics and electronics solutions employed in the SCALA components were also described in detail. Most parts used in the implementation of SCALA were custom designed and built for the system, including laser cut, machined or 3D printed components. However, some commercially available components were also used, and are listed in Table XXVII, available in Appendix C4. The vision system configuration was also shown, as well as the multi-agent control and path planning strategies.

Finally, a cost analysis of SCALA was performed, including the list of its several individual components and respective costs, and the cost of an example of system setup. The comparison made to a similar setup using existing automation solutions, shows that SCALA is a cost effective solution, even considering that the addition of commercial setup costs, profit margins, engineering costs, etc., would roughly increase the cost of SCALA by four times the estimated costs in Table XVII. It is also evident that by relying on a single robotic system, instead of three different robots, it becomes easier and more cost effective to run and maintain the installation. SCALA also leaves the floor space free for humans or other equipment, while existing solutions occupy this space, as depicted in Figure 4-38.

The results of current SCALA generation testing and the demonstrations are the subject of the next chapter.

Chapter 5

Results and Demonstrations

This chapter begins by introducing the small scale test-bed, built for the experiments and demonstrations with the SCALA system.

Then, it details the results from the testing and application of the several SCALA components. These experiments aim to characterize the positioning accuracy and precision of both mobile agents and parallel manipulator. In addition, the locomotion efficiency of the mobile agents on the rail mesh is also evaluated. In this dissertation, the locomotion efficiency is evaluated taking into account the success rate of mobile agent junction crossing and switching direction in the rail mesh, when this mesh is installed horizontally or vertically. The results shown here not only provide validation to the development process, including theoretical models, but also give a concrete measure of the performance of the system.

Finally, several demonstrations of the SCALA system, including pick and place, digital fabrication and autonomous surveillance, are shown and described, as proof of concept. The goal of these demonstrations is to validate the system as an effective tool for these applications, even though the reduced scale of the testbed, where the demonstrations take place, does not allow to fully explore all capabilities of the system.

5.1 SCALA Test-bed

For the SCALA testing and demonstrations, a small scale test-bed was implemented, as shown in Figure 5-1.

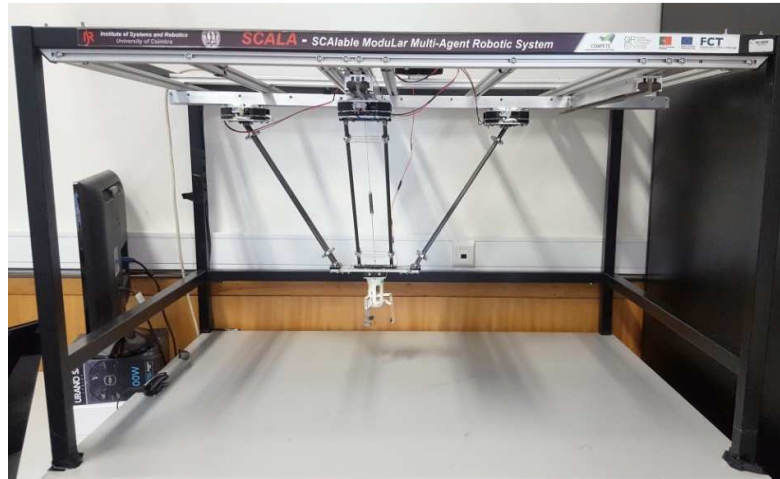


Figure 5-1 - Small scale test-bed built for the SCALA, with a parallel manipulator and three mobile agents.

The test-bed dimensions are $1200 \times 705 \times 850 \text{mm}$ and its rail mesh is constituted by four rail segments of 455mm in length, three rail segments of 185mm in length and two junctions. The detailed drawings for the SCALA test-bed are available in the Appendix A5. The base rail arrangement was designed so that all demonstrations could be achieved, including fine manipulation in a single block and parallel manipulator reconfiguration.

SCALA was remotely controlled by a computer with an AMD A6-7400K Radeon R5 processor, 6 Compute Cores (2C+4G) at 3.50 GHz, 8Gb of RAM, with a Bluetooth communications module. The control software used was the one developed specifically for SCALA, and presented in section 4.3.5.

5.2 Component Testing

For industrial robots, the testing methods and performance evaluation criteria, as for instance accuracy or repeatability, are defined in the International Standard ISO 9283, prepared by the Technical Committee ISO/TC 184, Industrial automation systems and integration, Subcommittee SC 2, Robots for manufacturing environment[258]. Even though such methodology is not employed in this work in a strict way, the adopted procedures can still provide an indicative measure of the system performance.

Two different experiments, with distinct purposes, were performed to assess the system performance. The first experiment intended to test the efficiency of the mobile agents drive system, while the second experiment intended to test the accuracy and repeatability of the whole system, including both agents and PM. The experimental setups, methodology and results are reported in this section.

5.2.1 Mobile agent locomotion efficiency

This experiment was conceived to test the mobile agents' success rate while crossing the junction, to either continue moving in the same direction or change to a perpendicular one. The procedure is done automatically by pre-programming the agent trajectory and using closed loop control. Ten trials were made in each case, and for two scenarios, where the rail mesh is horizontal or vertical. In Figure 5-2, the still images from these tests are reproduced. The results are presented in Table XIX.

One can see that almost all junction crossings were successful. Only one test out of ten failed, on the vertical mesh scenario. Switching direction also achieved an inferior success rate, with a couple of failed attempts. Two main reasons for junction crossing or switching direction failure were identified: incorrect positioning of the robot in the junction center, mostly due to gravitational effects combined with gear backlash, when the rail mesh is positioned vertically; and rack and drive gear teeth collisions. The first can be solved with the use of anti-backlash drive gears. Regarding the second, one can add a feedback sensor on the exact angular position of the drive gear. A simple encoder could be added to the drive motors so that one could be sure that the gear angle would enable teeth engagement with no collisions. These solutions shall be investigated in future work.

Table XIX – Results from the mobile agent locomotion tests.

Movement	Mesh Orientation	N° of Trials	Success Rate
Junction Crossing	Horizontal	10	100%
	Vertical 1	10	100%
	Vertical 2	10	90%
Switching Direction	Horizontal	10	90%
	Vertical	10	80%

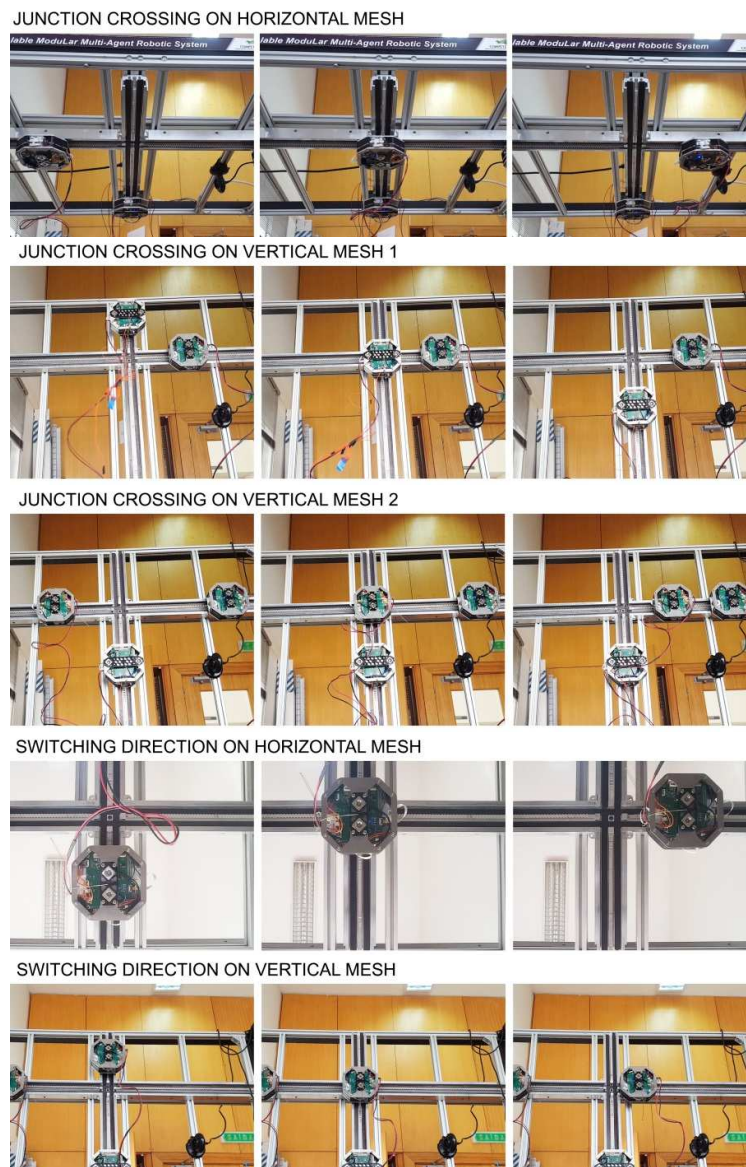


Figure 5-2 - Performance tests conducted. Images from left to right show the movement of the agent.

5.2.2 Mobile agent localization accuracy

The next set of experiments were made in order to access the accuracy and repeatability of both the agents' localization system and also the PM platform. The accuracy of a system is defined as the closeness of agreement between n observed values, *ObsValue*, and an accepted reference value (gold standard), *RefValue*:

$$Accuracy = RefValue - \frac{1}{n} \sum_{i=1}^n ObsValue_i \quad (5-1)$$

On the other hand, *repeatability* is the ability to replicate a given result. The International Standard ISO 9283 [258] defines the translational *repeatability*, considering that there is only movement in the direction of interest, as:

$$Repeatability = \bar{D} + 3.S_D \quad (5-2)$$

Where $\bar{D} = \frac{1}{n} \sum_{i=1}^n |ObsValue_i - AvgValue|$, being *AvgValue* the arithmetic average of the observed values, and S_D is a standard deviation given by:

$$S_D = \sqrt{\frac{\sum_{i=1}^n (|ObsValue_i - AvgValue| - \bar{D})^2}{n-1}} \quad (5-3)$$

This is the definition adopted in this dissertation work for the *repeatability* measure. As the gold standard for absolute position, the Polhemus Liberty 240 6 DOF high accuracy tracking solution [23] was used. This electromagnetic system requires a source to be the fixed system's reference frame, and a sensor attached to the object being tracked, either the mobile agent or the platform. The system's reported tracking resolution, for a maximum distance between the source and sensor of *600mm*, is inferior to *0.005mm* for position and *0.0014°* for orientation. The complete specs for this sensor are included in Annex D. A special 3D printed support, made from ABS, was used to connect the sensor to the tracked object, thus placing it far from any metallic parts. The electromagnetic source was also placed far from the prototype metallic structure, to avoid as much as possible interference in the generated magnetic fields. Prior to the experiments, a calibration procedure was used to align the cartesian coordinate system (*x*, *y*, *z*) of the Polhemus system to the SCALA's point of origin (*0*, *0*, *0*). Also, the orientation signals of the sensor were calibrated to a standard orientation. The experimental setup is depicted in Figure 5-3.

The agent localization system employed, based on magnetic encoders, is capable of measuring linear displacements as small as *0.025mm*. However, the real accuracy depends mainly on the system mechanical realization tolerances, drive system backlash and system

control. The goal of this test is to quantify the positioning accuracy of the agents. Two sets of tests were conducted. In the first set, the accuracy of the agents was measured in a single rail segment placed horizontally, with no junction crossing and using only the continuous strip readings. Ten trials were made for each of five displacements.

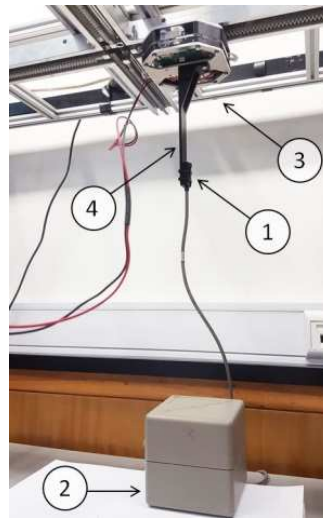


Figure 5-3 - Setup for the Polhemus System in the agent accuracy/precision tests. 1- Sensor; 2- Source; 3- Mobile agent; 4- ABS support.

The position absolute error results are shown in Figure 5-4.

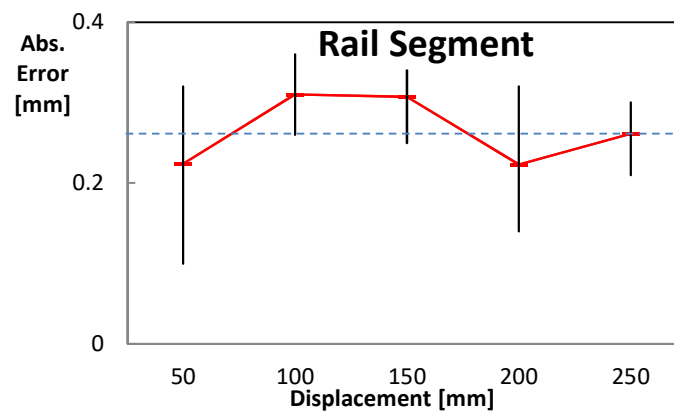


Figure 5-4 - Average results with range for 10 localization accuracy trials, for each of the 5 displacements on a single rail segment. The average error of all displacements is represented by the horizontal blue dashed line.

As can be seen, the average accuracy is 0.27mm for all displacements and the maximum error is below 0.40mm . Another conclusion one can draw from these results is that there was no noticeable accumulation of error with the increase of the distance paved. The amplitude of the error (maximum error minus minimum error) was, in average, 0.14mm , which indicates an excellent precision. The repeatability for the five displacements (50 trials), was 0.14mm .

The second set of tests was similar to the first one, but this time only two displacements were considered, and they involved crossing a junction. The agent position error was not reset on the junction. Once again, ten trials were made for each displacement, and the results are shown in Figure 5-5. This time, the average accuracy was 0.43mm and the amplitude of the results was 0.32mm . The repeatability for the two displacements (20 trials), was 0.62mm .

While both accuracy and precision levels were lower, the difference is not large enough to conclude that there is a loss of accuracy by crossing a rail junction. In fact, for the first displacement of 265mm , the precision and accuracy obtained are on the same level of the ones obtained from moving on a single rail segment.

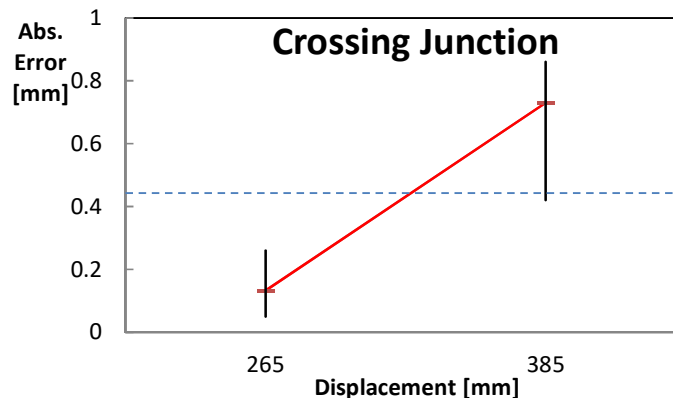


Figure 5-5 - Average results with range for 10 localization accuracy trials, for each of the 2 displacements, with a junction crossing. The average error of all displacements is represented by the horizontal blue dashed line.

5.2.3 Parallel manipulator static accuracy

Having tested the agents' localization accuracy and precision, the next goal was to access the accuracy of the PM driven by three agents. As seen previously, parallel machines precision is susceptible to the positioning accuracy of their drives, the manufacturing tolerances and even the machine pose.

Once again two sets of tests were conducted. The experimental setup is depicted in Figure 5-6. The first assembly mode was used for this test.

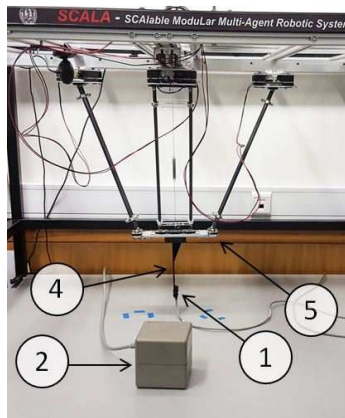


Figure 5-6 - Setup for the Polhemus System in the PM accuracy/precision tests. 1- Sensor; 2- Source; 4- ABS support; 5- Parallel manipulator.

For the first set, five points were chosen randomly from the PM's workspace. Then the manipulator, starting from a random location, moves to the set point on the workspace and the absolute position error is measured. The random starting point of the PM displacement is chosen so that it requires all three agents to move at least *100mm*, to reach the target point. The random target positions used were $P1(250, 231, 312)$, $P2(250, 249, 297)$, $P3(290, 289, 273)$, $P4(290, 312, 246)$ and $P5(390, 389, 76)$. For each position, ten trials were made, and the results are shown in Fig. 25.

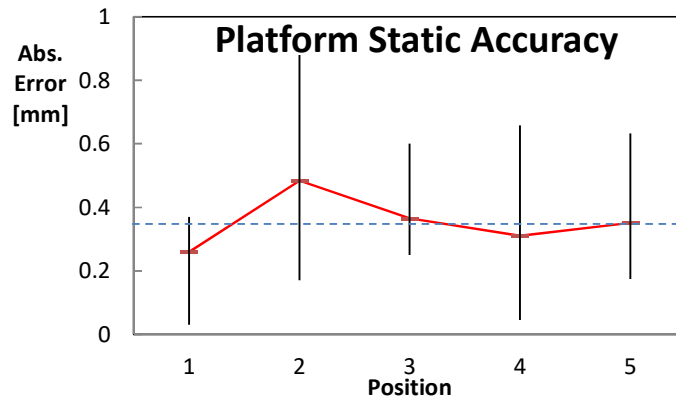


Figure 5-7 - Average results with range for 10 static localization accuracy trials, for each of the PM mobile platform 5 random points in its workspace. The average error of all points is represented by the horizontal blue dashed line.

The obtained average accuracy of all positions was 0.35mm and, in all 50 trials, accuracy level was below 1mm , indicating high PM precision. These results, however, have limited significance since, for some particular poses of a parallel machine, usually either close to the boundary of the workspace or to singularities, a small actuator displacement leads to a large displacement of the mobile platform. The tool displacement errors are then amplified in equal measure. This is called anisotropic behavior and, as previously discussed in Chapter 3, is a common characteristic of parallel machines.

Because of this, a study was made using the interval analysis algorithms developed and described in Chapter 3, to determine the expected static accuracy of the PM, given its architecture, geometry, actuator accuracy and pose. For a chosen horizontal plane $z = 310\text{mm}$, the workspace and expected accuracy ranges for the PM poses were determined, and are shown in Figure 5-8.

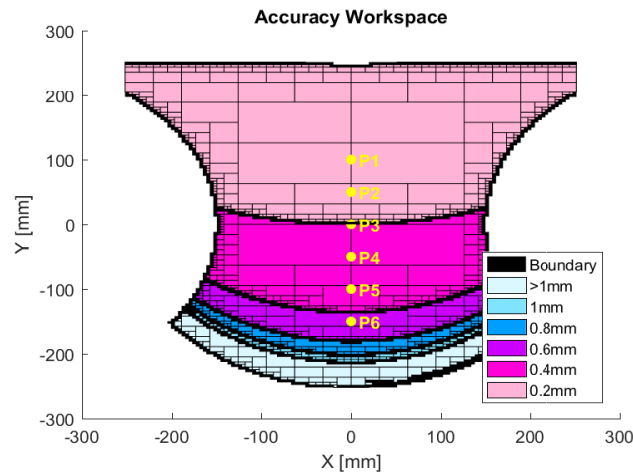


Figure 5-8 - Static accuracy range determined for the PM mobile platform, for 6 positions P along the y axis, in a horizontal plane $z = 310mm$.

Then 6 positions along the y axis were chosen, $P1-6$, and the PM precision tests were performed for these points. The results are shown in Figure 5-9 and Table XX.

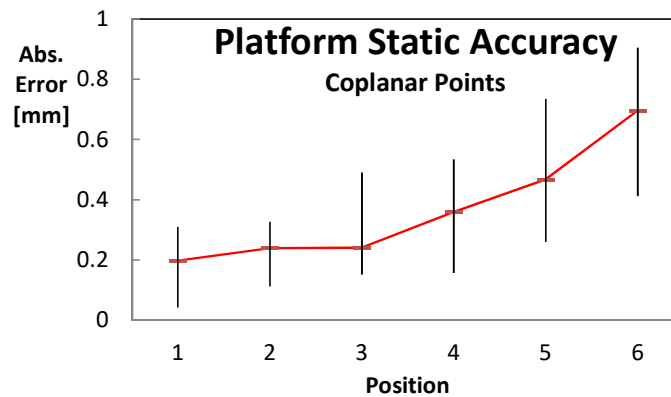


Figure 5-9 - Average results with range for 10 static localization accuracy trials, for each of the PM mobile platform 6 positions along the y axis, in a horizontal plane $z = 310mm$.

The obtained position accuracy is either very near or inside the expected accuracy ranges for the manipulator, which means that the mechanical tolerances adopted in its construction are very strict and that the prototype performs as expected.

Table XX – Comparison between the expected and obtained PM accuracy.

Pos.	Coordinates	Calculated Ac. Range [mm]	Obtained Average Ac. [mm]
P1	(0,100,310)	< 0.20	0.20
P2	(0,50,310)	< 0.20	0.24
P3	(0, 0,310)	~ 0.20	0.24
P4	(0,-50,310)	< 0.40	0.36
P5	(0,-100,310)	< 0.40	0.47
P6	(0,-150,310)	< 0.60	0.69

The mobile platform accuracy, considering all trials, is equal to $0.36mm$, while the repeatability value is $0.56mm$.

5.2.4 Parallel manipulator path following accuracy

The PM dynamic or path following accuracy is also important to evaluate, since, for a machine which can be used for 3D printing, it is important to ensure that the real path of the tool is faithful to the programmed one. The testing procedure involved programming a trajectory for the robot end-effector to perform, in our case, a circle on a horizontal plane, with a diameter of $100mm$, centred at $(0, 0, 320mm)$, to be done in 8 seconds. The starting point was set to be $(50mm, 0, 320mm)$ and it performed the circle in a counter clockwise direction. The manipulator used the first assembly mode for this test. The robot performed this planned trajectory with the gripper tool attached, and in two different conditions: no load and carrying a load of $800g$. The Polhemus Liberty sensor was once again used for position tracking of the end-effector, collecting over 400 points during the trajectory. The metal plate of the end-effector was replaced by one made from acrylic, to reduce the interferences with the sensor, which was attached to it, as shown in Figure 5-10.

The trajectory accuracy tests, whose results can be seen in Figure 5-11, reveal some deviations from the goal position, which are most evident in the load test. The average positioning error and standard deviation values of $1.63mm$ and $1.11mm$ were obtained for the no-load test. For the load tests, the average positioning error and standard deviation values of $1.96mm$ and $1.88mm$ were obtained.

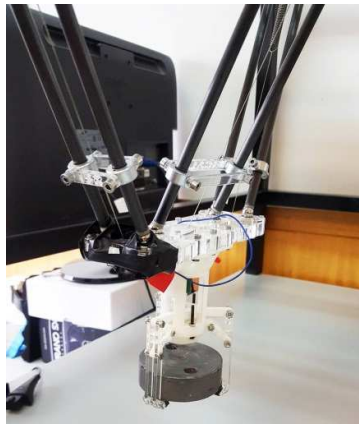


Figure 5-10 - Manipulator carrying a payload of 800 g.

The second test, with load, shows a larger deviation of the circular path, due to the increased forces the robot actuators and the parallel structure need to support, which bear a negative effect on their accuracy and rigidity. However, the main reason which seems to cause this disparity between manipulator static and dynamic precision is control problems on the agents. Because, for dynamic trials, the time variable plays an important role. For the PM to be able to reach the desired position at the desired time, involves perfect synchronization between its actuators, in this case the agents. If a single agent is slower than the others, it causes systematic errors which propagate until the end of the trajectory.

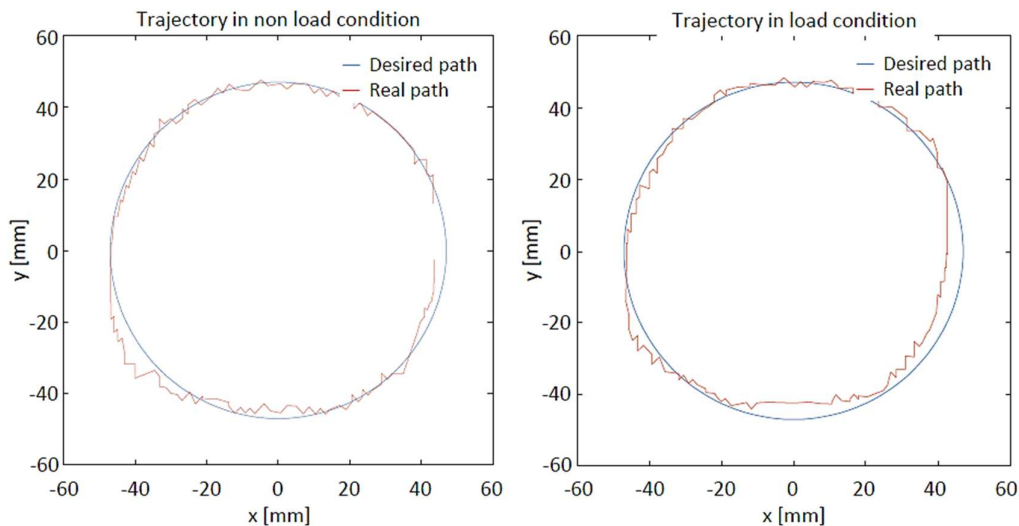


Figure 5-11 - Platform path-following accuracy tests. Plot of desired vs actual trajectory (dimensions in meters) for no load (left) and 800 g load test (right).

This problem was not investigated further, but some causes and possible solutions to it are mentioned here. In fact, the manipulator dynamic model was not implemented in the control strategy, which could aid in producing better results for dynamic conditions with different load values. Because the mechanical tolerances vary slightly between several agents and even rails, this dynamic model should include the right individual friction parameters for each agent, obtained through actual testing.

5.2.5 Parallel manipulator reconfiguration

The developed parallel manipulator is capable of dynamic reconfiguration, which can be used for workspace enlargement and dynamic property improvement, by selecting the most suitable assembly for each task, when possible.

Despite the small scale of the testing rail mesh, one could still demonstrate:

- Reconfiguration and assembly mode switching on the same work block (Figure 5-12 a));
- Transition to another work block (Figure 5-12 b));

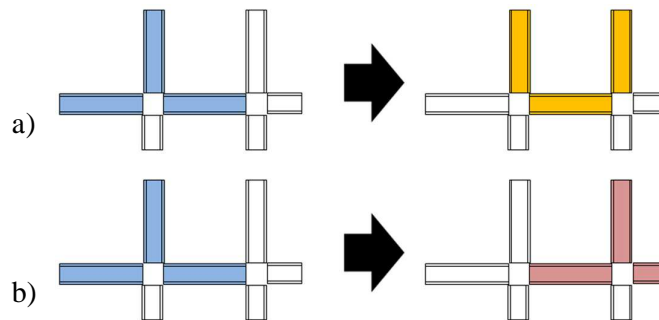


Figure 5-12 - Different test scenarios involving parallel manipulator translation or reconfiguration in the small scale test-bed: a) AM switching; b) PM translation.

A led strip was mounted around the mobile platform to get a better perception of where it is located during the tests. Automatic reconfiguration and translation was achieved, but the tests have shown that the performance is very sensitive to the agents junction crossing efficiency and the multiple agent coordination. A single agent getting stuck in a rail junction was enough to stall the entire process. During the tests, the

manipulator did not carry any tools to reduce the risk of cable entanglement. This was also one of the reasons why reconfiguration is not used in the final demonstrations of pick and place or digital fabrication. Figure 5-13 and Figure 5-14, show the process of transition from one workblock to another, from two different views.

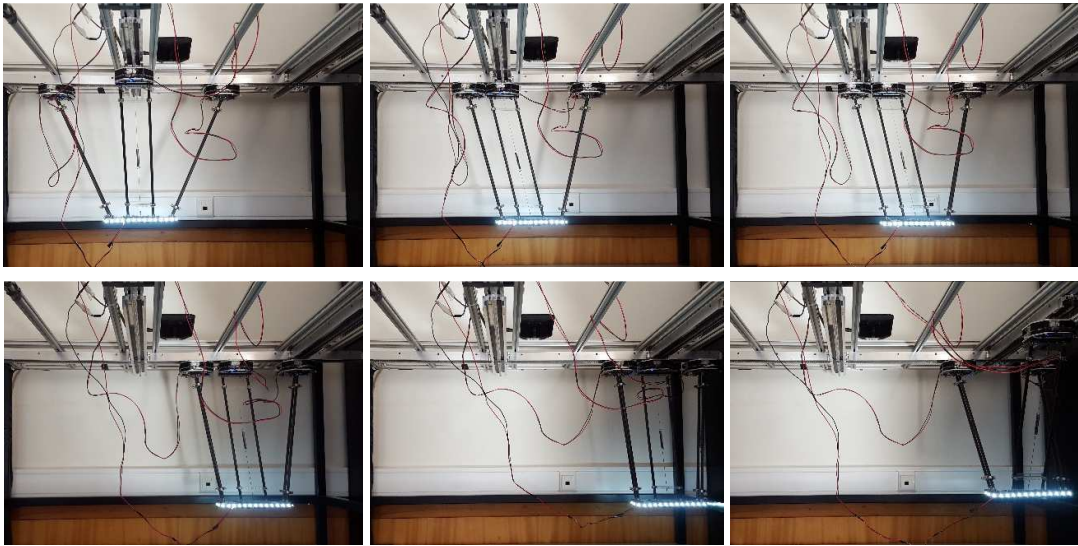


Figure 5-13 – PM translation from one work block to another, viewed from the front.

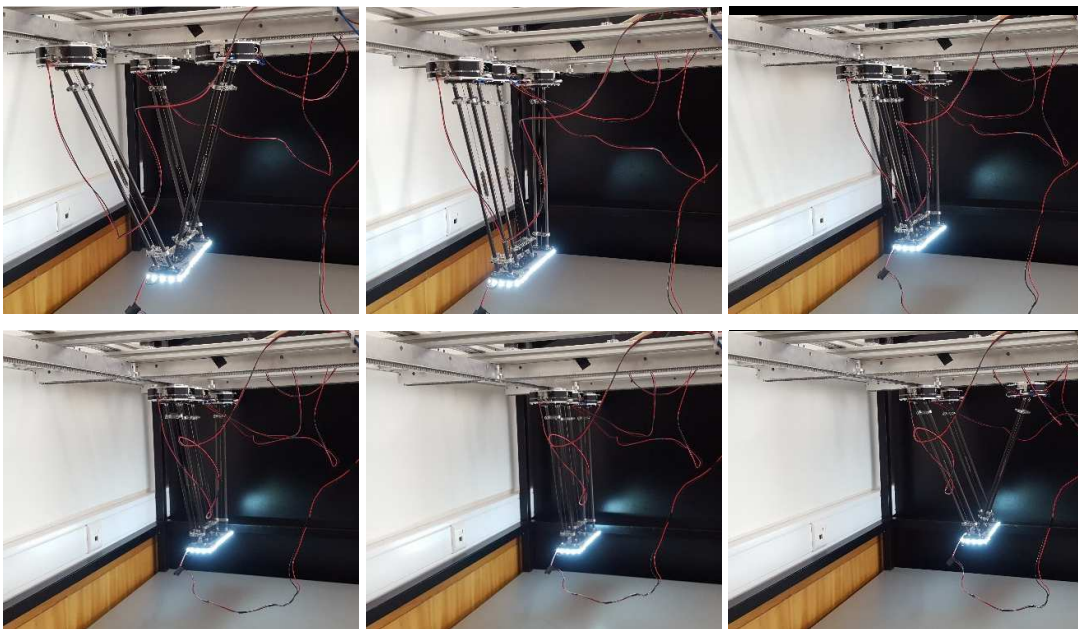


Figure 5-14 - PM translation from one work block to another, viewed from the side.

5.2.6 Discussion

The SCALA component testing demonstrated that it is possible to achieve high accuracy for both the agents' localization and the parallel manipulator positioning. The experimental results are summed in Table XXI.

Table XXI – Results for SCALA accuracy and repeatability tests.

Component	Accuracy [mm]	Repeatability [mm]	n° of trials
Mobile agent (no junction crossing)	0.27	0.14	50
Mobile agent (with junction crossing)	0.43	0.62	20
Parallel manipulator tool	0.36	0.56	110

These results fall within the expected ranges for this architecture and are *on par* with the performance of some industrial solutions presented in Table XXIV and Table XXV. This is remarkable, considering it is an initial prototype of the system. Thus, one can validate the design, project and realization of the system and its several components. Still, the author reckons some improvements can be made, regarding the mechanical construction (by adopting tighter tolerances in the mechanical realization of the manipulator and making stiffer joints and links) and also the control scheme of the system. This becomes evident in the results of the dynamic accuracy of the manipulator, where the trials under load revealed an average deviation of *1.96mm* from the trajectory.

Platform translation and reconfiguration was performed and accomplished. The tests revealed that more improvements on the agent locomotion are required to enhance this process.

5.3 Pick and Place

5.3.1 Methodology

A pick and place routine was pre-programmed for the SCALA parallel manipulator, using the gripper as its tool. The goal was to demonstrate a fully autonomous pick and

place routine, requiring perfect coordination between SCALA agents and manipulator tool to perform a rather complex task, without any human intervention.

This task consisted of picking two objects and placing them in a basket, one after the other. The two objects chosen were a sphere made of soft foam, and an apple. For this, four main waypoints were spread across the tri-dimensional workspace of the manipulator, in its first assembly mode. These points are *Point-H*, which was considered to be the home or idle position of the manipulator, *Point-B*, where the basket is located and the manipulator is supposed to drop the picked objects, *Point-A* which is the apple location, and *Point-S*, which corresponds to the sphere position. The task sequence was defined by a state-machine, and is illustrated in Figure 5-15.

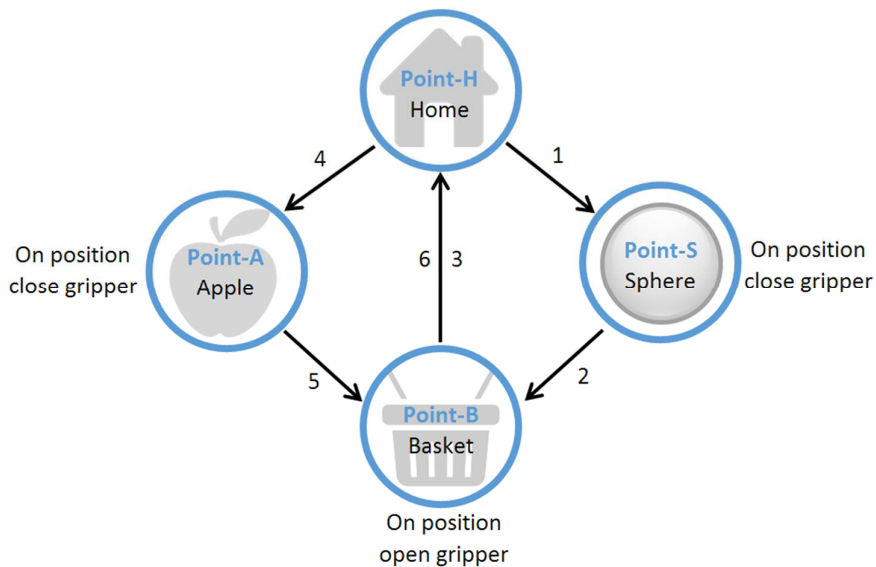


Figure 5-15 – Task sequence implemented in the state machine, for autonomous pick and place task.

No sensing system was required to know where the objects were, since the position of the waypoints was pre-programmed in advance. However, this also meant that if such reference positions needed to be changed after, programming of the new positions to the autonomous routine was required.

The performed autonomous procedure starts with the manipulator in the set home position, in *Point-H*. Then, it moves to the *Point-S*, and positions the gripper at the perfect height to grab the sphere. Once the sphere position is achieved, which corresponds to the

fulfillment of a set accuracy threshold, an interrupt event is generated and the state is changed. Next state controls the gripper actuator, more specifically, it sends commands to close the claw and grab the sphere. This is accomplished by driving the motor in open loop and during a duration of time, which was pre-determined during calibration tests with the object. When the time counter is over, another interrupt event is generated, which corresponds to raise the manipulator and move to the basket position. When *Point-B* is reached, the event of gripper opening is raised. This is the same event of the gripper closing, except this time, the motor runs in the opposite direction, thus opening the claw. Once the sphere falls in the basket, the manipulator returns to home position and repeats the same process to pick the apple at *Point-A*.

5.3.2 Results

The state machine was implemented by software using a *switch-case* module, where each case represents an *i* state. This implementation is described in detail in[246]. The interrupt and progression event in each state was raised when all agents reached their set position, within a certain threshold. The used threshold value was set to be ± 20 tick counts, which corresponds to $\pm 0.5mm$ for the agents' position. Lower thresholds could be used, but given the relative size of the objects and gripper, this tool positioning accuracy was enough to provide consistency and 100% task execution success rate. Figure 5-16 contains still images taken during the pick and place task execution.

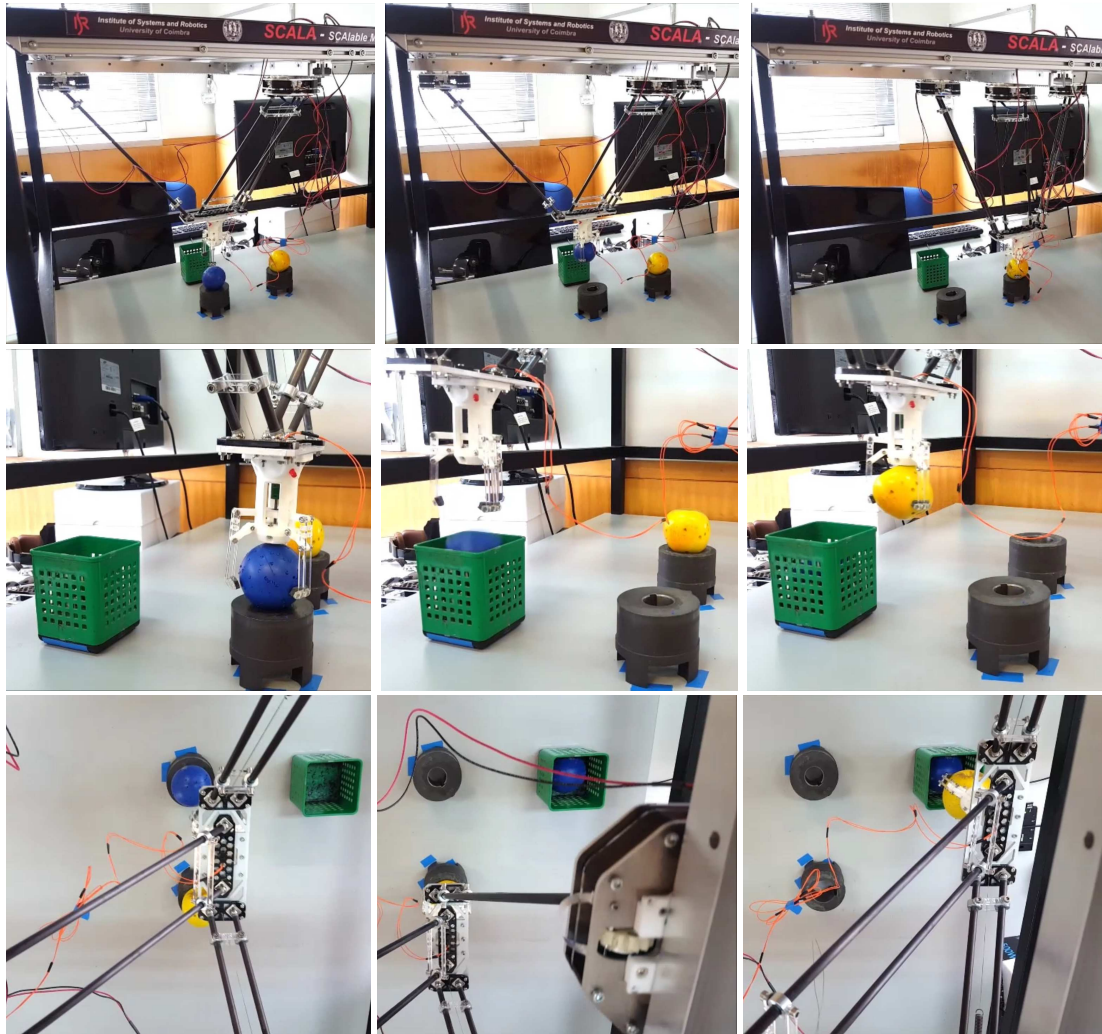


Figure 5-16 – Video captures during pick and place routine of the SCALA system.

5.3.3 Discussion

The task sequence was executed for at least 20 times, without any failure to report. This reveals good system robustness and repeatability. Even without any feedback from extra sensors as, for instance, a pressure sensor or cameras in the gripper, the picking and releasing of the objects was always successful and precise. The only drawback was that it required a pre-calibration phase, for the objects and basket position, and gripper operations. Future developments using agents with cameras, and tools with sensors, could improve further the system and its flexibility. However, for basic and repetitive tasks in

automation, where the picked objects and their positions are always the same, this same system and procedure, in its current state, can be used.

In this sense, through this demonstration, one could reproduce an experiment that is not far from a real application. In other words, one was able to prove the full functionality of SCALA as a pick and place system.

5.4 Digital Fabrication

5.4.1 Methodology

Digital fabrication machines transform a digital representation of a part or component, whether it is a 3D model or a 2D drawing, into a real prototype. This is the case of 3D printers, laser cutters or CNC machines. This transformation involves several steps, which are illustrated in Figure 5-17, and are different depending on the input given to the digital fabrication machine and the expected output.

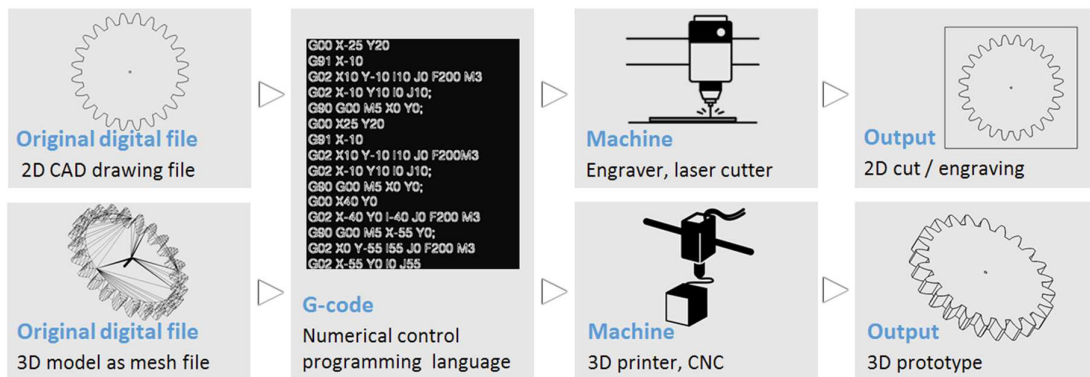


Figure 5-17 – Digital fabrication from original source file to final output.

To produce a 2D cut or engraving, typical source files include CAD drawings in a common format, such as DXF (Drawing Exchange Format). This format does not store information regarding the depth of the model, as it is intended only for planar fabrication. On the other hand, 3D models are required to fabricate parts in 3D printers or CNC

machines. These models often originate from STL (Stereo Lithography) files, which consist of many linked triangles (called a “mesh”) that simulate the surface of the object to fabricate.

The next step includes the common denominator in the digital fabrication process, the g-code generation. g-code (also RS-274), is the common name for the most widely used numerical control programming language. It includes a set of instructions for the machine tool, like the path it should follow, the moving speed, the cutting or extrusion speed, among others... A g-code can be automatically generated from source files. For instance, in 3D printing, the g-code is generated by a slicer software. This software “slices” the 3D model of the part into layers, and then they generate g-code that extrudes plastic to fill each layer.

Since SCALA can be used for multi-type digital fabrication machine, a g-code interpreter was implemented, so that one could perform both 2D and 3D digital fabrication tasks. This interpreter was directly implemented in the SCALA control GUI and enables the loading of a g-code file. It then computes the required trajectory for the manipulator tool and the corresponding agent trajectories. This control uses again a state machine, as the one implemented for the pick and place task. Each state corresponds to a point or instruction given by the g-code. Once a state is accomplished, it proceeds to the next state, until the end of the task.

As digital fabrication demonstration, two tasks were envisioned. The first task was to show the SCALA manipulator working on a single plane, as in a laser engraving or cutting machine. This was divided into two approaches. In the initial approach, a pen and a white board were used. This was done to test the robustness of the system. The pen was attached to the gripper, using a special printed support. The g-codes of several shapes, including a *10cm* diameter circumference, a *10cm* square and the word SCALA were loaded and drawn in a single plane. The second approach involved the laser assembly. The laser and its driver board were mounted on the manipulator tool. A potentiometer was used to control the laser power. Once again, the same shapes were marked on a black paper. An additional test was included, where the laser engraving was done in a concave surface, forcing the laser to move vertically, in addition to its planar movements.

The second task demonstrated 3D printing using the SCALA manipulator. For this task, the plastic extruder was used. The same g-code interpreter, for the first task, was employed. However, this time, the user had to select the starting plane for printing, the part and filament thickness. The program then automatically calculated the number of layers. Once the first planar layer was finished, it was programmed to repeat the same layer in a plane some tenths of millimeter (depending on the filament thickness) above the previous one. This process was then repeated until printing all layers. In the meantime, the stepper motor responsible for feeding the plastic, was programmed to run continuously. No coordination between the movement of the tool and the stepper control was implemented. This was done to quickly implement this demonstration procedure, but future developments should include such coordination for better printing performance.

A power source for the stepper motor and the heating element on the extruder head, as well as a stepper motor control board, an additional screen and the filament spool, were mounted on top of the SCALA testbed.

5.4.2 Results

Figure 5-18 depicts the demonstrations for the first task, using a pen and a white board, to draw a circle, a square and the word SCALA.

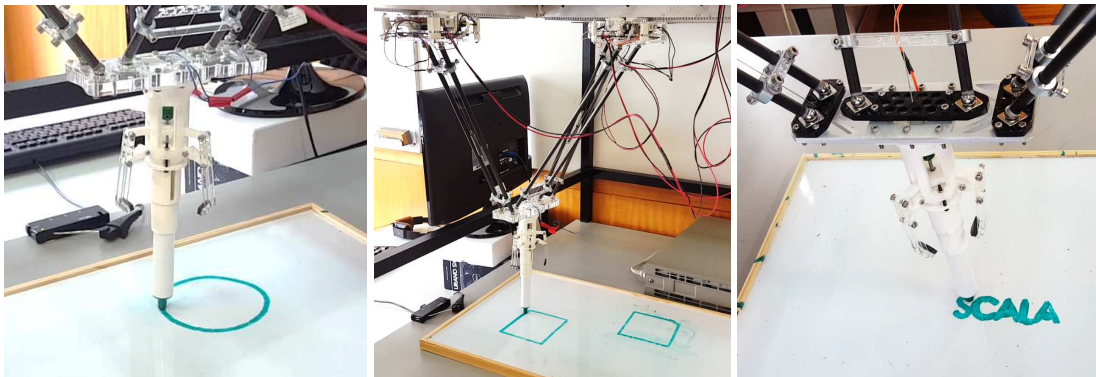


Figure 5-18 – Digital fabrication task one demonstration, by drawing on a white board.

The SCALA manipulator, using its first assembly mode, was able to draw all geometries. The word SCALA was the more challenging task, as its 715 line g-code included vertical displacements of the tool, to create spaces between the individual letters. However, due to the large diameter of the pen tip, it is not possible to observe these fine details, nor the tool accuracy.

The second subtask of the engraving/cutting demonstration is depicted in Figure 5-19. All shapes were made in the black paper, with good precision. To perform the engraving on the paper, in the concave surface, the vertical movement of the tool had to be modified in the g-code, to follow the curved shape of the surface. The resulting shapes on the black paper were digitized and are shown in Figure 5-20, with their colors inverted, for better visualization of the laser marks. As one can see, the laser marks are not a continuous line, but instead a set of dots. This was due to laser focus and driver problems and should be improved in the future developments. Nevertheless, one can see that the desired geometry was followed by the manipulator.

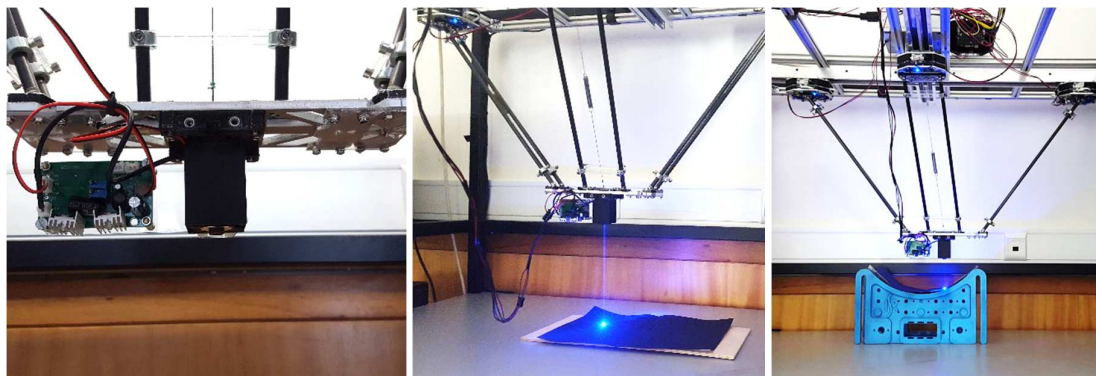


Figure 5-19 - Digital fabrication task one demonstration, using the laser, on a planar and concave surface.

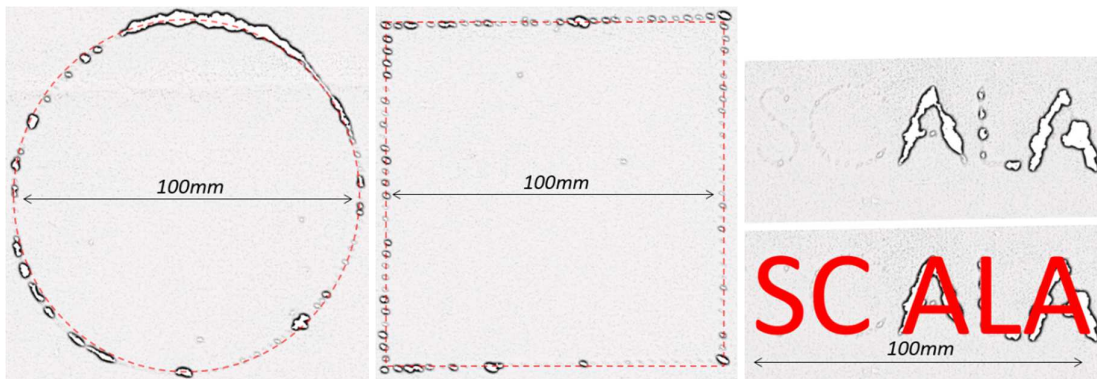


Figure 5-20 – Negatives of the results from the laser engraving demonstration on the planar surface. The desired shape is shown in red while the marks show the laser engraving/cut spots.

The 3D printing demonstration is shown in Figure 5-21. All parts were printed successfully, and for each part, all layers were deposited precisely on top of the previous ones, showing a good 3D positioning accuracy of the manipulator tool. However, the print quality was much inferior to the one obtained in commercial printers. This is due to control employed for the robot. By relying solely on a PID position control, with no force or velocity control, the agents' movement becomes very jerky, propagating vibrations to the manipulator tool and causing this low quality print. Another problem which affected the print quality was the independent control of the stepper motor, which fed the plastic. Because it was continuously feeding the plastic at a constant rate, when the manipulator was moving between positions, where there should be no plastic material, it still deposited plastic. This resulted in a low quality print of the SCALA letters, where one can see deposited material between the letters. This is visible in the final prints, shown in Figure 5-22.

One important future development shall be improvement of the trajectory planning algorithm, with a third order function which takes into consideration a continuous velocity and acceleration function on the intermediate points, for a jerk-free and smooth motion.

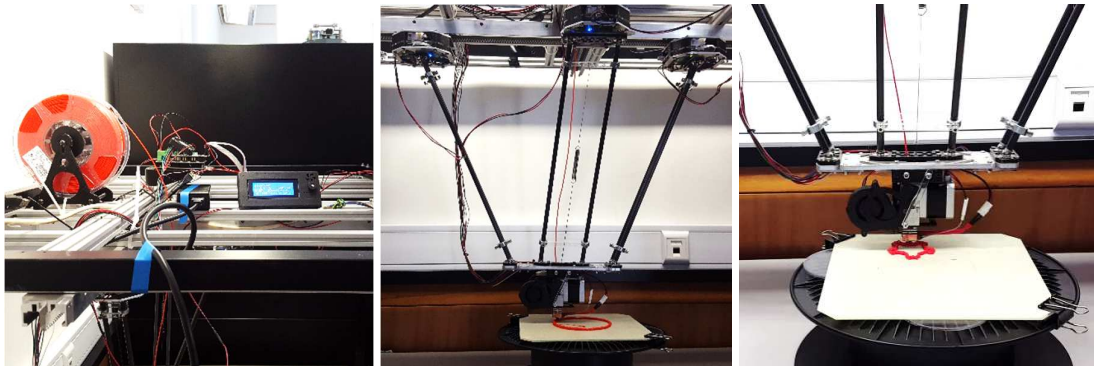


Figure 5-21 – SCALA 3D printing demonstration.



Figure 5-22 – Parts 3D printed by SCALA.

5.4.3 Discussion

All digital fabrication tasks were accomplished successfully, in terms of proof of concept. In general, the manipulator performed as expected, and was able to follow the desired trajectory.

Regarding the laser cutting tasks, the poor laser focus prevented from achieving better results. However, the demonstration validated SCALA as a laser cutter or

engraving tool. It even shown SCALA potential to make large parts on a tridimensional surface, involving large vertical displacements of the tool.

The achieved 3D printing quality was low, mostly due to control problems of the agents. This resulted in vibrations which were propagated to the whole structure, including the printing head, causing the low printing quality of the parts. This should be sorted in future developments with the adoption of better control strategies.

All fabrication demonstrations were performed using a single assembly mode. The reasons for this were that it was complicated to change the assembly mode of the manipulator due to the fact that external power and control cables were attached to both the laser and plastic extrusion assembly. Changing of the assembly mode was tried, but during this process, the cables got entangled causing the failure of the AM switching. In a future version of the manipulators tools, the power source for the laser and plastic extruder, as well as the filament spool, should be placed in the manipulator end-effector, to grant it total freedom to move in the large rail mesh. This was not done in the current SCALA prototype, as it was not robust enough to support the extra weight and size of these components.

The control of the laser power, as well as the plastic feeder, should also be included in the main SCALA control program for better fabrication results. This can be achieved by using any available ports in one of the SCALA agents control boards. Then, the implemented g-code interpreter can send synchronized commands to control the manipulator tool positioning and also the laser or extruder functioning. This will largely improve the part fabrication quality.

5.5 Target Following

5.5.1 Methodology

Three experiments were set up for the SCALA autonomous vision system. Even though the scale of the experiment was low, due to the small dimension of the setup, the tests intended to reproduce a situation where it was possible to demonstrate the functioning

of the system and its advantages over existing solutions. The results obtained can be scaled up to real world applications.

In all experiments, the target was constantly and autonomously monitored by the individual visual tracking system of each robot, which reported its position, velocity, heading or the lack of detection.

To perform the visual tracking in the target object, a fiducial marker system [259] was used. This marker system is composed of a set of valid markers and an algorithm which performs its detection, and possibly correction, in images. Although it is possible to generalize object detection by training a personalized cascade classifier [260], fiducial markers are more reliable, computationally cheaper and have better position and rotation accuracy. This marker was installed in a ground mobile robot capable of being remotely controlled in real time or to perform pre-programmed trajectories.

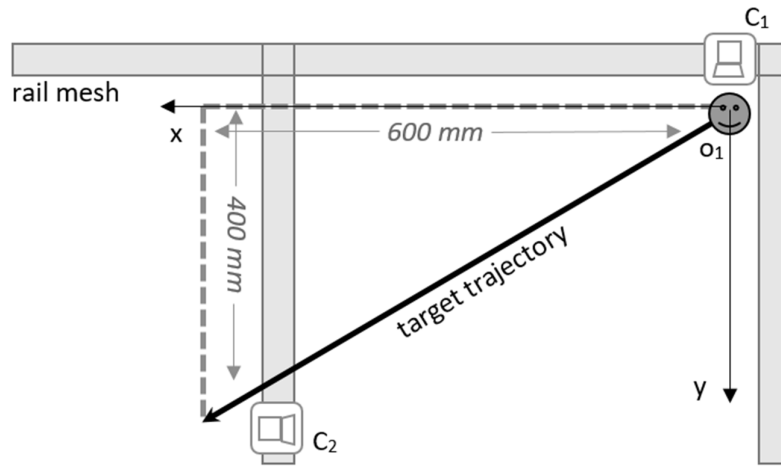


Figure 5-23 - Scheme of the test bed setup, showing cameras 1 and 2 and the target in their starting position. The target diagonal trajectory is also marked.

In the three experiments, the same trajectory was pre-programmed into the ground moving robot target, and also the cameras start from the same position, as shown in Figure 5-23. The target followed its trajectory at a constant speed of 3.5cm/s , taking about 20 seconds to complete it. For each experiment, the target tracking was performed differently:

Experiment 1

In this experiment, target tracking was done by two fixed cameras, which were located as depicted in Figure 5-23. This experiment intended to reflect the tracking performance of a vision system based on static sensors.

Experiment 2

In this experiment, both cameras c_1 and c_2 performed target tracking and were able to move only on their axis, i.e. c_1 was able to translate in its rail along the x direction and c_2 translated along the y direction. This experiment intended to reflect the tracking performance of a vision system based on mobile sensors restricted to translations in one dimension.

Experiment 3

In this experiment, only one camera (c_1) will be used for target tracking. To be able to follow the target from start to finish, it will have to switch rails, and go from a translation along x to a translation along y . This experiment takes full advantage of the 2D mobility of the proposed novel system.

During these experiments, the following variables were measured:

- The position of each mobile camera, given by the encoders on the SCALA agents;
- Position of the target relative to the world frame of reference and each mobile camera, measured by camera vision;
- The target tracking efficiency measured by the percentage of the target's trajectory that is detected by at least one camera, during the target's movement.

5.5.2 Results

The Figure 5-24, Figure 5-25 and Figure 5-26 illustrate the first, second and third experiments, respectively.

The marker position tracking results for each experiment are shown in Figure 5-27, Figure 5-28 and Figure 5-29. The absolute distance between the target and the cameras

(DTC), for each experiment, is shown in Figure 5-30. The results from all three experiments are presented in Table XXII.

Table XXII – Results from SCALA vision demonstrations.

	Experience 1	Experience 2	Experience 3
Tracking efficiency [%]	96.8	100.0	97.3
Tracking R^2	0.999	0.991	0.977
Average DTC [mm]	157	87	130
Standard deviation DTC [mm]	69	51	54

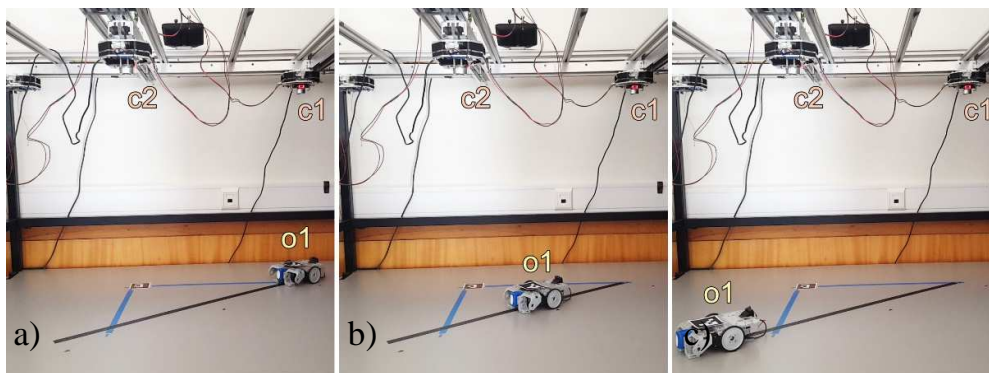


Figure 5-24 - Video captures from experience 1: a) target o_1 at the trajectory start, tracked by static camera c_1 ; b) target tracked by both c_1 and c_2 ; c) target at the end of trajectory, tracked by c_2 .

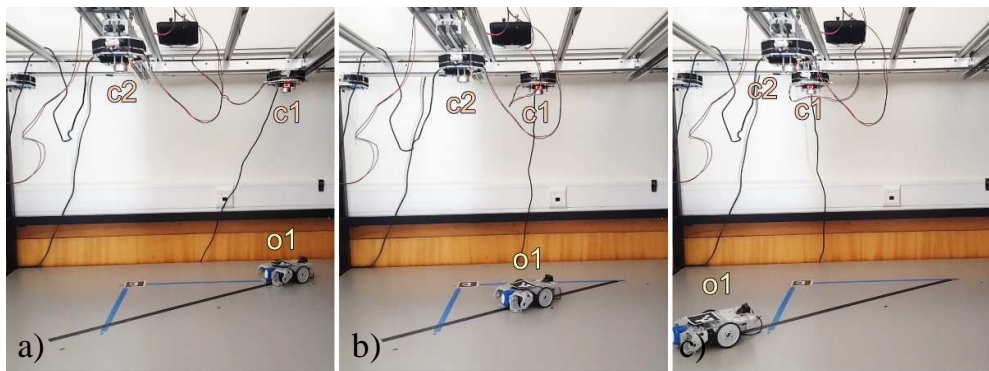


Figure 5-25 - Video captures from experience 2: a) target o_1 at the trajectory start, tracked by mobile camera c_1 ; b) target tracked by both c_1 and c_2 ; c) target at the end of the trajectory, tracked by c_2 .

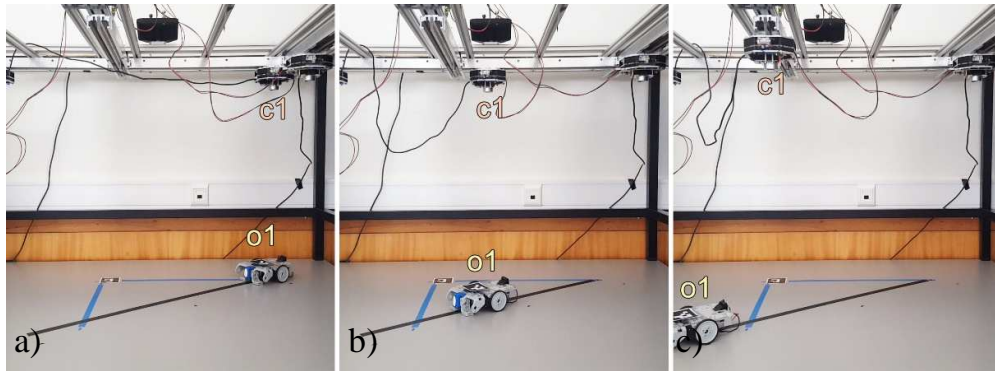


Figure 5-26 - Video captures from experience 3: a) target o_1 at the trajectory start, tracked by mobile camera c_1 ; b) target leaves camera FOV and c_1 proceeds to change axis; c) target at the end of the trajectory, tracked by c_1 on a different axis.

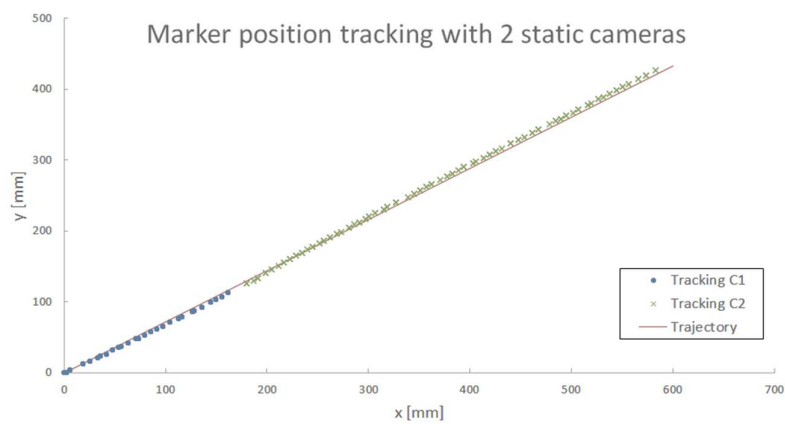


Figure 5-27 - Target position tracking results using two static cameras c_1 and c_2 .

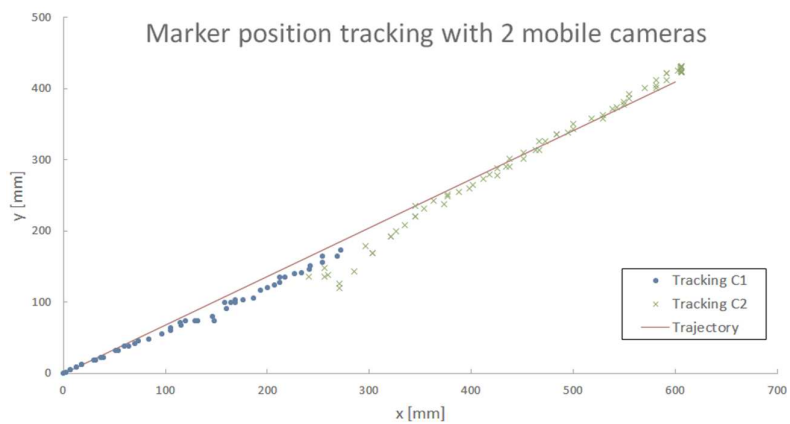


Figure 5-28 - Target position tracking results using two mobile cameras c_1 and c_2 .

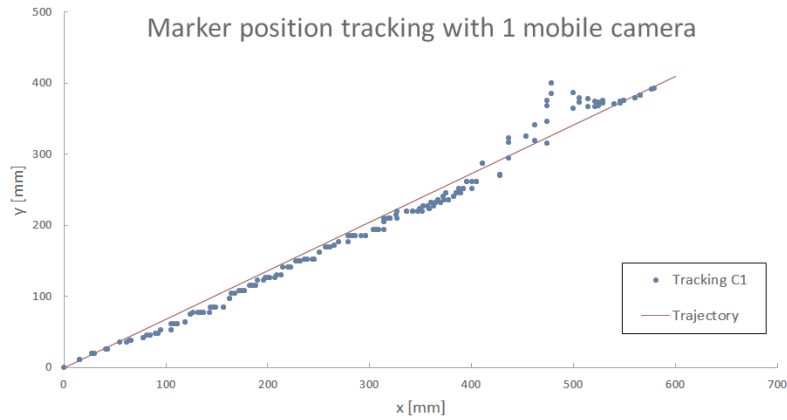


Figure 5-29 - Target position tracking results using one mobile camera c_1 .

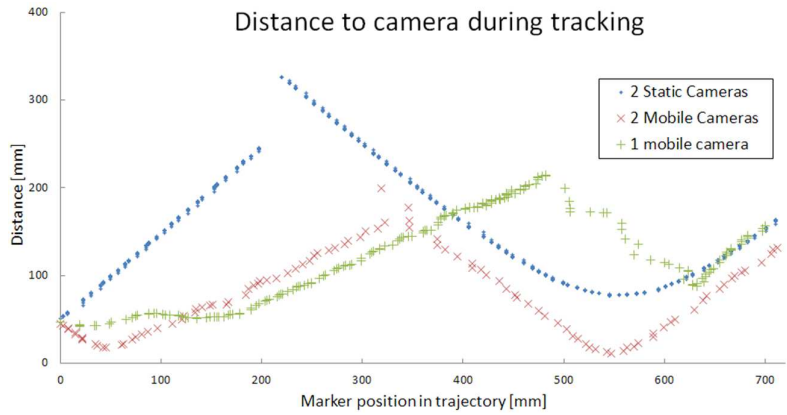


Figure 5-30 – Absolute distance to camera results of the three experiments.

The tracking efficiency was determined as the percentage of the total target trajectory which was detected by at least one camera. A linear regression was made to the position points resulting from vision tracking, using the linear trajectory as approximation, and an r-squared coefficient was determined. This coefficient relates how close the visual tracking was to the real target trajectory and its purpose is to provide a means of comparing the accuracy of each tracking method. The average and standard deviation for the distance to camera (DTC) results were also determined.

In the experiment 1, with two static cameras, as expected the DTC is very high, as the cameras are not capable of moving and following the target. This also results in the lowest tracking efficiency, since there is a part of the target trajectory (approximately the

position of the marker shown in Figure 5-24 b)) which is not inside the *FOV* of any of the two cameras. The strong point of using static cameras is the accuracy of the tracking, as the referential is always fixed.

The DTC is the lowest for the second experiment with two mobile cameras. Being able to move and follow the target allows them to continuously track its trajectory from start to finish. When the target begins its movement, it is being followed by camera 1, which moves along a rail with the orientation of the *x axis*. At some point in its trajectory, the target enters the *FOV* of camera 2, which moves on a perpendicular axis. Since camera 2 is free, it receives the order to move to follow the target. For a brief period, both cameras follow the target up to the point where the target distance to camera 2 is inferior to the distance to camera 1 (approximately the position of the marker shown in Figure 5-25 b)). Then, and because the target is moving to the outside of camera 1 *FOV*, the camera 2 assumes the main target tracking and following function. Accuracy of tracking is slightly lower in this case, especially when the mobile camera is moving faster. This may be explained by software and control issues and more specifically the lack of synchronization between the reading and printing of the encoder values and the vision outputs. In Figure 5-31 it is shown the distance to 2 mobile cameras in both *x* and *y axis*. It can be seen that, while the camera 1 is following the target and moving on an *x oriented rail*, the distance to the camera in *x axis* is constant and maintained low. The same happens when the target is being followed by camera 2, but this time on the *y axis*, as this is the orientation of the camera movement.

The experiment 3 intended to simulate the functioning of the SCALA vision system, performing target tracking and following with a single mobile camera, capable of moving in 2D. The camera 1 tracks and follows the target up until the point where it leaves its *FOV* (approximately the tag position shown in Figure 5-26 b)). At this point, the camera searches for the nearest perpendicular rail, where it can switch moving direction and resume the target tracking, which is done a couple of seconds after.

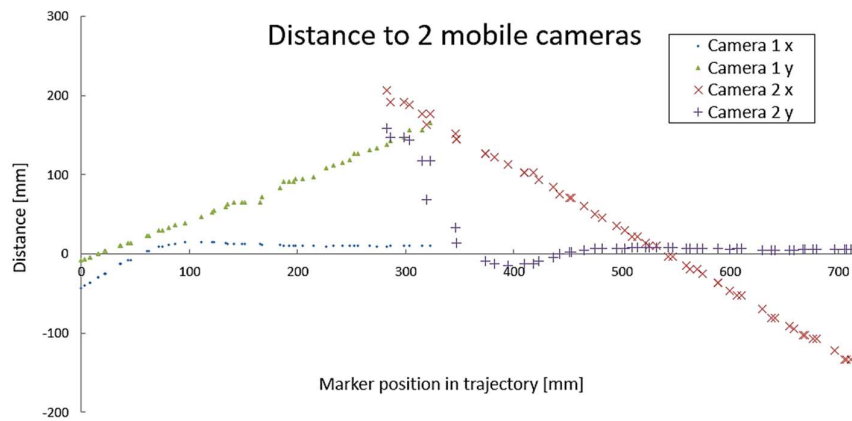


Figure 5-31 – Distance to 2 mobile cameras, in x and y axis.

Because of this process, there is no detection of the entire target trajectory. However, it is shown that the DTC results are better than using static cameras. Once again, tracking accuracy is lower, due to the already mentioned reading and printing synchronization problems when the mobile robot velocity is higher. In Figure 5-32 it is shown the distance to the mobile camera in both *x* and *y* axis. It can be seen that, while the camera is following the target and moving on an *x* oriented rail, the distance to the camera in *x* axis is constant and maintained low. Then, when switching to the perpendicular axis, the distance in *y* axis is minimized.

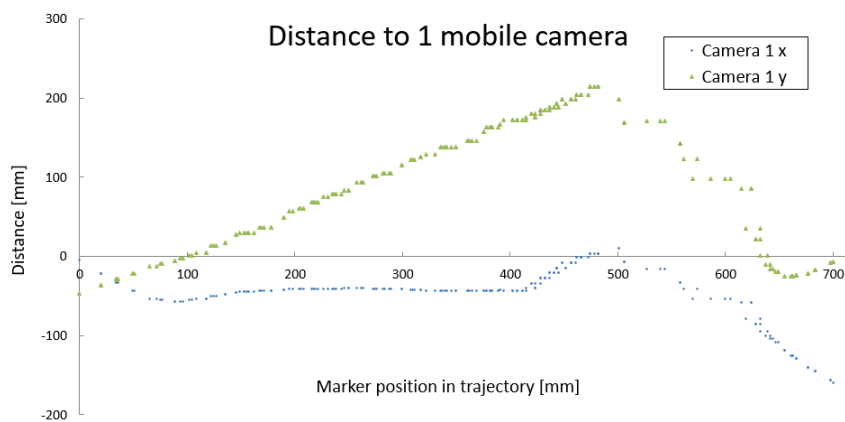


Figure 5-32 - Distance to 1 mobile camera, in x and y axis.

5.5.3 Discussion

The SCALA system for vision applications has advantages over fixed camera systems since it allows to cover a vast space with a reduced number of sensors. It can also overcome problems such as target occlusion, dead angles or large camera/target distances. Regarding the 1D mobile camera systems, SCALA offers more freedom and flexibility by allowing 2D movement on walls and ceiling.

The demonstrations performed to compare SCALA performance against static and 1D mobile systems reveal similar performances, even when performing tracking and following with a single camera. Given the reduced scale of the testing bed, the obtained results can only be considered as representative, but show that a high tracking efficiency can be achieved with the proposed system. This efficiency depends on the speed of the moving target, and the faster it moves, the more difficult will be to follow it while switching rails. However, the rail mesh can also be optimized for each application and each space, and more rails and intersections can be installed, thus minimizing this effect. Using multiple 1D cameras to follow a target achieves better tracking results, but requires a large number of cameras for a large number of targets. With a single camera capable of moving on 2D, the same tracking can be done with little impact on the efficiency. This strategy is then more suitable for large and complex spaces, with multiple targets to be followed.

The lack of tracking accuracy when the mobile cameras move at higher speeds should also be solved in future developments. Experiments on a large scale, should also be made, using state of the art vision methods, as done by *Linder T. et al* [261]. These will allow to infer the true performance of the system on real applications, and establish again a comparison to other similar existing systems.

It is also interesting to explore the possibility of adding pan-tilt-zoom control to the cameras, to improve functionality with face recognition and other complex vision methods, as described in [262], [263]. This possibility has not been explored in this work and it would be interesting to see if better tracking results can be achieved by using cameras with pan-tilt-zoom capabilities.

Chapter 6

Conclusion

6.1 Final Remarks

In this work, a novel framework called SCALA - SCALable moduLar multi-Agent robotic system on ad-hoc pathways for automation and surveillance, was presented and developed, from conceptual stage to design, implementation, testing, verification and final demonstrations. The motivation for this research work was to fill the gap between the high precision fixed base industrial manipulators, and mobile robots capable of working in large spaces, by delivering a solution capable of performing precision work with speed, efficiency and repeatability, over a large workspace.

The first stage of this research work consisted in the characterization of existing systems, identifying their strong features and learning the best strategies to overcome their limitations. A system based on multi-agents moving on a passive bi-dimensional rail mesh was the result of this conceptual development. It took several design iterations, prototype developments and improvements, until reaching the final architecture. This cycle of hypothesis, experiments, reevaluation, modification and extension of the original hypothesis is what constitutes the scientific method which was the basis of this dissertation work. Its final result was a novel mechanical solution in the field of mobile robotic systems, the SCALA Railbot II. Even though some systems with multi-agents moving on rail grids, can be found, and are mentioned here, none can offer all the characteristics which the patented SCALA system possesses, including continuous movement of multiple mobile agents on a passive rail grid which can be mounted in any inclination.

After the development of the bi-dimensional multi-agent system, the next task described in this dissertation work was the study and development of the novel reconfigurable parallel manipulator. The concept of having 2D mobile agents employed to control a PKM is new to the state-of-the-art. This solution offers many advantages and enables to take advantage of several strategies to increase the workspace of the manipulator, including base translation, drive range extension and reconfiguration. To the best of the author's knowledge, this was the first parallel system to combine all three strategies simultaneously and dynamically. Given the novelty of the solution developed, an extensive analysis was performed on the kinematics, dynamics, static properties and workspace of the PKM. A new methodology for the design of a family of PKM which ensures a set of desired properties was conceived, using the latest tools in interval arithmetic and analysis. This methodology was used to determine the geometrical parameters for the SCALA manipulator, given set requirements of workspace size, accuracy and force. It was also used to analyze in detail the property workspace of the PKM, which was critical to understand and justify the behavior of the manipulator during the accuracy tests. In the end, the contribution of this part of the dissertation work, was not only the novel solution in the field of parallel machines, but also a method, which proved to be efficient to design and study a parallel manipulator given various properties of different nature.

The implementation of SCALA was also a process which involved several iterations. Three generations were made, and throughout their evolution, their design, component arrangement and materials used was subject to constant optimization. This process is described in detail, from the mechanical to the electronic, mechatronic and control solutions employed. The management of the multi-agent system is also addressed with the development of custom made path planning tools for SCALA. This also shows the multiple areas of research involved in this dissertation work. A comparative cost analysis was made to back up the claim of SCALA being an automation solution that is cheaper than existing systems. Despite being only an indicative cost study, it shows that setting up the proposed system may not involve a large investment, thus representing a disruptive development in the field of industrial automation systems.

After implementation, all SCALA components were thoroughly tested to assess their performance and identify their main problems, in order to be able to propose improvements in the system. In overall, the system performed as expected. The agents revealed good performance in the junction crossing tests, in both horizontal and vertical or hanging down scenarios, with an overall success rate of around 90%. The few failure causes were identified and solutions were proposed. Regarding the static accuracy tests of both agents and parallel manipulator, the accuracy results below $0.45mm$ and repeatability results below $0.65mm$ reflect the robustness of the solution and its mechanical implementation. They are also comparable to the performance level of available industrial manipulators. Regarding the results of the dynamic accuracy tests, the obtained value of $1.96mm$ for the parallel platform accuracy under load reveals essentially problems with the agents' synchronization.

In the reduced space of the test-bed, it was also shown the parallel manipulator reconfiguration. The tests revealed that this process is very sensitive to the agents synchronization and junction crossing performance, thus to decrease the failure rate it is crucial to optimize the agent control and design.

Finally, the SCALA real potential was shown in a few demonstrations of applications where it can be used, including automation, digital fabrication and surveillance. The pick and place demonstration revealed high robustness and repeatability of the system, with no failure occurrences to register. This involved picking and transporting two different objects, from two different 3D locations, to a basket. The locations of each object and the basket were pre-programmed in the pick and place routine, as there were no external sensors used, such as cameras, to detect the objects' position. In the future, these can be used to dynamically perform this task, and even recognize the shape and size of the object, to better configure both the gripper and the manipulator.

The more challenging digital fabrication demonstration also revealed good results, with all parts being made successfully. This demonstration included the use of three different tools, a pen, a laser and a plastic filament extruder. The first two were used to draw and engrave several shapes, including a circumference, a square and the word SCALA, while the latter was used to print several parts. The fabrication quality was low

but its causes were identified and future improvements to the system were suggested. However, the main objective, which was to validate the system as a framework for multiple high accuracy applications in large workspaces, was achieved.

The autonomous surveillance task demonstrated the true potential of this platform for vision applications. For this demonstration, two mobile agents were fitted with low cost web cameras, and a tag recognition software was used in coordination with the SCALA control, to allow the agents' movement to track and follow a tag placed in a mobile robot. Even though the test scale was reduced, the results showed that SCALA can achieve similar performance of the fixed camera systems and 1D mobile camera systems, using fewer cameras. This was a very important achievement which may one day contribute to scalable, cheaper and more efficient surveillance and vision systems.

Despite the successful accomplishment of the system demonstrations, several problems of the current prototype were observed. Their causes were identified and their solutions were proposed and are discussed in the next section.

Several articles were published in the top international peer reviewed journals in the areas of mechanics and automation, while others have been submitted and are currently awaiting acceptance. A provisional patent of the SCALA system was also filled, in the National Institute of Intellectual Property. The published work is listed in section 6.3.

In the end, all tasks proposed were successfully accomplished, despite the many challenges faced in the multiple areas of research involved. The objectives which were set out for this work were fulfilled, in the sense that the developed prototype is capable of performing fine manipulation over a large 3D workspace, in a fast, safe, reliable and repeatable fashion. Comparing to existing SOA systems, it is faster since its movement is continuous, even when switching movement direction at the junctions. The reliability and repeatability were demonstrated in the SCALA component testing. The system is also designed so it can work in a rail mesh installed on the walls or the ceiling. This allows to separate the system actuation space from human space, thus increasing the safety factor. The rail and junction components were modular built, so they could be assembled to form any rail mesh configuration, and scalable to any size. It was also demonstrated, through the

cost analysis, that this is a low cost and simple system, when compared to existing solutions. The resulting prototype can then be considered a relevant tool for several applications and a framework for further research and development. The technical specifications of the developed prototype are summed in Table XXIII.

Table XXIII – technical specifications of the developed SCALA prototype.

	SCALA
Agent movement	Planar, continuous and restricted on a 2D grid
Agent drive	4 DC motors and gear/rack drive system
Agent max. speed	0.10 m.s ⁻¹
Agent localization accuracy*	0.43 mm
Agent localization repeatability*	0.62 mm
Sensors	Magnetic position encoders
Agent voltage and current	9 V at 0.3 A
Agent mass	345 g
Agent controller and communication	Onboard control board with Bluetooth
Manipulator mechanical structure	3-PU^R reconfigurable parallel architecture
Manipulator DOF	3 translational DOF (spatial movement)
Manipulator workspace area**	0.627 m ²
Manipulator work/inst. area ratio**	1.25
Manipulator drive	3 Mobile agents' movement (no additional actuators)
Manipulator accuracy***	0.36 mm
Manipulator repeatability***	0.56 mm
Manipulator reconfiguration	Dynamic
Central control station	AMD A6-7400K Radeon R5 processor, 6 Compute Cores (2C+4G) at 3.50 GHz, 8Gb of RAM, with a Bluetooth communications module

*average experimental results with junction crossing; **in a workblock and for $z = 310\text{mm}$;

***average experimental results.

6.2 Outlook

Three key research and improvement directions have been identified, which could follow-up on the methodological contributions of this thesis and will be described below:

First, a couple of solutions have been proposed to the problem of junction crossing failure of the mobile agents. This is a critical procedure from which the whole functioning of SCALA depends. These solutions include both mechanical design and electronic improvements. The use of antibacklash driving gears can help improve the agent placement accuracy in the junction. By installing a single turn encoder on the drive gears, one can also control their rotation angle to avoid collision with the rack teeth. Both these solutions should improve the junction crossing performance of the mobile agents. Regarding the scaffold, their fabrication by extrusion and the inclusion of power lines to grant infinite autonomy to the mobile agents are also improvements which are to be made. Rail embedded copper lines can be used to conduct the power through the mesh, and carbon brushes placed in the agents sliders can draw the power from these lines. In addition, a more robust version of the SCALA manipulator would allow the installation of the auxiliary components of the laser and 3D printing assemblies, such as the power sources or the plastic filament spool, in the mobile platform. This would allow the manipulator to move freely in the rail mesh, and be able to re-configure itself, which is something not achievable by the present prototype, when carrying tethered tools. Larger and heavier objects could also be manipulated in the pick and place tasks.

The second improvement proposition is regarding the control of the system, by adopting more robust synchronization strategies to improve the dynamic accuracy of the parallel manipulator. A control strategy based on position, velocity and force control would also contribute to better practical results in dynamic conditions. This should improve the quality of the laser cut and 3D printing tasks, by making the tool movement smoother and more precise. An interesting research direction related to this topic is in the parallel manipulator optimal path planning and assembly mode selection. Because there are areas in the manipulator workspace which can be reached by several assembly modes, it is important to find a control strategy to autonomously select the most suitable configuration

for the current task. For instance, a pick and place operation may require superior load bearing performances from the configuration, while digital fabrication would favor precision. For the same workspace point, one assembly mode might be superior in one aspect and inferior in other, to another assembly mode, which shares that same workspace point. A suitable selection of assembly modes might then be critical to the successful accomplishment of a task.

The third research direction goes towards large scale testing and demonstration of real world applications with a robust prototype. Pick and Place and digital fabrication demonstrations were performed using a single AM. The reason for this was the limited scale of the test bed and low complexity of the tasks demonstrated. However, for more demanding tasks, the use of several AM might be needed. Even though the changing of AM was demonstrated here, in future developments, it would be interesting to demonstrate reconfiguration as a means to aid in the accomplishment of complex SCALA operations. The same applies for the surveillance demonstration. Even though, to some extent, the obtained results can be scaled up, one can only fully validate the proposed system by testing it in real applications and scenarios, where several moving targets, occluding objects, light and environment changes and other variables may have a decisive role in the performance of SCALA.

6.3 Published Scientific Output

From this dissertation work resulted four published articles. Two articles are directly related to the parallel manipulator design and development, and were published in the Mechanisms and Machine Theory (MMT) journal from Elsevier. The subject of another article was the SCALA conceptual development, and was published in the Journal of Intelligent & Robotic Systems (JIRS), from Springer. The fourth article concerned the mechanical design and development of the SCALA prototype, and was published in the IEEE/ASME Transactions on Mechatronics. All journals are from the best quartile (Q1) in the areas of mechanical engineering and industrial and manufacturing engineering, for MMT and JIRS, respectively (relative to the year 2015).

Additionally, there are two submitted journal articles, which currently await acceptance.

A provisional patent of the SCALA system, containing a description of the concept and the mechanical realization of the agents was filled, in the National Institute of Intellectual Property.

List of publications

- Carlos Viegas, Mahmoud Tavakoli, Pedro Lopes, Riccardo Dessi, Aníbal T. de Almeida. "SCALA - A scalable rail-based multi-robot system for large space automation: design and development" *IEEE/ASME Transactions on Mechatronics*, vol. 22, issue 5, (2017): 2208-2217.
- Carlos Viegas, Mahmoud Tavakoli, and Aníbal T. de Almeida. "A novel grid-based reconfigurable spatial parallel mechanism with large workspace." *Mechanism and Machine Theory* 115 (2017): 149-167.
- Carlos Viegas, David Daney, Mahmoud Tavakoli, M., and Aníbal T. de Almeida. "Performance analysis and design of parallel kinematic machines using interval analysis." *Mechanism and Machine Theory*, 115 (2017): 218-236.
- Mahmoud Tavakoli, Carlos Viegas, Lucio Sgrigna, and Aníbal T. de Almeida. "SCALA: Scalable Modular Rail based Multi-agent Robotic System for Fine Manipulation over Large Workspaces." *Journal of Intelligent & Robotic Systems* (2017), 1-18.

Under review

- Carlos Viegas, Mahmoud Tavakoli, Riccardo Dessi, Pedro Lopes, Aníbal T. de Almeida. "Control and Path Planning of a Multi-Agent Grid-based Ceiling Robotic System" *Journal of Control, Automation and System*.
- Carlos Viegas, José Prado, Mahmoud Tavakoli, Pedro Lopes, Aníbal T. de Almeida. "Scalable Modular Multi Mobile Agent Autonomous Computer Vision System for Large Spaces" *Autonomous Robots*.

Patent

Mahmoud Tavakoli, Carlos Viegas. "System for moving robots on two dimensional scaffolds" *Patent Request INPI 109859 U*, September 28th, 2017.

References

- [1] Committee on Visionary Manufacturing Challenges, *Visionary Manufacturing Challenges for 2020*. Washington, D.C.: National Academic Press, 1998.
- [2] European Commission, “ManuFuture, A Vision for 2020,” Report of the High-Level group - Assuring the future of manufacturing in Europe, Brussels, 2004.
- [3] A. Quilligan, “Digital Industry 4.0 - Accenture,” 2016. [Online]. Available: <https://www.accenture.com/gb-en/blogs/blogs-digital-industry-4-0>. [Accessed: 05-Feb-2017].
- [4] P. Leitão, “Agent-based distributed manufacturing control: A state-of-the-art survey,” *Eng. Appl. Artif. Intell.*, vol. 22, no. 7, pp. 979–991, Oct. 2009.
- [5] J. Biers, “3D Printing Could Become A \$13 Billion Industry,” *Business Insider*, 2014, url: <http://www.businessinsider.com/afp-from-earphones-to-jet-engines-3d-printing-takes-off-2014-11>.
- [6] M. A. Manyika James, Chui Michael, Bughin Jacques, Dobbs Richard, Bisson Peter, “Disruptive technologies: Advances that will transform life, business, and the global economy,” Report McKinsey Global Institute, May 2013.
- [7] D. Kucera, “Amazon Acquires Kiva Systems in Second-Biggest Takeover,” 2012. [Online] Available: <http://bloom.bg/Gzo6GU>, [Accessed: 01 Feb 2015]
- [8] Economic Policy Committee and the European Commission (DG ECFIN), “The impact of ageing on public expenditure: projections for the UE25 Member States on pensions, health care, long-term care, education and unemployment transfer, 2004-2050,” 2006.
- [9] “BEST Performance Group,” 2015. [Online]. Available: <http://bestperformancegroup.com/>.
- [10] Dassault Systemes, “3D CAD Design Software SOLIDWORKS.” Dassault Systemes, 2017.
- [11] Microsoft IDE, “Visual Studio - Developer Tools and Services.” Microsoft IDE, 2017.
- [12] MathWorks, “MATLAB.” MathWorks, 2017.
- [13] M. Tavakoli, C. Viegas, L. Marques, J. Norberto Pires, and A. T. de Almeida, “OmniClimber-II: An omnidirectional climbing robot with high maneuverability and flexibility to adapt to non-flat surfaces,” in *2013 IEEE International Conference on Robotics and Automation*, 2013, pp. 1349–1354.
- [14] M. Tavakoli, C. Viegas, L. Marques, J. Norberto, and A. T. de Almeida, “Magnetic omnidirectional wheels for climbing robots,” in *2013 IEEE/RSJ International Conference*

- on Intelligent Robots and Systems*, 2013, pp. 266–271.
- [15] M. Tavakoli, C. Viegas, L. Marques, J. N. Pires, and A. T. de Almeida, “OmniClimbers: Omni-directional magnetic wheeled climbing robots for inspection of ferromagnetic structures,” *Rob. Auton. Syst.*, vol. 61, no. 9, pp. 997–1007, Sep. 2013.
 - [16] M. Tavakoli and C. Viegas, “Analysis and application of dual-row omnidirectional wheels for climbing robots,” *Mechatronics*, vol. 24, no. 5, pp. 436–448, Aug. 2014.
 - [17] C. Viegas and M. Tavakoli, “A single DOF arm for transition of climbing robots between perpendicular planes,” in *2014 IEEE/RSJ International Conference on Intelligent Robots and Systems*, 2014, pp. 2867–2872.
 - [18] C. Viegas, “Design and implementation of an omni-directional climbing robot for inspection of ferromagnetic structures,” University of Coimbra, 2013.
 - [19] M. Tavakoli, C. Viegas, L. Sgrigna, and A. T. de Almeida, “SCALA: Scalable Modular Rail based Multi-agent Robotic System for Fine Manipulation over Large Workspaces,” *J. Intell. Robot. Syst.*, 2017, pp. 1–18.
 - [20] Carnegie Mellon University, “Unimate,” *The Robot Hall of Fame*. [Online]. Available: <http://www.robothalloffame.org/inductees/03inductees/unimate.html>. [Accessed: 10-May-2017].
 - [21] KUKA AG, “KR 1000 titan.” [Online]. Available: <https://www.kuka.com/en/de/products/robot-systems/industrial-robots/kr-1000-titan>. [Accessed: 18-Feb-2017].
 - [22] Omron Adept Technologies Inc., “Adept Quattro s650H.” [Online]. Available: <http://www.adept.com/products/robots/parallel/quattro-s650h/intro>. [Accessed: 18-Feb-2017].
 - [23] Y. Jin *et al.*, “Kinematic Analysis and Dimensional Synthesis of Exechon Parallel Kinematic Machine for Large Volume Machining,” *J. Mech. Robot.*, vol. 7, no. 4, p. 41004, Nov. 2015.
 - [24] “KIVA Systems.” [Online]. Available: <http://www.kivasystems.com/>. [Accessed: 01-Feb-2015].
 - [25] Egemin Automation Inc., “Tugger Automated Guided Vehicle (AGV),” 2015. [Online]. Available: http://www.egeminusa.com/pages/agvs/agvs_tuv.html. [Accessed: 01-Jun-2015].
 - [26] JBT Corporation, “Unit Load Automatic Guided Vehicles,” 2015. [Online]. Available: <http://www.jbtc-agv.com/en/Solutions/Products/Unit-Load-Automatic-Guided-Vehicles-AGVs>. [Accessed: 01-Jun-2015].
 - [27] Egemin Automation Inc., “Forklift Automated Guided Vehicles (AGVs),” 2015. [Online]. Available: http://www.egeminusa.com/pages/agvs/agvs_flv.html. [Accessed: 01-Jun-2015].
 - [28] M. Bengel, K. Pfeiffer, B. Graf, A. Bubeck, and A. Verl, “Mobile robots for offshore inspection and manipulation,” in *2009 IEEE/RSJ International Conference on Intelligent Robots and Systems*, 2009, pp. 3317–3322.
 - [29] Carnegie Mellon University’s National Robotics Engineering Center, “Sensabot: A Safe and Cost-Effective Inspection Solution,” *J. Pet. Technol.*, vol. 64, no. 10, pp. 32–34, 2012.

-
- [30] R. Bischoff, U. Huggenberger, and E. Prassler, "KUKA youBot - a mobile manipulator for research and education," in *2011 IEEE International Conference on Robotics and Automation*, 2011, pp. 1–4.
- [31] M. Rostkowska and M. Topolski, "On the Application of QR Codes for Robust Self-localization of Mobile Robots in Various Application Scenarios," Springer International Publishing, 2015, pp. 243–252.
- [32] X. YUAN, X. Yuan, Y. Yang, Z. Jiang, and C. Zhou, "A high precision visual localization sensor and its working methodology for an indoor mobile robot," *Front. Inf. Technol. Electron. Eng.*, vol. 17, no. 4, pp. 365–374, Apr. 2016.
- [33] R. Fukui, H. Morishita, T. Mori, and T. Sato, "HangBot: A Ceiling Mobile Robot with Robust Locomotion under a Large Payload," Springer Berlin Heidelberg, 2014, pp. 685–694.
- [34] Young-Ho Choi and Kwang-Mok Jung, "Windoro: The world's first commercialized window cleaning robot for domestic use," in *2011 8th International Conference on Ubiquitous Robots and Ambient Intelligence (URAI)*, 2011, pp. 131–136.
- [35] SPIDERCAM GMBH, "spidercam," 2017. [Online]. Available: <http://www.spidercam.tv/>. [Accessed: 10-May-2017].
- [36] R. Yao, X. Tang, J. Wang, and P. Huang, "Dimensional Optimization Design of the Four-Cable-Driven Parallel Manipulator in FAST," *IEEE/ASME Trans. Mechatronics*, Dec. 2010.
- [37] A. MING, M. KAJITANI, and T. HIGUCHI, "On the Design of Wire Parallel Mechanism," *Int. J. Japan Soc. Precis. Eng.*, vol. 29, no. 4, pp. 337–342, 1995.
- [38] G. Stepan and et. al., "ACROBOTER: a ceiling based crawling, hoisting and swinging service robot platform," in *Beyond Gray Droids: Domestic Robot Design for the 21st Century Workshop at HCI*, 2009.
- [39] S. Takahiro, T. Suzuki, M. Torikawa, and S. Suzuki, "Development of a ceiling-robots system and its motion control," in *2014 IEEE 13th International Workshop on Advanced Motion Control (AMC)*, 2014, pp. 179–184.
- [40] "Amazon Prime Air," 2015. [Online]. Available: <http://www.amazon.com/b?node=8037720011>. [Accessed: 01-Jun-2015].
- [41] N. Lavars, "How drones are poised to help build the cities of tomorrow," *Gizmag*, 2015.
- [42] H. Hodson, "Spider-drones weave cables into high-rise structures," *New Sci.*, vol. 220, no. 2942, p. 20, Nov. 2013.
- [43] Gramazio Kohler Research, "Aerial Construction, ETH Zurich, 2013-2015," 2015. [Online]. Available: <http://gramaziokohler.arch.ethz.ch/web/e/forschung/240.html>. [Accessed: 01-Jun-2015].
- [44] F. Outamazirt, L. Fu, Y. Lin, and N. Abdelkrim, "A new SINS/GPS sensor fusion scheme for UAV localization problem using nonlinear SVSF with covariance derivation and an adaptive boundary layer," *Chinese J. Aeronaut.*, vol. 29, no. 2, pp. 424–440, Apr. 2016.
- [45] S. Chen, S. Guo, and Y. Li, "Real-time tracking a ground moving target in complex indoor and outdoor environments with UAV," in *2016 IEEE International Conference on Information and Automation (ICIA)*, 2016, pp. 362–367.

- [46] V. Kumar, *Vijay Kumar: Robots that fly ... and cooperate* / TED Talk. 2012.
- [47] L. Christensen, N. Fischer, S. Kroffke, J. Lemburg, and R. Ahlers, “Cost-Effective Autonomous Robots for Ballast Water Tank Inspection,” *J. Sh. Prod. Des.*, vol. 27, no. 3, pp. 127–136, 2011.
- [48] E. Nunes *et al.*, “DORIS - Monitoring Robot for Offshore Facilities,” in *OTC Brasil*, 2013.
- [49] Y. Chen, Y. Yang, H. Qian, and Y. Xu, “The design of robot for space station operation,” in *2012 IEEE International Conference on Robotics and Biomimetics (ROBIO)*, 2012, pp. 247–252.
- [50] Sung-Min Moon, Daehie Hong, Sung-Won Kim, and Sora Park, “Building wall maintenance robot based on built-in guide rail,” in *2012 IEEE International Conference on Industrial Technology*, 2012, pp. 498–503.
- [51] Lucas France, “Lucas Robotics Systems.” [Online]. Available: <http://www.lucas-robotic-system.com/en/robots/lrs-en>. [Accessed: 20-Feb-2017].
- [52] G. L. H. Robert R DeWitt, “Material handling apparatus for delivering or retrieving items,” US8622194 B2, 2014.
- [53] OPEX Corporation, “Perfect Pick® Warehouse Automated Picking System.” [Online]. Available: <https://www.opex.com/material-handling/perfect-pick>. [Accessed: 20-Feb-2017].
- [54] Swisslog, “AutoStore Small Parts Storage System.” [Online]. Available: <http://www.swisslog.com/en/Products/WDS/Storage-Systems/AutoStore>. [Accessed: 20-Feb-2017].
- [55] J. L. Scheie, J. P. Røyseth, P. Grøssereid, L. Zheng, and G. F. Rolandsen, “Bachelor Thesis - AutoStore,” Norwegian Business School, 2012.
- [56] Autodesk, “Project Escher.” [Online]. Available: <http://projectescher.com/>. [Accessed: 17-Feb-2017].
- [57] J. McClellan, “Mars homes could be built in 24 hours using 3D printers,” *Tech Times*, 2014.
- [58] K. S. Saidi, J. B. O’Brien, and A. M. Lytle, “Robotics in Construction,” in *Springer Handbook of Robotics*, Berlin, Heidelberg: Springer Berlin Heidelberg, 2008, pp. 1079–1099.
- [59] Construction Robotics, “Semi-automated mason.” [Online]. Available: <http://www.construction-robotics.com/>. [Accessed: 20-Feb-2017].
- [60] S. Martinez, A. Jardon, J. M. Navarro, and P. Gonzalez, “Building industrialization: robotized assembly of modular products,” *Assem. Autom.*, vol. 28, no. 2, pp. 134–142, Apr. 2008.
- [61] S. Martínez, A. Jardón, J. Gonzalez Vítores, and C. Balaguer, “Flexible field factory for construction industry,” *Assem. Autom.*, vol. 33, no. 2, pp. 175–183, Apr. 2013.
- [62] “3D Print Canal House,” 2015. [Online]. Available: <http://3dprintcanalhouse.com/>. [Accessed: 01-Feb-2015].
- [63] “WASP – World’s Advanced Saving Project,” 2015. [Online]. Available:

- <http://www.wasproject.it/w/en/us/>. [Accessed: 01-Feb-2015].
- [64] Max Planck Society, “New technology for animation film experts: Movie heroes to be transferred to virtual worlds more easily, realistically,” *Phys.org*, 2013.
- [65] A. Ess, B. Leibe, K. Schindler, and L. Van Gool, “A mobile vision system for robust multi-person tracking,” in *2008 IEEE Conference on Computer Vision and Pattern Recognition*, 2008, pp. 1–8.
- [66] A. Sikandar and et. al., “Multi-view pictorial structures for 3d human pose estimation,” in *British Machine Vision Conference. Vol. 2.*, 2013.
- [67] Leyard, “OptiTrack - Motion Capture Systems.” [Online]. Available: <http://optitrack.com/>. [Accessed: 31-May-2017].
- [68] M. Riberto and et. al., “Setting up a Human Motion Analysis Laboratory: Camera Positioning for Kinematic Recording of Gait,” *Int J Phys Med Rehabil*, vol. 131, no. 1, 2013.
- [69] C. Rougier, J. Meunier, A. St-Arnaud, and J. Rousseau, “Fall Detection from Human Shape and Motion History Using Video Surveillance,” in *21st International Conference on Advanced Information Networking and Applications Workshops (AINAW'07)*, 2007, vol. 2, pp. 875–880.
- [70] E. Culurciello, P. Lichtsteiner, and T. Delbruck, “Fall detection using an address-event temporal contrast vision sensor,” in *2008 IEEE International Symposium on Circuits and Systems*, 2008, pp. 424–427.
- [71] R. Cucchiara, A. Prati, and R. Vezzani, “A multi-camera vision system for fall detection and alarm generation,” *Expert Syst.*, vol. 24, no. 5, pp. 334–345, Nov. 2007.
- [72] G. Diraco, A. Leone, and P. Siciliano, “An active vision system for fall detection and posture recognition in elderly healthcare,” in *2010 Design, Automation & Test in Europe Conference & Exhibition (DATE 2010)*, 2010, pp. 1536–1541.
- [73] M. Kobilarov, G. Sukhatme, J. Hyams, and P. Batavia, “People tracking and following with mobile robot using an omnidirectional camera and a laser,” in *Proceedings 2006 IEEE International Conference on Robotics and Automation, 2006. ICRA 2006.*, pp. 557–562.
- [74] D. Culler and J. Long, “A Prototype Smart Materials Warehouse Application Implemented Using Custom Mobile Robots and Open Source Vision Technology Developed Using EmguCV,” *Procedia Manuf.*, vol. 5, pp. 1092–1106, 2016.
- [75] K. Dewangan, A. Saha, K. Vaiapury, and R. Dasgupta, “3D Environment Reconstruction Using Mobile Robot Platform and Monocular Vision,” Springer, Singapore, 2016, pp. 213–221.
- [76] M. Reinstein and M. Hoffmann, “Dead Reckoning in a Dynamic Quadruped Robot Based on Multimodal Proprioceptive Sensory Information,” *IEEE Trans. Robot.*, vol. 29, no. 2, pp. 563–571, Apr. 2013.
- [77] Savant Automation, “The Basics of Automated Guided Vehicles,” 2015. [Online]. Available: <http://www.agvsystems.com/vehicles/>. [Accessed: 01-Jun-2015].
- [78] Mobile Robots Inc., “Mobile Robots Specifications,” 2007. [Online]. Available: <http://forkliftsystems.com/wp-content/uploads/2014/01/specifications-for-platforms.pdf>.

- [Accessed: 01-Jun-2015].
- [79] S. Lynen, M. W. Achtelik, S. Weiss, M. Chli, and R. Siegwart, “A robust and modular multi-sensor fusion approach applied to MAV navigation,” in *2013 IEEE/RSJ International Conference on Intelligent Robots and Systems*, 2013, pp. 3923–3929.
- [80] A.-M. Ahmad and H. Al Youssef, “3D sensor-based Moving Human Tracking Robot with Obstacle Avoidance,” in *2016 IEEE International Multidisciplinary Conference on Engineering Technology (IMCET)*, 2016, pp. 9–14.
- [81] Y. E. Abdelgabar, J. H. Lee, and S. Okamoto, “Motion Control of a Three Active Wheeled Mobile Robot and Collision-Free Human Following Navigation in Outdoor Environment,” in *Proceedings of the International MultiConference of Engineers and Computer Scientists*, 2016, vol. 1.
- [82] Revolutionary Robotics, “Revolutionary Robotics – Advanced IP CamTrack,” 2013. [Online]. Available: http://www.revolutionary-robotics.com/downloads/Revolutionary_Robotics_AIPCT.pdf. [Accessed: 01-Aug-2013].
- [83] Tyco Integrated Fire & Security, “Tyco SensorRail™ IV - Rail Video System,” 2015. [Online]. Available: <https://www.tycoemea.com/English/Products/CCTV/rail.asp>. [Accessed: 01-Jun-2015].
- [84] Sentry Tecnologies, “VideoRailway,” 2017. [Online]. Available: <http://investorshub.advfn.com/Sentry-Technology-Corp-SKVY-4211/>. [Accessed: 28-Mar-2017].
- [85] M. Tavakoli, G. Cabrita, R. Faria, L. Marques, and A. T. de Almeida, “Cooperative multi-agent mapping of three-dimensional structures for pipeline inspection applications,” *Int. J. Rob. Res.*, vol. 31, no. 12, pp. 1489–1503, Oct. 2012.
- [86] “Robotis Ltd.” [Online]. Available: <http://en.robotis.com/index/>. [Accessed: 22-Feb-2017].
- [87] IGUS, “igus® Portugal - Plastics for longer life®.” [Online]. Available: <http://www.igus.pt/>. [Accessed: 26-Feb-2017].
- [88] K. Tadakuma *et al.*, “Omnidirectional driving gears and their input mechanism with passive rollers,” in *2012 IEEE/RSJ International Conference on Intelligent Robots and Systems*, 2012, pp. 2881–2888.
- [89] Liban Robert De, “Guidance systems,” US3147817 A, 08-Sep-1964.
- [90] Egemin Automation Inc., “Egemin Navigation System on Robot,” 2015. [Online]. Available: http://www.egeminusa.com/pages/software/agvs_ensor.html. [Accessed: 01-Jun-2015].
- [91] Ben Einstein | Robohub, “Meet the drone that already delivers your packages, Kiva robot teardown.” [Online]. Available: <http://robohub.org/meet-the-drone-that-already-delivers-your-packages-kiva-robot-teardown/>. [Accessed: 26-Feb-2017].
- [92] Jean-Jacques Lucas, “Module for transferring a robotic carriage between guiding elements that are not joined end-to-end and adjacent,” EP2829364 A1, 2014.
- [93] C. R. J. B. Lars Sverker Ture Lindbo, Robert Rolf Stadie, Matthew Robert Whelan, “Apparatus for retrieving units from a storage system,” WO2015019055 A1, 2014.
- [94] C. Viegas, M. Tavakoli, and A. T. de Almeida, “A novel grid-based reconfigurable

- spatial parallel mechanism with large workspace,” *Mech. Mach. Theory*, vol. 115, pp. 149–167, 2017.
- [95] C. Viegas, D. Daney, M. Tavakoli, and A. T. de Almeida, “Performance analysis and design of parallel kinematic machines using interval analysis,” *Mech. Mach. Theory*, vol. 115, pp. 218–236, 2017.
- [96] L.-W. Tsai, *Robot analysis: the mechanics of serial and parallel manipulators*. John Wiley & Sons, 1999.
- [97] F. Gao, W. Li, X. Zhao, Z. Jin, and H. Zhao, “New kinematic structures for 2-, 3-, 4-, and 5-DOF parallel manipulator designs,” *Mech. Mach. theory*, vol. 37, no. 11, pp. 1395–1411, 2002.
- [98] Festo, “Sistemas cartesianos - Manipuladores 3D.” [Online]. Available: https://www.festo.com/cat/pt_pt/products_YXCR. [Accessed: 05-Mar-2017].
- [99] G. C., “Kinematic analysis optimization and programming of parallel robotic manipulators,” McGill University, Montréal, 1988.
- [100] Universal Robots, “UR5 - The flexible and collaborative robotic arm.” [Online]. Available: <https://www.universal-robots.com/products/ur5-robot/>. [Accessed: 05-Mar-2017].
- [101] Symétrie, “Breva - High Accuracy Adjustment Hexapod.” [Online]. Available: <http://www.symetrie.fr/en/products/positioning-hexapods/breva/>. [Accessed: 05-Mar-2017].
- [102] A. Cauchy, “Deuxième mémoire sur les polygones et les polyèdres,” *J. l'École Polytech.*, pp. 87–98, 1813.
- [103] R. Bricard, “Mémoire sur la théorie de l’octaèdre articulé,” *J. Math. Pures Appl.*, pp. 113–148, 1897.
- [104] V. E. Gough, “Contribution to discussion of papers on research in automobile stability, control and tyre performance,” in *Proc. Auto Div. Inst. Mech. Eng.*, 1956, vol. 171, pp. 392–394.
- [105] V. E. Gough and S. G. Whitehall, “Universal tyre test machine,” in *Proc. FISITA 9th Int. Technical Congress*, 1962, pp. 117–137.
- [106] K. Cappel and Others, “Motion simulator,” US Patent 3,295,224, 1967.
- [107] D. A. Steward, “A platform with 6 degree of freedom,” *Proc. Inst. Mech. Eng.*, no. part 1, pp. 371–386, 1965.
- [108] H. McCallion and P. D. Truong, “The analysis of a six degree of freedom work station for mechanized assembly,” in *Proc. 5th World Congress on Theory of Machines and Mechanisms*, 1979, vol. 611, p. 616.
- [109] C. Reboulet and A. Robert, “Hybrid control of a manipulator with an active compliant wrist,” *3th ISRR, Gouvieux, Fr.*, vol. 7, pp. 76–80, 1985.
- [110] J.-P. Merlet and D. Daney, “Appropriate design of parallel manipulators,” in *Smart Devices and machines for advanced manufacturing*, Springer, 2008, pp. 1–25.
- [111] E. F. Fichter, “A Stewart platform-based manipulator: general theory and practical construction,” *Int. J. Rob. Res.*, vol. 5, no. 2, pp. 157–182, 1986.

- [112] M. Griffis and J. Duffy, "A forward displacement analysis of a class of Stewart platforms," *J. Robot. Syst.*, vol. 6, no. 6, pp. 703–720, 1989.
- [113] Z. Affi, L. Romdhane, and A. Maalej, "Dimensional synthesis of a 3-translational-DOF in-parallel manipulator for a desired workspace," *Eur. J. Mech.*, vol. 23, no. 2, pp. 311–324, 2004.
- [114] R. Clavel, "Une nouvelle structure de manipulation parallèle pour la robotique légère," *RAIRO AP11*, vol. 23, no. 6, 1986.
- [115] J. M. Hervé, "Design of parallel manipulators via the displacement group," in *Proceedings of the Ninth World Congress on the Theory of Machines and Mechanisms*, 1995, vol. 3, pp. 2079–2082.
- [116] J. M. Hervé and F. Sparacino, "Structural synthesis of parallel robots generating spatial translation," in *Proceedings of the 5th IEEE international conference on advanced robotics*, 1991, pp. 808–813.
- [117] L. Romdhane, "Design and analysis of a hybrid serial-parallel manipulator," *Mech. Mach. Theory*, vol. 34, no. 7, pp. 1037–1055, 1999.
- [118] L. Romdhane, Z. Affi, and M. Fayet, "Design and Singularity Analysis of a 3-Translational-DOF In-Parallel Manipulator*," *J. Mech. Des.*, vol. 124, no. 3, pp. 419–426, 2002.
- [119] A. Tremblain and L. Baron, "Geometrical synthesis of parallel manipulators of star-like topology with a geometric algorithm," in *IEEE International Conference on Robotics and Automation, Detroit, MI*, 1999.
- [120] L.-W. Tsai, "Kinematics of a three-dof platform with three extensible limbs," in *Recent advances in robot kinematics*, Springer, 1996, pp. 401–410.
- [121] M. A. Laribi, L. Romdhane, and S. Zeghloul, "Analysis and dimensional synthesis of the DELTA robot for a prescribed workspace," *Mech. Mach. Theory*, vol. 42, no. 7, pp. 859–870, 2007.
- [122] R. Clavel, "Delta, a fast robot with parallel geometry," in *Proc. 18th Int. Symp. on Industrial Robots, Lausanne, 1988*, 1988, pp. 91–100.
- [123] P. Vischer and R. Clavel, "Kinematic calibration of the parallel Delta robot," *Robotica*, vol. 16, no. 2, pp. 207–218, 1998.
- [124] M. Stock and K. Miller, "Optimal kinematic design of spatial parallel manipulators: application to linear delta robot," *J. Mech. Des.*, vol. 125, no. 2, pp. 292–301, 2003.
- [125] J.P. Merlet, *Parallel Robots*. Springer Science & Business Media, 2012.
- [126] Z. Pandilov and V. Dukovski, "Comparison of the characteristics between serial and parallel robots," *ACTA TEHNICA CORVINIENSIS - Bulletin of Engineering*, vol. 1, pp. 2067–3809, 2014.
- [127] R.-M. A. Nzue, J.-F. Brethé, E. Vasselin, and D. Lefebvre, "Comparison of serial and parallel robot repeatability based on different performance criteria," *Mech. Mach. Theory*, vol. 61, pp. 136–155, Mar. 2013.
- [128] R. Clavel, "Robots parallèles," *Tech. l'Ing{é}nieur*, 1994.
- [129] M. Hebsacker, T. Treib, O. Zirn, and M. Honegger, "Hexaglide 6 dof and triaglide 3 dof

- parallel manipulators,” in *Parallel Kinematic Machines*, Springer, 1999, pp. 345–355.
- [130] K.-H. Wurst and others, “Systematic design of hexapods and other parallel link systems,” *CIRP Ann. Technol.*, vol. 46, no. 1, pp. 291–295, 1997.
- [131] F. L. O. Company F. Pierrot and C. Fioroni, “Modeling and preliminary design issues for 3-Axis parallel machine-tool,” in *Proc. Parallel Kinematic Machines Int. Conf, Ann Arbor, MI (USA)*, 2000, pp. 14–23.
- [132] T. Brogårdh, S. Hanssen, and G. Hovland, “Application-oriented development of parallel kinematic manipulators with large workspace,” in *2nd International Colloquium of the Collaborative Research Center*, 2005, vol. 562, pp. 153–170.
- [133] D. Zhang and Z. Bi, “Development of reconfigurable parallel kinematic machines using modular design approach,” *Proc. Can. Eng. Educ. Assoc.*, vol. 0, no. 0, 2011.
- [134] K. H. Wurst, “The conception and construction of a modular robot system,” *Proc. 16th Int. Sym. Ind. Robot.*, pp. 37–44, 1986.
- [135] and H. J. F. Stechert, C., “Oriented configuration of parallel robotic systems,” *Futur. Prod. Dev. Proc. 17th CIRP Des. Conf.*, pp. 259–68, 2007.
- [136] C. Brisan and A. Csiszar, “Computation and analysis of the workspace of a reconfigurable parallel robotic system,” *Mech. Mach. Theory*, vol. 46, no. 11, pp. 1647–1668, Nov. 2011.
- [137] R. Fisher, R. P. Podhorodeski, and S. B. Nokleby, “Design of a reconfigurable planar parallel manipulator,” *J. Robot. Syst.*, vol. 21, no. 12, pp. 665–675, Dec. 2004.
- [138] D. P. and N. P. and A. V. and B. P. and B. G. and D. Lese, “Kinematics and design of two variants of a reconfigurable parallel robot,” in *2009 ASME/IFTOMM International Conference on Reconfigurable Mechanisms and Robots*, 2009, pp. 624–631.
- [139] N. Plitea, D. Lese, D. Pislă, and C. Vaida, “Structural design and kinematics of a new parallel reconfigurable robot,” *Robot. Comput. Integr. Manuf.*, vol. 29, no. 1, pp. 219–235, Feb. 2013.
- [140] G. Coppola, D. Zhang, and K. Liu, “A 6-DOF reconfigurable hybrid parallel manipulator,” *Robot. Comput. Integr. Manuf.*, vol. 30, no. 2, pp. 99–106, Apr. 2014.
- [141] P. Grosch, R. Di Gregorio, J. López, and F. Thomas, “Motion planning for a novel reconfigurable parallel manipulator with lockable revolute joints,” in *2010 IEEE International Conference on Robotics and Automation*, 2010, pp. 4697–4702.
- [142] M. Palpacelli, L. Carbonari, G. Palmieri, and M. Callegari, “Mobility Analysis of Non-overconstrained Reconfigurable Parallel Manipulators with 3-CPU/3-CRU Kinematics,” Springer, Cham, 2016, pp. 189–200.
- [143] D. Chablat, R. Jha, and S. Caro, “A Framework for the Control of a Parallel Manipulator with Several Actuation Modes,” in *14th International Conference on Industrial Informatics IEEE*, 2016.
- [144] R. Rizk, J. C. Fauroux, M. Munteanu, and G. Gogu, “A comparative stiffness analysis of a reconfigurable parallel machine with three or four degrees of mobility,” *J. Mach. Eng.*, vol. 6, no. 2, pp. 45–55, 2006.
- [145] Y. Jin, B. Lian, M. Price, T. Sun, and Y. Song, “QrPara: A New Reconfigurable Parallel Manipulator with 5-Axis Capability,” Springer, Cham, 2016, pp. 247–258.

- [146] W. Ye, Y. Fang, and S. Guo, "Design and analysis of a reconfigurable parallel mechanism for multidirectional additive manufacturing," *Mech. Mach. Theory*, Mar. 2016.
- [147] M. Zein, P. Wenger, and D. Chablat, "Non-singular assembly-mode changing motions for 3-RPR parallel manipulators," *Mech. Mach. Theory*, vol. 43, no. 4, pp. 480–490, Apr. 2008.
- [148] J. Hesselbach, M. B. Helm, and S. Soetebier, "Connecting assembly modes for workspace enlargement," in *Advances in Robot Kinematics*, Dordrecht: Springer, 2002, pp. 347–356.
- [149] C. Budde, P. Last, and J. Hesselbach, "Development of a Triglides-robot with enlarged workspace," in *Robotics and Automation, 2007 IEEE International Conference on*, 2007, pp. 543–548.
- [150] O. K. Sakamoto Y. and M. Horie, "A Type Synthesis of Spatial Mechanism with Consideration of Degrees of Freedom of Mechanism.," *Nippon Kikai Gakkai Ronbunshu*, vol. 59, no. 559, pp. 939–946, 1993.
- [151] J. Angeles and C. Gosselin, "Determination du degre de liberte des cha{î}nes cinematiques simples et complexes," in *7th World Congress on Theory of Machines and Mechanisms*, pp. 199–202.
- [152] R. Franke, *Vom Aufbau der Getriebe*, vol. 1. VDI-Verlag, 1958.
- [153] M. Shoham and B. Roth, "Connectivity in open and closed loop robotic mechanisms," *Mech. Mach. theory*, vol. 32, no. 3, pp. 279–293, 1997.
- [154] N. Rakotomanga and I. A. Bonev, "A 3-RPR Parallel Mechanism With Singularities That are Self-Motions," *J. Mech. Robot.*, vol. 2, no. 3, p. 34502, 2010.
- [155] D. N. Nenchev, S. Bhattacharya, and M. Uchiyama, "Dynamic analysis of parallel manipulators under the singularity-consistent parameterization," *Robotica*, vol. 15, no. 4, pp. 375–384, 1997.
- [156] P. Wenger and D. Chablat, "Workspace and assembly modes in fully-parallel manipulators: A descriptive study," in *Advances in Robot kinematics: Analysis and control*, Springer, 1998, pp. 117–126.
- [157] X. Kong and Y. Jin, "Type Synthesis of 3-DOF multi-mode translational/spherical parallel mechanisms with lockable joints," *Mech. Mach. Theory*, vol. 96, pp. 323–333, Feb. 2016.
- [158] P. Chedmail and M. Gautier, "Optimum Choice of Robot Actuators," *J. Eng. Ind.*, vol. 112, no. 4, p. 361, 1990.
- [159] C. Germain, S. Caro, S. Briot, and P. Wenger, "Optimal Design of the IRSBot-2 Based on an Optimized Test Trajectory," in *Volume 6A: 37th Mechanisms and Robotics Conference*, 2013, p. V06AT07A056.
- [160] V. Potkonjak, "Thermal criterion for the selection of dc drives for industrial robots," in *Proc. of the 16th ISIR*, 1986.
- [161] E. D. W. Khalil, *Modeling, Identification and Control of Robots*. Butterworth-Heinemann, 2004.
- [162] H. Olsen and G. Bekey, "Identification of robot dynamics," in *Proceedings. 1986 IEEE*

-
- International Conference on Robotics and Automation*, vol. 3, pp. 1004–1010.
- [163] M. Gautier and S. Briot, “New method for global identification of the joint drive gains of robots using a known inertial payload,” in *IEEE Conference on Decision and Control and European Control Conference*, 2011, pp. 1393–1398.
- [164] J. Hollerbach, W. Khalil, and M. Gautier, “Model Identification,” in *Springer Handbook of Robotics*, Cham: Springer International Publishing, 2016, pp. 113–138.
- [165] W. Khalil, M. Gautier, and P. Lemoine, “Identification of the payload inertial parameters of industrial manipulators,” in *Proceedings 2007 IEEE International Conference on Robotics and Automation*, 2007, pp. 4943–4948.
- [166] S. Briot and W. Khalil, *Dynamics of Parallel Robots: From Rigid Bodies to Flexible Elements*, vol. 35. Cham: Springer International Publishing, 2015.
- [167] W. Q. D. Do and D. C. H. Yang, “Inverse dynamic analysis and simulation of a platform type of robot,” *J. Robot. Syst.*, vol. 5, no. 3, pp. 209–227, Jun. 1988.
- [168] P. Guglielmetti and R. Longchamp, “A Closed Form Inverse Dynamics Model of the Delta Parallel Robot,” *IFAC Symp. Robot Control. (September 1994)*, pp. 51–56, 1994.
- [169] and D. K. Tsai, K. Y., “Modified Newton-Euler Computational Scheme for Dynamic Analysis and Simulation of Parallel Manipulators with Applications to Configuration Based on RL Actuators,” in *Proceedings of the 1990 ASME Design Engineering Technical Conferences*, 1990.
- [170] M. Ahmadi, M. Dehghani, M. Eghtesad, and A. R. Khayatian, “Inverse Dynamics of Hexa Parallel Robot Using Lagrangian Dynamics Formulation,” in *2008 International Conference on Intelligent Engineering Systems*, 2008, pp. 145–149.
- [171] G. Lebret, K. Liu, and F. L. Lewis, “Dynamic analysis and control of a stewart platform manipulator,” *J. Robot. Syst.*, vol. 10, no. 5, pp. 629–655, Jul. 1993.
- [172] A. Elkady, G. Elkobrosy, S. Hanna, and T. Sobh, *Cartesian Parallel Manipulator Modeling, Control and Simulation*. Citeseer, 2008.
- [173] Y. Li and Q. Xu, “Kinematics and inverse dynamics analysis for a general 3-PRS spatial parallel mechanism,” *Robotica*, vol. 23, no. 2, pp. 219–229, Mar. 2005.
- [174] A. Codourey, “Dynamic modelling and mass matrix evaluation of the DELTA parallel robot for axes decoupling control,” in *Proceedings of IEEE/RSJ International Conference on Intelligent Robots and Systems. IROS '96*, vol. 3, pp. 1211–1218.
- [175] L.-W. Tsai, “Solving the Inverse Dynamics of a Stewart-Gough Manipulator by the Principle of Virtual Work,” *J. Mech. Des.*, vol. 122, no. 1, p. 3, 2000.
- [176] K. Miller, “Optimal Design and Modeling of Spatial Parallel Manipulators,” *Int. J. Rob. Res.*, vol. 23, no. 2, pp. 127–140, Feb. 2004.
- [177] S. Küçük, *Inverse Dynamics of RRR Fully Planar Parallel Manipulator Using DH Method*. INTECH Open Access Publisher, 2012.
- [178] W. Khalil and O. Ibrahim, “General solution for the dynamic modeling of parallel robots,” in *IEEE International Conference on Robotics and Automation, 2004. Proceedings. ICRA '04. 2004*, 2004, p. 3665–3670 Vol.4.
- [179] C. F. Adetu, C. A. Moore, and R. G. Roberts, “Dynamic modeling and control of the OMEGA-3 parallel manipulator,” in *2009 IEEE International Conference on Systems*,

- Man and Cybernetics*, 2009, pp. 3599–3604.
- [180] H. Baruh, *Analytical dynamics*. WCB/McGraw-Hill Boston, 1999.
- [181] C. Canudas de Wit and A. Aubin, “Parameters identification of robots manipulators via sequential hybrid estimation algorithms,” in *Proceedings IFAC Congress*, 1990, pp. 178–183.
- [182] Brian Armstrong-Hélouvy, *Control of Machines with Friction*. Springer Science, 2012.
- [183] C. C. de Wit, P. Noël, A. Aubin, and B. Brogliato, “Adaptive Friction Compensation in Robot Manipulators: Low Velocities,” *Int. J. Rob. Res.*, vol. 10, no. 3, pp. 189–199, 1991.
- [184] P. R. Dahl, “Measurement of Solid Friction Parameters of Ball Bearings,” in *Proceedings of the 6th Annual Symposium on Incremental Motion Control Systems and Devices*, 1977.
- [185] P. Hamon, M. Gautier, P. Garrec, and A. Janot, “Dynamic identification of robot with a load-dependent joint friction model,” *2010 IEEE Conference on Robotics, Automation and Mechatronics*. pp. 129–135, 2010.
- [186] M. Leonesio and G. Bianchi, “Self-locking analysis in closed kinematic chains,” *Mech. Mach. Theory*, vol. 44, no. 11, pp. 2038–2052, 2009.
- [187] C. Gosselin and J. Angeles, “Singularity analysis of closed-loop kinematic chains,” *IEEE Trans. Robot. Autom.*, vol. 6, no. 3, pp. 281–290, Jun. 1990.
- [188] S. Bhattacharya, H. Hatwal, and A. Ghosh, “On the optimum design of Stewart platform type parallel manipulators,” *Robotica*, vol. 13, no. 2, p. 133, Mar. 1995.
- [189] M. Badescu and C. Mavroidis, “Workspace Optimization of 3-Legged UPU and UPS Parallel Platforms With Joint Constraints,” *J. Mech. Des.*, vol. 126, no. 2, p. 291, 2004.
- [190] A. G. Erdman, *Modern kinematics: developments in the last forty years*. John Wiley & Sons, 1993.
- [191] I. Das and J. E. Dennis, “A closer look at drawbacks of minimizing weighted sums of objectives for Pareto set generation in multicriteria optimization problems,” *Struct. Optim.*, vol. 14, no. 1, pp. 63–69, Aug. 1997.
- [192] M. L. Keler, “Dual Expansion of an Optimal in-Parallel Spherical Platform Device into a Spatial One,” in *Advances in Robot Kinematics: Analysis and Control*, Dordrecht: Springer Netherlands, 1998, pp. 79–86.
- [193] W. Chen, M. M. Wiecek, and J. Zhang, “Quality Utility—A Compromise Programming Approach to Robust Design,” *J. Mech. Des.*, vol. 121, no. 2, p. 179, 1999.
- [194] W. Chen, A. Sahai, A. Messac, and G. J. Sundararaj, “Exploration of the Effectiveness of Physical Programming in Robust Design,” *J. Mech. Des.*, vol. 122, no. 2, p. 155, 2000.
- [195] D. Chablat and P. Wenger, “Architecture optimization of a 3-DOF translational parallel mechanism for machining applications, the orthoglide,” *IEEE Trans. Robot. Autom.*, vol. 19, no. 3, pp. 403–410, Jun. 2003.
- [196] H. S. Kim and L.-W. Tsai, “Design Optimization of a Cartesian Parallel Manipulator,” in *Volume 5: 27th Biennial Mechanisms and Robotics Conference*, 2002, pp. 865–872.
- [197] A. H. Land and A. G. Doig, “An Automatic Method of Solving Discrete Programming Problems,” *Econometrica*, vol. 28, no. 3, p. 497, Jul. 1960.
- [198] J. D. C. Little, K. G. Murty, D. W. Sweeney, and C. Karel, “An Algorithm for the

- Traveling Salesman Problem,” *Oper. Res.*, vol. 11, no. 6, pp. 972–989, Dec. 1963.
- [199] L. Jaulin, *Applied interval analysis: with examples in parameter and state estimation, robust control and robotics*. Springer Science & Business Media, 2001.
- [200] R. E. Moore, *Interval analysis*. Prentice-Hall Englewood Cliffs, 1966.
- [201] F. Hao and J.-P. Merlet, “Multi-criteria optimal design of parallel manipulators based on interval analysis,” *Mech. Mach. Theory*, vol. 40, no. 2, pp. 157–171, Feb. 2005.
- [202] J.-P. Merlet and D. Daney, “Dimensional Synthesis of Parallel Robots with a Guaranteed Given Accuracy over a Specific Workspace,” in *Proceedings of the 2005 IEEE International Conference on Robotics and Automation*, pp. 942–947.
- [203] M. Tannous, S. Caro, and A. Goldsztejn, “Sensitivity analysis of parallel manipulators using an interval linearization method,” *Mech. Mach. Theory*, vol. 71, pp. 93–114, Jan. 2014.
- [204] J.-P. Merlet, “An improved design algorithm based on interval analysis for spatial parallel manipulator with specified workspace,” in *Proceedings 2001 ICRA. IEEE International Conference on Robotics and Automation (Cat. No.01CH37164)*, vol. 2, pp. 1289–1294.
- [205] and S. C. Kaloorazi, M. Hadi Farzaneh, Mehdi Tale Masouleh, “Interval-analysis-based determination of the singularity-free workspace of gough-stewart parallel robots,” in *Electrical Engineering (ICEE), 2013 21st Iranian Conference on. IEEE*, 2013.
- [206] S. Caro, D. Chablat, A. Goldsztejn, D. Ishii, and C. Jermann, “A branch and prune algorithm for the computation of generalized aspects of parallel robots,” *Artif. Intell.*, vol. 211, pp. 34–50, Jun. 2014.
- [207] N. Ramdani, M. Gouttefarde, F. Pierrot, and J.-P. Merlet, “First results on the design of high speed parallel robots in presence of uncertainty,” in *2008 IEEE/RSJ International Conference on Intelligent Robots and Systems*, 2008, pp. 2410–2415.
- [208] A. Goldsztejn, S. Caro, and G. Chabert, “A three-step methodology for dimensional tolerance synthesis of parallel manipulators,” *Mech. Mach. Theory*, vol. 105, pp. 213–234, Nov. 2016.
- [209] R. Di Gregorio and V. Parenti-Castelli, “Geometric error effects on the performances of a parallel wrist,” in *3rd Chemnitz Parallelkinematik Seminar*, 2002, pp. 1011–1024.
- [210] A. Goldsztejn, C. Michel, and M. Rueher, “Efficient handling of universally quantified inequalities,” *Constraints*, vol. 14, no. 1, pp. 117–135, Mar. 2009.
- [211] L. Jaulin and É. Walter, “Guaranteed tuning, with application to robust control and motion planning,” *Automatica*, vol. 32, no. 8, pp. 1217–1221, Aug. 1996.
- [212] S. Ratschan and Stefan, “Efficient solving of quantified inequality constraints over the real numbers,” *ACM Trans. Comput. Log.*, vol. 7, no. 4, pp. 723–748, Oct. 2006.
- [213] D. Ratz and T. Csendes, “On the selection of subdivision directions in interval branch-and-bound methods for global optimization,” *J. Glob. Optim.*, vol. 7, no. 2, pp. 183–207, Sep. 1995.
- [214] A. Goldsztejn and L. Jaulin, “Inner and Outer Approximations of Existentially Quantified Equality Constraints,” Springer, Berlin, Heidelberg, 2006, pp. 198–212.
- [215] W. Oettli and W. Prager, “Compatibility of approximate solution of linear equations with given error bounds for coefficients and right-hand sides,” *Numer. Math.*, vol. 6, no. 1, pp.

- 405–409, Dec. 1964.
- [216] W. Oettli, “On the Solution Set of a Linear System with Inaccurate Coefficients,” *J. Soc. Ind. Appl. Math. Ser. B Numer. Anal.*, vol. 2, no. 1, pp. 115–118, Jan. 1965.
- [217] O. Beaumont, “Algorithmique pour les intervalles: Comment obtenir un résultat sûr quand les données sont incertaines,” Université de Rennes, 1999.
- [218] G. Rex and J. Rohn, “Sufficient Conditions for Regularity and Singularity of Interval Matrices,” *SIAM J. Matrix Anal. Appl.*, vol. 20, no. 2, pp. 437–445, Jan. 1998.
- [219] C. Jansson and J. Rohn, “An Algorithm for Checking Regularity of Interval Matrices,” *SIAM J. Matrix Anal. Appl.*, vol. 20, no. 3, pp. 756–776, Jan. 1999.
- [220] J.-P. Merlet and D. Daney, “A formal-numerical approach to determine the presence of singularity within the workspace of a parallel robot,” in *2nd Workshop on Computational Kinematics*, 2001, pp. 167–176.
- [221] C. Han, J. Kim, J. Kim, and F. C. Park, “Kinematic sensitivity analysis of the 3-UPU parallel mechanism,” *Mech. Mach. Theory*, vol. 37, no. 8, pp. 787–798, Aug. 2002.
- [222] Chang-Soo Han, J. C. Hudgens, D. Tesar, and A. E. Traver, “Modeling, synthesis, analysis, and design of high resolution micromanipulator to enhance robot accuracy,” in *Proceedings IROS '91:IEEE/RSJ International Workshop on Intelligent Robots and Systems '91*, pp. 1157–1162.
- [223] H. S. Kim and Y. J. Choi, “The kinematic error bound analysis of the Stewart platform,” *J. Robot. Syst.*, vol. 17, no. 1, pp. 63–73, Jan. 2000.
- [224] O. Masory, J. Wang, and H. Zhuang, “On the accuracy of a Stewart platform. II. Kinematic calibration and compensation,” in *[1993] Proceedings IEEE International Conference on Robotics and Automation*, pp. 725–731.
- [225] A. J. Patel and K. F. Ehmann, “Volumetric Error Analysis of a Stewart Platform-Based Machine Tool,” *CIRP Ann. - Manuf. Technol.*, vol. 46, no. 1, pp. 287–290, 1997.
- [226] T. Ropponen and T. Arai, “Accuracy analysis of a modified Stewart platform manipulator,” in *Proceedings of 1995 IEEE International Conference on Robotics and Automation*, vol. 1, pp. 521–525.
- [227] J. Hubert and J.-P. Merlet, “Singularity Analysis through Static Analysis,” in *Advances in Robot Kinematics: Analysis and Design*, Dordrecht: Springer Netherlands, 2008, pp. 13–20.
- [228] S. et al Ratschan, “Rsolver.” 2004.
- [229] G. Chabert and L. Jaulin, “Contractor programming,” *Artif. Intell.*, vol. 173, no. 11, pp. 1079–1100, Jul. 2009.
- [230] G. Chabert, “A simple slam example with ibex.” 2013.
- [231] J.-P. Merlet, “Alias: an interval analysis based library for solving and analyzing system of equations,” *SEA Autom.*, pp. 1964–1969, 2000.
- [232] Europeumaq, “ITEM Profiles and accessories,” 2015. [Online]. Available: <http://www.item24.pt/pt/home/produtos/catalogo-de-produtos/products/profile-und-zubehoer-1.html>. [Accessed: 01-Jun-2015].
- [233] Shapeways, “Strong & Flexible Plastic Material Information,” 2015. [Online]. Available:

- <http://www.shapeways.com/materials/strong-and-flexible-plastic>. [Accessed: 01-Jun-2015].
- [234] IGUS, “IGUS.” [Online]. Available: <http://www.igus.pt/>. [Accessed: 01-Jun-2015].
- [235] “Joints for Delta Printer,” *Reprap.org*, 2014. [Online]. Available: http://reprap.org/wiki/Joints_for_Delta_Printer. [Accessed: 01-May-2015].
- [236] HKCM Engineering, “HKCM Engineering - Specialists for Magnets,” 2015. [Online]. Available: <https://www.hkcm.de/expert.php?fav=>. [Accessed: 01-Jun-2015].
- [237] Pololu Robotics & Electronics, “Micro Metal Gearmotors,” 2015. [Online]. Available: <https://www.pololu.com/category/60/micro-metal-gearmotors>. [Accessed: 01-Jun-2015].
- [238] Eclipse Magnetics, “Energise to Hold Electromagnets,” 2017. [Online]. Available: <http://www.eclipsemagnetics.com/row/product-range/magnet-materials-assemblies/m52175-240va-energise-to-hold.html>.
- [239] BQ, “HeatCore Unibody extrusion kit,” 2017. [Online]. Available: <https://www.bq.com/en/heatcore-unibody>.
- [240] OSRAM, “Blue Laser | Visible Laser | OSRAM Opto Semiconductors.” [Online]. Available: https://www.osram-os.com/osram_os/en/products/product-catalog/laser-diodes/visible-laser/blue-laser/. [Accessed: 19-Jun-2017].
- [241] A. Stock, “Comparing Performance and Efficiency of Linear Motors, Ball Screws, and Rack-and-Pinion Drives. | Archive content from Machine Design,” 2010.
- [242] Steven Gauthier, “Developing a High-Accuracy Multipole Strip Magnet for Noncontact Linear and Rotary Position Measurement | Sensors,” *Sensors Online*.
- [243] AMS, “AS5304 Linear Sensor.” [Online]. Available: <http://ams.com/eng/Products/Magnetic-Position-Sensors/Linear-Position/AS5304>. [Accessed: 21-Mar-2017].
- [244] ARM, “Cortex-M4 Processor.” [Online]. Available: <http://www.arm.com/products/processors/cortex-m/cortex-m4-processor.php>. [Accessed: 01-Jun-2015].
- [245] Microchip, “RN42,” 2016. [Online]. Available: <http://www.microchip.com/wwwproducts/en/RN42>.
- [246] R. Dessi, “Coordination and Path Planning of a Multi Robot System for Fine Manipulation and 3D Printing Over Large Workspace,” Politecnico di Torino, 2016.
- [247] Y. Wang and A. Cavallaro, “Prioritized target tracking with active collaborative cameras,” in *2016 13th IEEE International Conference on Advanced Video and Signal Based Surveillance (AVSS)*, 2016, pp. 131–137.
- [248] E. G. Tsardoulis, A. Iliakopoulou, A. Kargakos, and L. Petrou, “A Review of Global Path Planning Methods for Occupancy Grid Maps Regardless of Obstacle Density,” *J. Intell. Robot. Syst.*, vol. 84, no. 1–4, pp. 829–858, May 2016.
- [249] P. P. Raja and S. Pugazhenthii, “Optimal path planning of mobile robots: A review,” *Int. J. Phys. Sci.*, vol. 7, no. 9, pp. 1314–1320, Feb. 2012.
- [250] I. Chaari, A. Koubaa, H. Bennaceur, S. Trigui, and K. Al-Shalfan, “smartPATH: A hybrid ACO-GA algorithm for robot path planning,” in *2012 IEEE Congress on*

- Evolutionary Computation*, 2012, pp. 1–8.
- [251] M. Alajlan, A. Koubaa, I. Chaari, H. Bennaceur, and A. Ammar, “Global path planning for mobile robots in large-scale grid environments using genetic algorithms,” in *2013 International Conference on Individual and Collective Behaviors in Robotics (ICBR)*, 2013, pp. 1–8.
- [252] N. A. Shiltagh and L. D. Jalal, “Optimal path planning for intelligent mobile robot navigation using modified particle swarm optimization,” *Int. J. Eng. Adv. Technol.*, vol. 2, no. 4, pp. 260–267, 2013.
- [253] E. Masehian and M. R. Amin-Naseri, “A Tabu Search-based Approach for Online Motion Planning,” in *2006 IEEE International Conference on Industrial Technology*, 2006, pp. 2756–2761.
- [254] I. Châari *et al.*, “On the Adequacy of Tabu Search for Global Robot Path Planning Problem in Grid Environments,” *Procedia Comput. Sci.*, vol. 32, pp. 604–613, 2014.
- [255] P. Hart, N. Nilsson, and B. Raphael, “A Formal Basis for the Heuristic Determination of Minimum Cost Paths,” *IEEE Trans. Syst. Sci. Cybern.*, vol. 4, no. 2, pp. 100–107, 1968.
- [256] A. Zhang, C. Li, and W. Bi, “Rectangle expansion A \square pathfinding for grid maps,” *Chinese J. Aeronaut.*, vol. 29, no. 5, pp. 1385–1396, 2016.
- [257] Ken Thayer, “What Is the Real Cost of an Industrial Robot Arm?,” *Engineering 360*, 2017.
- [258] Technical Committee ISO/TC 184, “ISO 9283:1998(en), Manipulating industrial robots — Performance criteria and related test methods,” 1998.
- [259] S. Garrido-Jurado, R. Muñoz-Salinas, F. J. Madrid-Cuevas, and M. J. Marín-Jiménez, “Automatic generation and detection of highly reliable fiducial markers under occlusion,” *Pattern Recognit.*, vol. 47, no. 6, pp. 2280–2292, 2014.
- [260] P. Viola and M. Jones, “Rapid object detection using a boosted cascade of simple features,” in *Proceedings of the 2001 IEEE Computer Society Conference on Computer Vision and Pattern Recognition. CVPR 2001*, vol. 1, p. I-511-I-518.
- [261] T. Linder, S. Breuers, B. Leibe, and K. O. Arras, “On multi-modal people tracking from mobile platforms in very crowded and dynamic environments,” in *2016 IEEE International Conference on Robotics and Automation (ICRA)*, 2016, pp. 5512–5519.
- [262] N. Krahnstoever, T. Yu, S.-N. Lima, and K. Patwardhana, “Collaborative control of active cameras in large-scale surveillance,” *Multi-Camera Networks Princ. Appl. H. Aghajan A. Cavallaro, Eds. Elsevier Sci. Inc*, pp. 165–188, 2009.
- [263] A. Del Bimbo, F. Dini, A. Grifoni, and F. Pernici, “Pan-tilt-zoom camera networks,” *Multi-Camera Networks Princ. Appl.*, p. 189, 2009.
- [264] ABB, “ABB Robotics - Manufacturer & Supplier of Industrial Robots.” [Online]. Available: <http://new.abb.com/products/robotics>. [Accessed: 05-Mar-2017].
- [265] FANUC, “FANUC Industrial Robots.” [Online]. Available: <http://www.fanuc.eu/uk/en/robots/robot-range-page>. [Accessed: 05-Mar-2017].
- [266] KUKA AG, “Industrial robot | KUKA AG.” [Online]. Available: <https://www.kuka.com/en-de/products/robot-systems/industrial-robots>. [Accessed: 05-Mar-2017].

- [267] Omron, "Omron Adept Technologies, Inc." [Online]. Available: <http://www.adept.com/>. [Accessed: 06-Mar-2017].
- [268] Symetrie, "Symetrie." [Online]. Available: <http://www.symetrie.fr/en/home/>. [Accessed: 06-Mar-2017].
- [269] B. S. Armstrong, "Dynamics for robot control: friction modeling and ensuring excitation during parameter identification," DTIC Document, 1988.

Appendix A

Prototype Drawings

Appendix A1 – SCALA GEN ONE prototype;

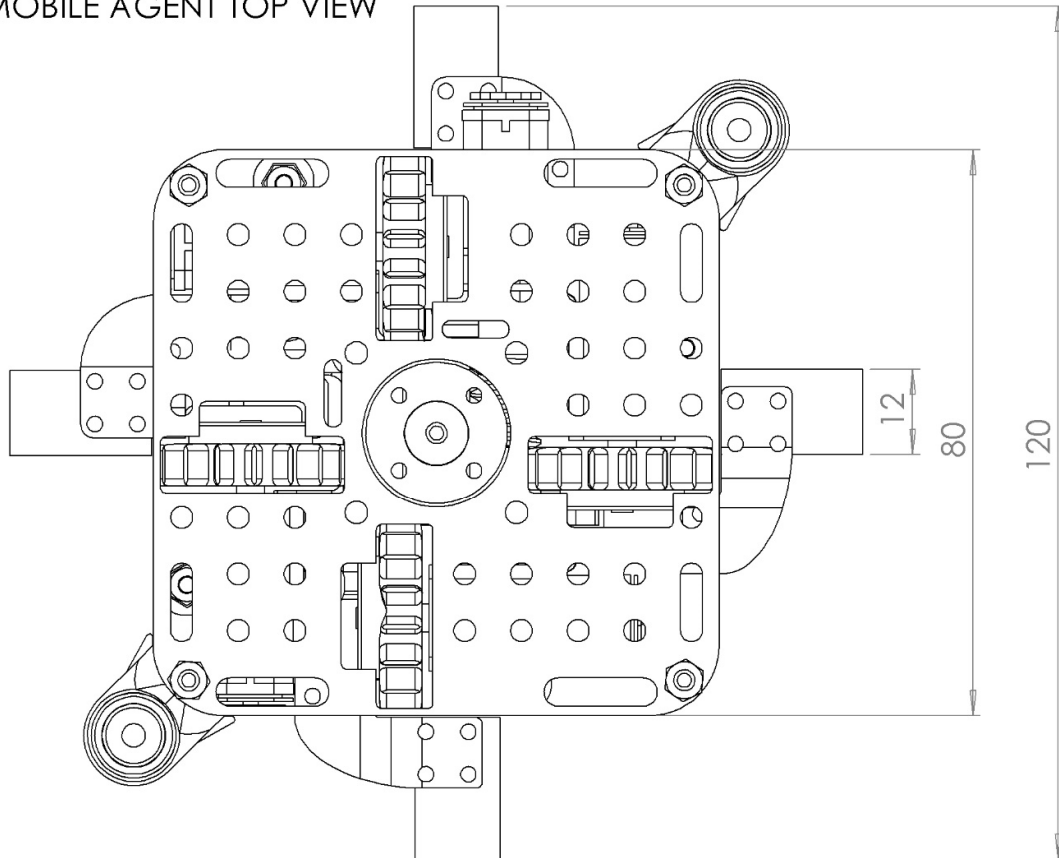
Appendix A2 – SCALA GEN TWO prototype;

Appendix A3 – SCALA GEN THREE prototype;

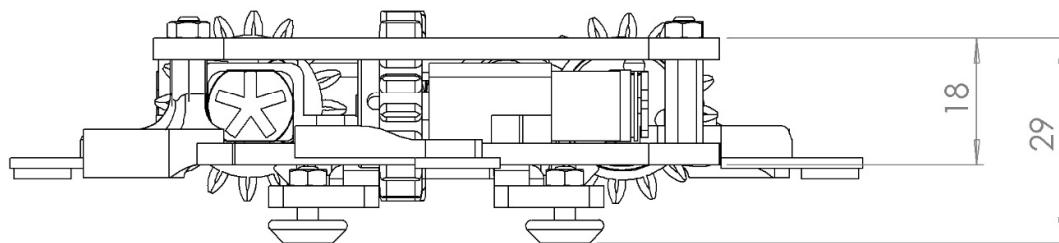
Appendix A4 – SCALA manipulator and tools;

Appendix A5 – SCALA test-bed.

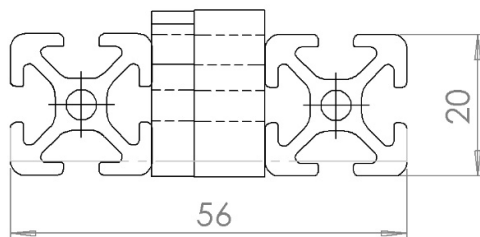
MOBILE AGENT TOP VIEW



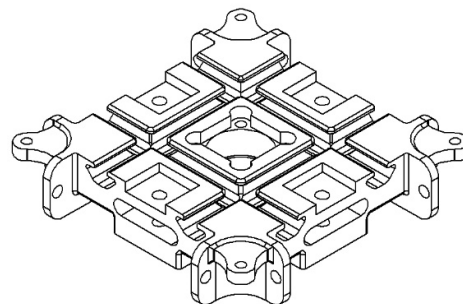
MOBILE AGENT FRONT VIEW



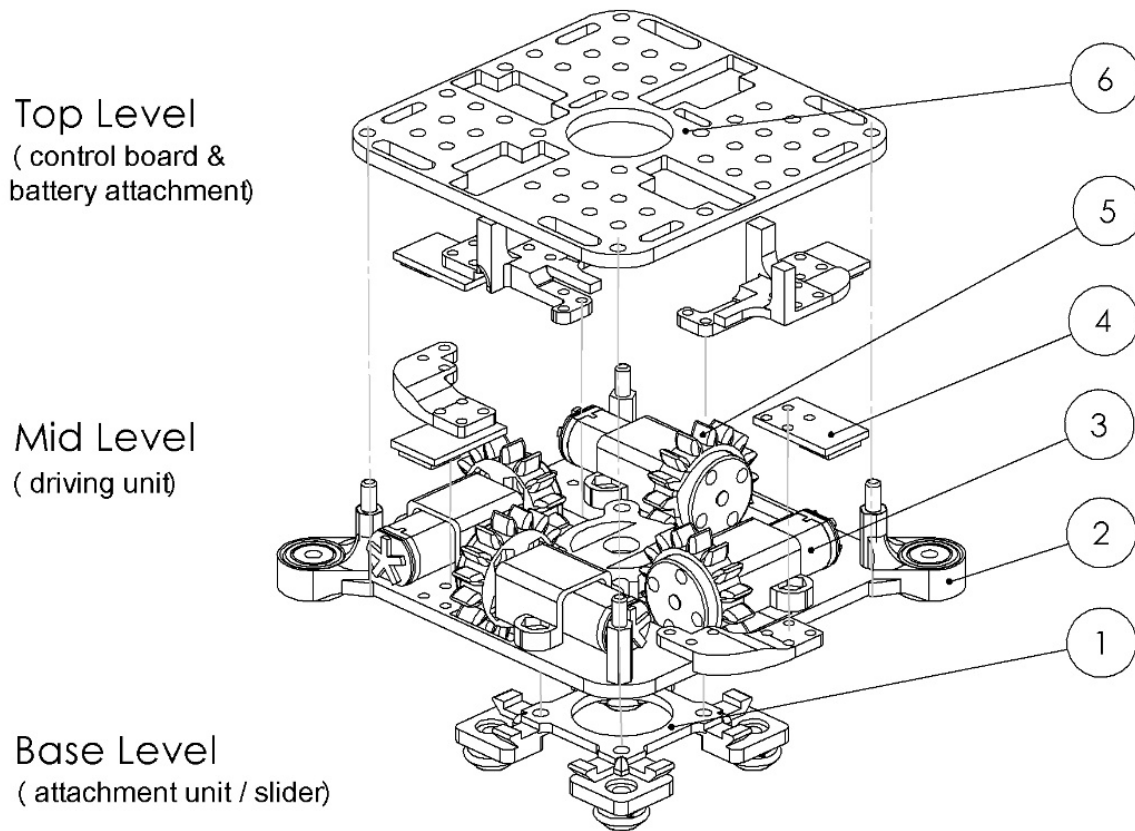
RAIL SECTION VIEW



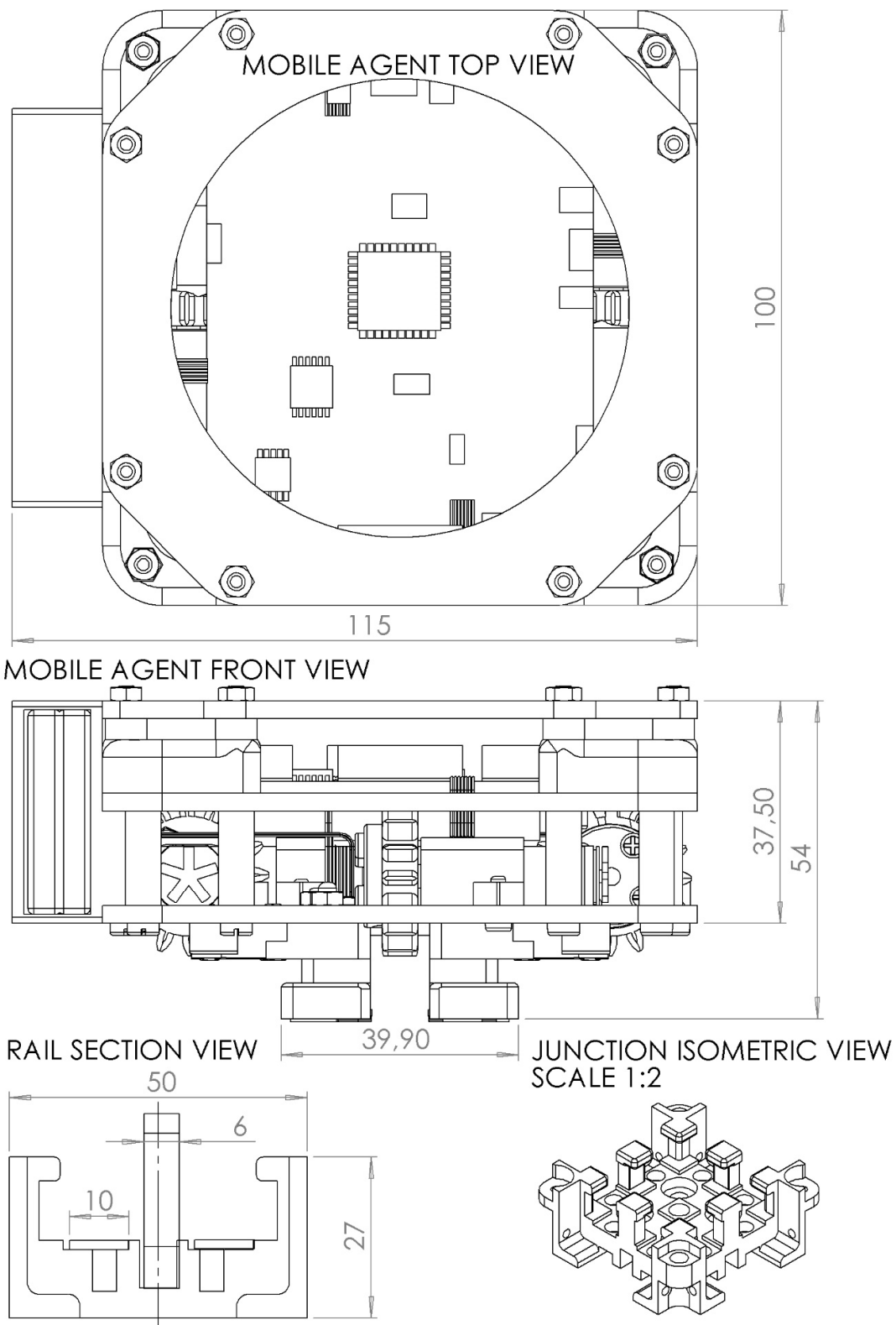
JUNCTION ISOMETRIC VIEW



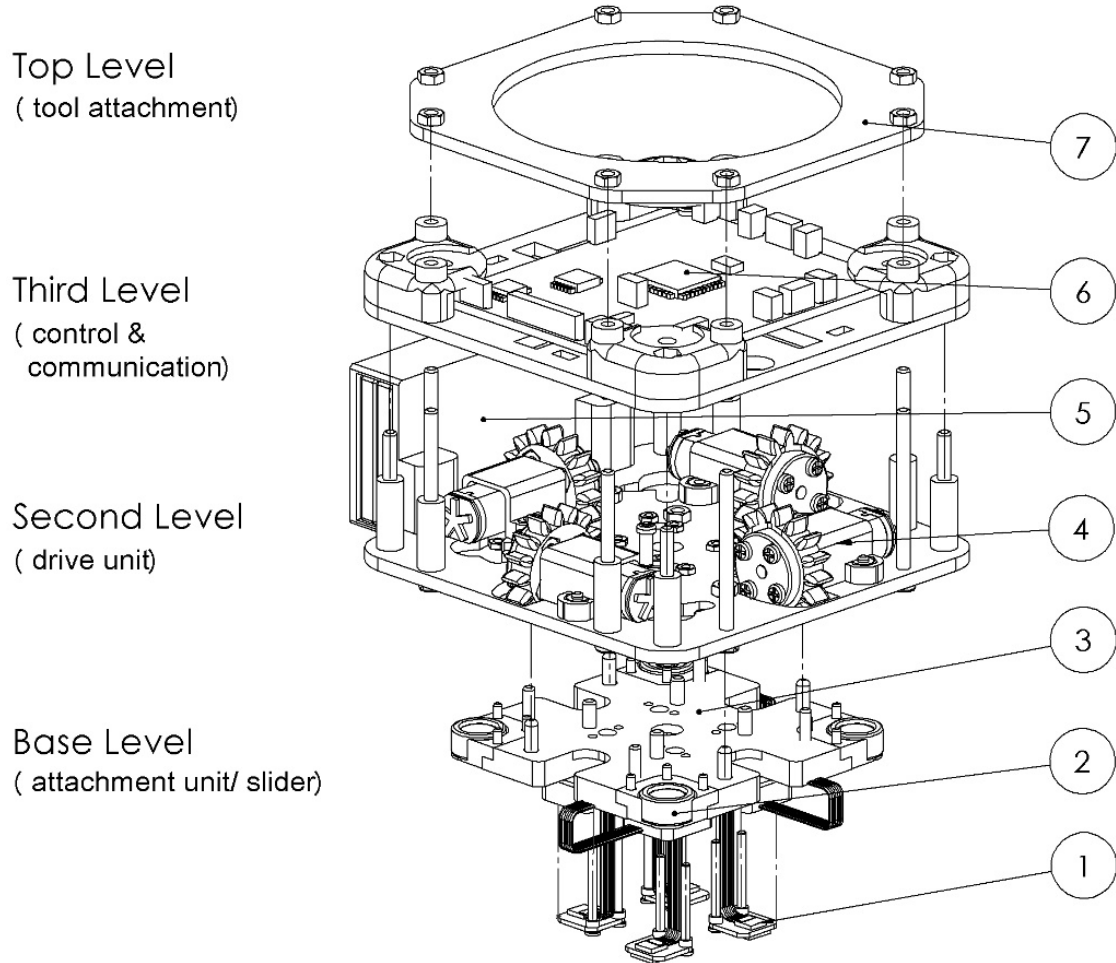
Appendix A1 – SCALA GEN ONE Prototype (scale 1:1).



Appendix A1 – SCALA GEN ONE Prototype exploded view, not showing control board and batteries. 1- Slider; 2- Magnets; 3- Drive motor; 4- Magnetic encoder; 5- Drive gear; 6- Battery and PCB support.

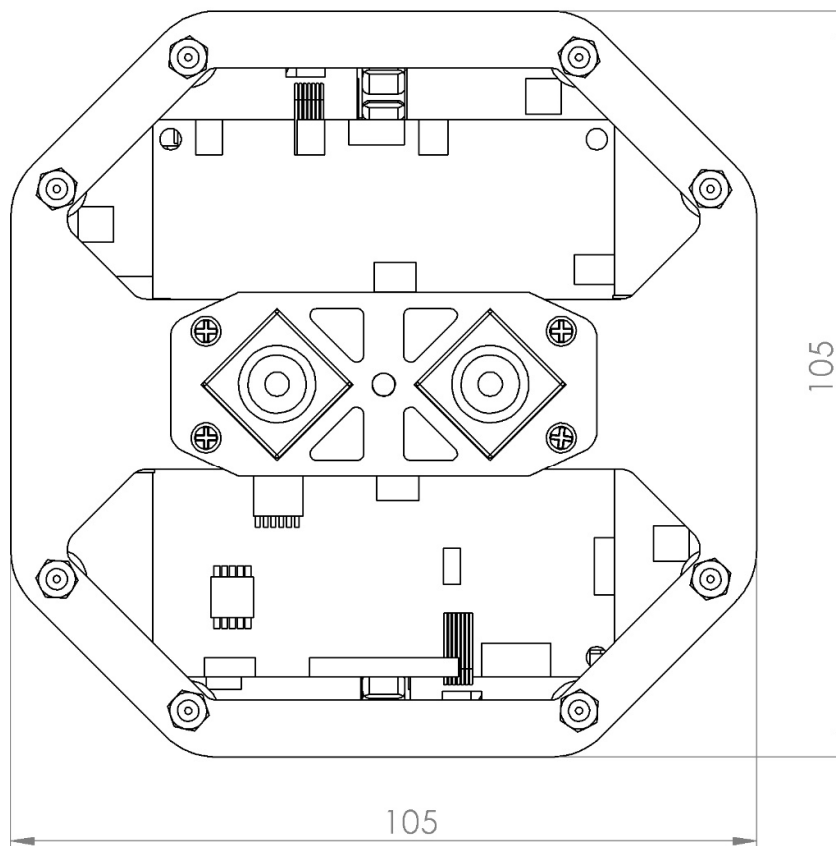


Appendix A2 – SCALA GEN TWO Prototype (scale 1:1).

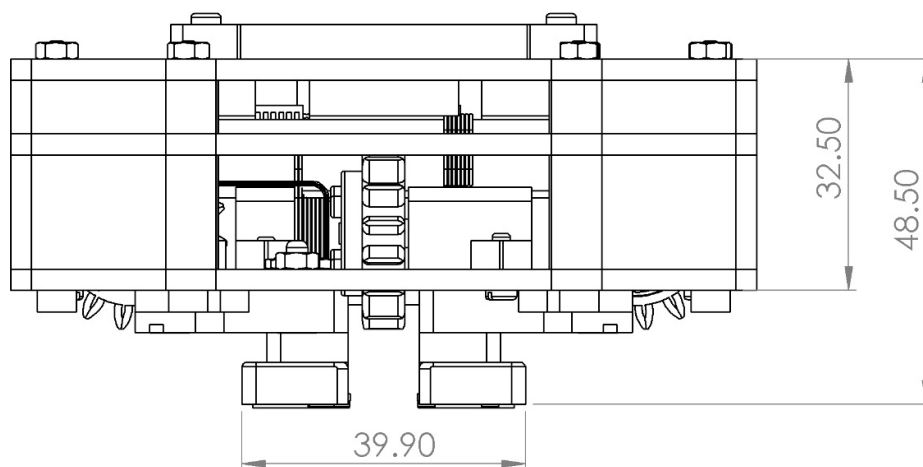


Appendix A2 – SCALA GEN TWO Prototype exploded view, showing its components: 1- Magnetic encoder; 2- Magnet; 3- Slider; 4- Drive motor; 5- Battery; 6- PCB; 7- Tool support.

MOBILE AGENT TOP VIEW

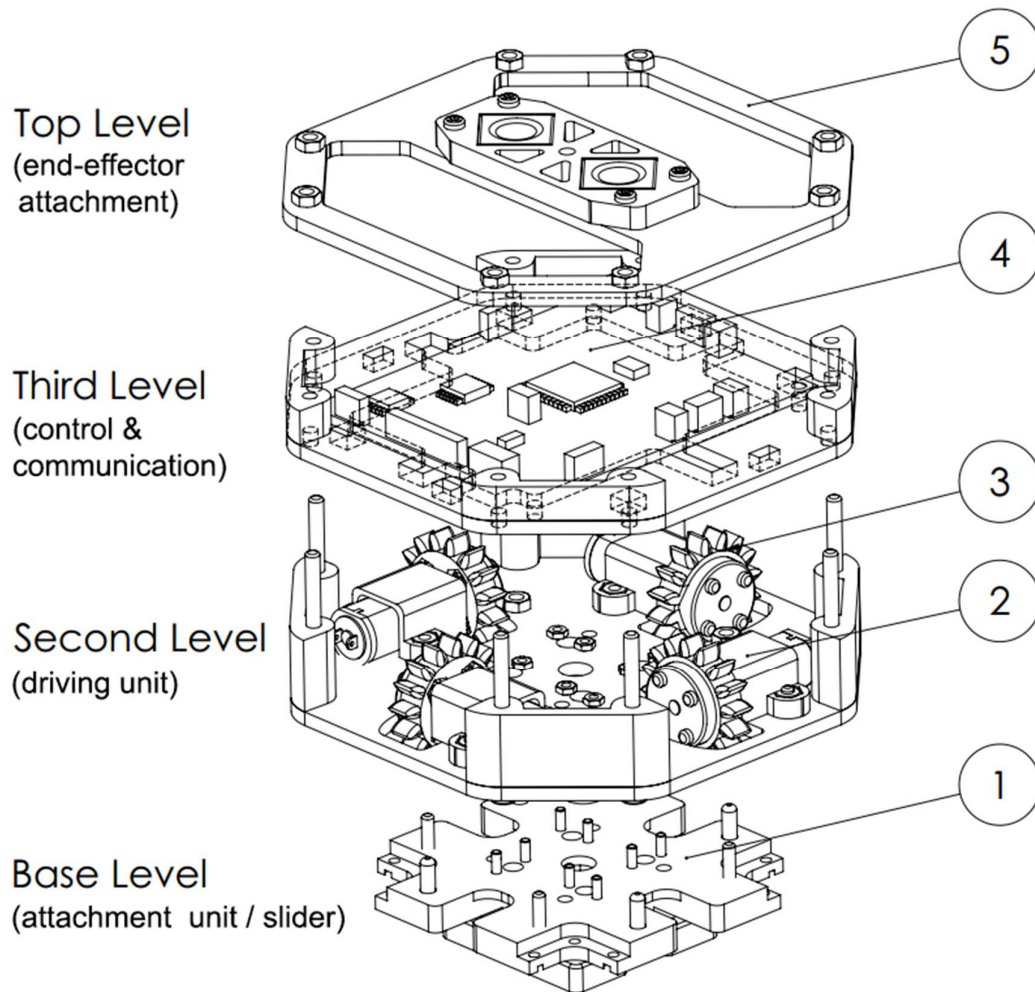


MOBILE AGENT FRONT VIEW

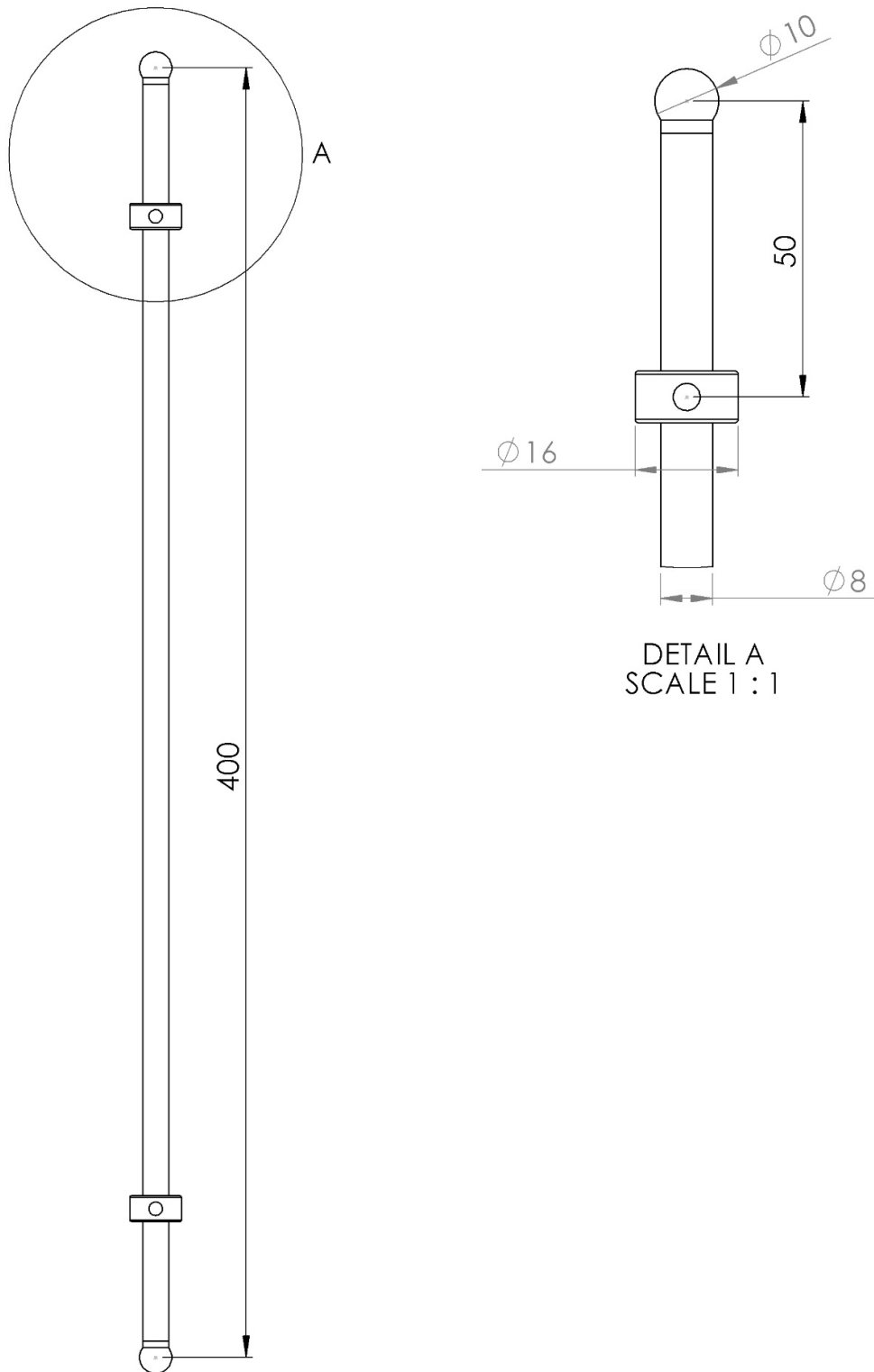


SAME RAIL AND JUNCTION FROM GEN TWO

Appendix A3 – SCALA GEN THREE Prototype (scale 1:1).

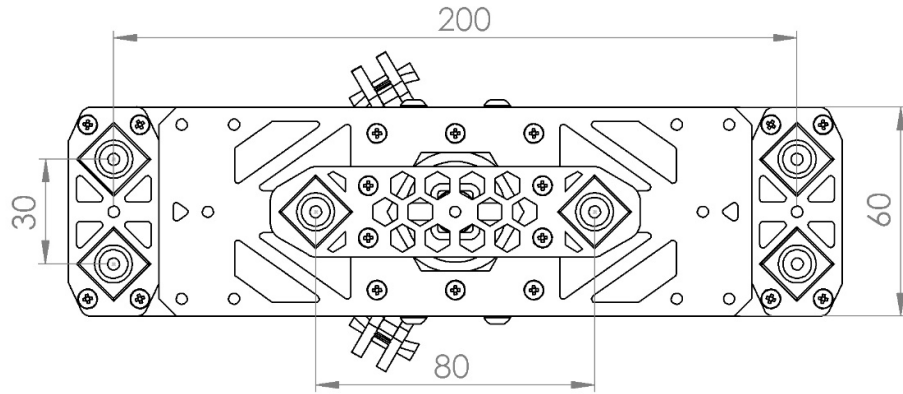


Appendix A3 – SCALA GEN THREE Prototype exploded view, showing its components: 1- Slider with embedded magnetic encoders; 2- Drive motor; 3- Drive gear ; 4- PCB; 5- Tool support.

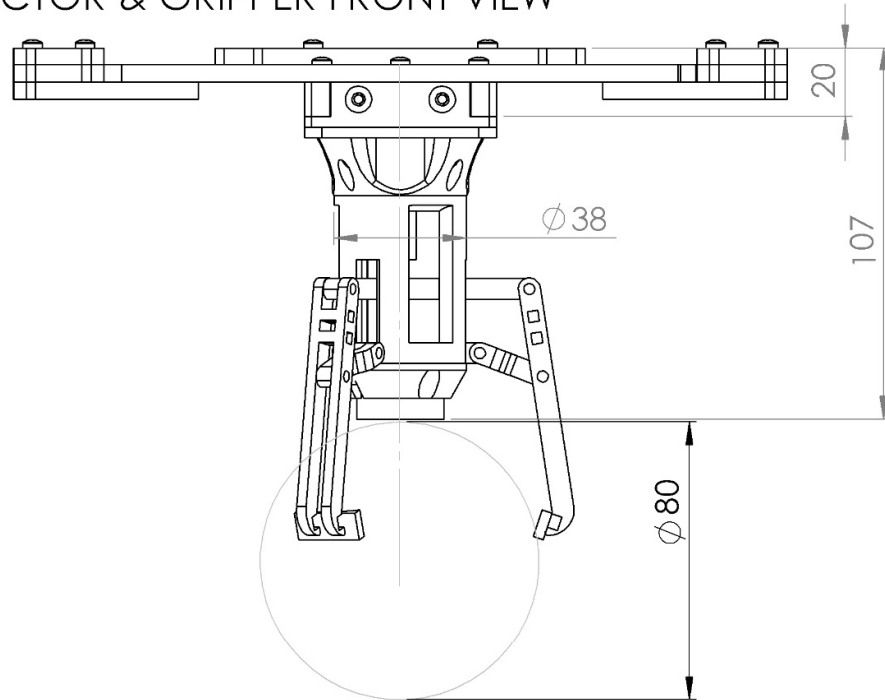


Appendix A4 – SCALA manipulator link (scale 1:2).

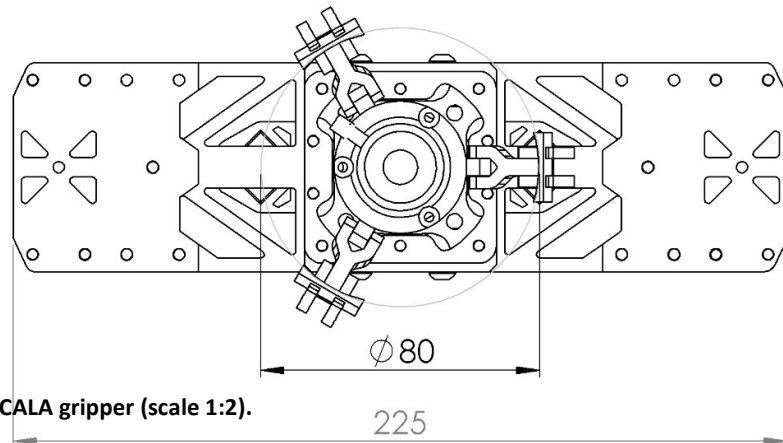
END-EFFECTOR & GRIPPER TOP VIEW



END-EFFECTOR & GRIPPER FRONT VIEW

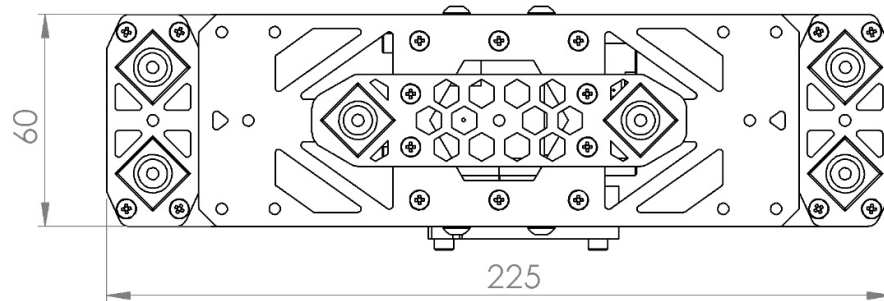


END-EFFECTOR & GRIPPER BOTTOM VIEW

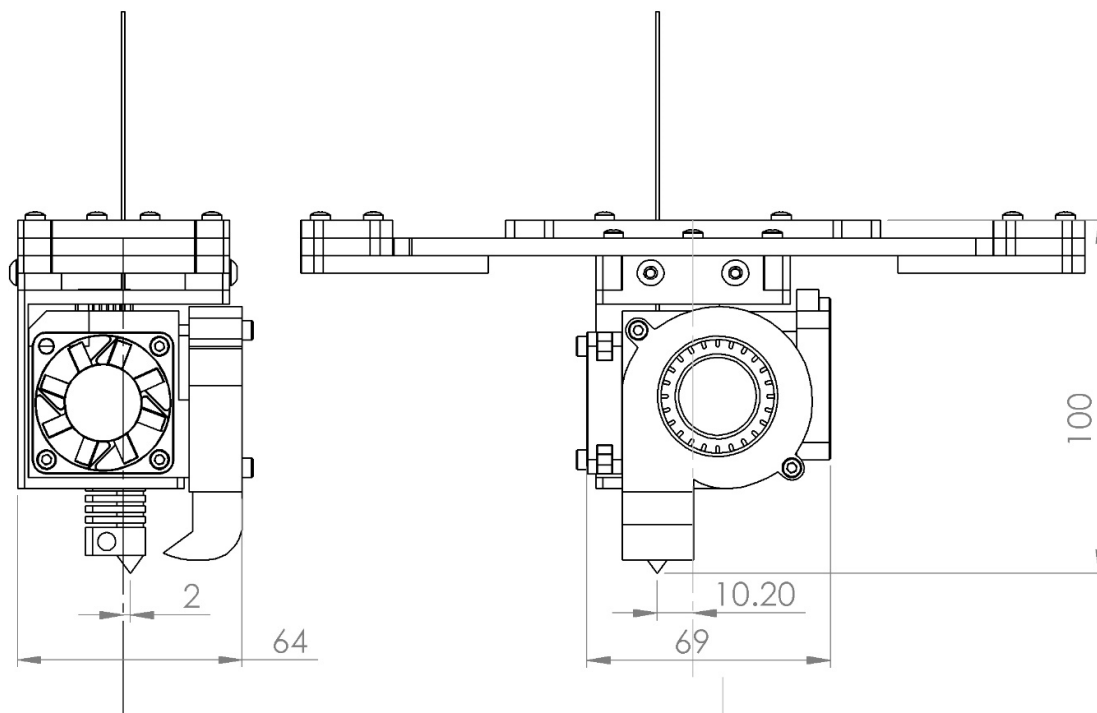


Appendix A4 – SCALA gripper (scale 1:2).

END-EFFECTOR & PLASTIC FILAMENT EXTRUDER TOP VIEW

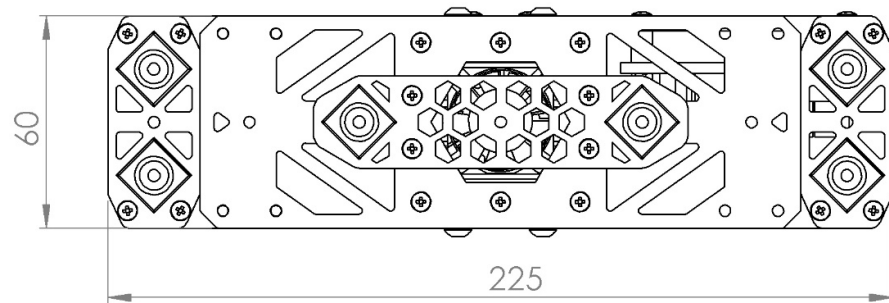


END-EFFECTOR & PLASTIC FILAMENT EXTRUDER LEFT AND FRONT VIEW

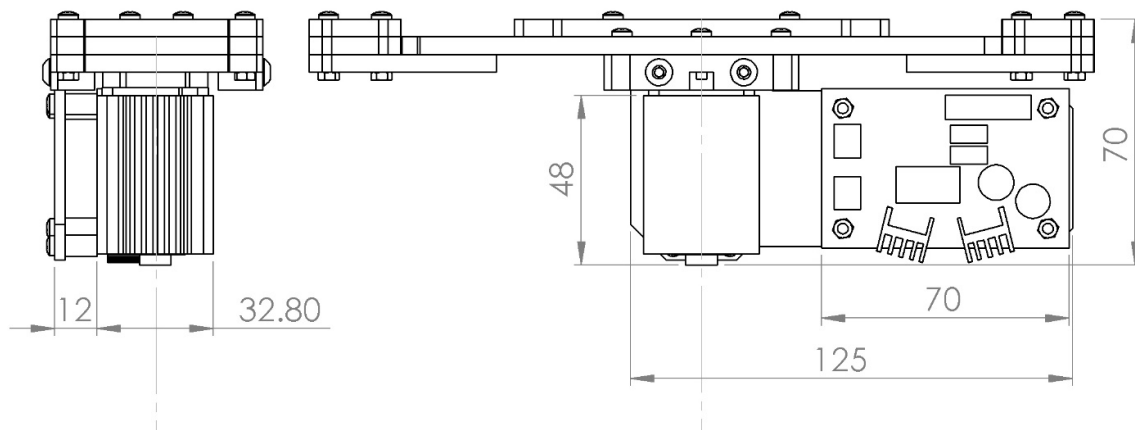


Appendix A4 – SCALA plastic filament extruder (scale 1:2).

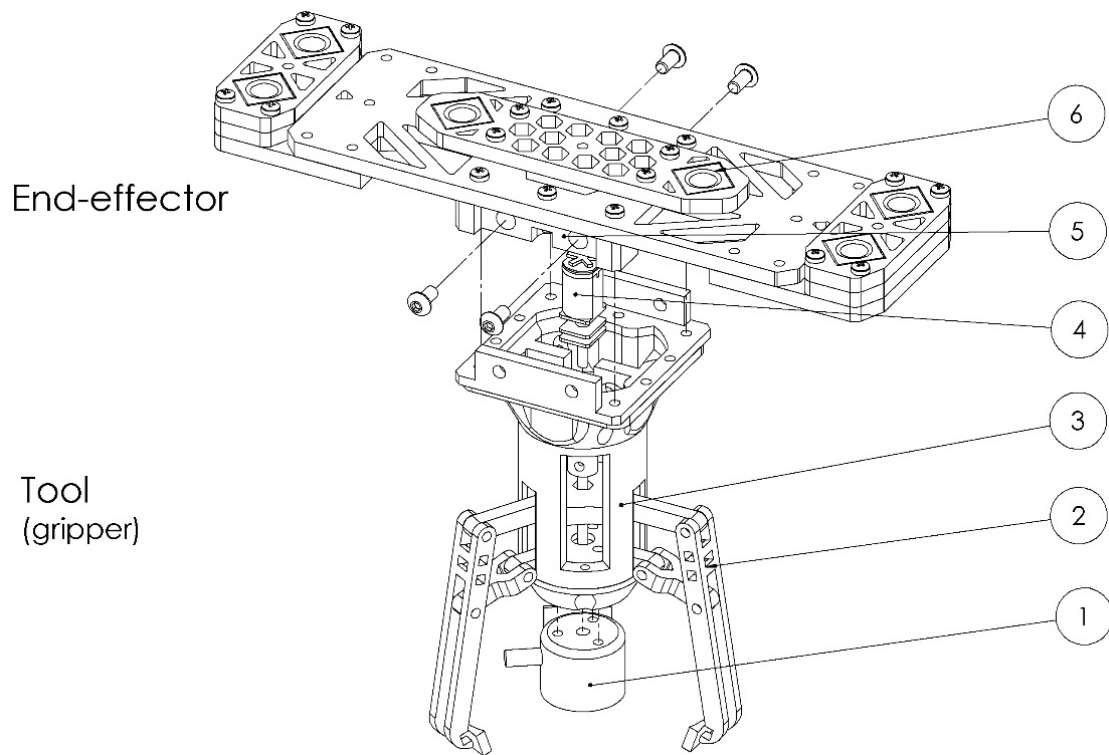
END-EFFECTOR & LASER TOP VIEW



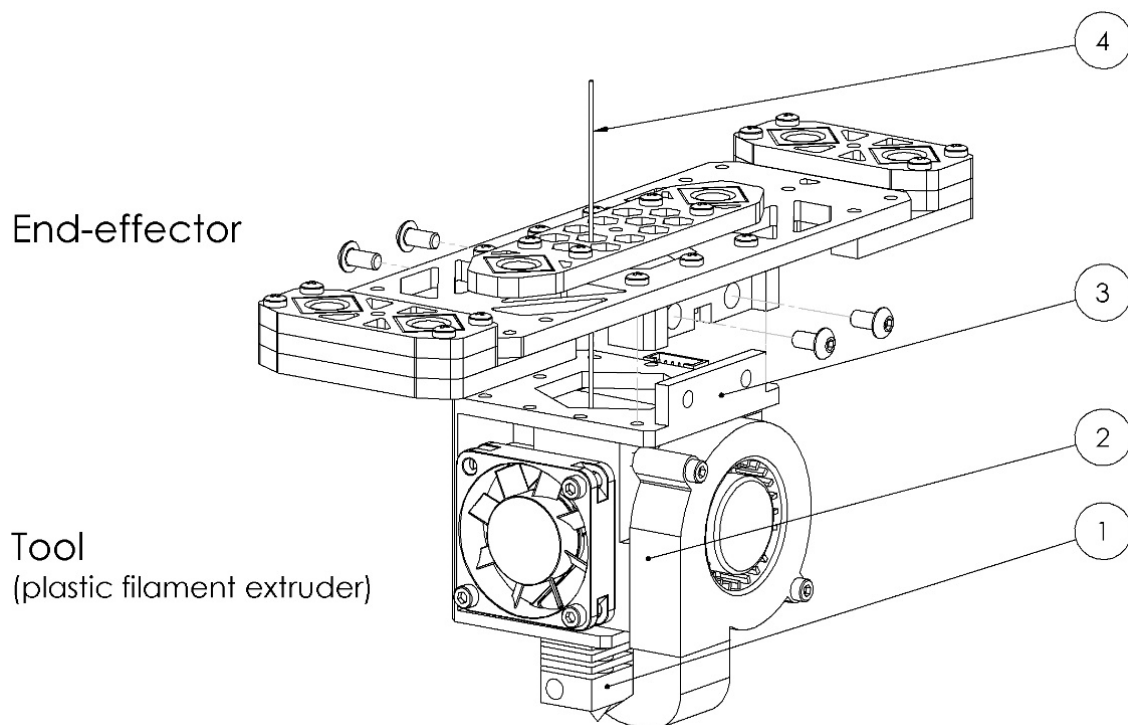
END-EFFECTOR & LASER LEFT AND FRONT VIEW



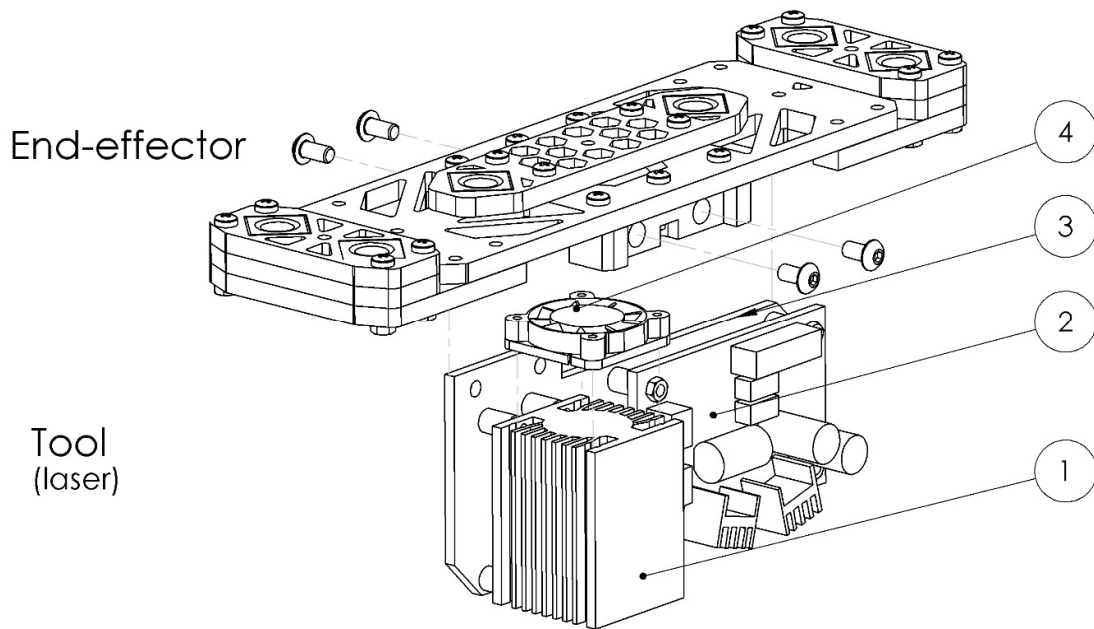
Appendix A4 – SCALA laser (scale 1:2).



Appendix A4 – SCALA gripper exploded view: 1- Electromagnet; 2- Claw finger; 3- Gripper body; 4- Actuator; 5- Modular tool attachment; 6- N35 magnet for PM links.

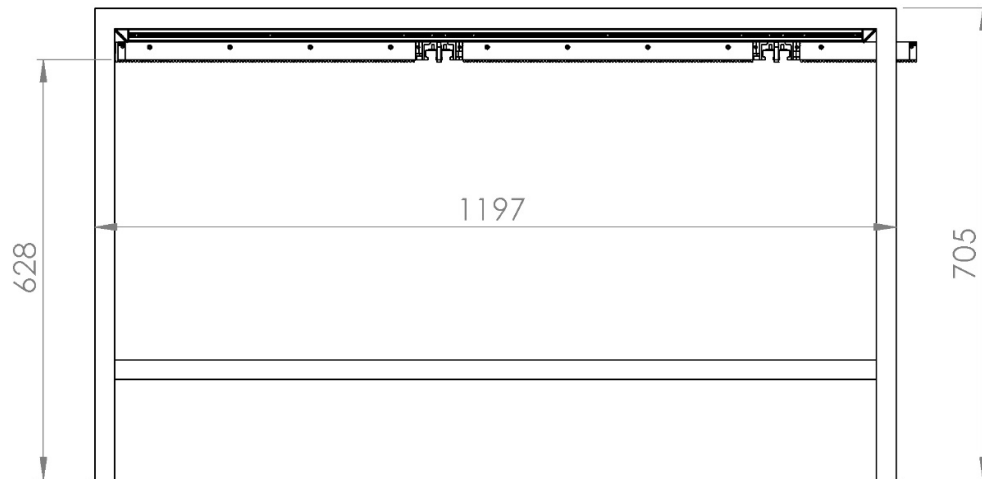


Appendix A4 – SCALA plastic filament extruder exploded view: 1- Plastic extruder; 2- Extrusion kit; 3- ABS support; 4- Plastic filament.

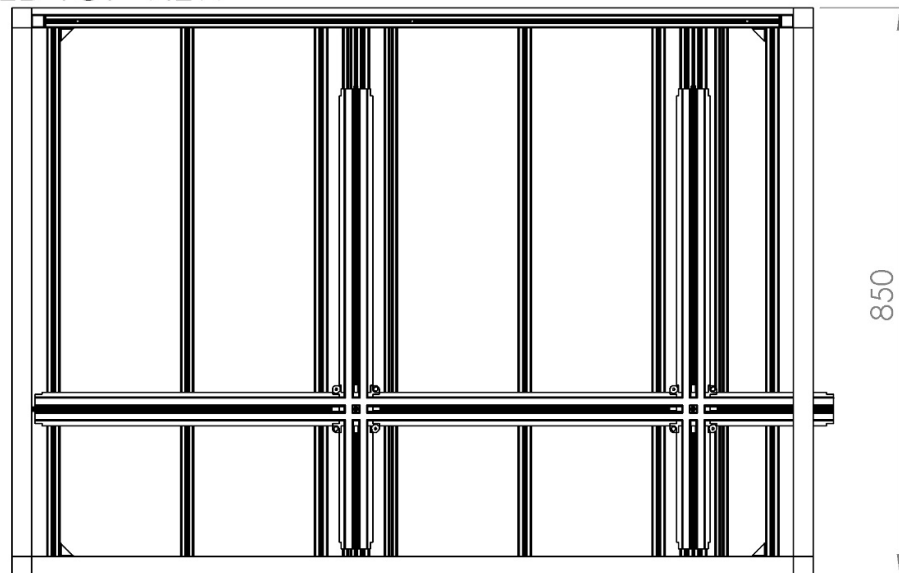


Appendix A4 – SCALA laser exploded view: 1- Laser; 2- Driver; 3- Acrylic support; 4- Cooling fan.

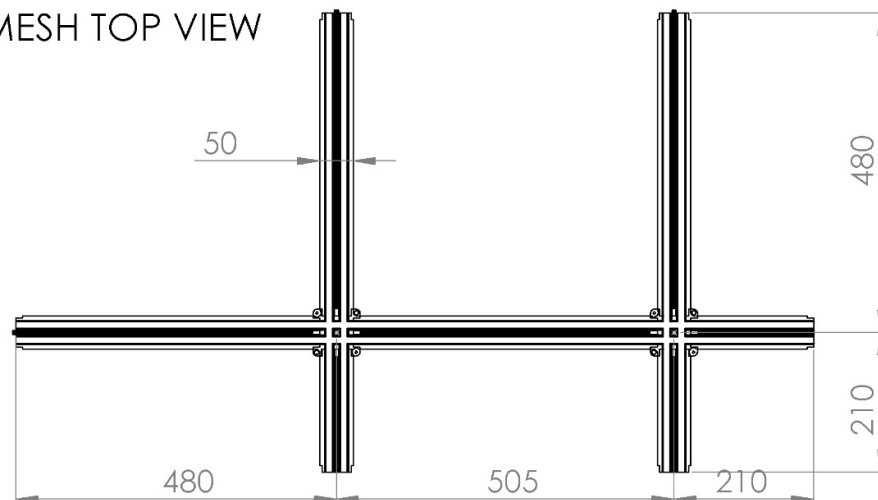
TEST BED FRONT VIEW



TEST BED TOP VIEW



RAIL MESH TOP VIEW



Appendix A5 – SCALA testbed (scale 1:10).

Appendix B

Algorithms

Appendix B1 – Algorithm 1 – Property verification routine;

Appendix B2 – Algorithm 2 – Design routine;

Appendix B3 – Algorithm 3 – Optimal path search routine for path planning.

Algorithm 1 Verification Routine

```

1: procedure WORKSPACE DETERMINATION
2:   inputs: [Qa]; [ΔXa]; [τ]; p;
3:   for i = 1, ..., m do
4:     ℒ = {initial[x]}; n = size(ℒ);
5:     while n > 0 do
6:       [b] = ℒ(1); ▶ take 1st box of ℒ
7:       ℒ(1) = []; n = n - 1; ▶ erase 1st box of ℒ
8:       [bnew] = Contract [b];
9:       if Contract fails then
10:        goto 5;
11:      end if
12:      if ∀x ∈ [bnew], Ci(x,p) met then
13:        [Wi] = [Wi] ∪ [bnew];
14:      else if ∀x ∈ [bnew], Ci(x,p) not met then
15:        goto 5;
16:      else
17:        if [bnew] > minDim then
18:          ℒ ← bisect [bnew]; n = n + 2;
19:        else
20:          ℬi ← [bnew]; ▶ list of boundary boxes
21:        end if
22:      end if
23:    end while
24:  end for
25:  return [W];
26: end procedure

```

Algorithm 2 Design Routine

```

1: procedure DESIGN CERTIFICATION
2:   inputs: [Qa]; [ΔXa]; [τ]; [W];
3:   [D0] = {initial[p]};
4:   for i = 1, ..., m do
5:     ℒ = [Di-1]; n = size(ℒ);
6:     while n > 0 do
7:       [b] = ℒ(1); ▶ take 1st box of ℒ
8:       ℒ(1) = [ ]; n = n - 1; ▶ erase 1st box of ℒ
9:       [bnew] = Contract [b];
10:      if Contract fails then
11:        goto 6;
12:      end if
13:      if ∀x ∈ [W], ∀p ∈ [bnew], Ci(x,p) met then
14:        [Di] = [Di] ∪ [bnew];
15:      else if ∀x ∈ [W], ∀p ∈ [bnew], Ci(x,p) not met then
16:        goto 6;
17:      else
18:        if [bnew] > minDim then
19:          if Eq. (3-71) > 0.8 then
20:            ℒ ← bisect [bnew]; n = n + 2;
21:          else
22:            bisect [W]; goto 13;
23:          end if
24:        else
25:          ℒ ← [bnew]; ▶ list of boundary boxes
26:        end if
27:      end if
28:    end while
29:  end for
30:  return [D];
31: end procedure
    
```

Algorithm 3 A* Optimal Path Search Routine

```

1: procedure OPTIMAL PATH SEARCH
2: init. variables:  $n_i = n_s$ ;  $n_t = target$ ;  $value(n)$ ;
3: repeat
4:    $value(n_i) = 0$  ▶ current node becomes non transitable
5:   for  $d = -2, -1, 1, 2$  do ▶  $d$  moving direction for adjacent position: -2 left, -1 down, 1 up, 2 right
6:      $n_j = adj(n_i, d)$  ▶ chooses adjacent node  $j$  a function of  $d$ 
7:     if  $value(n_j) = 1$  then ▶ adjacent node  $j$  is transitable
8:        $direction(n_j) = d$ 
9:       if  $direction(n_j) = direction(n_i)$  then
10:         $g(n_j) = 1$ 
11:       else
12:         $g(n_j) = 3$ 
13:       end if
14:       calculate  $f(n_j)$  ▶ determine evaluation function (eq. 4-6) score
15:        $\mathcal{L}_{open} \leftarrow n_j$  ▶ add  $n_j$  to open node list
16:     end if
17:   end for
18:    $n_i = \min( f(n) ) \forall n \in \mathcal{L}_{open}$  ▶ next  $n_i$  is then node with lowest score in the open node list
19:    $\mathcal{L}_{open} \rightarrow n_i$  ▶ remove  $n_i$  from open node list
20: until  $n_i = n_t$ 
21: repeat
22:    $path = path \& n_i$ 
23:    $path\_cost = path\_cost + g(n_i)$ 
24:    $n_i = adj(n_i, -direction(n_i))$  ▶ moves backwards until the start node
25: until  $n_i = n_s$ 
26: return  $path$ ;  $path\_cost$ ;
27: end procedure

```

Appendix C

Complementary Tables

Appendix C1 – Table XXIV – Characteristics of industrial serial manipulators;

Appendix C2 – Table XXV – Characteristics of industrial parallel manipulators;

Appendix C3 – Table XXVI – Spatial parallel manipulator configurations.

Appendix C4 – Table XXVII – Commercial components used in SCALA.

Table XXIV - Characteristics of industrial serial manipulators from ABB[264], Fanuc[265] and KUKA[266].

Robot	Mass [kg]	Load [kg]	Repeatability [mm]	Load/Mass	Reach [m]	Base Size [m]	WorkS/InstS	Max Vel. [m.s ⁻¹]	Max Acc. [m.s ⁻²]
IRB 140	98	6	±0.03	0.061	0.81	0.45	12.96	2.5	20
IRB 2600	272	12	±0.04	0.044	1.65	0.67	24.26	NA	NA
IRB 4400	1040	60	±0.19	0.058	1.96	0.92	18.16	NA	NA
IRB 6620	900	150	±0.03	0.167	2.20	1.01	18.98	NA	NA
Fanuc CR7	53	7	±0.02	0.132	0.72	0.30	23.04	NA	NA
Fanuc M710	540	12	±0.15	0.022	3.12	0.55	128.72	NA	NA
Fanuc M20iA	250	20	±0.08	0.080	1.81	0.34	113.36	NA	NA
Fanuc M410	2430	450	±0.50	0.185	3.13	1.08	33.60	NA	NA
Kuka KR16	254	26	±0.05	0.102	1.61	0.65	24.54	NA	NA
Kuka KR1000	4750	750	±0.10	0.158	3.60	1.36	28.03	NA	NA

Table XXV - Characteristics of industrial parallel manipulators from ABB[264], Fanuc[265], Adept[267] and Symétrie[268].

Robot	Mass [kg]	Load [kg]	Repeatability [mm]	Load/Mass	Reach [m]	Base Size [m]	WorkS/InstS	Max Vel. [m.s ⁻¹]	Max Acc. [m.s ⁻²]
IRB 360	120	3	±0.10	0.025	0.40	0.74	1.17	10	100
Fanuc M1 HL	21	1	±0.03	0.048	0.21	0.37	1.29	NA	NA
Fanuc M2 6H	115	6	±0.10	0.052	0.40	0.80	1.00	NA	NA
Adp. Q. s650H	117	6	±0.10	0.051	0.65	NA	NA	10	150
Adp. H. 565	52	3	±0.10	0.058	0.57	0.89	1.64	NA	NA
Sym. Sirius	85	200	±0.000006	2.353	0.15	0.88	0.12	0.008	NA
Sym. Notus	100	200	NA	2.000	0.25	1.20	0.17	0.8	10
Sym. Mistral	450	1000	±0.50	2.222	0.460	2.28	0.16	1	10
Sym. Sirocco	850	2000	NA	2.353	0.600	3.35	0.13	2	6
Sym. Aquilon	3000	6000	NA	2.000	0.800	4.50	0.13	1.8	7

Table XXVI – Spatial parallel manipulator configurations and their complexity level.

DOF of each limb	Examples	Complexity Level	
		Number of Joints	Number of Links
3,3,3	3-PU*	21	9
	3-U*P	21	9
4,4,4	3-PU*R	24	9
	3-P^UR	21	6
	3-CU^	18	6
	3-^UC	18	6
	3-RPC	9	3
	3-RRC	9	3
5,5,5	3-PU*U	21	9
	3-P^UU	21	6
	Delta	15	9
5,5,3	2-PU*U & 1-PU*	20	9
6,6,3	2-PUS & 1-PU*	12	5

Table XXVII – Main technical specifications of the commercial components used in SCALA.

Designation	Manufacturer / Supplier	Reference / Model	Technical data
Drive motors	Pololu, USA	2218	Available in annex A
Motor mounting bracket	Pololu, USA	1089	Plastic, mass: 1g
Motor hubs	Pololu, USA	1996	17.5×5mm diam/thick, mass: 2.8g
Magnetic linear sensors	AMS, Austria	AS5304	Available in annex B
Magnetic strip	AMS, Austria	MS20-150	Available in annex C
Shaft collar	BearingKing, UK	CABU08Z	Steel 16x8x8mm OD/ID/W
Steel balls	Imporseal, Portugal	-	Chrome Steel AISI 52100, Grade 10, 10mm diam
Links	Decathlon, France	795700	Carbon, 8x6mm OD/ID
Magnets	HKCM, Germany	9960-3494	Material, Grade: NdFeB, N35, holding force*: 41N, mass: 8.4g
6DOF tracking sensor	Polhemus, USA	Liberty	Available in annex D
Laser	OSRAM, Germany	PL TB450B	Available in annex E
Extrusion kit	BQ, Spain	HeatCore DDG	Available in annex F

*on a steel plate

Annex

Data Sheets

Annex A – POLOLU MicroMotors Specs

Annex B – AS5304 Linear Encoders Specs

Annex C – MS20-150 Magnetic Multipole Strip Specs

Annex D – Polhemus Liberty Specs

Annex E – OSRAM Laser Specs

Annex F – BQ HeatCore Extrusion kit Specs

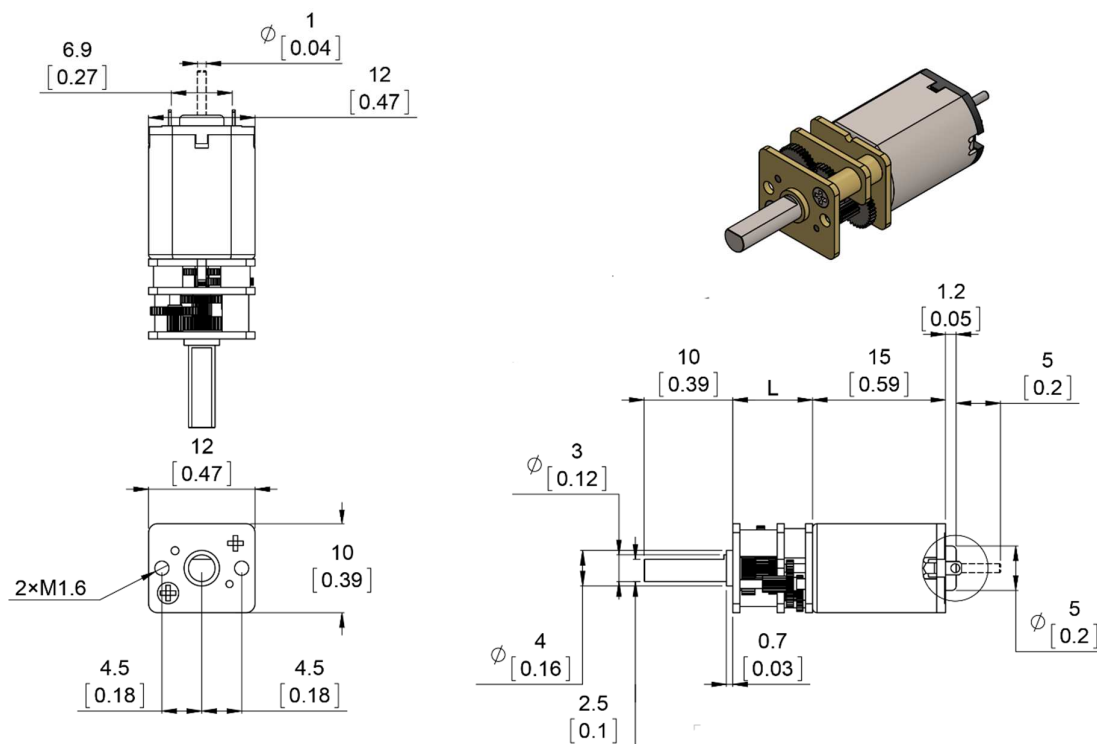
Annex A - POLOLU MicroMotors Specs

Overview

The brushed DC gearmotors, of high-power (HP) type, are intended for use at 6V, though in general, these motors can run at voltages in the 3 – 9V range. The brass gearbox has a 3mm diameter D-shaped metal output shaft, and a gear ratio of 298:1. The gearmotor can have an additional output shaft, in the rear of the motor, to install an encoder, to provide motor speed or position feedback.

Product specs

Nominal voltage	Stall current @ 6V	No-load speed @ 6V	Stall torque @ 6V	Mass
6 V	1600 mA	100 rpm	0.5 N.m	10 g



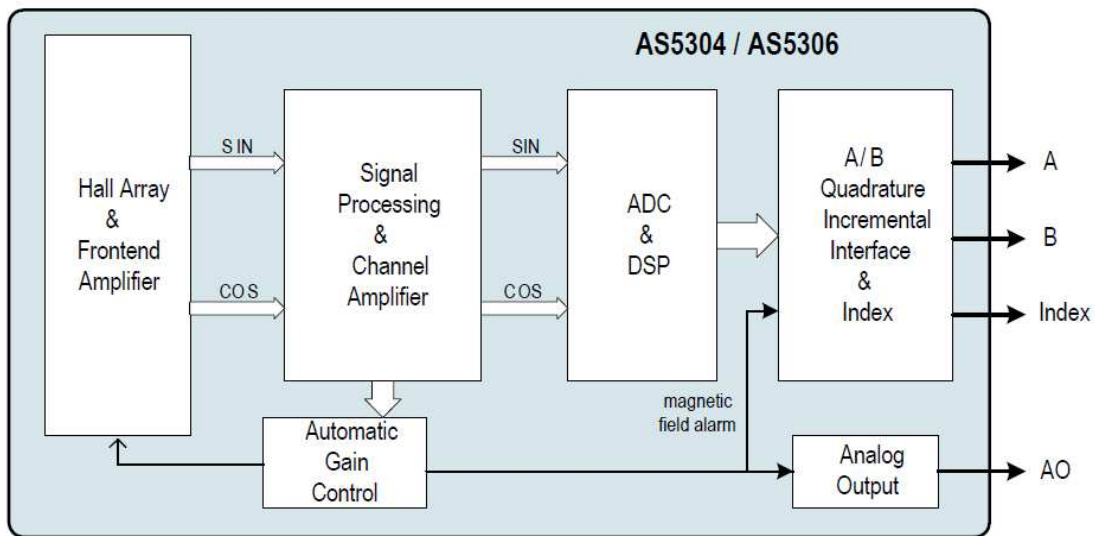
Micro metal gearmotor dimensions (units: mm [in]). L = 9mm.

Available in: <https://www.pololu.com/product/2218>

Annex B - AS5304 Linear Encoders Specs

Overview

The AS5304 is an incremental position sensor for linear and rotary off-axis applications based on contactless magnetic sensor technology. To measure position and motion a multi-pole magnet strip or ring has to be used. There are *160 pulses* per *4mm* pole pair length on the standardized quadrature output interface with an index pulse (ABI interface) with a maximum speed of *20m/s*.



Key Features

- Contactless motion and position sensing
- High speed measurement
- Immune to external magnetic stray fields

Product specs

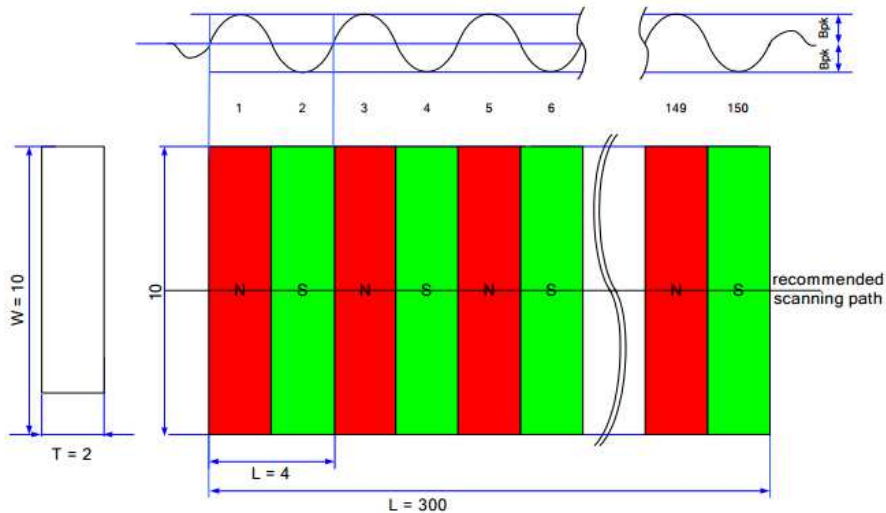
Resolution	Minimum pole pair length	Max speed	Voltage	Temp. range
160 step	4 mm	20 m.s ⁻¹	5 V	-40 to +125 °C

Available in: <http://ams.com/eng/Products/Position-Sensors/Linear-Incremental-Magnetic-Position-Sensors/AS5304>

Annex C - MS20-150 Magnetic Multipole Strip Specs

Overview

This specification defines the dimensional and magnetic properties of a multipole magnetic strip for use with the AS5304 magnetic linear motion and off-axis rotary angle encoder. Material: Strontium ferrite bonded. The MS20-150 magnet strip is magnetized on the top side and bonded on a steel support with elastomer adhesive (bottom). Note that the polarization of the magnet will change when it is rotated as the pole arrangement not symmetric. In order to get a stable 12-bit absolute reading, it may be necessary to filter the values by averaging, e.g. a moving average calculation in the external microcontroller. Averaging 4 readings results in $6dB$ ($=50\%$) noise and jitter reduction. An average of 16 readings reduces the jitter by a factor of 4. The vertical distance between the magnet strip and the top of the IC package should be $\leq 0.8mm$. Note that the vertical distance depends on the strength of the magnet. The AS5304 automatically adjusts for fluctuating magnet strength by using an automatic gain control (AGC).



MS20-150 strip dimensions (units in mm).

Product specs

Pole length	Number of poles	Resolution	Max cumulative error	Air gap
2 mm	150	25 μm	25 $\mu m/m$	< 0.8 mm

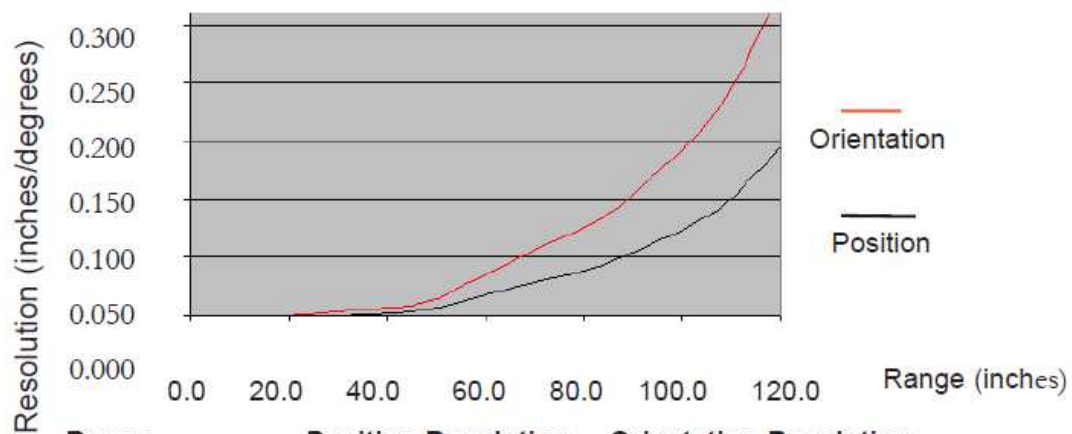
Available in: <http://ams.com/eng/Products/Magnetic-Position-Sensors/Magnets/AS5000-MS20-150>

Annex D – Polhemus Liberty™ Specs

Overview

The fastest, most accurate, scalable electromagnetic tracker available, LIBERTY™ represents a quantum leap in new technology. State-of-the-art Digital Signal Processor electronics make it the perfect real-time solution for 6 Degree-of-Freedom needs. LIBERTY has speed, ease-of-use via an intuitive Graphical User Interface, scalability, distortion sensing, and improved signal-to-noise ratios which increase stability and resolution while providing consistent high quality data. Note that large metallic objects, such as desks or cabinets, located near the source or sensor, may adversely affect the performance of the system.

Range vs. Resolution



Range (inches)	Position Resolution (inches)	Orientation Resolution (degrees)
12.0	0.00005	0.0004
24.0	0.0002	0.0014
36.0	0.001	0.0048
48.0	0.005	0.0117
72.0	0.031	0.060
120.0	0.145	0.280

Product specs

Update rate	Number of sensors	Position static accuracy	Orientation static accuracy
240 Hz	1 to 8	0.03 in.	0.15°

Available in: <http://polhemus.com/motion-tracking/all-trackers/liberty>

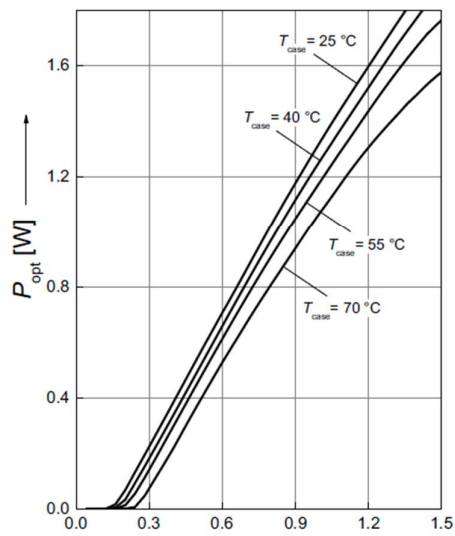
Annex E – OSRAM Laser Specs

Features

- Optical output power (continuous wave): 1.6 W ($T_{case} = 25\text{ }^{\circ}\text{C}$)
- Typical emission wavelength: 450 nm
- Efficient radiation source for cw and pulsed operation

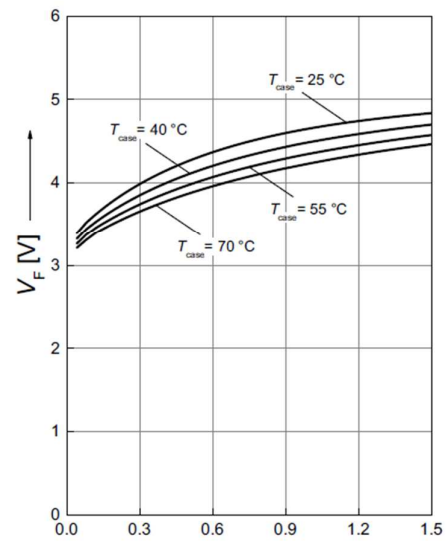
Optical Output Power

$$P_{opt} = f(I_F)$$



Operating Voltage

$$V_F = f(I_F)$$



Product specs

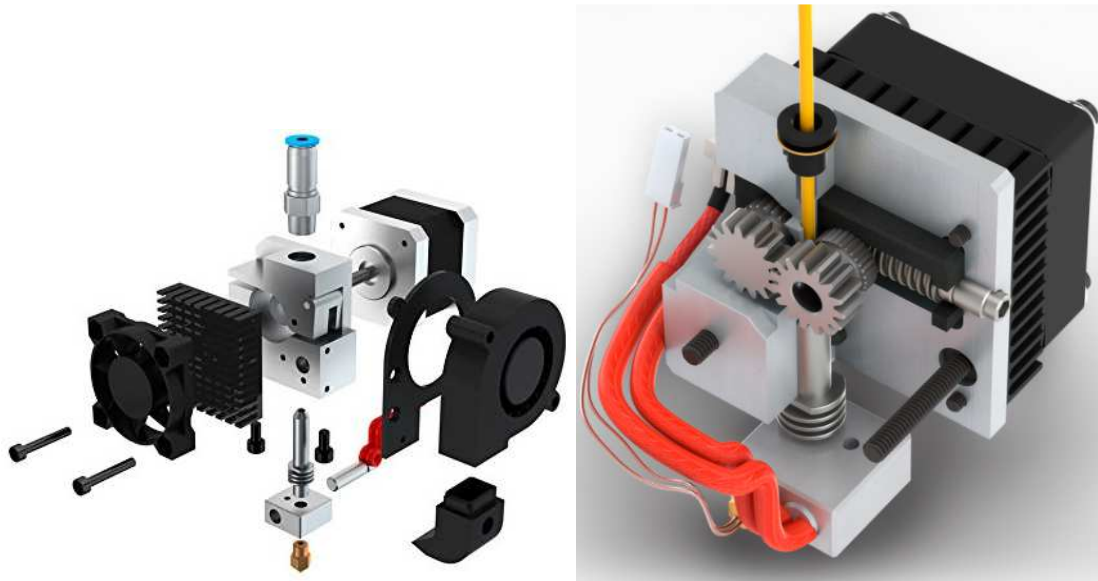
Optical output power	Operating current	Operating voltage	Emission wavelength
1.6 W	1.5 A	4.8 V	450 nm

Available in: https://www.osram-os.com/osram_os/en/products/product-catalog/laser-diodes/visible-laser/blue-laser/

Annex F – BQ HeatCore Extrusion kit Specs

Overview

The HeatCore Unibody was designed with the priority of ensuring that the printing system was stable and free from leaks. The best way to do this was by reducing the number of parts and joints. This is why the HeatCore Unibody hot-end is formed of a single piece of AISI 303 stainless steel. This material was selected for its high thermal conductivity which enables the system to reach the desired printing temperature even faster. What's more, to facilitate passage of the filament, the HeatCore Unibody has been electro-polished: electro-polishing is a chemical and electrical process that polishes the internal walls and reduces the number of irregularities, which optimizes the passage of the filament and reduces the chance of blockage.



Extrusion kit 3D model with an exploded and cut views.

Product specs

Nozzle diam.	Filament	Stepper	Heater	Thermistor	Mass
0.4 mm	1.75 mm	NEMA 17	40 W ceramic cartridge	NTC 100K	650 g

Available in: <https://www.bq.com/en/heatcore-ddg-extruder-kit>